Small Satellites for Gravitational Waves Observation

Laser Interferometer CubeSat Constellation Antenna (LICCA)

DSE Group 15

TUDelft

[This page was left blank intentionally.]

Small Satellites for Gravitational Waves Observation

Laser Interferometer CubeSat Constellation Antenna (LICCA)

by

Design Synthesis Exercise (DSE) Group 15

Final Report Draft

Under guidance of Dr. A. Menicucci (Tutor), Dr. C. Siemes (Coach) and G. I. Kus (Coach)

Delft University of Technology, Faculty of Aerospace Engineering

June 30, 2020

Name	Student Number
J. Achterberg	4685652
F. Bagchus	4454081
I. Boshuizen	4662776
T. Eppenga	4541677
S. Falckenheiner	4563387
F. Magri	4663438
G. Mettepenningen	4682343
J. Oduber	4534581
P. Silvagni	4652649
V. Tunjov	4548485
F. Weijand	4478762

TUDelft

Version Control

Changes were made on the 30th of June unless stated otherwise. The changes are shown in table 1.

Table 1: Log of the changes made to this report

Chapter	Changes
Payload	• The requirement source is specified. • The component selection is merged in the final design.
Astrodynamics	• Redundant text was eliminated. • References specified. • Equations explained in more detail.
Attitude Determination & Control System	• Magnitudes for disturbance torques added • Sources and explanation about $flux/m^2$ threshold added in pointing stability subsection.
Propulsion	• Take manufacturing into account for tank.
Conclusion & Recommendations	• Recommendation about centre of mass fluctuations added. • Conclusion adapted
General	• Feedback implemented. • Report formatting. • GTO to GEO transfer added. • Deployer section added. • Phase shift maneuver section added.
The merging of chapters	• RAMS and Risk. • Sustainability and Mission & design overview • Finance: Cost and System characteristics, Market analysis and Mission & design overview
Formatting	• Removing some pictures • Table of Content, List of acronyms on separate page.

Acknowledgements

Executive Summary

"Laser Interferometer CubeSat Constellation Antenna (LICCA) aims to complement current ground-based gravitational wave observations by measuring in the range of 1-10 Hz, using a CubeSat constellation in orbit around Earth" [3]. The objective of this final report is the detailed design of this mission's concept. Furthermore, a sustainability strategy, verification and validation procedures, finances and technical risk management are addressed in this report.

Mission & Design Overview
In the previous phases, eight design concepts for the LICCA mission were generated. These were traded off to identify the best performing result: two constellations of three satellites, utilising Sagnac interferometry. In the current design phase, each subsystem is designed in detail. This was done through an iterative process, going into more detail after each iteration.

Astrodynamic Characteristics
The designed lifetime of the LICCA CubeSats is 2 years, a result of a compromise between component degradation and the measurement of gravitational waves. The measurements will continue after this lifetime if possible. As the LICCA CubeSats will be in Geosynchronous Equatorial Orbit (GEO), they will experience radiation from cosmic rays, Van Allen belt radiation, and solar radiation. The Space Environment Information System (SPENVIS)[1] was used to get an estimate for the Total Ionising Dose (TID) and Single Event Effects (SEE). The ΔV budget was estimated to be 1.82 km/s including the Geostationary Transfer Orbit (GTO) to GEO transfer. If this transfer is not taken into account, the remaining ΔV is 0.37 km/s. The General Mission Analysis Tool (GMAT) from the National Aeronautics and Space Administration (NASA) was used to analyse non-impulsive transfers. Furthermore, a tool was developed to calculate relative Sun positions and eclipses. The maximum eclipse period is estimated to be around 72 minutes.

Sustainable Development Strategy
The main focus of the sustainability analysis lies in the Life Cycle Assessment (LCA) of the mission. The handbook developed by European Space Agency (ESA) is used as a guideline for this LCA [28]. For each of the phases of this mission, the sustainability is determined in terms of environmental and socioeconomic impact:

1. **Feasibility & Preliminary definition**
   - *Environmental*: Gas and electricity used by eleven students working from home.
   - *Socioeconomic*: Education of the eleven students and the introduction of the team to experts in mission related fields.

2. **Detailed definition & Qualification and Production**
   - *Environmental*: Mostly Commercial Off-The-Shelf (COTS) components were used which decreases Research and Development (R&D) costs, but tracing resource materials of these components is difficult.
   - *Socioeconomic*: Manufacturing, assembly, integration, and testing creates jobs. The worker welfare is vastly different per country.

3. **Launch and Commissioning**
   - *Environmental*: Emissions are reduced as the six spacecraft will piggy-back in one launcher vehicle. Still, rocket launch emissions are large. Two transfer vehicle are used to transport the CubeSats to GEO, however these vehicles will not expel non-green emissions.
   - *Socioeconomic*: New jobs will be created in mission research, maintenance and control. The impact differs per country.

4. **Utilisation**
   - *Environmental*: The propellant for the propulsion system is clean by LCA standards, and debris mitigation strategies are set up. No explosive or radioactive materials are used. The satellite uses radiofrequency bandwidth during its lifetime, which has a negative sustainability impact on a finite resource.
   - *Socioeconomic*: A transparent emission profile policy will be used to satisfy the general public about the negative impact of propulsion in the atmosphere. Jobs will be created, which are safe due to the radiation- and toxicity-free design.

---

[1] https://www.spenvis.oma.be/, accessed 8/06/2020

5. **Disposal**
   - *Environmental*: The spacecraft will enter a graveyard orbit, and all propulsion tanks and batteries will be depleted.
   - *Socioeconomic*: Sustainable approaches to space systems engineering and complex science-centered space missions are broadcast to the public. Processing measured data creates new jobs. Media coverage may inspire future engineers and scientists.

Payload

The payload will consist of an interferometer, including a laser setup, two transponders and two telescopes. The transponder will contain one laser each, and the telescopes contain two mirrors, a pupil and a body. All components from the laser setup are COTS options. The telescope body and mirrors must be manufactured, and will be made out of invar and zerodur, respectively. The properties of the payload are shown in table 2.

Table 2: The properties of the payload. Note that 1 U is 10x10x10 cm^3.

Mass [kg]	Volume [U]	Power consumed [W]
5.75	4	5.114

Attitude Determination & Control

The Attitude Determination and Control System (ADCS) will use only COTS options and consists of two star sensors, six Sun sensors, one Earth sensor, one Inertial Measurement Unit (IMU), four reaction wheels and two thrusters. The star sensors, Sun sensors and Earth sensor provide pointing accuracies of 0.0083°, 0.5°and 0.2°respectively. The IMU provides accelerometers and inclinometers and has a gyro bias instability of 0.3 °/h. The four reaction wheels are positioned in a tetrahedral configuration and rotate the spacecraft 180°in 107 s. The thrusters can dump a total angular momentum of 5.68 Nms per axis. The properties of the ADCS are shown in table 3.

Table 3: The properties of the ADCS

Mass [kg]	Volume [U]	Power consumed [W]
2.843	1.134	9.9

Propulsion

For the propulsion subsystem, the EPSS C1 thruster from Nanoavionics will be used, along with LMP-103S as chemical propellant. The thruster is a COTS option, but the propellant tank was designed specifically for the LICCA project and needs to be manufactured. The thruster will provide a thrust of 1 N at Begin-of-Life (BoL), down to 0.22 N at End-of-Life (EoL). The time required for realignment burns will be 65 s at BoL, and 270 s at EoL. For all manoeuvres, a total of 2.74 kg of propellant is required. As a result the propellant tank should have a capacity of 2.39 U. The propulsion subsystem will not perform the transfer from GTO to GEO, this will be done by the launcher instead. The properties of the propulsion subsystem are shown in table 4.

Table 4: The properties of the propulsion subsystem

Mass [kg]	Volume [U]	Power consumed [W]
4.40	3.98	11.49

Telemetry, Tracking & Command

The Telemetry, Tracking & Command (TT&C) subsystem will consist of a Ultra-High Frequency (UHF) system, and an S-band system. All components will be COTS options. The spacecraft UHF system will use a monopole antennae system and a UHF transceiver, both from Nanoavionics. The UHF ground segment will use Yagi antennae from ISIS. The UHF system will primarily be used for uplinking data. The spacecraft S-band system consists of one S-band patch antenna from GOMSpace, and two S-band transceivers from Satlab. The S-band ground segment will use stations in Kourou in French Guiana, Villafranca in Spain, and Dongara in Australia, all part of the ESA ESTRACK network. The S-band system will primarily be used for downlinking data and tracking. The properties of the TT&C subsystem are shown in table 5. It should be noted the power required to utilise the TT&C subsystem is only 1.05 W if no data is being transmitted.

Table 5: The properties of the TT&C subsystem

Mass [kg]	Volume [U]	Power consumed [W]
0.528	0.56	5.5

Command & Data Handling

The Command & Data Handling (CDH) subsystem will use the OBC-P3 from Space Inventor, along with an Input/Output (I/O) board. The OBC-P3 has two independent cores. One will function as the ADCS control system, and the other core will function as the main On-Board Computer (OBC). The two cores will be connected, such that data and commands may be transferred between them. The OBC will come with Error Detection And Correction (EDAC) software and watchdogs. The I/O board is connected to the OBC via an I2C connection. In total, 80 sensors will be connected to the I/O board. The properties of the CDH subsystem are shown in table 6.

Table 6: The properties of the CDH subsystem

Mass [kg]	Volume [U]	Power consumed [W]
0.285	0.285	3.3

Electrical Power System

The Electrical Power System (EPS) will consist of a battery, two Power Conditioning and Distribution Units (PCDU) and six deployable solar panels, each with 16 solar cells. As for the battery, a Li-Ion ICP-20 will be used. The QJ Solar Cell 4G32C from AZUR SPACE was chosen and the Starbuck NANO Plus will be used as PCDU. This comes with Battery Charge Regulators (BCR) and Maximum Power Point Trackers (MPPT). The battery can store up to 96 Wh. The total solar panel area is 0.3072 m², and they generate on average 40.46 W while exposed to sunlight. The PCDU's are the only EPS components with power consumption, and this is equal to 0.8 W. The properties of the EPS are shown in table 7.

Table 7: The properties of the EPS

Mass [kg]	Volume [U]	Power Generated [W]	Power consumed [W]
1.200	0.750	40.46	0.8

Thermal

The thermal subsystem consists of a thermal coating, louvers, and heat sources. The coating will be aluminised kapton foil of 2mm thick and will cover the main spacecraft structure and the backsides of the solar panels. The louvers will be the CubeSat Form Factor Thermal Control Louvers, invented by Allison L. Evans and patented by NASA. Underneath the louvers, a coating of aluminized kapton foil, with the metallic side facing outwards, will be applied. The heat sources will be simple resistance circuits, consuming up to 10 W. They will only be active during eclipses. The thermal subsystem will be able to freely control and maintain the temperature in the range of 3.7 °C up to 32.8 °C. The properties of the thermal subsystem are shown in table 8. It should be noted that volume on the outside of the main structure is not included.

Table 8: The properties of the thermal subsystem

Mass [kg]	Volume [U]	Power consumed (eclipsed) [W]
0.433	0.010	0 (10)

Structure

The structure will consist of a main structure, radiation shielding, solar panels and a deployment mechanism for the ADCS thrusters. For the main structure, the 12-Unit CubeSat structure from ISIS will be used. The radiation shielding will be located around the main structure, must be manufactured, and will be made of aluminium 6082-T6 of differing thicknesses, depending on the location. The solar panels must be manufactured, and will be made of AM162-AlBeMet with a thickness of 2.0615 mm. The Hold-And-Release Mechanism (HRM) of the solar panels and ADCS thrusters will utilise springs, nylon wires with retractable reels and burn circuits. The properties of the structure are shown in table 9.

Table 9: The properties of the structure

Mass [kg]	Volume [U]	Power consumed [W]
3.7	0.060	0

System Characteristics

The configuration of the spacecraft has been determined, and is shown in figure 1. For the communication protocol I^2C has been selected. This results in an additional 10-20% mass for the cabling. For the launcher, either Ariane 5 or Ariane 6 will be used, depending on the retirement of the Ariane 5 and the development of the Ariane 6. In order to reach GEO from GTO, the VIGORIDE solution will be used. This consists of a spacecraft that brings a payload from a relative low Earth orbit to a higher one, which for the case of the LICCA mission two of these will be needed. Regarding the mission operations, the spacecraft will enter GEO by piggybacking off the transfer vehicle. After which it performs a phase shift of 120°per satellite in each constellation. While operating, the spacecraft will downlink every day, and the constellation is aligned every 15 days. This is done because the satellites drift with respect to each other and this is not desired. At the end of life, the spacecraft will enter a graveyard orbit, where it may continue operating while enough propulsion is available. The budgets are summarised in table 10.

Table 10: The system characteristic budgets

Mass [kg]	Volume [U]	Power consumed [W]
22.3 ±2.50	10.9	30.60 ±2.30

For an overview of the system, system characteristic diagrams were developed and maintained throughout the project.

Finances

The total mission cost was estimated to be 14.67 million EUR, including inflation and excluding operations costs. Operation costs were estimated to be 5.36 million EUR. In the market analysis, two markets were identified and predicted in size. The first market includes all gravitational wave measurements, and is estimated to be 2 815 million EUR. The second market includes all CubeSats, and is estimated to be 956 million EUR. The LICCA mission will have shares on these markets of 0.45% and 1.33% respectively. A Strengths, Weaknesses, Opportunities and Threats (SWOT) analysis was made. Most strengths and opportunities originate from the unique mission goal and simple CubeSat form-factor, whereas most weaknesses and threats originate from the competitiveness of the CubeSat market and the experimental technology required for measuring gravitational waves.
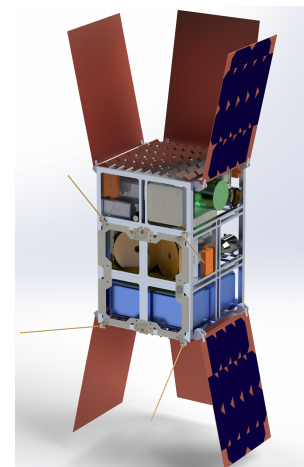

Figure 1: The configuration of the spacecraft

Technical Risk Management

All technical risks and risks concerning the subsystems were mapped. Then the most severe risks were identified and mitigated. These risks are mitigated by introducing tests, increasing redundancy or setting guidelines on handling components.

RAMS

The Reliability, Availability, Maintainability and Safety (RAMS) of the design are estimated. The reliability has been empirically estimated to be 56%. The reliability is increased by the usage of certified COTS components, as well as introduced tests which mitigate risks. The reliability is lowered due to low redundancy of the system, caused by volume constraints. As the main function of the system is to measure gravitational waves, the availability is a measure of the ability to detect these waves. As two constellations are used, at least one dataset will always be available. Constellations are available for taking measurements while uplinking, but not while downlinking. The system will operate in space, and can thus not be maintained physically. Software updates can be uplinked and processed by the CDH. The safety of the system depends on the subsystem. Safety features and mechanisms are introduced to mitigate safety risks. Component failure does not cause safety issues to people nor environment, as guaranteed by sustainability measures.

Sensitivity Analysis

A system-wide sensitivity analysis was performed to determine the maximum impact of the introduced margins on the system characteristic budgets. The total variation of the system characteristic budgets is given in table 11.

Table 11: The total variation in the system characteristic budgets of the spacecraft

Mass range [kg]	Volume range [U]	Power consumption range [W]
19.6 - 26.8	10.5 - 11.6	27.4 - 46.6

Verification & Validation Procedures

All developed tools were verified using unit tests and system tests, and validated using other validated tools, or tested with similar calculations from literature. For verification of the product, verification guidelines were set up per requirement. The accurate testing environments were determined per requirement that should be verified with tests. Environments include the CubeSat Support Facility and the Maxwell Test Chamber from ESA, the Cyclotron Resource Centre from UCL, and Environmental Test Facilities from ISIS.

For the validation of the product, four tests are proposed: end-to-end information system tests, mission scenario tests, operations readiness tests, and stress tests.

List of Abbreviations

For the purpose of this document, the following abbreviations apply:

Abbreviation	Meaning	Abbreviation	Meaning
ADCS	Attitude Determination & Control System	FRAM	Ferroelectric Random Access Memory
ASAP-5	Ariane 5 Structure for Auxiliary Payloads	GEO	Geosynchronous Equatorial Orbit
ASAP-S	Arianespace Structure for Auxiliary Payloads for Soyuz	GMAT	General Mission Analysis Tool
BCR	Battery Charge Regulators	GMSK	Gaussian Minimum Shift Keying
BER	Bit Error Rate	GNSS	Global Navigation Satellite System
BoL	Begin-of-Life	GPIO	General Purpose Input/Output
CBS	Cost Breakdown Structure	GS	Ground Station
CDH	Command & Data Handling	GTO	Geostationary Transfer Orbit
CG	Centre of Gravity	HRM	Hold and Release Mechanism
CMOS	Complementary Metal–Oxide–Semiconductor	HTP	Hydroxytryptophan
COTS	Commercial Off-The-Shelf	HWBD	HardWare Block Diagram
CPU	Central Processing Unit	ID	Identification
DBMS	DataBase Management Software	I/O	Input/Output
DOD	Depth of Discharge	IMU	Inertial Measurement Unit
DORIS	Doppler Orbitography and Radiopositioning Integrated by Satellite	ISIS	Innovative Solutions In Space
DOT	Design Option Tree	ISO	International Organisation for Standardisation
DSE	Design Synthesis Exersice	ITU	International Telecommunication Union
EDAC	Error Detection And Correction	LCA	Life Cycle Assessment
EEMCS	Electrical Engineering, Mathematics and Computer Science	LEO	Low Earth Orbit
EIRP	Effective Isotropic Radiator Power	LET	Linear Energy Transfer
EoL	End-of-Life	LICCA	Laser Interferometer CubeSat Constellation Antenna
EPS	Electrical Power System	LIGO	Laser Interferometer Gravitational wave Observation
ESA	European Space Agency	LISA	Laser Interferometer Space Antenna
ESTRACK	European Space Tracking	MBU	Multiple Bit Upset
EUR	Euro	MEO	Medium Earth Orbit
FBS	Functional Breakdown Structure	MPPT	Maximum Power Point Tracking
FEEP	Field Emission Electric Propulsion	NASA	National Aeronautics and Space Administration
FET	Field-Effect Transistor	NIU	Neutron Induced Upset
FFD	Functional Flow Diagram	OBC	On-Board Computer
FFM	Free Falling test Mass	PCDU	Power Conditioning and Distribution Unit
FM	Flight Model	PCU	Power Conditioning Unit
FoV	Field of View	PDU	Power Distribution Unit

PSU	Power Storage Unit	SEL	Single Event Latch-up
QM	Qualification Model	SEU	Single Event Upset
RAMS	Reliability, Availability, Maintainability and Safety	SET	Single Event Transient
R&D	Research and Development	SNR	Signal-to-Noise Ratio
RAM	Random Access Memory	SWBD	SoftWare Block Diagrams
RTD	Resistance Temperature Detector	TID	Total Ionising Dose
RTG	Radioisotope Thermometric Generator	TRL	Technology Readiness Level
RTOS	Real-Time Operating System	TSO	Air force CubeSat mission
RW	Reaction Wheels	TT&C	Telemetry, Tracking and Command
SAGE	SagnAc interferometer for Gravitational	USA	United States of America
SEB	Single Event Burnout	VHF/UHF	Very/Ultra High Frequency
SEFI	Single Event Functional Interrupt	WBS	Work Breakdown Structure
SEGR	Single Event Gate Rupture	WFD	Work Flow Diagram

List of Symbols

For the purpose of this document, the following symbols apply:

Symbol	Meaning	Symbol	Meaning
A	Area	F_{tank}	Force on the tank
A_{cs}	Cross-sectional area	g	Gravitational acceleration constant
A_{enc}	Enclosed area	G_r	Receiver antenna gain
A_i	Projected area	G_t	Transmitting antenna gain
A_{is}	Isotropic antenna area	h	Height
A_r	Effective receiver antenna area	I_{xx}	Moment of inertia about the x-axis
A_s	Illuminated Area	i	Inclination
$A_{solar-cell}$	Area of the solar cell	J	Heat
$A_{surface}$	Surface area	J_a	Albedo irradiance
a	Albedo factor	J_{ir}	Infrared flux
a	Semi-major axis	J_s	Solar irradiance
$a_{l,max}$	Maximum launch acceleration	k	Heat flow constant , spring constant, Stefan-Boltzmann constant
a_T	Semi major axis transfer orbit	l	Length
B	Channel bandwidth	L_a	atmosphere loss factor
c	Speed of light	L_l	Feed line loss (transmitter)
C	Received power	L_r	Reception feeder loss
c_m	Center of mass	L_{pr}	Antenna pointing loss
c_{p_s}	Center of solar pressure	L_s	Space loss
D_r	Receiver antenna diameter	LAT_{GS}	Ground station latitude
e	Eccentricity	LAT_{SAT}	Satellite latitude
E	Youngs elasticity modulus	M_d	Mass density
E_a	Eccentric anomaly	m_{sp}	Mass of solar panel
E_b	Received energy per bit	m_{tank}	Mass of the tank
e_t	Pointing offset angle	N	Total received noise power
f	Signal frequency	N_0	White noise spectral density
F	Visibilty factor	P	Power of the signal generated by transmitter
$F_{n,max}$	Maximum normal force	P_d	Power needed during daytime

P_e	Power needed during eclipse		$V_{solar-panels}$	Volume of the solar panels
P_{req}	Power required		V_{tank}	Volume of the tank
p	Pressure		V_{th}	Threshold voltage
$\dot{Q}_{absorbed}$	Absorbed heat flow		w	Width
$\dot{Q}_{sc,sp}$	Heat flow from spacecraft to solar panel		W_f	Power flux density
q	Reflective Index		$\alpha_{1/2}$	Antenna half-power beamwidth
$q_{emitted}$	Emitted heat		α_s	Absorptivity of spacecraft
R_e	Earth radius		γ	Central angle
R_{orbit}	Radius of orbit		δ	Difference between the longitudinal coordinates of the satellite and ground station
R_{planet}	Radius of planet		δV	Change in velocity
R_s	Distance between satellite and ground station		ϵ	Emissivity
r	Distance between satellite and Earth centre		ϵ_{IR}	infrared emissivity
r_a	Radius in apocentre		η	Solar cell efficiency, Receiver antenna efficiency
r_{dep}	Radius of the departure orbit		η_{bat}	Battery efficiency
$r_{E,S}$	Distance from the Earth to the Sun		$\eta_{charge-bat}$	Charge efficiency of the battery
r_p	Radius in pericentre		η_{cond}	Conditioning efficiency
$r_{S,E}$	Distance from the Sun to the Earth		η_d	Efficiency during daytime
r_{tar}	Radius of the target orbit		$\eta_{discharge-bat}$	Discharge efficiency of the battery
S	distance between transmitting and receiving antennae		η_{dist}	Distribution efficiency
T_e	Effective temperature		η_e	Efficiency during eclipse
T_{ir}	Infrared temperature		θ	Incidence angle
T_s	System noise temperature		θ_a	True anomaly
T_{sc}	Spacecraft temperature		λ	Degradation factor of the solar cells, Signal wavelength
T_{sp}	Solar panel temperature		μ	Gravitational parameter
t	Lifetime, thickness		ρ	Density
t_d	Day time		σ	Stress
t_e	Eclipse time		Φ	Solar flux
$t_{solar-cell}$	Thickness of the solar cell		ϕ	Angle of Incidence
t_{tank}	Thickness of the tank		Ω	Angular velocity
V_{apo}	Velocity in apocentre		ω_n	Natural frequency
V_c	Circular velocity		$\#_{cells}$	Amount of solar cells
V_{per}	Velocity in pericentre			

Contents

Introduction

"Spanning from the composition of atoms to the structure of galaxies, the appeal of physics is its drastic scope in aiming to explain the universe mathematically and experimentally. However, gravity, the engine behind many events in the universe, operates most of the time in the dark. Investigating this phenomenon will broaden the knowledge boundaries further than anything else. The starting point for this are gravitational waves. The concept of gravitational waves was theorised by Albert Einstein in 1916. He predicted that huge accelerating objects, namely neutron stars and black holes, orbiting each other would ripple space-time, forming waves, propagating in every direction at the speed of light and carrying information about their origin. On the 14th of September 2015 when Laser Interferometer Gravitational wave Observation(LIGO) for the first time in history sensed the gravitational waves generated by two colliding black holes 1.3 billion light-years away, Einstein's theory of general relativity was proven [21].

This discovery opened a new era for research in physics and astronomy. LIGO, along with other ground based interferometers, have a sensitivity centred at 10^3 Hz allowing it to detect the shorter waves, caused by binary neutron stars and supernovae. The proposed Laser Interferometer Space Antenna(LISA) mission is centred at around 10^{-2} Hz, measuring waves from super-massive black holes, allowing for a map of the structure of the space-time around these black holes. The missing frequencies, from $1 - 10$ Hz, measure gravitational waves produced by compact binary systems in the Milky Way, allowing for tracking and eventually studying of these complex gravitational phenomena. To obtain this intermediate frequency range, satellites orbiting Earth can be used. This will be done in the LICCA mission. The goal for this mission is to increase the knowledge about the exotic topic that is gravitational waves, of which so little is known. Every little piece of scientific information will help develop a better understanding." [4]

To measure gravitational waves, the principle of interferometry is utilised. An interferometer contains two laser beams which travel the same paths but in different directions and are then superimposed to measure their difference in phase. If a phase difference occurs, then one of the two laser beams must have travelled a diverging path length, meaning a gravitational wave may have passed. Because of the short wavelength of visible light, and the high velocity at which light propagates, this principle can measure tiny fluctuations in the space-time continuum over very large distances in a small amount of time.

"The primary objective for this project has been identified in the project plan. The Project Objective Statement is: "To design a cost-effective mission based on a constellation of CubeSats to detect gravitational waves in a group of 11 students during 10 weeks." [4] "Also secondary objectives can be identified for this project. These secondary objectives go hand in hand with the primary objective. They are to be accomplished next to it during the project. Achieving these objectives indicates the success of the project.

- Demonstrate the technology of CubeSats in high altitude orbits.
- Demonstrate that 11 students can set up and complete a design project with limited resources and time.
- Demonstrate the compatibility of highly accurate scientific instruments that fit in CubeSats, using readily available technology.
- Accomplish accurate gravitational wave measurements within a cost effective mission.
- Synthesise the knowledge gathered in the Aerospace Engineering bachelor into a design project." [3]

$ $

Mission & Design Overview

In this chapter, the design methodology followed in this detailed design phase is going to be structured and described. Section 2.2 gives a brief overview of the trade-off that was performed to select the design concept that would be further developed. Section 2.3 gives the market analysis performed on the chosen concept. The sustainability of the project is described in section 2.4. Section 2.5 explains how the iterations for the detailed design were performed with the aid of a design N2 chart. In section 2.6 the procedure followed by each subsystem is explained along with an outline of the rest of this report.

2.1. Mission description

The Mission Need Statement of LICCA is: *"To gain a more comprehensive view of the gravitational wave frequency spectrum, the mission will provide complementary measurements to the frequencies of current and planned gravitational wave measurements by detecting in the range of 1-10 Hz."* LICCA is a constellation of CubeSats in geostationary orbit that will measure these gravitational waves using laser interferometry. The mission will consist of six 12U CubeSats, which form two independent constellations of three satellites. Each satellite in the constellation will send and reflect lasers to the other satellites. When a wave passes the measurement point, there is a tiny fluctuation in the space-time continuum. Therefore, the relative distance between the satellites fluctuates, which can be detected with the interference of two separate laser paths. As mentioned, the mission will use CubeSats. These are small, lightweight and cheap, since most technology for the subsystems of the spacecraft can use COTS components which are readily available. The user requirements for which this mission has been designed for can be seen in table 2.1. These have been agreed upon with the client and it should be noted that deleted requirements have been omitted from this list.

Table 2.1: User requirements for the LICCA mission

ID	User Requirements
LICCA-SYS-Perf-01	The system shall be able to detect gravitational waves in the 1-10 Hz band.
LICCA-SYS-Perf-05	The system shall provide command uplink.
LICCA-SYS-Perf-06	The system shall provide a telemetry downlink to the ground station.
LICCA-SYS-Perf-07	The system shall provide scientific data download to the ground station.
LICCA-SYS-Perf-08	The mission shall be composed of at least 3 small satellites in formation.
LICCA-SYS-Perf-09	The constellation of satellites shall be flying with a distance of 72 000 km from each other.
LICCA-ST-Perf-01	The spacecraft shall carry a low power laser payload for interferometry.
LICCA-SYS-SR-01	The mission shall withstand a TID of at least 10^6 rad during the entire lifetime.
LICCA-ST-SR-02	The overall mission's reliability shall be estimated.
LICCA-ST-SR-03	The overall mission's availability shall be estimated.
LICCA-ST-Sus-01	An End-of-Life (EoL) strategy shall be identified.
LICCA-ST-Sus-02	Use of radioactive materials shall be avoided.
LICCA-ST-Sus-03	The propulsion system shall use sustainable propellant.
LICCA-ST-Sus-04	A strategy for sustainable manufacturing and integration of the satellite shall be identified.
LICCA-SYS-Bud-01	The spacecraft shall be compliant with the CubeSat form factor i.e. it should be made up of multiple cubic units each of 10 cm x 10 cm x 10 cm.
LICCA-SYS-Bud-02	The spacecraft shall have a size of ≤ 12 U.
LICCA-SYS-Bud-03	The total required electrical power shall not exceed 40 W.
LICCA-SYS-Bud-05	The required data rate shall not exceed 1 Mbps.
LICCA-SYS-Bud-06	A Commercial Off-The-Shelf (COTS) option shall be identified during the design of each subsystem, and included in the trade-off.
LICCA-SYS-Bud-07	The spacecraft design shall be compatible with existing launchers and CubeSat deployers.

LICCA-ST-Bud-01	The launch date shall be 2030.
LICCA-ST-Cost-01	The cost of the mission shall not exceed 20 million euro, excluding the launch cost and operation.
LICCA-ST-Cost-03	An estimation of the costs for launch shall be provided.
LICCA-ST-Cost-04	An estimation of the costs for operation shall be provided.

It is chosen to adjust one of the requirements. The rationale and the identifier for this requirement are shown in the changelog in table 2.2

Table 2.2: User Requirements changelog

ID	*Change*	*Rationale*
LICCA-SYS-SR-01	TID limit added.	Instead of the abstract 'withstand radiation environment', a total ionising dose value was added as a threshold.

2.2. Summary of previous design activities

The LICCA project started with a planning and organisational phase, resulting in the project plan [4]. Then the exploratory and creative phase was entered, represented by the baseline report [3]. The functions and requirements of the spacecraft were generated, based on a literature review of similar missions and the desires of the client and other stakeholders. Various design options were identified and some concepts were devised. These concepts were traded off during the preliminary design phase, represented by the midterm report [5]. In this report, the final report, the detailed design of the spacecraft is presented. This is the final phase of this project. Throughout the whole project multiple analyses are done during every phase, which include sustainability, risk and budgets. A more detailed explanation of the trade-off process is now given to understand the starting point of the detailed design.

In the mission and design exploration phase of this project, a study into the possibilities for the design concepts was performed. First, the structure of the constellation of the satellites had to be chosen. This includes the number of satellites that would be present in the constellation, along with which satellites are considered to be "passive" and "active". An active satellite initiates, can reflect the laser beam and performs the interferometry measurements, whereas a passive satellite simply reflects the beam. These different satellite types would drive the difference in components needed on board. Next, the type of scientific payload that would be used for the measurements also provided distinct concepts. Since any payload type could be used in any constellation, it was chosen to trade these off separately, namely in a constellation trade-off and a scientific payload trade-off. The constellation trade-off was also split into a high level and a detailed trade-off.
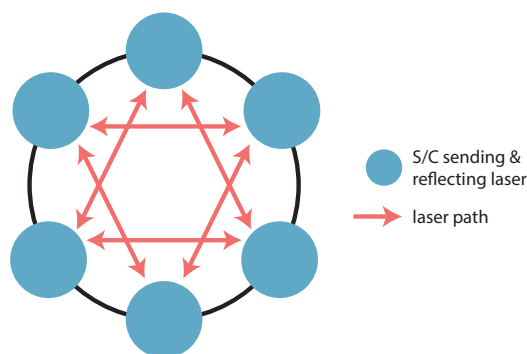
Figure 2.1: Winning constellation concept from trade-off

The high level constellation trade-off was first performed between six concepts. These concepts had differences in number of satellites, combinations of active and passive satellites, and orbital altitudes. The criteria that were used to evaluate the concepts were reliability, cost, sustainability, ΔV and quality of measurements. Three concepts remained after this trade-off. Then, the payload trade-off was performed. Three main aspects were considered. The first was the interferometry principle, meaning the setup of the laser paths that would interfere such that measurements can be taken. Then, the type of test mass that would experience the gravitational fluctuations and thus be used for the measurements was traded-off. And last, the method of reflection of the laser beams was also evaluated and selected. From these, the result was to use a Sagnac interferometer while using the CubeSat bodies themselves as the test masses, along with transponders to reflect the laser

signals between the satellites. The last step in the trade-off process was to repeat the constellation trade-off in more detail. The same criteria were considered to trade the last three concepts off, though this time they were quantified in more detail to further highlight the differences in the concepts. The best performing result uses six satellites that form two independent constellations of three active satellites. A visualisation of this concept is shown in figure 2.1. Sensitivity analyses were performed for all the trade-off and the results were deemed viable.

2.3. Market analysis

In the market analysis, the market in which this project is participating will be defined and the market trends will be addressed. Finally, a predicted share will be calculated and a SWOT analysis will be made.

2.3.1. Market definition, future prediction and share

In this section, the market in which the LICCA mission is will be defined, its trend specified and the share will be stated.

Market definition

Due to the fact that currently there are no CubeSat constellations measuring gravitational waves, this product can be considered as a new development in which no direct competitors exist. Nevertheless, it can be considered that this CubeSat constellation participates in two well-defined markets:

- Market 1: Measurement of gravitational waves
- Market 2: Cubesat design and manufacture

These two markets are chosen because the companies or organisations that participate have sufficient expertise to satisfy the same customer needs as this project. Therefore, these companies or organisations are considered direct competitors. There are also a few markets that can use the LICCA project as a spin-off to other applications, for example a laser market, or an earth gravity field measurement market. However, since the companies in these markets are no direct competitors, they will not be evaluated in much detail for now.

The client of the LICCA project is considered to be the TU Delft. Nevertheless, the function that the TU Delft has in this project can be replaced by another university or research centre as well. Therefore, to perform the market analysis in a broader manner, the clients will be universities or research centres. This way the focus can be centred in a bigger market instead of only a single client.

Future market prediction

The LICCA mission is planned for 2030. To estimate the predicted share, it is important to predict the markets at this point. Furthermore, it is important to address the two aforementioned markets in which this project will participate.

Gravitational wave measurement market
Current gravitational wave measurements are done in the 30-7000 Hz range by the LIGO project [13], based in the US. However, with the LIGO Voyager upgrade predicted to be operational near 2027-2028, it is estimated that the low-frequency cutoff will have been reduced to 10Hz [17]. The total cost up to now for the LIGO project has been estimated around 620 million USD in 2015. Using Consumer Price Index (CPI-U) data provided by the US bureau of labour statistics, the inflation from 2015 to 2020 is 8.9%. This brings the cost of LIGO in 2020 to 675 million USD. Converted to EUR at the average exchange rate in 2020, this would be equivalent to 615 million EUR.
Two similar projects to the LIGO project exist: the KAGRA project and the VIRGO project, based in Japan and Italy respectively. The KAGRA project is estimated to cost around 200 million USD, or equivalently 180 million EUR. The VIRGO project cost is not disclosed; however, the allocated budget is 10 million EUR per year. Since the project has spanned 27 years since its formation, its total cost will be estimated at around 270 million EUR. This means the current total market value of gravitational wave detection is around 1 065 million EUR.

In the 2030s, two more large-scale gravitational wave observation projects will likely enter the market:

- LISA, estimated to cost around 1 050 million EUR [21].
- TianQin, estimated to cost around 700 million EUR [41].

Both of these projects will observe gravitational waves in the range of 10^{-5}-10^{-1}Hz, meaning that although the projects have similar objectives, they do not form direct competition to the LICCA project.

Adding these space-based gravitational wave measurement projects costs to the current ground-based costs, the market of gravitational wave observation will have a value of around 2 815 million EUR.

Cubesat market
The CubeSat market size has been estimated based on the data available in Nanosats Database[1]. First, the data of the launched CubeSats was analysed year by year in order to estimate the market growth rate in

---

[1]https://www.nanosats.eu/database, accessed 22/06/2020

figure 2.2. The first problem encountered was that there are significant variations in the amount of CubeSats launched per year. This makes sense as the market is emerging. Therefore, a moving average of the amount of CubeSats launched per year was applied in order to give a better overview of the market. An initial number and a growth rate can be obtained in order to calculate the market size for the year 2030. Nevertheless, the growth rate changes considerably depending on the amount of years in which the moving average is applied. Therefore, it was decided to use 3 and 4 years moving average in order to get a positive growth and to consider these two results as lower and upper limits. The final results are 243 and 204 adjusted units launched in 2019 (U_{2019}) and 15.89% and 7.78% growth rate (r) as upper and lower limit respectively.
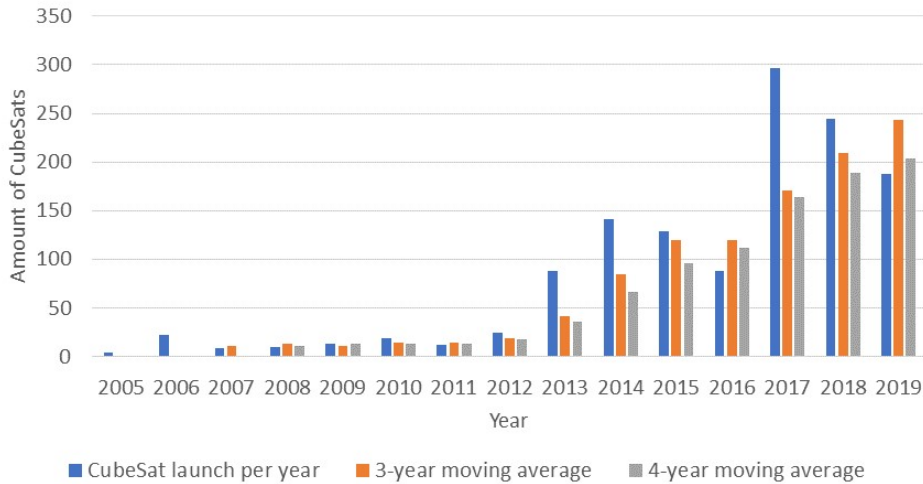
Figure 2.2: Amount of CubeSats launched per year and a 3-year and 4-year moving average

The next step is to calculate the average cost of a CubeSat. According to the same source, the market share of every type of CubeSat can be represented as it is in the nanosat database [1]. It should be considered that, as this is an emerging and technology intensive sector, the costs of manufacturing CubeSats have been decreasing year after year and the market size can still be considered small. This could explain why a bigger CubeSat is presented in the analysed data as cheaper than a smaller one.

Table 2.3: Market share and average price by CubeSat size

Size	Average bus cost (USD currency) $\bar{c}$	Market share x
1U	343 000	21%
2U	257 143	9%
3U	1 058 000	44%
6U	1 926 429	14%
8U	743 750	8%
12U	9 183 333	4%

Finally, the market size in the year 2030 (S_{2030}) can be estimated as it is stated in equation (2.1), in which S_{2030} is the size of the CubeSat market in 2030.

$$S_{2030} = \left(\sum_{i=1}^{6} \bar{c}_i \cdot x_i \right) \cdot U_{2019} \cdot (1+r)^{11} \tag{2.1}$$

The upper and lower limit yields 1 232 and 466 units launched respectively, which results in a market size of 1.524 and 0.577 billion USD. As this is a prediction of an emerging market which had a significant variation in the past few years, it makes sense that there is this difference in the upper and lower limit for a 11 year forecast. Therefore, the average value will be used, which is a market size of 1.05 billion USD, which represents 0.956 billion EUR.

2.3.2. Market share

Based on the results found in the previous section, the market shares of the project can be calculated. The total cost of the project is around 12.67 million EUR, as calculated in section 12.7. Since this project will participate in both the gravitational wave measurement market and the CubeSat market, it is assumed it will have value in both markets of 20 million EUR. The market share calculation can be seen in table 2.4

Table 2.4: The market share of project LICCA

Market	Total value	LICCA share
Gravitational wave measurement	2 815 million EUR	0.45%
Cubesat	956 million EUR	1.33%

It is also important to mention that, if the volume required is met and the possibility is given, the satellite could be used as a platform by another organization that wants to put in LICCA's orbit a specific payload. In this way, the budget of the project can increase, which would also increase the market participation while exceeding the sustainability objectives

2.3.3. SWOT Analysis

To perform a proper market analysis, a SWOT analysis has to be done. In this SWOT analysis, the strengths, weaknesses, opportunities and threats are described with relation to the product-market combination. This means that the strengths and weaknesses are described with relation to the product, whereas the opportunities and threats mostly come from the products relation to the market and competitors. In table 2.5, the SWOT analysis is given, followed by detailed descriptions of each SWOT entry.

Table 2.5: SWOT Analysis

Strengths	Weaknesses
1. The cubesat constellation can be launched with other cubesats 2. Many cubesat components are off-the-shelf 3. There are many reliable customers	1. The product has highly experimental technology 2. The Satellites need their own propellant to go from GTO to their destination orbit
Opportunities	**Threats**
1. The gravitational wave measurement market is in its launch phase 2. The knowledge areas are highly specialised 3. The cubesat constellation may be able to perform missions from third parties	1. A significant amount of cubesat businesses are established 2. New technologies for cheaper measurement of gravitational waves could be introduced

A more detailed analysis of all the strengths, weaknesses, opportunities and threats can be found in the baseline report [3]. As risks usually flow from threats described in the SWOT analysis, it is used in the risk management, as described in chapter 13.

2.4. Sustainable Development Strategy

At an early stage of the design process it was determined that the Life Cycle Assessment (LCA) is most suitable tool to determine the sustainability of the LICCA mission [3, 5]. The LCA method is a standardised method that assesses the environmental impact of each phase throughout the entire life cycle of a product and its parts [2]. ESA's Space system Life Cycle Assessment (LCA) handbook is used as a guideline [28] for this mission. This handbook is the ISO 14044 LCA standard method expanded and projected on space systems, as these systems have a unique low production rate, long development cycles and need for special materials and processes [1]. The LCA method is used as a guide to perform an extensive life cycle assessment of the system in this report. In this current section, the general philosophy of sustainable design and how it is applied to the space system and its phases is discussed. Next to that, each subsystem extensively discusses the sustainability of its own parts via the LCA method. As a result, the design of the complete space system is assessed in detail. In this section, first the definition of sustainability is explained, secondly the complete design process of the LICCA mission is discussed and its sustainability aspects explored and assessed regarding all three pillars of sustainability.

2.4.1. Definition of sustainability

The definition of sustainable development, as given in the Brundtland Report, is: "Development that meets the needs of the present without compromising the ability of future generations to meet their own needs" [11]. The concept 'sustainability' concerns three pillars, namely environmental, social and economic. To maximise the sustainability of a process or a product, the negative impact of the three aforementioned pillars must be minimised over the entire life cycle of the process and product. The environmental pillar mainly concerns emissions during manufacturing and transport or emissions directly in the high atmosphere, resource consumption, wildlife displacement and process hazard analysis, potential impacts of unintentional hazardous materials. The social and economic pillars mainly concern the creation of jobs, its effect on the local employment statistics and general public, and hazards during production [27]. It is chosen to combine these last two pillars into a 'socioeconomic' category, as both pillars are closely related.

2.4.2. Phased Life Cycle Assessment

ESA's Space system Life Cycle Assessment (LCA) guidelines define several distinct phases of space system development and utilisation. It is chosen to assess all three pillars per phase, such that the complete process is assessed. Each phase is described and assessed in the following subsections.

Feasibility and Preliminary definition

This phase mainly concerns office work and design facilities.

- **Environmental impact:** For this project, the design activities are performed by eleven students from their home. The environmental impact is the used electricity and gas of their respective homes and diets.
- **Socioeconomic impact:** No jobs are created for this project, this project is an introduction to space system engineering and introduces the student to the related work forces. This project is set up for educational purposes to the group of students. Guided by mentors, the students will gain insight in space system design and will get in contact with experts.

Detailed definition and Qualification and production

This phase mainly concerns the manufacturing, assembly, integration and testing phase.

- **Environmental impact:** As almost all of the used components in the design are COTS components, distinct drawbacks and advantages are identified. A drawback to COTS components is that it is very hard to trace the resource materials and their transportation, the exact production process is often also unknown. No process hazard analysis can be made. The only aspect that can be assessed in detail is the transportation of the component to the required location. A big advantage to COTS components is that all components have been certified and tested, vastly decreasing the resources required for R&D and the development of engineering models. The few components that are non-COTS, and thus will need to be developed, are required to minimise the environmental impact by avoiding the use of hazardous materials and production at local facilities is preferred. For the testing of the newly developed components, it is decided to only use already existing testing facilities to minimise the environmental impact.
- **Socioeconomic impact:** The manufacturing, assembly, integration and testing phase produce a large amount of jobs. The manufacturing jobs are widely spread across the globe, each country has a different attitude towards workforce welfare, concerning health, salary and longevity. This attitude is greatly affected by political stability and the different regulations maintained by the countries.

Launch and commissioning

This phase mainly concerns the transport to the launch site, the spacecraft and launcher preparation, mission control and ground control centres.

- **Environmental impact:** The environmental impact is vastly decreased as it is chosen for the mission to piggy back in an existing launcher and planned launch. This means that no launcher or special fairing needs to be developed for this mission and that a launch specifically for this mission is not required to be planned. The transport to the launch site will, however, require resources for protection of the CubeSats and provide emissions due to the transportation. The launcher will already be prepared for the main payload, so the required additional resource consumption for the preparation and the launch of the LICCA mission is minimal. However, it can not be neglected that a rocket launch expels a large amount of emissions into the lower and upper atmosphere. The transfer vehicle, used for the GEO transfer, is powered by (flight tested) water plasma engines. The water is stored in low pressure tanks, with no risk of combustion. The emissions of the water propellant are considered to be harmless to the space environment. At the time of writing, the transfer vehicle is expendable. Future versions are planned to be reusable, it is acknowledged that this might be the case at LICCA's launch date [2]. The mission control and ground control centres require electricity and gas, this will not be significantly increased by the LICCA mission.
- **Socioeconomic impact:** The propellant for the transfer vehicle is water, this is non-toxic to humans. The mission control will generate new jobs, mostly in research and in mission maintenance and control. Again,

[2]https://momentus.space/rides/, accessed 29/06/2020

the importance of the welfare of the workforce on ground and for what goal the new research information will be used is different for every country and thus can only be assessed when it is known where and how the research is conducted.

Utilisation
This phase mainly concerns the usage of sustainable propellant, radioactive materials and other hazardous materials in the spacecraft design. It also focuses on space debris collision mitigation and general data handling of the mission.

- **Environmental impact:** Propellant is considered clean if no green house gasses are expelled. Measures have to be taken to minimise the possible leakage of the propellant tank and the outgassing of other structural materials [36]. A debris mitigation strategy is set up: the ΔV required for this is taken into account in the orbit maintenance budget of the propulsion system and the ADCS is able to perform required manoeuvres without early saturation of the components. The CubeSat also utilises shielding for debris. No parts of the spacecraft are released during nominal operation, in addition no explosive or radio-active materials are used. The risk of explosion of components is mitigated per subsystem (depletion of tanks and battery before end-of-life) and the the status data is periodically monitored to prevent unexpected break-up, and for deployment a combination of springs and nylon string is used [36]. The radio frequency band is a limited resource that LICCA utilises. This source is increasingly congested with communication frequencies of the increasing amount of space missions, and LICCA is one of its contributors. In the TT&C subsystem design, the possible interference with the communications of other missions is taken into account. The design lifetime of the LICCA mission is two years, as a result the radio frequency will only be in use for that amount of time. This limited time, however, already has a sustainability impact.
- **Socioeconomic impact:** The general public is increasingly concerned with the negative impact of propulsion expellants in the lower and upper atmosphere. To put the public at ease, the LICCA mission should maintain an open and transparent emission profile policy. The health and well-being of the workforce is indirectly positively affected as it is chosen to not use any radio-active materials, and minimise the use of hazardous materials in the final design and during production. The space debris mitigation strategy allows for the sustainable use of space and the continuation and development of new space missions. As a result, this can generate jobs in the future and maintain the current ones. The scientific nature of this mission may spark interest in space missions and increase the amount of people interested in engineering.

Disposal
This phase mainly concerns the de-orbiting of the CubeSat system after use, the reuse possibilities and a possible second mission and the payload data processing centre.

- **Environmental impact:** A de-orbiting strategy is developed to enter the Cubesat into a graveyard orbit at its end-of-life, this manoeuvre is accounted for via the propulsion system and the ADCS. This manoeuvre is discussed in more detail in section 12.4.3. All propellant tanks must be completely emptied to minimise break-up by explosions due to chemical reactions and other hazards during the off-line time of the CubeSats after de-orbiting. The CubeSat systems lifetime will be extended as much as possible by taking scientific measurements in the graveyard orbit. The constellation of the LICCA mission allows for a secondary mission: The gravitational waves will not only be detected, but the source of the gravitational waves can be localised via trilateration. The payload data processing will be done at research centres on Earth, this will utilise resources.
- **Socioeconomic impact:** This mission broadcasts a sustainable approach for space systems engineering, and the use of CubeSats for complex science-centered space missions to the public. The payload data processing will mainly be done at research centres, this will generate new jobs. Any new media coverage of the scientific results may spark interest in science or space missions and increase the amount of future engineers and scientists.

2.5. Detailed design methodology

With the constellation and payload type known, some preliminary design was performed at the end of the previous design phase. This is the starting point of the detailed design phase. Before initiating this phase, a design N2 chart was constructed to identify the relationship between the various subsystems and to aid in structuring the design iterations. The full design N2 chart is presented in figure A.5. On the diagonal it shows the elements of the mission that are to be designed. These elements consist of the different subsystems of the satellites, together with the third parties directly involved in the mission, namely the ground segment and the launcher.

As mentioned, the starting point for the detailed design was the preliminary sizing performed during the midterm phase. A first estimation of some of the inputs were already found in that phase, which is referred to as iteration zero. The design N2 chart was used during the design iterations of the different subsystems. As the design advanced, the completed parameters were highlighted in green. This way it was also possible to check which subsystems needed more resources allocated to it, to make sure the iterations would proceed efficiently. The

design for a subsystem cannot continue until it receives the inputs it needs from other subsystems. Based on this, resources from another subsystem that is already completed in an iteration can be moved such that the needed outputs can be determined sooner. Note that due to the interdependency between the various subsystems, it will be impossible to start designing a subsystem only once all the required inputs have been defined. For this reason, an iterative process is followed, in which the entire procedure is repeated several times. This way the design will converge after a number of iterations. For this mission, three iterations were performed.

2.6. Detailed design overview

As mentioned, the design iterations were executed according to the design N2 chart. The results of these iterations are documented in this report for each of the subsystems. The following aspects of each subsystem are presented in their corresponding chapters. First, a functional analysis and the requirements of the subsystem are presented. Then, the design methodology that was followed for the subsystem is discussed. After that, the risk, sustainability and RAMS considerations are given. Lastly, the final design aspects of the subsystem are summarised.

Besides the subsystem design, this report also delves into the details of the astrodynamic characteristics of the mission. This includes the lifetime of the mission, the radiation experienced throughout the mission, the ΔV needed for the manoeuvres and the periods of eclipse. Furthermore, general risk, sustainability, RAMS and financial aspects are considered on a mission level in this phase as well. Verification and validation have been performed for the tools that were used during the detailed design. A sensitivity analysis of the entire final design was performed, along with a compliance check on all requirements.

3

Payload

This chapter describes the payload subsystem. For the LICCA mission, the payload consists of the lasers that forms the interferometers that are used to detect the gravitational waves.

3.1. Functional analysis

It should be noted that it is not the objective of this project to design the entire payload, but rather the satellite and constellation that encompass it. However, to be able to design these properly, the functions of the payload should be well understood. In case of the LICCA mission, the payload will perform the measurements from which gravitational waves can be detected. Via laser interferometry, fluctuations in the space-time continuum can be measured, which is the aim of this mission. The functions of the payload are visualised in figure 3.1.
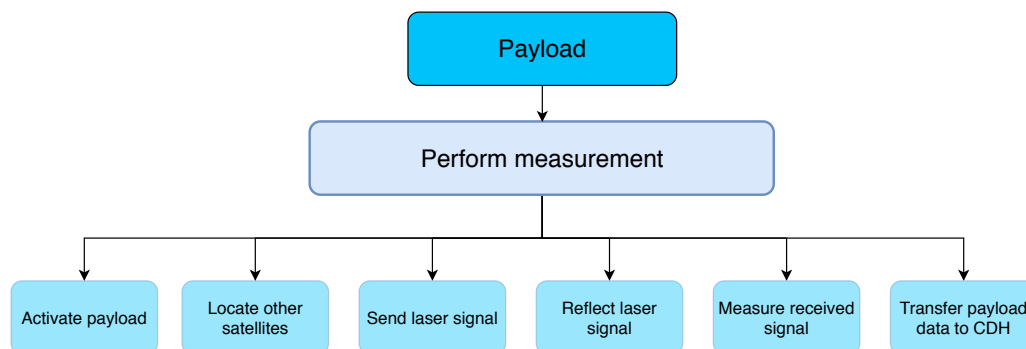
Figure 3.1: Functional breakdown structure of payload

3.2. Requirements

The requirements that the payload subsystem has to fulfill are presented in the table 3.1 below. These requirements have been identified as driving requirements for the design of the LICCA mission. The first three requirements were obtained from the SagnAc interferometer for Gravitational wavE (SAGE) project proposal [45], which operates in a similar manner as the LICCA mission so it was considered safe to use these same requirements. The last two requirements were considered to be adequate for a mission which will use a payload that still has not been developed.

Table 3.1: Payload requirements

ID	Payload
LICCA-SYS-Sub-PI-1	The interferometers shall operate with a maximum angle deviation of 5 arcmin.
LICCA-SYS-Sub-PI-2	The variation in power of the lasers that compose the interferometers shall not exceed 150 mW.
LICCA-SYS-Sub-PI-3	The variation in frequency of the lasers that are part of the interferometers shall not exceed 167 THz.
LICCA-SYS-Sub-PI-4	The distance from the interferometers to the centre of mass of the spacecraft shall not exceed 4 cm.
LICCA-SYS-Sub-PI-5	The components of the payload shall have a current TRL of 3 or higher.

3.3. Design methodology

In order to define the payload, first the interferometry principle, the type of test mass and the reflecting method were chosen in the midterm report [5]. This resulted in a Sagnac interferometer with the satellite body itself as a test mass and a transponder system to reflect the incoming signals. In this design stage, a further look will be taken into the measurement principle, followed by the component selection.

3.3.1. Measurement principle

To measure gravitational waves using a Sagnac interferometer, two laser beams are sent simultaneously in two different directions, after which they are reflected to follow the same path back to the source. Here the phase difference is measured, which might give a change in path length, potentially caused by a gravitational wave. The process of measuring the phase difference consists of five steps and is specified in figure 3.2. During the description of this process, only one laser beam is considered. First, the first satellite sends a laser beam towards a second satellite. Once the beam reaches this second satellite, it will be reflected back towards the first satellite. Then it will be reflected towards a third satellite, which reflects the beam back to the first satellite and it is compared to the laser beam that travelled the opposite path, and the phase difference between these two paths is measured.

By making the two paths equal and opposite, the measurements are not sensitive to the difference in distance between two individual satellites. With the measurement process determined, the required components can be selected.
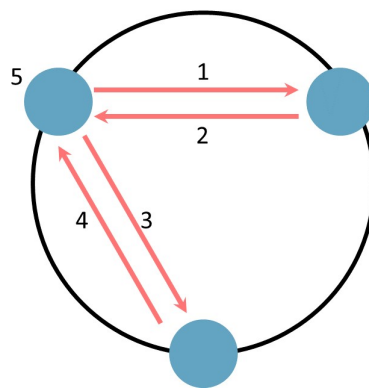
Figure 3.2: Phase difference measurement principle

3.3.2. Identification of required components

To select the required components, the steps in the measurement process from the previous section will be used. It should be noted that each of the satellites in the constellation will perform the above mentioned steps, meaning that each satellite will send outgoing laser beams as well as reflect incoming ones. Therefore, each satellite will be equipped with the same payload setup.

For step 1, a laser is required. As mentioned, two laser beams are sent out from each satellite towards the other two. To guarantee that both laser beams will have the same wavelength and intensity, only one laser will be used to send the initial laser beams. The laser will be guided inside the spacecraft using optic fibres. The emitted laser beams will be split equally using a fiber optic coupler. Then, their phases are regulated using two phase modulators. It is also important to note that the position of the satellites may drift over time. To accurately point the lasers in the correct directions, two piezo stages are needed.

For steps 2 and 4, two telescopes are required per satellite, since each satellite will receive beams from the other two. To detect the properties of the incoming laser beams, a pupil is required in each telescope. Further-more, two transponders are needed in each satellite to respond in both directions of the other satellites. Each transponder system will need a laser to provide the 'reflected' signal.

For step 3, each of the lasers in the transponder systems must be connected to the pupils in both telescopes. This way, both transponder lasers can act based on the incoming laser beams detected by either pupil, de-pending on the properties of the laser beams.

For step 5, to measure the phase difference between the incoming signals, three diodes will be used. One diode will compare the incoming laser beams, whereas the other two diodes will compare the phase differences between the two outgoing and incoming laser beams. To measure the outgoing signals, partially transparent mirrors are needed. To connect the three diodes, two more fibre optic couplers are required. For accurate measurements, an accurate clock is needed.

The full setup thus requires one laser, optical fibres, three fibre optic couplers, two phase modulators, three diodes, two transponder systems and two telescopes. Each transponder systems comprises of one laser. Each telescope comprises of two mirrors and a pupil. Now that all required components are determined, the selection procedure for each component will be described.

3.4. Risk

Now a technical risk assessment will be done for the payload. The payload is an important subsystem since it will actually perform the gravitational wave measurements and therefore it is crucial to identify all the risks that involve the payload. The payload consists of many components, all serving a specific purpose. There is, of course, the risk of the failure of one or more of these components. This could vary from a laser or transponder to a diode. In any case, it will have consequences for the measuring capabilities of the payload and therefore the entire mission.

Another risk has to do with the pointing of the lasers. The lasers have to point to the other satellites so that they can receive the signal. Therefore, a certain pointing accuracy is needed, such that the laser signal is successfully received by the other satellites. This pointing will be done by the piezo stages. If the accuracy degrades over time and the pointing becomes less accurate, then this will affect the mission. It may be needed to realign the satellites more often, therefore depleting the propellant sooner than expected and reducing the mission lifetime. Furthermore, if the piezo stage is jammed and it can not change its position anymore, accurate pointing of the laser will no longer be possible.

The third risk concerning the payload is the transponder system. Since it is not common to use such a system in a satellite, not much is as yet known about these systems and their reaction to the environment of space. This may lead to failures or malfunctioning earlier than expected.

The final risk that is identified in this analysis, is that the mirrors in the telescope are not oriented in the correct way. This risk seems unlikely to happen, though a similar problem occurred in the Hubble Space Telescope. However, a mission to repair this error is not likely for the LICCA CubeSats, meaning that the measurements would not be able to be performed correctly and the mission will not be able to continue with the constellation involving this satellite.

3.5. Sustainability

The following sustainability impacts can be highlighted for the payload subsystem. The mirrors will be made of Zerodur. The composition consists of silicon dioxide, aluminium oxide, phosphate rock and lithium carbonate. These are assumed to be obtained upstream of the production process, and will affect the environment during extraction and transport, namely contributing to emissions and the depletion of minerals. A controlled process is required to obtain the special properties that Zerodur provides. Factors that should be considered for the production of Zerodur itself are for example the energy consumption relating to all the necessary machines and the waste that will be produced by the process. The product may need to be polished and coated as well, which will increase the impacts on the environment. Also, safety hazards should be considered, for example fine glass shavings that occur during sanding.

The other optical elements of the payload have similar considerations to the Zerodur mirrors on a high level. Raw materials will be needed, thus harvested and transported. The processing will require energy and pro-duce waste. Also, polishing and coating will likely be needed, and hazardous production processes should be considered as well. The rest of the components will largely consist of electronic elements. Considerations for these include the raw materials needed, as well as the energy consumed during transport and fabrication. Chemical processes are also used during production of electronics, which can be hazardous to health and the environment.

Based on the above considerations, it is evident that the payload is not the most sustainable element of the LICCA mission. To limit this, the design of the payload should be well defined and thoroughly reviewed before

prototypes are constructed, and even the number of prototypes should be highly limited. The several different types of components will come from different providers. The integration of these components should be properly investigated beforehand, to avoid any mismatches. Lastly, high quality manufacturers should be chosen and clearly communicated with to reduce the chance of mistakes in the provided components.

3.6. RAMS

This section will discuss the reliability, availability, maintainability and the safety of the scientific.

3.6.1. Reliability

Several risks have been identified in the risk analysis of the payload. On a mission level, reliability is ensured by having two constellations that are independent of each other. If any malfunctions are present in one constellation, it will not affect the other. Within a given constellation each satellite serves as an interferometer, meaning that each constellation has three interferometers. The payload system should be designed in such a way that if the laser-sending capabilities of one satellite is compromised, it should still be able to reflect the signals of the other two. This can be done by making sure the transponder system can operate apart from the main laser system of the payload. Furthermore, if the transponders fail, there are still mirrors present in the system. Though the reflection of these will be much weaker, there is still a small chance of being able to use them for the measurements.

3.6.2. Availability

As described in the measurement procedure of the payload, one satellite will send laser beams toward both other satellites. This beams will be angled at 60°. Due to disturbances and drifting, the satellites may not be precisely aligned at this angle. Therefore, more precise pointing is achieved with the piezo stages, that can adjust the laser pointing by a displacing in 2 axes. As will be described in section 4.3, after 15 days the maximum drift will be beyond the reach of the piezo stages. Therefore, the satellites positions will need to be corrected for the drift that has occurred. Regarding the availability of the measurements, the payload will be able to measure continuously in those 15 days. Then, during realignment, measuring will not be possible.§ To still provide continuous measurements and not miss the chance of measuring a gravitational wave, two constellations are present. In this way, one constellation can still be measuring nominally while the other executes its realignment procedure.

3.6.3. Maintainability

Physical maintenance of the satellites during operations will likely not be possible, this also counts for the hardware of the payload. As previously stated, the payload will measure fluctuations in the distances between the satellites. Since the satellite body itself is used as the test mass, these fluctuations will also occur due to disturbances other than those caused by gravitational waves. These other disturbances, non-graviational accelerations, need to be modelled or measured and filtered from the measurements taken by the payload. This can be made maintainable by allowing for updates, for example in the event that a more accurate model is available for a certain type of disturbance.

3.6.4. Safety

As mentioned in the sustainability analysis of the payload, several procedures can be hazardous to those carrying out the production. This requires adequate precautionary measures to be taken. Furthermore, the payload is a system of lasers, most likely operating in the visible to near-infrared range of the spectrum. Lasers can be harmful to human eyes, and therefore safety precautions should be taken during the testing of the lasers. Lastly, safety mechanisms can be employed for the operation of the payload, by ensuring that it is only activated when needed. This can avoid unnecessarily sending stray laser beams into space, for example if the satellites are tumbling uncontrollably or after the mission has already concluded.

3.7. Final design

The selection of the components required has been done by contacting an expert in the field of gravitational wave detection using CubeSats, Dr. Sylvestre Lacour. Dr. Lacour has participated in the SAGE project, which has similar objectives as the LICCA project. Furthermore, for the selection of the transponder system and the pupil, an expert in the field of communication, Dr. Stefano Speretta, was contacted for recommendations of the required components. Based on the insights of these experts, a preliminary breakdown for the components of the payload has been defined and an estimate of the total mass, volume and power that will be required for this subsystem is calculated.

The chosen payload includes two piezo stages, one laser, three fibre optic couplers, three diodes, two phase modulators and one clock. As this payload is not in existence yet and will have to be specially constructed for this mission, several COTS options were considered to estimate the characteristics of the payload. These consist of both COTS options for Earth and space operations, since it is only meant to give a first estimate.

Thorlabs[1] was consulted for the lasers and fiber optics. The clock needed for the timing of the measurements was taken from Orolia[2]. The phase modulators were estimated from the ones of Jenoptik[3]. The diodes needed to measure the incoming light are from ID Quantique[4]. The characteristics of the piezo stages are estimated from a range of types and providers, such as Aerotech[5].

The transponder system must also be developed, as there is no existing component that meets the needs of the payload. For now, it is assumed that each transponder will be equipped with two of the same lasers as the main system. Furthermore, a large margin has been taken for electronics, to account for the rest of the elements that will be needed.

Lastly, the system will be enclosed by two telescopes that will be made out of invar, an alloy of iron and nickel. Invar is known for its low thermal expansion coefficient. This is beneficial for this project, as thermal expansion could influence the measurements. The two mirrors inside the telescope will be made out of Zerodur, a lithium-aluminosilicate glass-ceramic with a very low thermal expansion coefficient. A summary of all the mentioned payload characteristics per satellite can be found in table 3.2. It should be noted that a total volume of 4U has been assumed for the entire payload setup, as the exact configuration of the payload components is beyond the scope of this project.

Table 3.2: The characteristics of the payload

Components	Mass [kg]	Volume [U]	Power [W]
Main system			
Piezo stages	1.50		0.00
Laser	0.15		0.04
Fiber optic coupler 50:50	0.07		0.00
Diodes	0.06		1.80
Phase modulator	0.44		0.2
Fiber optic coupler 99:1	0.10		0.00
Clock	0.1		2.5
Electronics margin	0.48 (20%)		0.45 (10%)
Total main system	2.90		4.994
Transponders			
Laser	0.30		0.08
Electronics margin (50%)	0.15		0.04
Total transponders	0.45		0.12
Telescope			
Primary mirrors	1.52		0.00
Secondary mirrors	0.132		0.00
Margin for body (40%)	0.66		0.00
Margin for pupil (5%)	0.083		0.00
Total telescope	2.39		0
Total	**5.75**	**4**	**5.114**

[1]https://www.thorlabs.com/navigation.cfm, accessed 03/06/2020
[2]https://www.orolia.com/products/atomic-clocks-oscillators/lnmo, accessed 03/06/2020
[3]https://www.jenoptik.com/products/optoelectronic-systems/..., accessed 03/06/2020
[4]https://www.idquantique.com/quantum-sensing/products/..., accessed 03/06/2020
[5]https://www.aerotech.com/product-catalog/piezo-nanopositioners.aspx, accessed 03/06/2020

Astrodynamic Characteristics

This chapter discusses the astrodynamic characteristics of the LICCA mission. First, the choice of the lifetime is discussed in 4.1. Following that, the radiation to which the spacecraft is exposed is discussed in section 4.2. Furthermore, the ΔV budget, which is important to determine the amount of propellant that is needed for the mission, is discussed in section 4.3. Lastly, this chapter presents the eclipse considerations in section 4.4.

4.1. Lifetime

The frequency at which detectable gravitational waves occur is not yet known, specially at the frequency at which LICCA will operate. Therefore, in order to maximise the probability of detecting this phenomenon, the mission lifetime should be as long as possible. This is, however, limited by the use of CubeSats. The limiting factors of CubeSats are discussed later on in this section.

To determine a desired lifetime, an estimate on the frequency of gravitational waves needs to be computed. To do this, the phenomenon that causes these waves, in the LICCA mission frequency, was identified as compact binaries. Its occurrence was estimated using The Washington Double Star catalogue. This source presents a list of all the known double stars[1], but due to the difficulties with prospective it needs to be verified if these are indeed compact binaries. At this moment, the catalogue consists of up to 100 000 systems, from which 255 are identified to be compact binaries [64]. These span a frequency range of $10^{-4}\ Hz$ to $10^4\ Hz$ [62], from which less than 50 are in the frequency range measured by LICCA.

Current gravitational wave detecting technology is solely supported by ground-based detection systems, such as LIGO. This detector currently finds one gravitational wave approximately every two months. At full sensitivity it expects a weekly detection[2]. The LICCA mission is a pioneer in its field of CubeSats and it is not expected to detect at this optimal rate. The mission aims to discover new compact binary systems making it difficult to estimate how often a detection will take place. Therefore, the preliminary design is based on the measuring rate of LIGO, namely one wave every two months.

Returning to the issue of the CubeSats, the design is based on extensive use of COTS components. Most of these components are developed for missions in Low Earth Orbit (LEO), and will have a hard time withstanding the space environment in GEO. For example, an ADCS component is expected to degrade to non-functionality within six months[3] without protection. Shielding can be applied, but will not withstand all radiation. Another implication when extending the lifetime is the added volume. Volume is a tight constraint in CubeSat design, especially for this mission. Extending the lifetime stipulates extra propellant needed for orbit maintenance, of which only a limited amount can be taken on board due to the volume constraint.

A compromise must be made between these considerations. From a measurement perspective, a long lifetime would be preferred. However, this is not possible within the given constraints. Therefore, as a compromise, the designed lifetime of the LICCA CubeSats will be two years. The satellites will make use of shielding to protect them from the space environment and radiation. The measurements will continue after this lifetime if functioning is still possible.

4.2. Radiation

The space environment is hazardous and can, when not properly taken into account, cause the mission to end prematurely. This environment consists mostly of high energy electrons and protons which can cause ionising effects in the satellite's electronics and prevent it from operating [55]. These particles come from the Sun, and cosmic rays and are trapped by Earth's magnetic field in the so-called Van Allen belts [55]. These Van Allen belts are regions around the Earth with very high levels of radiation, as can be seen in figure 4.1. A satellite thus needs to have proper protection, while operating in or traveling through these regions.

Most CubeSat missions operate in LEO and experience lower levels of ionising radiation, than satellites operating in GEO. LEO missions mostly operate below the first Van Allen belt, GEO is an orbit in the upper Van Allen belt. The TID in GEO can be of an factor 1 000 higher than the TID in LEO. So far Cubesat missions have been deployed mainly in LEO and in order to survive the harsh radiation environment encountered in GEO, extra radiation shielding or space graded components would be needed. The TID the components receives is

---

[1] http://www.astro.gsu.edu/wds/, accessed 29/06/2020
[2] https://www.ligo.caltech.edu/page/faq, accessed 16/06/2020
[3] https://www.spenvis.oma.be/, accessed 16/06/2020
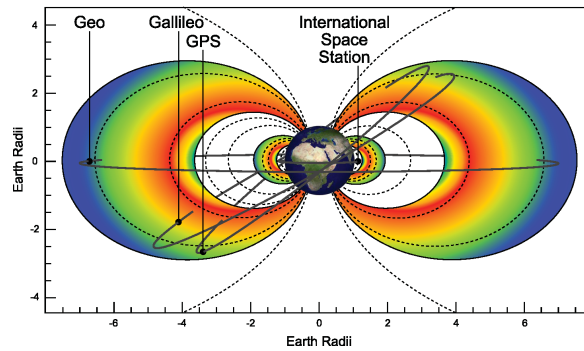
Figure 4.1: The Van Allen belts [4]

caused by electrons, protons, and heavy ions. Bremsstrahlung also contributes to the TID, which is caused by the deceleration of one of these ionising particles in materials which in turn releases energy, in the form of electromagnetic radiation [55].

The solar radiation fluctuates at all times, and differs for solar maxima and minima. A solar flare can send a high amount of high energy particles at once. High energy particles, such as electrons, cannot penetrate the Earth's magnetic field extensively and are therefore mostly trapped in the outer Van Allen belt. The lower energy protons can penetrate further and are trapped in the inner Van Allen belts. A transfer from GTO to GEO comes with serious radiation risks, as the transfer takes spacecraft through both Van Allen belts. Therefore, either the spacecraft needs to travel quickly though this region, or enough radiation shielding would need to be provided.

SPENVIS was used to get an estimate of the TID and the Single Event Effects (SEE). SPENVIS is an online tool from ESA to get an estimate of radiation effects on satellites for different orbits. To come to a value for the TID, SPENVIS was run for the inputs of two years in GEO, with no inclination, with the start of the mission on 1 MAR 2030. The AP/AE-9 models were run for the proton and electron populations in the outer Van Allen belts. The solar particle mission fluences, ESP-PSYCHIC, were run on a 95% interval. The Galactic Cosmic Ray (GCR) fluxes model, ISO 15390, was also run. In order to estimate the TID, the MULASSIS and SCHIELDOSE-2 models were run. The TID was calculated for the centre of a hollow aluminium sphere of varying thicknesses, where an aluminum sphere is taken to more accurately model the satellite, the results can be found in figure 4.2. Depending on the thickness of the aluminium equivalent shielding, the TID is between 5 000 and 50 000 rad (Si) per year in GEO, this is for 3-5 mm of equivalent aluminium thickness. Which is the normal skin thickness of satellites in GEO.
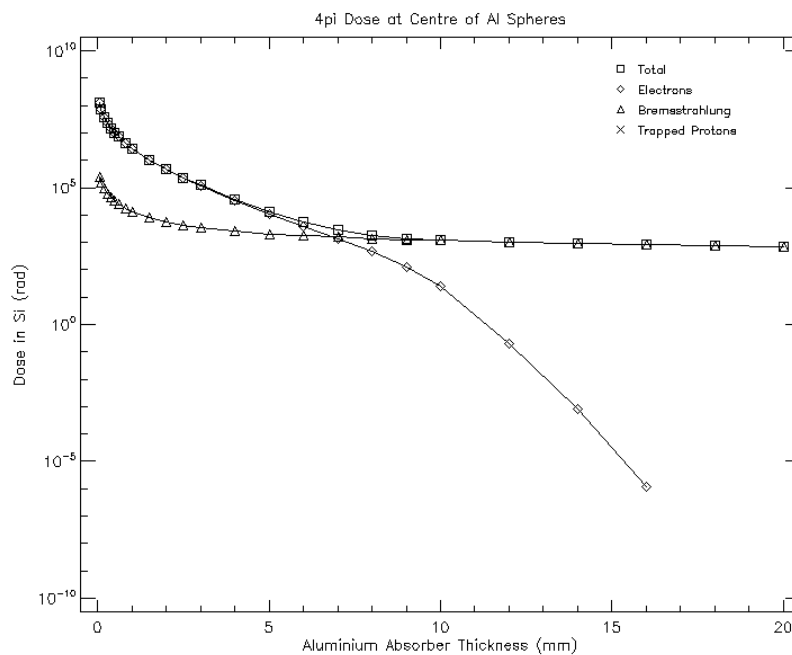

Figure 4.2: SCHIELDOSE-2 output for 2 years GEO.

[4]http://www.fp7-spacecast.eu/, accessed 30/06/2020

For the SEE, the long-term SEE and Linear Energy Transfer (LET) spectra were run, using the solar particles and GCR particles models of SPENVIS. There are many different kinds of SEE to be dealt with, but it is impossible to know which ones will occur. However, it is known that many SEE will be Single Event Upsets (SEU), which are less critical than other SEE. The method of determining the SEE is described in section 8.4.2.

4.3. Delta V budget

This section will discuss the ΔV budget, split into several parts: the transfer from GTO to GEO, once in GEO a phase shift to obtain the required relative position, realignment of the satellites, orbit maintenance and the EoL manoeuvre. The equations for important velocities are given from equation (4.1) to equation (4.4), in which a_T represents the semi major axis transfer orbit, r the radius, r_{dep} the radius of the departure orbit, r_{tar} the radius of the target orbit, μ the gravitational parameter, r_a the radius in the aphelion, r_p the radius in the perihelion, V_c the circular velocity, V_{apo} the velocity in the aphelion and V_{per} the velocity in the perihelion.

$$a_T = \frac{1}{2} \cdot (r_{dep} + r_{tar}) \quad (4.1)$$

$$V_c = \sqrt{\frac{\mu}{r}} \quad (4.2)$$

$$V_{apo} = \sqrt{\mu \cdot \left(\frac{2}{r_a} - \frac{1}{a_T}\right)} \quad (4.3)$$

$$V_{per} = \sqrt{\mu \cdot \left(\frac{2}{r_p} - \frac{1}{a_T}\right)} \quad (4.4)$$

When the satellites are launched into GTO, there can be a slight deviation in the apogee altitude. This deviation is 80 km as a maximum, so this will be considered in the ΔV budget [6]. The ΔV required can be calculated with a Hohmann transfer. These equations also hold for the EoL manoeuvre. The equations for a Hohmann transfer are presented from equation (4.5) to equation (4.7), in which $V_{c_{dep}}$ is the circular velocity at the departure and $V_{c_{tar}}$ is the circular velocity at the target orbit.

$$\Delta V = \Delta V_1 + \Delta V_2 \quad (4.5) \qquad \Delta V_1 = V_{per} - V_{c_{dep}} \quad (4.6) \qquad \Delta V_2 = V_{c_{tar}} - V_{apo} \quad (4.7)$$

The transfer from GTO to GEO using an impulsive shot was calculated with the cosine rule, since an inclination change has to be accounted for as well. Using figure 4.3, the ΔV can be calculated using equation (4.8).
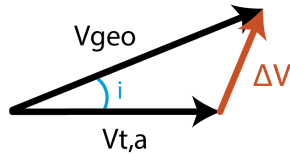
$$\Delta V = \sqrt{V_c^2 + V_{apo}^2 - 2\, V_c\, V_{apo}\, \cos i} \quad (4.8)$$

Figure 4.3: ΔV for transfer to GEO

Another ΔV component that has to be determined is the realignment manoeuvre. Once every 15 days the satellites have to realign their relative positions to maintain the quality of measurements. The realignment is a result of the drifting of the satellites. This drifting can result in an altitude change or a phase change. The ΔV needed to realign in the case of an altitude change can easily be calculated using the equations for the Hohmann transfer. When the satellites drift within the orbit, they have to undergo a phase change to realign. The equations for this phase change are presented from equation (4.9) to equation (4.11) in which T stands for the orbital period, N for the amount of revolutions and $\Delta\theta$ is the change in true anomaly. These equations can also be used for the phase shift that the satellites have to perform once they reach GEO in order to obtain the required distance between the satellites.

$$\Delta T = T_{GTO} \cdot N \quad (4.9)$$

$$\Delta a = \Delta\theta \frac{r_{GEO}}{3\pi} \frac{T_{GEO}}{\Delta T} \quad (4.10)$$

$$\Delta V = 2 \cdot \left(\sqrt{\mu \left(\frac{2}{r_{GEO}} - \frac{1}{r_{GEO} + \Delta a}\right)} - \sqrt{\frac{\mu}{r_{GEO}}} \right) \quad (4.11)$$

A more elaborate explanation on the realignment manoeuvre is visualised in figure 4.4. The satellite can drift up to 5 arcmin in 15 days [45] corresponding to 106 km in GEO. This drift can occur in every direction within the orbital plane. The worst case scenario is that the spacecraft drifts in altitude as well as in phase. This would ask for a combined manoeuvre using two sequential transfer orbits, implying three burns.
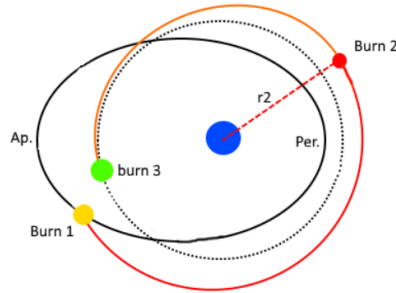
Figure 4.4: Example of a realignment manoeuvre

A burn sequence is executed as follows. First the ADCS rotates the spacecraft such that the thruster points in the direction of the required manoeuvre. Then the thruster fires, for which an impulsive shot is assumed. The manoeuvre ends with the ADCS rotating the spacecraft back towards its original orientation. During the slew and the burn itself, the measurements are interrupted, since the spacecraft is not pointed towards the other spacecraft. Also, the firing thruster generates signal noise, which is not beneficial for the measurements. Therefore the burn time should be taken into account for the realignment manoeuvre. Although, in between burns the satellites will be rotated back to the measurements attitude and data will be collected.

The last component of the ΔV budget is the orbit maintenance. The ΔV required is estimated using recommended values from Zandbergen [74, p. 226]. The mission lifetime is designed to be two years. Usually reserve fuel would be taken along such that the lifetime can be extended when the satellite is still functioning. However, this mission has a very tight volume constraint. Any increase in propellant would cause a snowball effect, increasing the volume of other subsystems as well. The ΔV calculated for the realignment manoeuvre estimates a drift of 106 km. However, it is unlikely that the spacecraft drift this maximum amount every 15 days. Therefore, for realignment and orbit maintenance a margin is already built in. This means that after EoL there will be propellant left and the mission lifetime can be extended.

In table 4.1, the total ΔV required for the LICCA mission is presented. Note that the ΔV for realignment is multiplied by a factor of 48, since realignment will take place once every 15 days. This will be 48 times in two years. Note that in table 4.1, the phase shift realignment is not accounted for in the total ΔV, since the ΔV required for Hohmann realignment is higher. This means that the Hohmann transfer is the critical case. When it comes to designing the propellant tank, this value is taken for the ΔV budget.

Table 4.1: Total ΔV required for the LICCA mission

Manoeuvre	*Required ΔV*
Transfer [km/s]	1.49
Apogee deviation [km/s]	0.0029
Phase shift [km/s]	0.102
Realignment (Hohmann) [km/s]	0.186
Realignment (Phase shift) [km/s]	0.039
Orbit maintenance [km/s]	0.027
End-of-Life [km/s]	0.0109
Total [km/s]	**1.82**

The presented equations hold for Hohmann transfers, which imply impulsive shots. Impulsive shots assume zero burn time and are thus only applicable for high thrust. This can be achieved by chemical propulsion. For electric propulsion, which uses low thrust, the orbital mechanics behind a manoeuvre are more complicated. Constant thrust is provided over a certain amount of time, slightly modifying the spacecraft's orbit every revolution. Since the manoeuvre takes time, gravity loss should be taken into account. A straightforward estimate for the ΔV including this gravity loss is 1.5 to 2 times the ΔV of an impulsive shot for the same manoeuvre [7]. The time to manoeuvre from one altitude to the other can be approximated using equation (4.12) [19].

$$t = \frac{m_0 \, g_0 \, I_{sp}}{T} \left[1 - e^{\frac{1}{I_{sp} \, g_0} \left(\sqrt{\frac{\mu}{r}} - \sqrt{\frac{\mu}{r_0}} \right)} \right] \qquad (4.12)$$
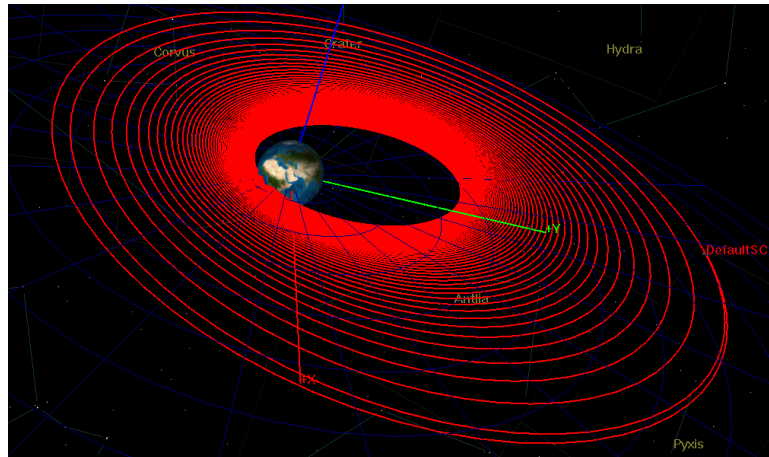
Figure 4.5: Electric transfer raising GTO periapsis to GEO

The General Mission Analysis Tool (GMAT) is software developed by NASA to simulate space missions. The tool was used in this project to simulate transfer and orbital maintenance manoeuvres, using both chemical and electric propulsion, and a combination of the two. The main goal was to visualise the transfer from GTO to GEO using multiple options for the propulsion subsystem and verifying their feasibility. An example can be seen in figure 4.5. This is explained in more detail in the propulsion subsystem design in chapter 6.

4.4. Eclipse

In order to account for sun pressure perturbations and eclipse conditions, a tool was developed in Python that could account for these phenomena. In order to divide the work to be done for this part, the system was divided in two parts: sun position calculation and eclipse calculation.

4.4.1. Sun position calculation

The objective of this program is calculating the sun position relative to the satellite. In order to arrive to this value, the system requires the inputs and outputs specified in table 4.2. The resolution and number of iterations in this table refer to the number of points in which the Sun position is calculated and the number of iterations in which numerical equations are solved respectively. This last input will be explained in the following paragraphs.

Table 4.2: Required inputs and outputs from the Sun position calculation program

Inputs	Outputs
Initial and end time	Sun position in Cartesian vectors
Resolution	Sun angles with respect to the CubeSat
Number of iterations	Time stamp

The assumptions made for this model are the following:

1. The satellite is in GEO. This is the intended mission's orbit.
2. The effects of external perturbations will not be taken into account. These effects could have an important influence in the final satellite orbit. However, as a realignment maneuver is performed every 15 days, it is assumed that the perturbations effects will not be strong enough to build up significantly for 15 days. These perturbations include:

    - N-body problem
    - Radiation pressure
    - J-effect
    - Changes in the rotational Earth axis

3. The satellite position with respect to the Sun will be equal to Earth's position with respect to the Sun. This can safely be assumed because the radius of the satellite's orbit is 42 164 km. This accounts for only the 0.028% of the mean distance of the Earth to the Sun. Furthermore, as the satellite rotates around Earth in GEO in the same direction as Earth, its orientation with respect to the Sun can also be assumed to vary at the same rate as the one of Earth.

The constants that are used, are the Earth's eccentricity (e), Earth's semi-major axis (a), the gravitational parameter of the Sun (μ), the Earth polar axis inclination (i) and the rotational rate of the Earth (Ω). Due to the assumption of considering the satellite in the same position as Earth, the position of the Sun with respect to the

Earth can be first calculated and then a transformation matrix can be applied in order to put the results such that they coincide with the body reference frame of the CubeSat. In order to calculate the position of the Sun relative to Earth, first the position of Earth relative to the Sun is calculated.

First, the reference frames are defined. In the Sun reference frame, the z-axis has positive values for points above the equator and the x- and y-axes are defined as specified in figure 4.6a. Here, θ_a represents the true anomaly and the location of Earth at $t = 0$ represents its perihelion where its z-value is minimum. The Earth centred reference frame will be used for Earth and as in the other sections of this report, the body axis will be used for the CubeSat in the way it is shown in figure 4.6b.

(a) Sun reference frame

(b) Earth and CubeSat reference frame
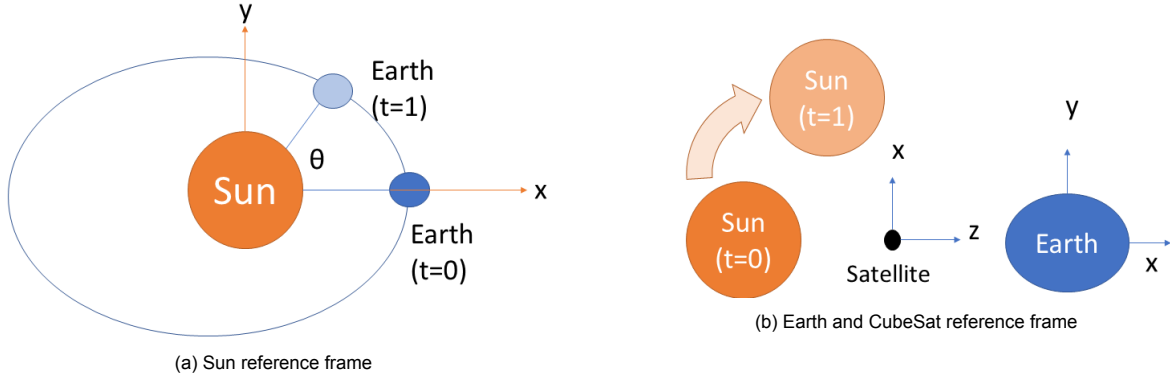
Figure 4.6: Sun, Earth and CubeSat reference frame

The location of Earth with respect to the Sun is calculated by first obtaining the mean anomaly (M_a) for every point in time (t), as specified in equation (4.13), in which t_p represents the time since last perihelion. Then the eccentric anomaly (E_a) is obtained by using equation (4.14). Because no analytical solution can be obtained from this equation, a recursive bisection is used to arrive to an answer for which the input "number of iterations" is used. Finally, the true anomaly, the module of the distance vector and the distance vector are obtained as specified in equation (4.15), equation (4.16) and equation (4.17) respectively, in which $\vec{r_{E,S}}$ is the distance of the Earth with respect to the Sun.

$$M_a = \sqrt{\frac{\mu}{a^3}}\left(t - t_p\right) \qquad (4.13)$$

$$M_a = E_a - e \cdot \sin E_a \qquad (4.14)$$

$$\theta_a = \arccos\left[\frac{\left(1 - e^2\right)}{e\left(1 - e\cos E_a\right)} - \frac{1}{e}\right] \qquad (4.15)$$

$$\|\vec{r_{E,S}}\| = \frac{a\left(1 - e^2\right)}{1 + e\cos\theta_a} \qquad (4.16)$$

$$\vec{r_{E,S}} = \|\vec{r_{E,S}}\|\begin{bmatrix} \cos\theta_a\cos i \\ \sin\theta_a \\ \cos\theta_a\sin i \end{bmatrix} \qquad (4.17)$$

Then, the transformations have to be performed. First, the transformation from the Sun's inertial reference frame to the Earth centred reference frame is done, which is a rotational reference frame. This transformation, specified in equation (4.18) in which $\vec{r_{S,E}}$ represents the distance of the sun with respect to Earth, varies with each point in time causing it to be calculated for each time iteration. Finally, the transformation to the satellite's body reference frame is done by switching the vectors in the following manner: The x-, y- and z-axis of Earth transforms into the z-, x- and y-axis of the satellite, as it was shown in figure 4.6b.

$$\vec{r_{S,E}} = -\begin{bmatrix} \cos\left(\Omega\cdot t\right) & \sin\left(\Omega\cdot t\right) & 0 \\ -\sin\left(\Omega\cdot t\right) & \cos\left(\Omega\cdot t\right) & 0 \\ 0 & 0 & 1 \end{bmatrix}\cdot\vec{r_{E,S}} \qquad (4.18)$$

4.4.2. Eclipse calculation

The position of the Sun and the satellite with respect to the Earth can be defined by parameters shown in figure 4.7. The vector $\vec{R_\Theta}$ denotes the position of the Sun while vector $\vec{r}$ gives the position of the satellite. It can be seen that $\vec{r}$ is decomposed in two components: $\vec{a}$ (perpendicular to $\vec{R_\Theta}$) and $\vec{d}$ (parallel to $\vec{R_\Theta}$). The angle Ψ is the angle between $\vec{R_\Theta}$ and $\vec{r}$.
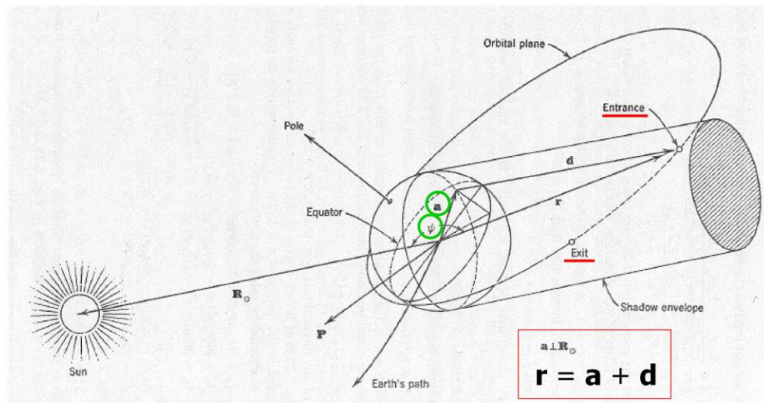
Figure 4.7: Three-dimensional eclipse scenario [29]

For a satellite to be in eclipse, two conditions have to be satisfied, namely that $\Psi > 90°$ and $\|\vec{a}\| < R_e$ (where R_e is the Earth radius)

Given that the satellite is in GEO, it is assumed that its position is fixed with respect to the Earth. Thus, only vector $\vec{R_\Theta}$ will change throughout the year. To satisfy the first condition, angle Ψ has to be found first. Since it is the angle between the Sun and satellite vectors, it can be found as follows:

$$\vec{R_\Theta} \cdot \vec{r} = R_\Theta \cdot r \cdot \cos\Psi \qquad (4.19) \qquad\qquad a = r \cdot \sin\Psi \qquad (4.20)$$

From equation (4.19), the first condition ($\Psi > 90°$) can be rearranged to $\cos\Psi < 0$. Magnitude of vector $\vec{a}$ can be found by relation given in equation (4.20). These equations can be applied to each state of the Sun with respect to the Earth. For each state it will be then calculated whether the satellite is in eclipse condition.

There are also other complications that will result in a longer period. These include penumbra effect, flattening of the Earth and refraction of light caused by atmosphere. However, maximum effect of all the three is only 120 seconds [58]. Thus, for simplicity, this effect will be added in the end.

5

Attitude Determination & Control System

This chapter presents the ADCS design for the LICCA mission. The ADCS will determine and control the pointing of the CubeSat and the drift thereof. This is done via a combination of actuators and sensors at specific locations in and on the CubeSat body.

5.1. Functional analysis

In order to design the ADCS, a functional analysis should be performed to account for all the functions that the subsystem shall execute and all scenarios the CubeSat shall experience. The diagram that specifies all these functions is shown in figure 5.1, in which the main functions of determining the attitude, satellite stabilisation, and data transfer were identified.
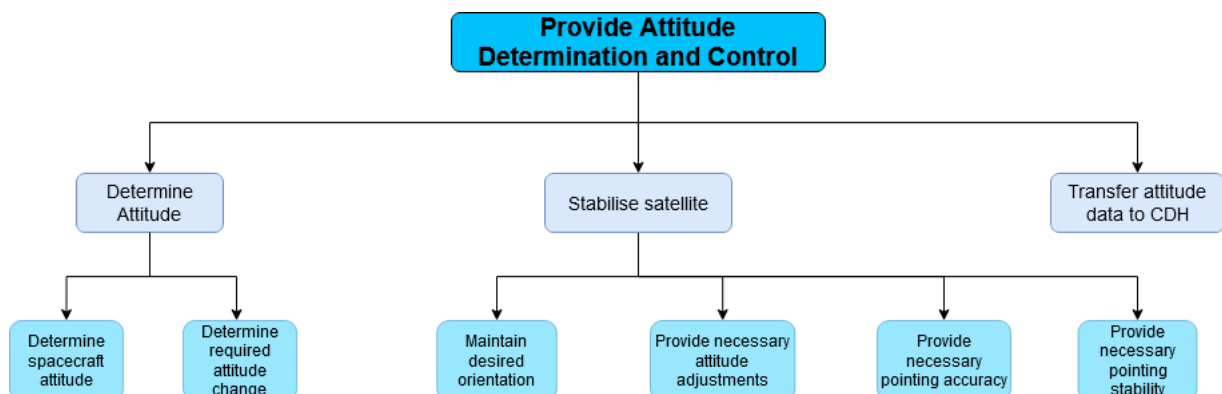
Figure 5.1: Functional diagram of the ADCS

5.2. Requirements

The subsystem requirements are obtained from the LICCA Baseline Report [3] and specified in table 5.1:

Table 5.1: ADCS requirements

ID	ADCS
LICCA-SYS-Sub-Ad-1	The ADCS shall be able to determine the attitude of the satellite about all three axes with an accuracy of 0.0023 rad.
LICCA-SYS-Sub-Ad-2	The ADCS shall be able to determine the necessary attitude adjustments about all three axes.
LICCA-SYS-Sub-Ad-3	The ADCS shall be able to adjust the attitude of the spacecraft about all three axes for the duration of its lifetime.
LICCA-SYS-Sub-Ad-4	DELETED
LICCA-SYS-Sub-Ad-5	DELETED
LICCA-SYS-Sub-Ad-6	The ADCS shall transfer attitude data to the CDH.
LICCA-SYS-Sub-Ad-7	The components of the ADCS subsystem shall have currently a TRL of 7 or higher.

It is determined that not all requirements are relevant anymore, and thus the requirement for pointing stability is deleted. The reasoning for this deletion can be found in more detail in section 5.3.3. A changelog of the ADCS requirements is found below in table 11.2.

Table 5.2: ADCS Requirements changelog

ID	Change	Rationale
LICCA-SYS-Sub-Ad-4	Deleted.	This requirement is automatically fulfilled if LICCA-SYS-Sub-Ad-1 is fulfilled, and thus is considered redundant.
LICCA-SYS-Sub-Ad-5	Deleted.	The pointing stability provided by the ADCS is seen as too abstract and out of the scope of this report for the LICCA mission.

5.3. Design methodology

In order to perform the previously specified functions and satisfy the requirements, a design of the ADCS is presented. To arrive to this final design, a design methodology was followed, which is treated in this section.

5.3.1. Subsystem modes

The first step to design the subsystem is to identify the modes in which it operates. These modes are listed below.

- **Standby mode:** The ADCS is put in standby. In the ideal case, this would happen just before or during deployment. In case of an unexpected power shortage or due to system failure, this mode shall be the response of the ADCS system. When the CDH subsystem determines it is safe for the spacecraft to operate, the ADCS can be switched on and start the De-tumbling mode.
- **De-tumbling mode:** In this mode the spacecraft corrects for possible high rotational speeds in order for the sensors to work properly. By the use of the Inertial Measuring Unit (IMU), it calculates its rotational speed and corrects it until all the optical sensors, such as Sun, Earth and star sensors can work properly. This mode can be activated either after the standby mode or after the spacecraft experiences an unexpected perturbation and it is placed in safe mode.
- **Attitude acquisition mode:** The ADCS starts to analyze the data from all the sensors, points the spacecraft in the nadir direction and maintains the necessary rotational speed.
- **Safe mode:** The spacecraft enters in a safe mode in which the current attitude is maintained. This is usually used when the ADCS experiences an emergency in which the regular mode fails. The spacecraft will use less power to meet its minimal needs [72, p. 569].
- **Nominal operation mode:** For an increased precision, the spacecraft points the payload to the other satellites of the constellation by using the feedback measurements provided by the payload sensors and the piezo stage. This can be done by using elements like a four quadrant photodiode, which allows position sensing with a greater precision and sensitivity in more than one axis. Although this is not a component of the ADCS, the subsystem has to negate the possible losses of contact with the constellation by changing the attitude of the spacecraft.

- **Slew mode:** The spacecraft rotates a certain amount of degrees, via internal torque generation, according to indications of the CDH subsystem.
- **Orbit correction mode:** This is the only manoeuvre in which the ADCS uses an external torque by means of a thruster system in order to desaturate the Reaction Wheels (RW). Then, slew manoeuvres will be performed before each time the propulsion system is activated in order to point the satellite in the intended direction at which the ΔV is applied. Once the spacecraft reaches its intended orbit, the "de-tumbling mode" is again activated.

5.3.2. Disturbances

The ADCS system is designed to ensure correct pointing stability and controllability of the CubeSat as it endures external and internal disturbances. The cause and effects that these disturbances have on the CubeSat are discussed in the following subsections. In addition, the magnitude and direction of the disturbance torques are determined if possible [72]. Not all internal torques are considered disturbance torques: the torque required for the slewing manoeuvre is discussed in the momentum budget, section 5.3.4.

External disturbances

The external disturbances are:

- **Solar Radiation:** Sunlight has momentum, therefore it exerts pressure on the object that it hits. The object can either absorb the light with all of its momentum or reflect the light and experience double the momentum. The starting point to model this disturbance is equation (5.1) [72], T_s is the solar torque, Φ is the solar flux, c is the speed of light, A_s is illuminated area, q is the reflective index, c_{p_s} is the center of solar pressure, c_m is the the center of mass and ϕ is the incidence angle. The satellites of LICCA mission orbit in GEO and they are Earth-oriented. Therefore the Sun-light area will vary in one orbital period [72]. To compute the torque exerted by the Sun, a model was developed that simulates the solar illumination on every face of the satellite of the Earth around the Sun for one year. This model is an adaptation of the one described in section 4.4. From this a cyclical behaviour was noticed and the maximum torque was extracted. This torque is estimated to be $8.03 \cdot 10^{-9}$ Nm.

$$T_s = \frac{\Phi}{c} A_s (1 + q)(c_{p_s} - c_m) \cos \phi \tag{5.1}$$

- **Aerodynamic Torque:** The aerodynamic torque is left out of consideration as spacecraft above the altitude of LEO will not experience noticeable aerodynamic torques, as the atmospheric density is extremely low at this altitude.
- **Magnetic Field:** The magnetic field of Earth causes cyclic torques acting on the CubeSat as it tries to align its dipole with the direction of the local magnetic field. The Earth's magnetic field is modeled as a dipole to simplify calculations and to find the maximum value of the magnetic torque. The torque is calculated with equation (5.2), where B is Earth's magnetic field strength and D the CubeSats magnetic dipole. Earth's magnetic field strength is approximated with the magnetic moment of Earth: $\mu_{Earth} = 7.96 \cdot 10^{15} Tm^3$, c is an approximation constant taken to be the value of 2 for an equatorial orbit and R is the arm from Earths dipole centre to the CubeSat. The magnetic dipole of the CubeSat is estimated as a function of mass with $D = c \cdot 10^3 \cdot m_{sc}$ as suggested by NASA's 'Spacecraft Magnetic Torques' report [24]. The CubeSat is estimated to be a 'Class I' spacecraft, as the magnetic dipole is minimised by minimising the looping of currents and magnetic materials. As a result, the net torque determined to be is $1.52 \cdot 10^{-10}$ Nm.

$$T_m = DB = D\left(\frac{M}{R^3}\lambda\right) \tag{5.2}$$

- **Gravity Gradient:** As the satellite is pointed nadir constantly during measurements, which accounts for the majority of the operation time, the angles that the satellite makes with respect to the Earth in the body-fixed reference frame are constant. Furthermore, these angles will be equal to zero in the defined reference frame. Therefore, by applying equation (5.3) [12], in which $\vec{T_g}$ represents the gravity torque gradient, there is no net torque present about any axis.

$$\vec{T_g} = \frac{3}{2} \cdot \frac{\mu}{a^3} \cdot \begin{bmatrix} (I_{zz} - I_{yy}) \sin 2\phi \cos^2 \theta \\ (I_{zz} - I_{xx}) \sin 2\theta \cos \phi \\ (I_{xx} - I_{yy}) \sin 2\theta \sin \phi \end{bmatrix} \tag{5.3}$$

All calculated torques are summed in the three axis they work in to obtain the total torque. If the torque could not be decomposed in the body axes of the spacecraft, the magnitude of the torque is considered to work in every axis at the original magnitude to effectively act as a 'safety margin'.

Internal torques are generated by various sources and via various causes. Below a list of most prevalent internal disturbance torques can be found.

- **Uncertainty in Center of Gravity (c_g):** It is possible that the c_g slightly deviates from the calculated value. When forces are not applied exactly through the c_g, torques are generated. Due to the emptying of propulsion tanks and the movement of parts within the spacecraft, the c_g of the CubeSat will change over time. Tracking the location of the c_g during operation is difficult and the path is hard to predict precisely. A typical range for the uncertainty is 1 to 3 cm. An estimate for the induced torque would be $1 \cdot 10^{-4}$ Nm. As the firing time is very small and its frequency very low, the momentum built up is considered to be very small in magnitude.
- **Thruster Misalignment:** If the thruster is misaligned with the intended alignment designed, a different torque than designed for is generated. A typical range for the uncertainty is 0.1 to 0.5 degrees.
- **Mismatch of Thruster Outputs:** Similar to 'Uncertainty in Center of Gravity'. A typical range for the uncertainty is $\pm$ 5 percentage difference in output thruster force.
- **Reaction Wheel Friction:** The friction causes the magnitude of the generated torque of the reaction wheel to be less than expected.
- **Rotating Machinery:** Rotating machinery within the CubeSat generate torques, in a similar fashion as the reaction wheels. As there are a limited amount of rotating components in the CubeSat, this magnitude in torque is considered to be small.
- **Liquid Slosh:** The propellant within the tanks slosh when the CubeSat changes attitude or translates, generating forces which are hard to predict and model. Due to the size and the very limited movement of the spacecraft, the generated torques are considered to be very small.
- **Dynamics of Flexible Bodies:** The expansion and shrinking of the structure due to thermal variations, the experienced vibrations during operation and eigenfrequencies of the CubeSat may induce unexpected movement and strains onto the structure. As a result torques may be generated.
- **Thermal Shocks:** Attitude can be disturbed due to extreme variations in temperature when entering and leaving the eclipse period. The magnitude of these torques is assumed to be limited as the solar arrays and the body of the CubeSat are small in size.

The magnitude of the internal torques is assumed to be very small, such that these can be accounted by taking margins when generating the momentum budget and sizing the reaction wheels, discussed in section 5.3.4.

5.3.3. Pointing stability
For correct pointing stability and tracking of the receiving satellites, the ADCS and the scientific payload components work together. As a first step, the components of the ADCS system fine tune the attitude of the CubeSat with respect to Earth with the help of the star sensors. Ideally, the nadir pointed side of the CubeSat is completely parallel to the vector tangent to the Earth. This tangential vector should be orthogonal to the vector between the c_g of the CubeSat and the centre of the Earth. If all three connected satellites in the system are pointed as previously described and the laser of each CubeSat is pointed $\pm$ 30 degrees of the vector between Earth and the CubeSat, the pointing system of the scientific payload takes over. The stability is achieved via two subsystems: the ADCS achieves its pointing with respect to celestial bodies, the scientific payload achieves its pointing with respect to the other CubeSats via the received and sent lasers. The laser of the payload is pointed via a piezo stage with a range of $\pm$ 0.13 degrees [44]. This piezo stage is used for the tracking and the precise pointing of the laser at the receiving CubeSats. The incidence angle and the flux received are very accurately monitored (more precisely than the star sensors) by the four quadrant diodes of the payload. It is determined that a $flux/m^2$ of $0.5 \cdot 10^{-7}$ is considered the threshold for proper laser registration and strength, as is shown in figure 5.2. This threshold for the $flux/m^2$ is determind via comparison to the LISA and SAGE mission [22], [45]. The range corresponding to this threshold can be extrapolated from figure 5.2. Taking a safety margin to account for non-gravitational accelerations, it is decided that at a $flux/m^2$ of $0.35 \cdot 10^{-7}$ the piezo stage should rotate to correct for the incidence angle and thus the decrease in $flux/m^2$ of the received laser. Via this pointing method, the ADCS components and the scientific payload components work together in a symbiotic mutualism.
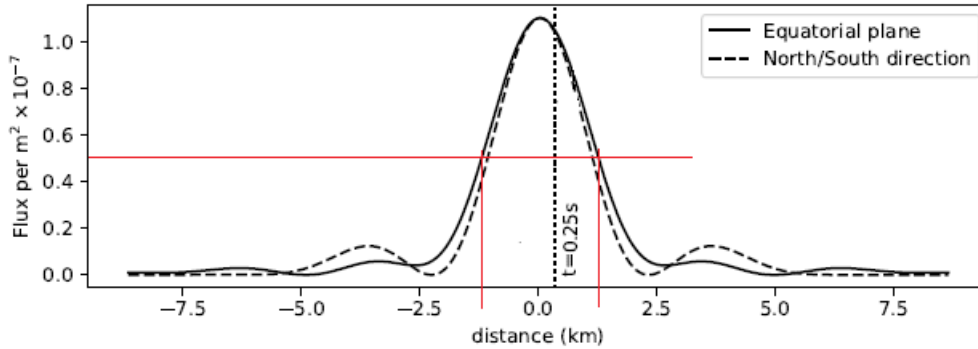
Figure 5.2: Diffraction of the laser at receiving CubeSat [45]

The laser beam travels at the speed of light, 300 000 km/s. As the arm between the CubeSats is equal to 72 000 km, the light takes 0.24 seconds to reach the receiving CubeSats. Furthermore, as the two receiving satellites have a velocity component orthogonal to the arm between the sending and receiving satellite of 1.77 km/s (determined via vector decomposition), the receiving CubeSat has already travelled 0.43 km. As shown in figure 5.2 by the vertical dotted line, the receiving CubeSat will not receive optimum flux. This can be fixed by pointing the laser ahead of the receiving CubeSat. However it is determined via trigonometry that this angle is very small and thus is neglected as it is accounted for by the $flux/m^2$ margin mentioned above.

The stability requirement, in this case, does not depend on the time required for obtaining measurements, but is highly dependent on the $flux/m^2$ and the incidence angle of the received lasers. These changes in flux and incidence angle are in their turn highly dependent on the experienced non-gravitational disturbances relative to all of the three measuring CubeSats in one of the two systems. These disturbances are highly unpredictable and impossible to model over the lifetime of two years. As a result, the pointing stability requirement can not be determined in the accustomed 'deg/s' unit, but is presented as a method to account for pointing stability as discussed above. Further exploration of this topic is considered out of the scope of this report.

5.3.4. Momentum Budget

The momentum budget is generated to determine the momentum originating from the external disturbance torques and the slewing torque over various time intervals. In an iterative nature, the wheels can be sized according to the maximum possible stored momentum and the maximum possible torque generated per wheel. After this sizing, the desaturation required for an assumed time interval is determined. For every torque a safety factor is taken into account to create a margin to prevent unexpected early saturation of the reaction wheels. This margin also accounts for the small torques generated by the internal disturbances and the small torques required for the tracking of the receiving satellites, as discussed in section 5.3.2 and in section 5.3.3 respectively.

- **Slew manoeuvre:** The torque required to be generated by the momentum wheels is calculated with equation (5.4).

$$T_{Slew} = \frac{4 \cdot \frac{\pi}{\theta_{slew}} \cdot I_y}{t_{slew}} \qquad (5.4) \qquad\qquad H_{Slew} = T_{Slew} \cdot \frac{t_{slew}}{2} \qquad (5.5)$$

It is required that scientific measurements can be taken during the realignment manoeuvre of the three CubeSats in the system. This requires the CubeSat to rotate 90 or 180 degrees before and after burn one, 90 or 180 degrees before and after burn two, and 90 or 180 degrees before and after burn three. The two rotations before and after every burn are always in opposite direction, this means that no momentum is built up in the reaction wheels. The momentum built up of every slew manoeuvre before each burn is still of importance to determine the desaturation strategy. As there is no total momentum built up in the reaction wheels over the entire realignment manoeuvre, a large margin is taken into account to account for any unexpected events during the realignment - the loss of the satellite during realignment has large consequences. This margin is equal in magnitude to three times the momentum built up of one slewing manoeuvre.
The slew manoeuvres required for the realignment using thrusters, instead of reaction wheels, is also considered. For this case, thrusters with a nominal thrust force of 0.01 N are used. After performing the calculations, it was determined that the propellant mass required for the realignment slewing manoeuvres was larger than budgetted for. This large propellant mass snowballed other subsystems out of proportion, as a result the use of thrusters for manoeuvring is not considered further.

- **External Disturbance Torques:** To determine the momentum built up about every axis, the total external disturbance torque per axis is determined. Each of these torques is multiplied by a time t, seen in

equation (5.6) to generate the stored momentum per axis.

$$H_{Dist} = T_{distx,y,z} \cdot t \qquad (5.6)$$

- **CubeSat Rotational Rate:** The positive z-axis of the CubeSat is required to point nadir at all times. As a result the CubeSat is required to rotate about the y-axis at a rotational rate (ω) of 360 degrees per day, or 0.0042 degrees per second. This rotational rate has to be 'applied' via an impulse to the CubeSat after every realignment manoeuvre. Thus, this momentum does not build up over time. The momentum required to be generated by the reaction wheel to facilitate this rotational rate is calculated using equation (5.7)

$$H_{Rot} = \omega \cdot I_y \qquad (5.7)$$

It is iteratively determined that the rotational rate of the slew manoeuvre is 1.5 deg/s, such that the reaction wheel about the y-axis is not fully saturated when the momentum of the slew and the momentum accumulated by counteracting external disturbances are summed before the next realignment manoeuvre. All calculated torques are kept below the possible maximum generated torque of the reaction wheels. As a result, only the possible maximum stored moment is taken into account when sizing the wheels. The accumulated momentum about all three axes is determined over multiple time intervals, as an iterative process. It is determined that a larger reaction wheel is required about the y-axis, that should be able to store at least 0.1 Nms in the time slot between two realignment manoeuvres such that the reaction wheel can be desaturated during the first burn of every realignment manoeuvre, every 15 orbits. About the x- and z-axis it is determined that in that same time interval, the time interval between the start of two realignment manoeuvres, a relatively small amount of momentum is stored. As a result, the reaction wheels about the x- and z-axis can be desaturated every 5 manoeuvres, 75 orbits. As both time intervals can be divided by 15, the desaturated of all reaction wheel can occur in the same time slot but at different intervals, before every realignment manoeuvre. As the stored momentum is of a large magnitude about the y-axis, desaturated with the use of momentum wheels is not a viable option. To desaturate the reaction wheel effectively, it is chosen to use thrusters to generate external torques to counteract the torques generated by the deceleration, desaturated, of the reaction wheels. This process is explained in detail in section 5.3.6.

5.3.5. Components trade-off

The ADCS components consist of sensors and actuators. The sensors are used to determine the attitude of the spacecraft to a certain degree of precision, the actuators are used to control the attitude of the spacecraft. These two types of components are heavily influenced by the required pointing accuracy and the moment of inertia of the spacecraft. As our mission concerns 12U CubeSats the moment of inertia is limited [23]. The combination of the strict pointing accuracy and the state of the art of ADCS components poses another challenge for the ADCS design [39]. It is required that the ADCS provides 3-axis attitude control and pointing, and to minimise correction delays the attitude will be determined on-orbit. The spacecraft encounter translation and rotational drift due to the external disturbances. The translational drift is accounted for by the realignment manoeuvre every fifteen days, the rotational drift is accounted for by the ADCS. In this section firstly a trade-off for the sensors is performed, secondly a trade-off for the actuators is performed. In the last section the components are synthesised in a final configuration.

Sensors

The sensors of the ADCS determine the attitude of the spacecraft. The pointing accuracy of the spacecraft should be below 0.13 degrees, as this is the range of the piezo stage. The sending spacecraft should be able to determine the location of the other spacecraft within this accuracy, such that the piezo stage can track the receiving spacecraft as they move trough the orbit and encounter possible non-gravitational disturbances. The sensors are required to measure the absolute and the relative attitude of the satellite [49]. The absolute attitude is determined by measuring two linearly independent vectors between the body frame of the spacecraft and a reference frame. Two coarse vectors are used to coarsely point the satellite nadir, star sensors are selected to finely determine the attitude of the spacecraft. Finally, the four-quadrant diodes and the piezo stages are used to finely tune and lock the laser paths. The relative attitude is determined by an Inertial Measurement Unit (IMU). A benefit is that the relative attitude measurements from the IMU are continuously available and independent of external sources, a drawback is that periodic alignment with absolute attitude measurements is required due to minimise pointing drift.

The following list discusses each sensor, the characteristics of the chosen COTS component and the rationale for the choice made.

- **Star Sensors:** For the star sensor the ST200[1] from 'Hyperion Technologies B.V.' (jointly developed by Berlin Space Technologies GmbH) is chosen, as this sensor has favorable mass, power and pointing accuracy properties. The pointing accuracy of the sensor (3σ) is 0.0083 degrees in pitch an yaw, and 0.055 degrees in roll. The sensor has a baffle for interfering Sun rays and a 5 Hertz update rate. The

---

[1]https://hyperiontechnologies.nl/, Star sensor ST200 datasheet, accessed 01/06/2020

component has flown on 14 missions since 2015. This star sensor allows for attitude determination and tracking[2].

- **Sun Sensors:** It is chosen to use the BiSon64-ET[3] fine Sun sensor for small satellites at GEO and beyond, manufactured by LENS R&D. The sensor measures to incident angle of the Sun in two axes (in plane of the sensor) over a field of view (FoV) of 64 degrees. This fine Sun sensor option is chosen due to its low mass, low power consumption, low volume and it sufficient coarse pointing precision (3σ) of 0.5 degrees. Input scales with cosine so the payload can be pointed nadir if orbital position is known via the communications subsystem. The sensor has a large temperature range, good radiation tolerance and is at current TRL 8. This Sun sensor is chosen under guidance of Johan Leijtens, systems engineer.

- **Earth Sensors:** For the earth sensor the CubeSpace's CubeSense N[4] (single sensor head) is chosen. This is a static optical sensor. An optical sensor is chosen because it is state of the art for CubeSats, and the albedo effect can be neglected contrary to an infrared horizon sensor. A static sensor is chosen because the other option, a scanning sensor, has a higher mass, higher power consumption and lower reliability due to moving parts and increased complexity. Furthermore, as the spacecraft is in GEO (high altitude) the FoV of the static sensor is sufficient for the Earth to be constantly in view and the precision of the sensor is increased in general. The pointing accuracy of the sensor (3σ) is 0.2 degrees over the entire 180 degree FoV. The sensor is chosen for its accurate pointing, low mass and power consumption and its flight heritage.

- **Magnetometers:** It is chosen to not use magnetometers, as the magnetic field is relatively weak in GEO, the sensor has to compare the measurements to a magnetic field model (required to be updated as it varies with time) on board, requiring processing time and power. It is also possible to use a magnetometer and measure the interplanetary magnetic field and compare it to a model. However, this requires processing power and this field is highly unpredictable due to its heavy dependence on solar winds.

- **GPS:** Attitude determination via GPS is not feasible as the satellite body is too small to determine the attitude sufficiently by placing GPS at every corner of the CubeSat. The orbital position of the satellite is determined via ground tracking, as discussed in chapter 7. As a result, it is decided to not use a GPS.

- **Gyroscopes:** Gyroscopes for CubeSats are not at a suitable TRL and thus are not considered further.

- **IMU:** It is chosen to use the STIM300 Multi-Axis Gyro Module ButterflyGyro[5] manufactured by Sensonor. This IMU is not aided by GPS and insensitive to magnetic fields. It contains three MEMS gyos, 3 accelerometers, 3 inclinometers and a low gyro bias instability (0.3 degrees per hour). It also has sufficient flight heritage.

- **Payload Four-quadrant Diode:** After the CubeSat is pointed via the ADCS, the scientific payload takes over to maintain contact with the other two satellites in one of the two three satellite systems. Once the satellite is pointed via ADCS towards the receiving satellites within the 0.13 degree pointing range of the piezo stage, the CubeSat tracking is done via the piezo stage and the four-quadrant diodes of the scientific payload.

Attitude sensors experience a multitude of errors, the most prevalent being systematic and random errors. Systematic errors, due to bias due to a manufacturing offset, imperfect calibrations or secondary effect (temperature offset). Random errors (noise), due to measurement noise or quantisation errors. In addition, errors are caused by outliers. Detailing the source and effects of these errors is deemed outside the scope of this project.

Actuators

The spacecraft is pointed by the generation of internal and external torques applied by the actuators. Actuators that can apply internal torques are reaction wheels, momentum wheels and control momentum gyros. Actuators that can provide external torques are thrusters and magnetic torquers. The actuators that are able to apply internal torques can get saturated if maximum rpm is reached. The actuators that apply external torques are used to desaturate the aforementioned actuators by applying torques in the required direction for deceleration of the actuators. Due to the strict precision required and the 3-axis attitude control and pointing, and the strict structural constraint for CubeSat design, passive means of attitude control are not feasible.

The following list discusses each actuator, the characteristics of the chosen COTS component and the rationale for the choice made.

- **Reaction Wheel:** Reaction wheels form a good solution to attitude control for CubeSats as these actuators have a low mass, low required power, low volume and are precise. It is chosen two use two types of reaction wheels of the same brand. It is chosen to use one larger reaction wheel about the axis that experiences the most disturbance torques and slewing manoeuvres, such that more momentum can be stored before saturation. The smaller reaction wheels are used to account for small external disturbances. The larger and smaller reaction wheels are the RWP050 and RWP100[6],respectively, manufactured by blue

---

[2]www.digitalcommons.usu.edu, Star sensor ST200 product specification, accessed 01/06/2020

[3]https://lens-rnd.com, Sun sensor BiSon64-ET datasheet, accessed 18/06/2020

[4]https://www.cubespace.co.za/, Earth sensor CubeSense N, accessed 01/6/2020

[5]www.sensonor.com, STIM300 Multi-Axis Gyro Module ButterflyGyro datasheet, accessed 11/6/2020

[6]https://www.bluecanyontech.com/, RWP050 and RWP100 datasheet, accessed 03/6/2020

Canyon Technologies Inc. The chosen reaction wheels are space graded and proven to function in orbit and have an expected lifetime of above five years.

- **Momentum Wheels:** To supply internal torques to account for external disturbance torques and to facilitate the required manoeuvring rate in orbit. A momentum wheel spinning at high speeds about one axis, provides gyroscopic stiffness around the other two axes. It is chosen to not use momentum wheels for this mission, as the wheels are spinning constantly and require a relatively high power. Furthermore, the combination of a low mass moment of inertia about all axes of the CubeSat and the possible friction, the constant spinning momentum wheel experiences, may cause the CubeSat to rotate, resulting in the opposite of the required stabilising effect of the momentum wheels.
- **Control Moment Gyro:** Control Moment Gyros for CubeSats are not at a suitable TRL for this mission and are thus not considered further.
- **Magnetic Torquers:** As previously mentioned, the Earth's magnetic field is weak in GEO and the interplanetary magnetic field is highly unpredictable. It is decided to not use a magnetic torquer as the generated torques are expected to be very small and highly unpredictable in GEO [20].
- **Thrusters:** It is chosen to use the End-Mounted Standard MiPS (Micro Propulsion System) X14029003-11[7] manufactured by VACCO. This MiPS consists of five thrusters for path, yaw and roll control. It provides a nominal thust of 10 mN, and it utlises a non-toxic R134a cold gas propellant.

Architecture

Six Sun sensors are used, one placed on every side of the CubeSat. Each Sun sensor has a FoV of 120 degrees, thus the attitude of the CubeSat relative to the Sun can be determined over 360 degrees about the spacecraft body. This allows, when the orbital position of the satellite and the Sun is known from the earth inertial reference frame, to coarsely point the satellite as at least two Sun sensor will register sunlight and its incidence when the CubeSat is at an angle towards the Sun. The most brightly lit Sun sensor will naturally have the smallest incidence angle towards the Sun. Although the sunlight pointed to the Sun sensors on the top and bottom of the satellite is partly obstructed by the solar arrays, it is still considered viable to receive sunlight coming from the positive z-direction. During measurements, most Sun sensors are in shadow but all Sun sensors are still considered of importance during the realignment manoeuvre and if attitude is lost. It is determined that with orbital position relative to the Sun and Earth, and the registered incidence angles of the Sun sensors, the CubeSat can be coarsely pointed towards Earth. The Earth sensor, positioned in nadir direction, as a result gets the Earth in FoV. The vector generated by the Earth sensor is the second absolute attitude vector that facilitates the coarse pointing of the CubeSat.

For fine pointing, the star trackers are placed orthogonal to each other to maximise accuracy. Each creating a vector between the spacecraft and a star. Two star trackers, pointed non-parallel, are required for three axis attitude determination. The star trackers are pointed in the negative z-direction, pointed opposite of nadir, to not let the starfield be obstructed by Earth. As the chosen earth sensor makes an optical Earth observation, during eclipse the sensor is not able to register the Earth as it is not lit by the Sun. During the eclipse the Sun sensors also fail to register the incidence angle of the incoming sunlight. In this scenario, the star trackers and the IMU ensure that the CubeSat's attitude is known. During the eclipse period, approximately 72 minutes, the IMU is still able to correct for its gyro bias as the star trackers are still operative.
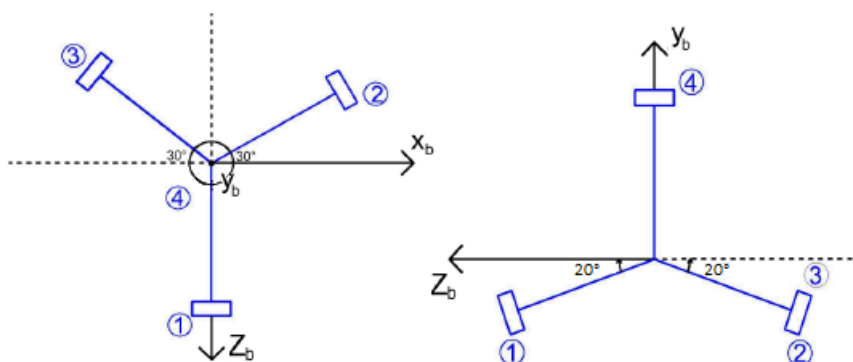
Figure 5.3: Tetrahedron configuration of reactionwheels in the bodyframe of the CubeSat

It is chosen to use a tetrahedron configuration for the reaction wheels. This configuration allows twice the maximum amount of torque about an axis compared to single wheel about an axis [43]. An additional benefit is the redundancy of the system, if one wheel fails the control systems still functions as required. Reaction wheels one, two and three make a 20 degree angle with the xz-plane of the CubeSat. Reaction wheel four, the largest reaction wheel, is rotating about the y-axis as the CubeSat will experience most momentum gain about

---

[7]https://www.vacco.com/, MiPS (Micro Propulsion System) X14029003-11 datasheet, accessed 07/6/2020

the y-axis. Additionally, the slew manoeuvre for the realignment manoeuvre is about the y-axis. The torques delivered by the system, and the relation between the wheel torques and the torques produced about each axis are studied iteratively by constructing the matrix system, as shown in system 5.8. It is determined that a 20 degree angle between reaction wheels one, two, and three allows the reaction wheels to provide sufficient torque to counteract external disturbances and perform slew manoeuvres about all axes.

$$
\begin{bmatrix}
cos(20) & -cos(20)cos(90-30) & -cos(20)cos(90-30) & 0 \\
0 & cos(20)cos(30) & -cos(20)cos(30) & 0 \\
-sin(20) & -sin(20) & -sin(20) & 1
\end{bmatrix}
\cdot
\begin{bmatrix}
T_1 \\ T_2 \\ T_3 \\ T_4
\end{bmatrix}
=
\begin{bmatrix}
T_x \\ T_y \\ T_z
\end{bmatrix}
\tag{5.8}
$$

The momentum budget shows that the larger reaction wheel, RWP100, should be desaturated before every realignment manoeuvre, the smaller reaction wheel, RWP050, should be desaturated every five manoeuvres. The desaturation strategy is explained in more detail in subsection 5.3.6.

The location of the thrusters is discussed in the following section, section 5.3.6. In table 5.3 a summary of the components, actuators and sensors, can be found along with their approximate position in the CubeSat.

Table 5.3: Summary of ADCS components describing their quantity (qnt), type, identifier (product number, manufacturer) and position in the body frame of the CubeSat

Qnt	Type	Identifier	Position (body frame)
2	Star Sensor	ST200, Hyperion Technologies B.V.	1 negative z direction, 1 positive x direction
6	Sun Sensor	BiSon64-ET, LENS R&D	1 on every side of the CubeSat
1	Earth Sensor	CubeSense N, CubeSense N	Pointed nadir in positive z direction
1	IMU	STIM 300, Sensonor	Internal, as shown on component
1	Reaction Wheel	RWP100, Blue Canyon Technologies Inc.	About y axis
3	Reaction Wheel	RWP050, Blue Canyon Technologies Inc.	about positive x axis, subsequent interval of 120 degrees
2	Thruster	X14029003-1X, VACCO	(x,y,z) [cm] 1:(10,10.55,0), positive x (x,y,z) [cm] 2:(-10,10.55,0), negative x

5.3.6. Desaturation strategy

The saturation of the RW occurs because they have a limited speed at which they can rotate. In order to desaturate them, an external torque has to be applied in the direction in which they are spinning due to angular momentum conservation. During the application of this external torque, the RW can decrease their rotational speed without changing the one of the spacecraft. There are two widely used devices for desaturation in CubeSats: magnetorquers and thrusters. The magnetorquers are used primarily in LEO, because the Earth magnetic field is dominant in that region. But as the satellite is in GEO, the presence of this magnetic field gets weaker, making thrusters a more suitable option. This subsection will focus in calculate the following characteristics for the thruster: thruster type, amount of thrusters to be used, position of the thrusters, orientation of the thrusters, thruster configuration and total impulse exerted for desaturation in each axis.

As COTS options are preferred, they were researched first in order to understand what level of development is now on the market. Surprisingly there were already components that have multiple thrusters and are made specifically for small satellite desaturation of RW and for ∆V changes. Such models were X14029003-0X[8] and X14029003-1X[9] which work with cold gas and are from VACCO, a manufacturer located in the United States of America (USA) which has experience with these devices. More thrusters were found, but they did not fit in the mass, volume and power budget, and therefore were disregarded.

[8] https://www.cubesat-propulsion.com/wp-content/..., Standard Micro-Propulsion System, accessed 14/06/2020
[9] https://www.cubesat-propulsion.com/wp-content/..., End-Mounted Standard MiPS, accessed 14/06/2020

Table 5.4: Comparison between X14029003-0X and X14029003-1X thrusters

Parameter	X14029003-0X	X14029003-1X
Volume [U]	0.3	0.25
Wet mass [kg]	0.542	0.676
Dry mass [kg]	0.430	0.439
Thrust [N]	0.010	0.010
ISP [s]	40	40
Total impulse [$N \cdot s$]	44	93
Standby power [W]	0.250	0.250
Maximum power [W]	10	10

Due to the volume restriction, which is considered to be dominant for the ADCS as it has a small volume, X14029003-1X was chosen to begin the analysis. This thruster, as shown in figure 5.4, has a cylindrical end which contains five thrusters: four of them are pointing 90 degrees apart each other, and the last one points normal to the plane. This position results beneficial because there is at least a force applied in the three dimensional axes.
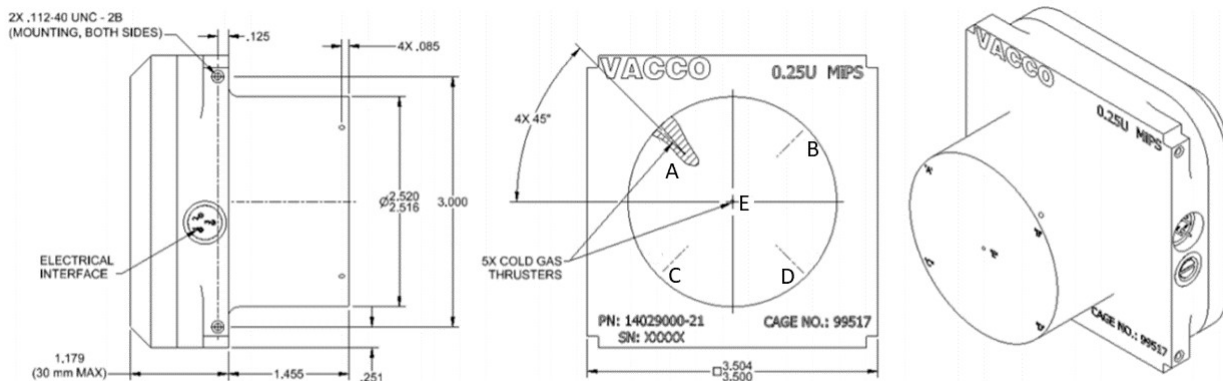
Figure 5.4: VACCO X14029003-1X technical drawing (units in inches)[10]

The method used in this analysis consists of calculating the torque that the system can deliver at maximum thrust configuration around the three body axes of the spacecraft. The reference system used has the z-axis going through the payload, pointing directly to the centre of Earth in measurement mode. The y-axis will go through the fuel tanks of the satellite, pointing north when measurements are performed. Finally, the x-axis will be at 90 degrees of z- and y-axes in order to make the coordinate system consistent, which is in east direction during measurements. Then, the total impulse needed to desaturate the RW in one axis is calculated in section 5.3.4 and is divided by this value to calculate the time needed to achieve desaturation. Finally, this calculated time will be multiplied by the delivered thrust in order to calculate the impulse delivered by the ADCS thrusters, which value has to be less than the capacity of these thrusters.

Many iterations were done to achieve a final thruster setting. The variables considered in order to perform an objective evaluation were the resultant force delivered to the system, independence of moments around the body axes, mass, volume and power consumed. The configurations could vary in number of thrusters used, orientation and position. The tool used to perform this evaluation was a spreadsheet in which the received thrusters configurations and as an output the system first will calculate the maximum torque that each thruster can exert in each axes. With that information, a linear combination of these values can be set up in which the objective is to get torque applied only in one axis with as little resultant net force as possible. This will give as a result the torques for the desaturation per axis, which as it was explained, will be used to calculate the total impulse that the system should deliver.

The assumptions made were the following:

1. The design of figure 5.4 has no deviations from the nominal values.
2. The component thrust is equal to the maximum thrust that it can deliver.
3. At maximum thrust condition $\sum_{i=1}^{5} F_i = 0.01[N]$ in which F_i represents the thrust per nozzle in one thruster.
4. The centre of mass is located at the centre of volume of the satellite.

---

[10] https://www.cubesat-propulsion.com/wp-content/uploads/..., End-Mounted Standard MiPS, accessed 14/06/2020

5. The volume of the satellite was approximated to the one of a cuboid with volume and dimensions equal to the standard 12U CubeSat.
6. Rigid body assumption.
7. No presence of external perturbations when performing the RW desaturation.

First, the nominal position is defined. This is the one in which the thruster "E" points in positive z-direction and is located at the coordinate origin, which is exactly in the centre of volume of the rectangular cuboid representing the satellite. Then, the rest of thrusters are oriented in the direction as it is indicated in figure 5.4 in the middle drawing, in which thruster B, A, C, and E are at 45°, 135°, 225° and 315° respectively with a radial distance of 32 mm. Afterwards, for the orientation of the applied thrust, transformation matrices are used such that $\vec{f}_{1,A} = T_z(\psi) \cdot T_y(\theta) \cdot T_x(\phi) \cdot \vec{f}_{0,A}$ in which $\vec{f}_{0,A}$ and $\vec{f}_{1,A}$ are the initial and final unit vectors of the applied thrust of thruster A respectively after the rotation, and $T_x(\phi)$, $T_y(\theta)$ and $T_z(\psi)$ are the transformation matrices around x-, y- and z-axis respectively. Then, the position of the thrusters is calculated in a similar manner. The initial position of, for example, thruster A ($\vec{x}_{0,A}$) is multiplied by the previously calculated transformation matrices and the displacement is added up such that the relation becomes $\vec{x}_{1,A} = T_z(\psi) \cdot T_y(\theta) \cdot T_x(\phi) \cdot \vec{x}_{0,A} + \vec{d}$, in which $\vec{x}_{0,A}$ and $\vec{x}_{1,A}$ are the initial and final position of thruster A and $\vec{d}$ is the displacement of the thruster. Once that the position and applied thrust are known in the body fixed frame, the torque caused by each thruster can be calculated by applying the equation $\vec{\tau} = \vec{r} \times \vec{F}$ where $\vec{\tau}$ is the resultant torque, $\vec{\tau}$ is the distance from the thruster to the centre of mass and $\vec{F}$ is the applied thrust, which for the thruster A equals $\vec{F}_A = n_A \cdot \vec{f}$, where n_A is the amount of thrust in Newtons that is applied by thruster A.

This gives as a result the torques and forces for an input of initial position and thrust configuration. After some iterations, the final position decided for the thrusters is shown in figure 5.5 and specified in table 5.3 in which they are located at the top of the satellite aligned by the x-axis. Then, the thrust configuration shown in table 5.5 indicates which thrusters have to be activated in order to rotate around each of the axes. In the configuration row, the letter represents the thruster activated according to figure 5.4 and the number next to it is the ID of the thruster. In this case, the thruster 1 is the one located in the positive x-part of the satellite and thruster 2 in the negative x-part, as specified in figure 5.5 and in table 5.3. The total thrust applied for these calculations is $0.01N$ per thruster, which is the maximum amount that this thruster can apply according to table 5.4.
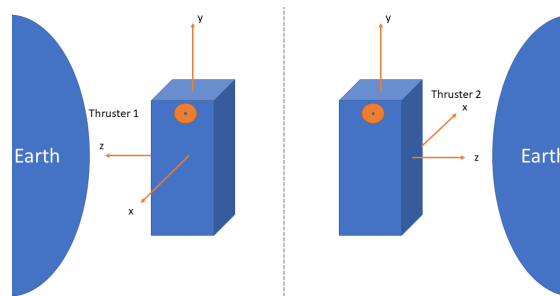
Figure 5.5: ADCS Thruster location

Table 5.5: Thrust configuration for rotation in each body-axis

	x-positive	*x-negative*	*y-positive*	*y-negative*	*z-positive*	*z-negative*
Configuration	B1,C1,A2,C2	A1,C1,B2,D2	A1,C1,A2,C2	D1,B1,D2,B2	C1,D1,A2,B2	A1,B1,C2,D2
Torque [$mN \cdot m$]	1.49	1.49	1.42	1.42	1.42	1.42
Force [mN]	14.14	-14.14	0.00	0.00	0.00	0.00
Axis	z-axis	z-axis				

By dividing the total stored momentum in each axis by the torque applied to desaturate each of the axes, the time for damping can be obtained. Then, the propellant used results by multiplying this term by the amount of thrusters and the thrust delivered per thruster. Finally, for the desaturation in the x-axis, the total impulse delivered to the satellite in the z-direction can be calculated by multiplying the time for dumping by the force delivered in table 5.5. This results in table 5.6, where the total propellant consumed per desaturation manoeuvre is calculated. If the period between each desaturation is 15 days, then a total of 49 manoeuvres have to be done in the period of two years, which is the nominal mission duration. This results in a consumed total impulse of $77.26Ns$, which is significantly lower than the $186Ns$ available by using two X14029003-1X thrusters at their full capacity specified in table 5.4. Therefore, it was decided to load the thrusters with enough propellant to last 2.5 years according to the previous calculations. This results in a total wet and propellant mass of $1.124kg$ and $0.246kg$ respectively for the two thrusters, which results in a reduction of $0.228kg$ from the fully-loaded thrusters.

Table 5.6: Damping results in each body axis

Axis	Time for damping [s]	Propellant impulse [Ns]	Applied impulse [Ns]
x-axis	6.36	0.1272	0.0899
y-axis	65.78	1.3156	0.0000
z-axis	6.70	0.1340	0.0000
Total	**78.84**	**1.5767**	**0.0899 (z-direction)**

Considering table 5.6 and table 5.5, the main motivations to put the thrusters in their final position are:

1. There is no coupling between moments in more than one axis. e.g. The stored moment in x-axis can be desaturated without applying torque in another axis.
2. Only two sets of thrusters are needed to desaturate the stored moments in three axes.
3. There is only one resultant force present when desaturation takes place, which points in the same direction as the main thruster of the propulsion system when the desaturation is in positive-x direction. This direction is, according to the momentum budget in section 5.3.4, the direction in which the resultant moment due to disturbances will be. This can be used as an advantage during the realignment manoeuvre by positioning first the spacecraft in the intended burn direction for the realignment, and then perform the desaturation, which will produce an estimated impulse of $0.0899Ns$ in the intended thrust direction.

5.4. Risk

The risk associated with the components chosen can be further classified in risk associated with sensors and actuators. The first ones consist of optical devices and accelerometers, which have a different sensitivity towards different factors compared to actuators, which consist of moving parts. In the following subsections, the risks related to each of these components are explained.

5.4.1. Sensors

This subsection includes the following components: Sun sensor, Earth sensor, Star sensor and IMU. The risks identified for these components are the following:

1. **Radiation:** Radiation can be identified as the principal risk of the ADCS sensors because the tolerances of the system towards this phenomenon is relative low. Due to the near exponential increase of this problem in GEO, many components are not prepared to handle this environment and they degrade much faster compared to what would happen in LEO, as it was already explained in section 4.2. If the COTS sensors for the ADCS were used without taking this into account, they probably will not last more than a year because their radiation tolerances levels, which are in between 24 and 30 krad, are what is usually is expected for a year orbiting in GEO.
2. **Temperature:** As the sensors have to be placed close the outside surface of the satellite, they are prone to a high radiation dose and temperature changes. Their temperature tolerance range is between -20 °C and 40 °C, which can differ significantly from the surface temperature of the satellite.
3. **Component failure:** If a component fails before the planned EoL, the ADCS should provide enough redundancy to compensate this shortcoming.

5.4.2. Actuators

1. **Reaction wheel failure:** Reaction wheels are used to rotate the satellite in its three dimensional axes. In order to rotate in all of these axes, at least three reaction wheels are needed. The problem arises when only three reaction wheels are used and one of these fails. Then, control around the axis of the broken reaction wheel is no longer possible.
2. **Thruster failure:** The thrusters in the ADCS are used to desaturate the angular momentum that is accumulated by the reaction wheels. Therefore, if one of these fails, the momentum can be desaturated in a limited amount. In this scenario, external forces will be produced too that would need to be counteracted with the propulsion subsystem or by a well defined desaturation strategy. This is an improving point that can be considered in further iterations.
3. **Variations in the centre of mass:** The centre of mass of the spacecraft can vary due to several reasons such as propellant consumption, solar panels deployment and liquid slosh, among others. This can introduce uncertainties in the ADCS, which could result in a decrease of accuracy.

5.5. Sustainability

All components of the ADCS are COTS components. They all consist of electronic elements, except the for thrusters. For the electronic components, the main considerations are sourcing the required raw materials, the energy consumed and the emissions during transport and the energy consumed during fabrication of the components. Chemical processes are often used during the the production of electronics, this can be dangerous for

organisms and nature. The drawback for COTS components is that the source material is very hard to locate, as a result it is hard to determine the sustainability impact of the COTS components. As the components are commercially available, a R&D phase is not required - reducing the amount of testing and resources required. The star, Sun and Earth sensors are sourced from The Netherlands, minimising the emissions for transport. The IMU is sourced from Norway, a country relatively close-by where the welfare of workers and the impact on the environment is considered of great importance. It is assumed the sustainability of the IMU is high.

The chosen MiPS is made from an aluminium alloy, requiring more energy to manufacture. The thruster utilises the cold gas, non-toxic R134a propellant. The propellant is non-flammable, reducing the hazard. The chemical substances however have a high lethal concentration[11], concluding to a Toxic and Environmental Hazard Figure of 0.69, which is quite high [34]. This propellant is considered environmentally friendly, since it does not produce any green house gases[12]. Nevertheless it does not contribute to a circular ecology system, as the propellant can not be decomposed after use. As a result the thrusters have a low sustainability, and are only chosen because there is no reasonable alternative. If development in the future allow for a more environmentally sustainable ADCS thruster, this option will be considered.

5.6. RAMS

In this section the reliability, availability, maintainability and the safety of the ADCS is discussed.

5.6.1. Reliability

The system reliability needs to be high because no maintenance can be done after launching. To ensure this, COTS components were used with proven flight heritage. A problem could arise if it is taken into account that the flight heritage of some of these components is proven to be in LEO. In order to counteract this, significant testing should be performed to the components that do not have a GEO heritage to ensure that these parts can withstand the GEO environment. Furthermore, redundancy was added in the star sensors, Sun sensors and reaction wheels in order to increase the system reliability. These components were chosen because they were considered the most prone to fail. The IMU can be placed inside the satellite, where it is more protected from radiation hazards and does not consist of intensively moving parts. Although the thrusters are placed outside the satellite, they are considered to be reliable due to their relative TRL value, which is reported to be between 8 and 9 [59, p. 101].

5.6.2. Availability

The locations of the sensors is chosen such that the attitude of the CubeSat can be determined in every scenario, like in eclipse or at high rotational speeds and lost attitude. All sensors are active at all times to ensure 3-axis attitude control. If any sensor breaks, the sensor configuration is designed such that attitude can be kept. The reaction wheels can be fired at any time, assuming the desaturation strategy is executed properly. If one reaction wheel reaches a momentum close to the maximum momentum, the wheel can be desatured by firing the MiPS at any time. During the desaturation of reaction wheels no measurements can be taken due to the induced vibrations of the process. If the is no desaturation process taking place, or the CubeSat is not performing a slew manoeuvre measurements can be taken uninterrupted. The MiPS can only be used after they have been deployed, this will be done after the deployment of the solar arrays and can only be done once.

5.6.3. Maintainability

Physical maintenance is not possible once the CubeSats are in orbit, thus any hardware defects can not be amended. However, the software the components utilise can be reset and updated from the ground. The IMU has its own integrated software package for maintenance and self assessment.

5.6.4. Safety

The following elements were considered critical for the satellite safety:

- **Thruster operation:** the thrusters of the ADCS contain a cold gas green propellant. Therefore, even though a leakage would occur, it is not expected that this could harm other components. A trade-off should be performed in later iterations to evaluate whether the spacecraft can handle a leakage of these thrusters or it should initiate its manoeuvre to be brought to the graveyard orbit.
- **Reaction wheels:** If these components are brought to rotational velocities above their designed values they could fail and harm other spacecraft components. Therefore, a strict control of these design values has to be done in order to avoid this to happen. Furthermore, degradation of these wheels should be taken into account in following iterations to asses how this maximum allowable speed could change over time and the implications of friction in this degradation.

---

[11]https://www.cdc.gov/niosh/idlh/7790912.html, accessed 18/06/2020
[12]http://www.afrox.co.za/en/images/R134a_tcm266-27719.pdf, R134a datasheet, accessed 18/06/2020

5.7. Final design

The final configuration for the ADCs sytem includes six Sun sensors, one Earth sensor, two star sensors, one IMU, one large reaction wheel, three smaller reaction wheels and two MiPS thrusters. All components are available commercially of the shelf. The type and amount of sensors is determined via an iterative process, taking into account all situations the CubeSat encounters. All disturbances, manoeuvres and possible manufacturing misalignments are taken into account by allowing a large margin. The momentum acquired by the reaction wheels about each axis is budgeted and the reaction wheels are sized accordingly. It is determined that MiPS are required for desaturation of the reaction wheels. All components used in the ADCS can be found in table 5.3.

6

Propulsion

This chapter presents the propulsion subsystem design for the LICCA mission. The propulsion system is important since it delivers the thrust needed for manoeuvres during the mission.

6.1. Functional analysis

Before starting the design of a subsystem, first it has to be clear what its functions are. The propulsion subsystem is the engine of the satellite, and has to provide thrust for the entire mission. The required thrust for the launch shall be provided by a launcher, so this should not be accounted for in the subsystem design. The manoeuvres that have to be done during the lifetime of the LICCA mission along with the other functions of the propulsion system are shown in figure 6.1.
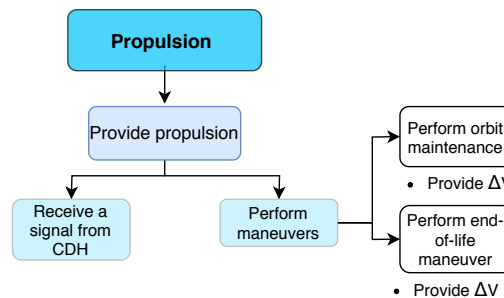
Figure 6.1: Functional breakdown propulsion subsystem

6.2. Requirements

For the propulsion system some requirements were established in the baseline report [3] and are presented below.

Table 6.1: Propulsion requirements

ID	Propulsion
LICCA-SYS-Sub-Prp-1	The propulsion system shall be able to receive signals from the CDH system.
LICCA-SYS-Sub-Prp-2	The propulsion system shall be able to provide 1.49 km/s ΔV for the transfer manoeuvre.
LICCA-SYS-Sub-Prp-3	The propulsion system shall be able to provide 0.0108 km/s ΔV for the end-of-life manoeuvre.
LICCA-SYS-Sub-Prp-4	The propulsion system shall be able to provide 0.129 km/s ΔV for orbit maintenance
LICCA-SYS-Sub-Prp-5	The components of the propulsion subsystem shall have a current TRL level of 7 or higher.
LICCA-ST-Sus-03	The propulsion system shall use sustainable propellant.
LICCA-SYS-Sus-Hm-2	The propellant shall have a Standard Practice for System Safety classification of "critical" or higher.

6.3. Design methodology

As described in section 4.3, the manoeuvres are split up in the different phases of the mission. When designing the subsystem, these four phases are used as well. The required ΔV was calculated for every phase and possible manoeuvre during the lifetime of the mission in section 4.3. The conclusion was reached that the total ΔV required for the mission is 1.82 km/s.

Now that the required ΔV is known, the type of propulsion can be chosen. Three forms of propulsion are considered, namely chemical propulsion, electrical propulsion and a combination of the two. When choosing the type of propulsion, volume and transfer time are important constraints. Logically, more ΔV requires more propellant, and thus more volume is needed for the subsystem. If electrical propulsion is used, a longer transfer time compared to chemical propulsion is required, since electrical propulsion can not do an impulsive shot manoeuvre. This means that a small amount of thrust is applied for a long period of time increasing the orbital parameters until the target orbit is reached.

6.3.1. GTO to GEO transfer

As can be seen in section 4.3, the largest portion of the ΔV-budget comes from the transfer manoeuvre from GTO to GEO. If chemical propulsion were to be used for this, the propellant tank would take up a volume of approximately 9 U. This is far beyond the volume budget allocated to the propulsion subsystem, and therefore considered non-feasible. A second option would be using electric propulsion. However, due to a limited power constraint of 40 W, only little thrust can be generated. This significantly increases transfer time, as can be seen from equation (4.12). For example an IFM Nano Thruster would be selected, based on the principle of Field Emission Electric Propulsion (FEEP)[1]. Given a power of 35 W (with 5 W reserved for communication and positioning during the transfer), this thruster can maximally provide 0.37 mN of thrust, according to the lowest specific impulse within the dynamic range (see figure 6.2). For a GTO to GEO transfer it was calculated that the transfer time will take six years, which would not make much sense for a two years mission. Furthermore, it would certainly not be beneficial for radiation levels and some components would not be able to perform the mission due to radiation. Therefore, solely electric propulsion is also considered as a non-feasible option for the transfer. Finally, a hybrid propulsion system is considered, combining both chemical and electric propulsion. However, since this would imply having two systems implemented, it was found that this would increase volume significantly due to the fact that two thruster systems are needed. Furthermore, the combined system would result only in a slight decrease in transfer time. Therefore, this is not a feasible option. It can be concluded that a transfer from GTO to GEO can not be done by the CubeSat itself, using existing means of propulsion. Technology is rising for small satellites to be transferred by a transfer vehicle towards GEO and not performing the transfer themselves. The transfer vehicle used is elaborated upon in section 12.3.
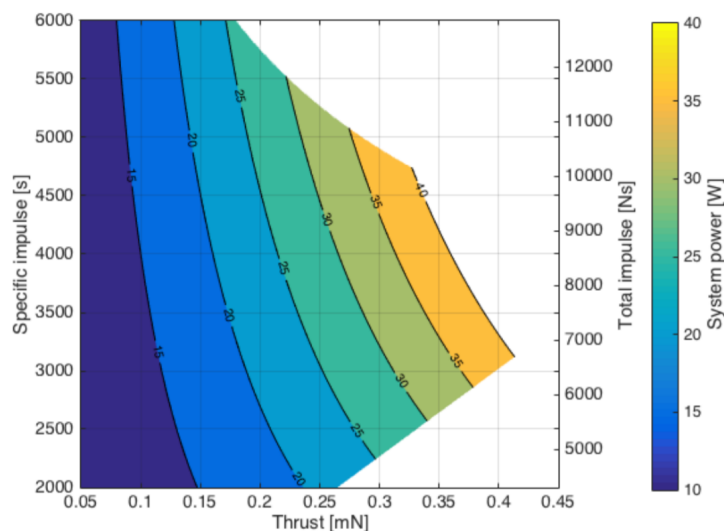
Figure 6.2: Dynamic range of the IFM Nano Thruster COTS+[1]

Disregarding the transfer, only the operational manoeuvres need to be taken into account. These include orbit maintenance, the realignment and the EoL manoeuvre, summing to a ΔV of 367 m/s. Again, the decision has to be made between chemical and electric propulsion. Special attention should be paid towards the realignment manoeuvre. Every 15 days the constellation of satellites should be realigned to compensate for translational drifting. This mission makes use of two constellations, generating two independent data sets. If the realignment is performed at different times for each of the constellations, the other constellation could still measure and data

could always be provided. However, if the electric thruster mentioned above would be used, it is calculated that this realignment would cost nine days, according to the method presented in section 4.3. This means continuous measurements are no longer guaranteed. Following from this, chemical propulsion, which is able to perform the manoeuvre with impulsive shots, is preferred.

6.3.2. Thruster selection
Since it is decided to use chemical propulsion, the thruster can now be selected. Microthrusters for CubeSats were considered, and the ones suitable for this mission are presented in the following. Initially, a thruster is chosen and the first thruster considered is the GR-1 thruster. However, this thruster uses 22 W of nominal operational power [66]. This is too much for this mission since only 40 W is available for the entire satellite. Therefore, the thruster is discarded. The next thruster considered is the Hydros-C thruster. However, similar to the GR-1 thruster, the power of this thruster is in the range from 5-25 W, meaning it is not feasible[2]. Two more thrusters are considered, namely the EPSS C1 and the 1N HPGP thruster. The characteristics of these two thrusters are listed in table 6.2 below.

Table 6.2: Thrusters deemed feasible for the LICCA mission [3] [4]

Type of thruster	Mass [kg]	Volume [U]	Power [W]	Thrust (BoL-EoL) [N]
EPSS C1	3.70	3.41	11.49	1-0.22
1N HPGP	3.84	2.74	8-10	1-0.25

A few things can be taken from table 6.2. First of all is that the mass and thrust are similar, so these will not be the decisive criteria. Secondly, the power of the HPGP seems lower. However, two things have to be noted: the power of the EPSS includes 9.6W of preheat power which does not have to be used constantly during the mission. The other thing is that the power of the HPGP is purely preheat power and no information is available about the operational power consumption. Lastly, the volume is an important factor in designing a CubeSat. Note that the volume presented in table 6.2 is the volume the propulsion subsystem would have, if that specific thruster would be used. The HPGP system is smaller than the EPSS, since the EPSS already incorporates a small propellant tank and feed system. However, it is decided that this tank will not be used, since a much bigger tank is needed for the LICCA mission.

To conclude, the two thrusters are similar. Although it seems that the 1N HPGP thruster is slightly better due to its lower volume, much is known about the safety features of the EPSS C1 thruster. Another aspect is that the EPSS C1 thruster already incorporates a feed system, and no information was found on a feed system compatible with the 1N HPGP thruster. Furthermore, not much is known about the software of the HPGP and since the operational power is also unknown, it is decided that the EPSS C1 thruster will be used for the LICCA mission.

6.3.3. Propellant selection and tank sizing
The next step in designing the propulsion subsystem is to determine the propellant that is going to be used. There are some constraints, since it was decided to use chemical propulsion and a green propellant is required (LICCA-ST-Sus-03). The propellant should be compatible with the thruster, namely ammonium dinitramide based (ADN). An important feature of the propellant is the density, since this is directly related to volume. The higher the density of the propellant, the lower the required volume, which is essential in designing a CubeSat. Therefore, research was conducted into high density, green propellants. Upon recommendation of Dr. K.V. Mani from the Politecnico di Milano (an expert in Space Systems and Propulsion), LMP-103S was chosen as propellant[5], which is ADN based and has a density of 1.26 g/cm^3.

Now that the propellant volume and characteristics are known, the propellant tank can be sized. The material used is Ti-6Al-4V because of its strength[6]. The optimal shape for a pressure vessel is a cylindrical tank. However, this is not an optimal shape to implement in a rectangular CubeSat. A rectangular tank is chosen and to counteract stress concentrations in sharp edges, the corners are rounded. The size of the tank is determined as follows. To fit in the configuration of the CubeSat, it was determined that the tank should have a height of 10 cm and a length of 20 cm. The width of the tank then is determined by the propellant volume. A margin of 10% in the volume is accounted for the rounded corners. The thickness of the tank is determined using equation (6.2), [40], for which the crossectional area A_{cs} needed to handle the loads can be taken from equation (6.1). The propellant in the tank is pressurized to 22 bar and a safety margin of 10% is used [75, p.60]. To calculate the thickness, the width and height are taken, since this would give the smallest cross-sectional area to carry the loads and thus the largest thickness. For simplicity, this thickness is used for the entire tank. However, the

---

[2] https://www.tethers.com/wp-content/uploads/2019/09/2019-HYDROS.pdf, Hydros-C datasheet, accessed 11/06/2020
[3] https://nanoavionics.com/cubesat..., datasheet EPSS C1, accessed 11/06/2020
[4] https://www.ecaps.space/products-1n.php, datasheet 1N HPGP, accessed 11/06/2020
[5] https://www.ecaps.space/hpgp-performance.php, LMP-103S propellant, accessed 11/06/2020
[6] http://asm.matweb.com/search/SpecificMaterial.asp?bassnum=MTP641, Ti-6Al-4V datasheet, accessed 08/06/2020

tank has to be manufactured. Therefore it is important to know the minimum required thickness to manufacture titanium. It is found that this minimum thickness is 0.2 mm [50] [31]. Since the calculated thickness is lower than this, namely 0.10 mm, it is decided to extend the thickness to 0.2 mm. Knowing the dimensions and material properties of the tank, its added volume (excluding internal volume for propellant) and mass can be determined.

$$F_{tank} = p \cdot A_{enc} = \sigma \cdot A_{cs} \qquad (6.1)$$

$$V_{tank} = (2wh + 2wl + 2hl) \cdot t_{tank} \qquad (6.3)$$

$$t_{tank} = \frac{A_{cs}}{2w + 2h} \qquad (6.2)$$

$$m_{tank} = V_{tank} \cdot \rho \qquad (6.4)$$

A final remark regarding the propulsion subsystem design is the burn time. It was found that during operations of the thruster no measurements can be taken, as explained in section 4.3. The burn time can be calculated as the propellant mass needed for the manoeuvre divided by the mass flow. For the realignment manoeuvre the propellant mass needed is 30.6 g. At BoL the burn time is 65 seconds with a mass flow of $4.68 \cdot 10^{-4}$ kg/s. At EoL the burn time is 4 and a half minutes with a mass flow of $1.14 \cdot 10^{-4}$ kg/s. For one realignment, three burns are needed, as already explained in section 4.3.

6.4. Risk

In order to analyse the different risk for the propulsion subsystem, the tank and propellant are taken into account. Since the chosen thruster has a lot of safety features, for example thruster catalyst heater protections, which are implemented in the software, the risk of a potential thruster failure does not seem significant.

There are two major risks concerning the propellant tank. A rectangular tank was chosen to optimise the volume within the CubeSat. Although the edges of this rectangular tank are rounded, it is still not an optimal shape for a pressurised vessel. Therefore stress concentrations might occur which can potentially lead to failure of the tank. When this event occurs, the mission will no longer be able to continue due to leakage of propellant. This leakage in general is also a risk concerning the tank [23, p.56]. If a tiny hole is present in the tank, propellant might leak affecting other subsystems. It would also mean that there is less propellant available to use. The combination of these two events would be catastrophic for the continuation of the mission.

The third and final risk discussed in this section concerns the EoL manoeuvre. It is important to do this manoeuvre to make sure that the satellites do not orbit in GEO anymore. Sending them to a graveyard orbit lowers the risk of potential space debris. Therefore it is crucial to perform this manoeuvre to not overcrowd GEO with dead satellites. To conclude, the risk is that the EoL manoeuvre can not be performed due to lack of propellant or power for example, causing space debris.

6.5. Sustainability

An important requirement regarding sustainability is LICCA-ST-Sus-03: "The propulsion system shall use sustainable propellant." The most significant variable in a sustainability analysis of the propulsion is the propellant. The propellant is considered clean if it does not exhaust green house gasses. An approach to implement this in the design was already determined in the Baseline report [3]. The sustainability of the propellant can be quantified based on the Toxic and Environmental Hazard Figure (TEHF), as stated in subrequirement LICCA-SYS-Sus-Hm-1.4. The propellant used is ADN-based, which is generally considered non-toxic for humans [53]. However, in a certain dose it is lethal, making the calculated TEHF 0.0023. On the scale of TEHF this is considered negligible and thus zero [34]. This means the propellant can be considered clean and thus sustainable. Another measure for sustainability of the propellant is the Standard Practice for System Safety classification. A classification of "critical" implies less probability of leakage. This reduces the safety measures for the propellant tank in the spacecraft itself, as well as for the infrastructure of manufacturing and testing [23, p.56].

Extra fuel is taken along for extension of the lifetime or unexpected manoeuvres. This propellant should be burnt at the EoL, such that it cannot form any hazard when the system is shut down and uncontrolled. Lastly, the propulsion system will also take care of the EoL manoeuvre, a transfer to a graveyard orbit. This prohibits the satellite from becoming space debris.

6.6. RAMS

In this section, the reliability, availability, maintainability and safety characteristics of the propulsion subsystem are presented.

6.6.1. Reliability

Since no maintenance is possible in orbit, a high reliability of the system is needed. The thruster chosen is tested, flight-proven and safe, and thus considered highly reliable. The propellant accounts for maximum drift and orbit maintenance, thus it can be assured that every manoeuvre can be performed during the lifetime of the mission.

From statistical data it can be seen that the propulsion subsystem usually is not a major factor in CubeSat failure [46]. Complimentary, the in section 6.4 defined risks have a low probability since the system includes multiple safety features. Therefore it can be concluded that the propulsion subsystem is highly reliable.

6.6.2. Availability

The thruster should be preheated in order to be able to fire. This preheat uses a significant amount of power, which should be available. If all other subsystems use their entire power budget at that moment, the preheat is not possible. The probability of this situation is however very small, since for example communication only uses its nominal power once a day.

Another aspect of availability is the influence of the propulsion system on measurements. During a burn, the satellite is rotated in the direction of the burn. Also, firing the thruster generates a lot of noise which is not beneficial for the measurement signal. This concludes to the measurements not being available during operation of the thrusters. For simple orbit maintenance and realignment this happens every 15 days for approximately 15 minutes at BoL, including rotation, and up to 25 and a half minutes at EoL.

6.6.3. Maintainability

Maintenance is not possible nor accounted for during operations. The thruster has its own integrated software package for regulation and safety features. This could be updated in orbit when an update is provided by the manufacturer, compatible with the system and if the processor of the On-Board Computer (OBC) is available. This will only be done when it is necessary to continue the mission and unavoidable.

6.6.4. Safety

A safety critical function of this subsystem is the functioning of the thruster. However the system has a lot of safety features built in by the manufacturer: overheat, overcurrent, and freeze protection for thruster, tank and feed system, overpressure protection, single event upset resistant circuits, redundant switches and sensors, and even more[7].

The propellant is considered safe since it is non-flammable without a catalyst. The propellant tank will need leakage seals for safety measures. Also additional valves could be implemented, however this is not needed for a safe propellant. As mentioned in section 6.5, the propellant should be burnt entirely at EoL to avoid any unexpected hazards.

6.7. Final design

The final design for the propulsion subsystem was obtained using the methodology of section 6.3. It was determined that chemical propulsion will be used since electrical propulsion is not feasible for the realignment. The GTO to GEO transfer will not be taken into account due to the too high required ΔV and thus too much volume would be needed for the propellant. The thruster selected for the mission is the EPSS C1 thruster and the propellant used is LMP-103S. A feed system is already incorporated in the thruster module. A rectangular titanium tank with rounded corners to reduce stress concentrations is chosen. In table 6.3 the final properties of the system are shown.

Table 6.3: Final properties of the propulsion subsystem

Property	Value	Unit	Property	Value	Unit
Final properties			*Tank*		
Mass	4.40	kg	Cross sectional area	0.55	cm^2
Power	11.49	W	Enclosed area	0.02	m^2
Volume	3.98	U	Force	48400	N
Thruster			Width	0.16	m
Mass	0.9	kg	Mass	121	g
Thrust	1-0.22	N	Pressure	24.2	bar
Volume	1.01	U	Thickness	0.2	mm
Propellant			Volume	3.21	U
Mass	3.38	kg	Density	4.43	g/cm^3
Volume	2.67	U	Stress	968	MPa
Density	1.26	g/cm^3			

---

[7]https://nanoavionics.com/cubesat-components/cubesat-propulsion-system-epss/, accessed 12/06/20

7

Telemetry, Tracking & Command

In this chapter, the detailed design of the Telemetry, Tracking & Command (TT&C) subsystem is presented. This subsystem is needed to allow for communication between the ground stations and the satellites, making uploading commands to the satellites and downloading the scientific payload data possible. Furthermore, it also allows for tracking of the satellites in orbit.

7.1. Functional analysis

In previous stages of this project, the TT&C and Navigation were considered to be two separate subsystems. The main functions of the TT&C can be defined as follows:

- **Telemetry:** The telemetry downlink provides the ground segment with the information gathered from the scientific measurements. Information on the status of the spacecraft is also provided in the telemetry downlink of the housekeeping data.
- **Tracking:** Tracking can be defined as measuring the position as well as direction and magnitude of the motion of a spacecraft. It can be noted that navigation entails using this tracking information to then control the movement of the spacecraft.
- **(Tele)command:** The command uplink is used by the ground segment to provide commands to the spacecraft for its operation.

From this point it is clarified that the "tracking" part of TT&C will be designed to provide the inputs needed for navigation. The navigation itself will not be a responsibility of the TT&C subsystem, but rather a part of the control architecture of the mission.

Before initiating the design, the functions to be performed by the subsystem have to be identified. In the functional breakdown structure presented in the baseline report, preliminary functions were identified [3, p. 4]. The updated functional breakdown structure is shown below in figure 7.1. It can be seen that based on the above descriptions, the functions needed for the telemetry and telecommand parts can be combined. During the detailed design phase, more specific and accurate functions were identified for these parts, resulting in a new functional breakdown structure.

For the tracking part, instead, it was not possible to determine specific functions at the beginning of the of the detailed design phase. This is due to the fact there are several tracking methods that can be used, which differ greatly in the measurement principles that are used. For example, the functions pertaining to tracking performed by a ground station or space-based system rather than an on-board tracking system will be different. For this reason, the functional breakdown is now kept general, and will be specified in more detail once a tracking method is chosen.
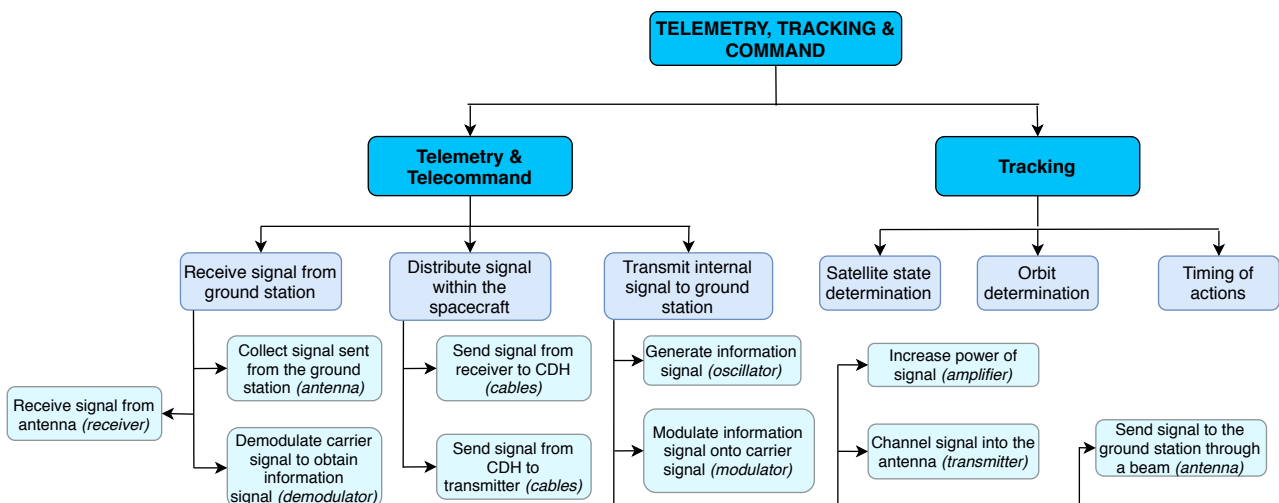
Figure 7.1: Functional breakdown structure of T&T subsystem

7.2. Requirements

During the mission definition and exploration phase, technical requirements were identified. Some of these have been discarded in this design phase, as they would drive the design to an extent outside the scope of the mission. These are presented in table 7.1, below.

Table 7.1: Technical requirements for communication subsystem

ID	Navigation
LICCA-SYS-Sub-Nav-1	The navigation system shall determine the velocity of the satellite, relative to the earth, with an accuracy of 1.0 meter per second (3σ).
LICCA-SYS-Sub-Nav-2	The navigation system shall determine the position of the satellite, relative to the earth, with an accuracy of 1000 meters (3σ).
LICCA-SYS-Sub-Nav-3	DELETED
LICCA-SYS-Sub-Nav-4	DELETED
LICCA-SYS-Sub-Nav-5	DELETED
LICCA-SYS-Sub-Nav-6	The navigation shall communicate the position of the satellite with the CDH.
LICCA-SYS-Sub-Nav-7	The components of the navigation subsystem shall have a current TRL of 7 or higher.
	TT&C
LICCA-SYS-Sub-TTC-1	The TT&C system shall receive the scientific data from the CDH system.
LICCA-SYS-Sub-TTC-2	The TT&C system shall receive the spacecraft housekeeping data from the CDH system.
LICCA-SYS-Sub-TTC-3	The time required for a downlink shall not exceed 1 hour.
LICCA-SYS-Sub-TTC-4	The TT&C system shall modulate the digital signals that are to be downlinked.
LICCA-SYS-Sub-TTC-5	DELETED
LICCA-SYS-Sub-TTC-6	DELETED
LICCA-SYS-Sub-TTC-7	DELETED
LICCA-SYS-Sub-TTC-8	DELETED
LICCA-SYS-Sub-TTC-9	The TT&C system shall demodulate the received uplink signals.
LICCA-SYS-Sub-TTC-10	DELETED
LICCA-SYS-Sub-TTC-11	The TT&C system shall transfer uplink data to the CDH system.
LICCA-SYS-Sub-TTC-12	The TT&C system shall be able to receive a shutdown command from the ground station at any point during the mission.
LICCA-SYS-Sub-TTC-13	The bit error probability shall not be greater than 10^{-6} for the uplink.
LICCA-SYS-Sub-TTC-14	The bit error probability shall not be greater than 10^{-6} for the downlink.
LICCA-SYS-Sub-TTC-15	The components of communication subsystem shall have a current TRL of 7 or higher.

Regulations

On top of customer and technical requirements, the design of the communication subsystem has to take into consideration constraints stemming from international, regional and national regulations. These are necessary as the radio frequency spectrum and the geostationary orbits are finite resources, hence the use of different frequencies by different stations has to be regulated, to avoid interference between different services and regions [42, p. 212]. The body coordinating these regulations and ensuring compatibility between the national systems worldwide is the International Telecommunication Union (ITU). Yet, it does not enforce these regulations, as the principle behind them is the voluntary undertaking of them. Important parameters for ITU regulations are the following [32, p. 422]:

- Allocated frequency band.
- Orbital location: this needs to be negotiated between the different satellite networks through the Space Service Department. This is necessary in order to provide sufficient separation between spacecrafts, allowing ground stations' antennae to discriminate between them.
- Maximum permitted power flux density at Earth's surface.

In order to obtain permission from the ITU, an application needs to be sent and approved. This process can take up to two years, hence it was omitted for this report and is going to be left as a recommendation for the further development of this mission [14, slide 41]. By looking at other CubeSat missions, such as the Delfi-n3xt [69], and at ITU standards, the requirements presented in table 7.2 were identified.

Table 7.2: Regulations requirements for communication subsystem

ID	Regulations Requirements
LICCA-SYS-Comm-Reg-01	The spacecraft shall be able to switch off any transmitter on board.
LICCA-SYS-Comm-Reg-02	Any data transmitted to the spacecraft, other than telecommands, shall not be encrypted.
LICCA-SYS-Comm-Reg-03	Any data transmitted from the spacecraft shall not be encrypted.
LICCA-SYS-Comm-Reg-04	In case of S-band usage, the channel used must be narrower than 6 MHz, for both uplink and downlink.
LICCA-SYS-Comm-Reg-05	In case of UHF usage, the channel used must be narrower than 25 kHz, for both uplink and downlink.

The first requirement stems from the need to be able to remove possible interference in case of emergencies in which the used bandwidth would be important. The second and third stem from the amateur nature of the UHF band, which makes it common practice to provide access to other amateurs to the spacecraft's data. The fourth and fifth requirements stem from ITU regulations, based on the most frequently used bandwidth in the CubeSat sector [37]. Note that, due to time constraint, it was not possible to specify the chosen bandwidth to the extent required by the last two requirements, as this requires obtaining specific data on the current bandwidth allocation of those frequencies, which is considered outside the scope of this project.

To keep track of the changes applied to the requirements and to better explain the rationale behind these changes, a change log is added, shown in table table 7.3.

Table 7.3: Requirements changelog

ID	Change	Rationale
LICCA-SYS-Sub-Nav-3	Removed	The tracking part of the TT&C will determine the orbital position and relative velocity, as specified in LICCA-SYS-Sub-Nav-1 and LICCA-SYS-Sub-Nav-2. Other necessary parameters can be derived from these and would be computed on the ground.
LICCA-SYS-Sub-Nav-4	Removed	The TT&C will not be responsible for any computations, this will be done on the ground.
LICCA-SYS-Sub-Nav-5	Removed	The TT&C will not be responsible for any computations, this will be done on the ground.
LICCA-SYS-Sub-TTC-5	Removed	Encryption methods have not been looked into, but are left as recommendation.
LICCA-SYS-Sub-TTC-6	Removed	Required data rate is already specified in user requirement "LICCA-SYS-Bud-05".
LICCA-SYS-Sub-TTC-7	Removed	Required data rate is already specified in user requirement "LICCA-SYS-Bud-05".
LICCA-SYS-Sub-TTC-10	Removed	Encryption methods have not been looked into, but are left as recommendation.
LICCA-SYS-Comm-Reg-01	Added	Regulations have been looked into as of this design phase.
LICCA-SYS-Comm-Reg-02	Added	Regulations have been looked into as of this design phase.
LICCA-SYS-Comm-Reg-03	Added	Regulations have been looked into as of this design phase.
LICCA-SYS-Comm-Reg-04	Added	Regulations have been looked into as of this design phase.
LICCA-SYS-Comm-Reg-05	Added	Regulations have been looked into as of this design phase.

7.3. Design methodology: telemetry & telecommand

This section will describe the approach for the design of the communications of the mission, namely the telemetry subsystem. First, section 7.3.1 will provide an overview of the literature study performed, which was done to gain background knowledge and served as a starting point for the design. Then, the link budget is presented in section 7.3.2. This section also describes how the link budget was used throughout the iterations, as well as how it led to the final design of the subsystem, which is presented later in section 7.8.

7.3.1. General overview

The undermentioned basic elements of an Earth-space communication link can be identified based on the functional analysis described in section 7.1. The link consists of the ground segment and the space segment. In each direction, it is desired to transfer an information signal from one segment to the other. This is first done by modulating the information onto a carrier signal, which is done with a modulator. This signal can then be sent by the transmitter, and can be directed towards the receiver by an antenna. In a transceiver, the function of transmitting and receiving is combined into one component. For simplicity, the term transceiver will be used to refer to these. Upon receiving the signal, it is then demodulated to obtain the desired information. All of the mentioned elements should be present in both segments.

Several main characteristics that influence the performance of the communication subsystem can be identified. Their exact contribution will be explained in the link budget in section 7.3.2. These characteristics will also influence what design options are needed of the system. They are briefly mentioned below:

- **Size of message & Data rate:** It is desired to send a certain number of bits in each transmission. The rate at which this occurs is governed by the data rate. In traditional CubeSat missions operating in LEO, it is usually desired to 'maximise' the data rate, since the satellite is only in contact with the ground station for limited time during each pass. The LICCA CubeSats will operate in GEO, meaning that the contact time will not be a limitation. The data rate is instead limited by the requirement LICCA-SYS-Bud-05. Still, the transmission should not take too long such that the ground stations are not used excessively, making a higher data rate more efficient.
- **Quality of transmission & Power of signal:** There are many parameters that govern the quality of the transmitted signal. The link budget is used to determine if this quality is sufficient, and is described in detail in section 7.3.2. One of the main aspects is the power of the signal. The transmitted signal will experience several types of losses on its journey between the segments. There will also be noise present in the system, from which the signal should be able to be distinguished. The subsystem should be designed such that enough power is left in the signal for it to be received successfully. This will influence the choice of antenna and transceiver on board the satellite, since they will need to be able to provide this power. The ground station also plays a role in the signal power, though it is less constrained than the space segment. Therefore, more powerful ground systems can be used to compensate for the limitations on board the satellites.
- **Frequency & Bandwidth:** The carrier signal that is used will have a certain frequency. Since the electromagnetic spectrum is limited, frequency use is regulated by the ITU, as described in section 7.2. The selected frequency will also affect the choice in components and ground stations. The bandwidth dictates the width of the spectrum that is used for the transmission, which should also comply with ITU regulations. The bandwidth has an influence on the rate at which the data can be sent, a larger bandwidth allows for more data to be sent at the same time.
- **Interface between segments & Ground coverage of satellites:** As previously mentioned, both segments must have the components required to make a communication link. This interface must be compatible, in the sense that selected frequencies and modulation method should match. Also as previously mentioned, the LICCA CubeSats will be orbiting in GEO, which provides a constant view of the same portion of the Earth. The ground stations will have to be chosen such that they are in view of the satellites. Furthermore, the satellites will have a longitudinal separation of 120 degrees. This means that several ground stations will need to be used.

Typically, the approach for designing the components of the communications subsystem first starts with performing the link budget calculations. From this, the required parameters such as the antenna aperture size and transmitter power can be determined and sized accordingly. The system requirement LICCA-SYS-Sub-1 states: *The use of COTS components for the system shall be maximised*. For this reason, the approach for the design of the LICCA communications subsystem is flipped. First, a number of COTS components are identified. Then, the link budget will be used to evaluate if the components are suitable. From the remaining suitable candidates, a trade-off will be performed to select the best option.

A preliminary study of typical CubeSat communications subsystems was performed, along with an investigation of what COTS components are currently on the market. As previously mentioned, it has been identified that the main elements needed on each end of the link are an antenna and a transceiver. It is assumed that the COTS transceivers are complete solutions, meaning that they will include the necessary radio elements, such as filters, amplifiers, oscillators, modulator/demodulators, and encoders/decoders. The main difference between the COTS options stem from what frequency band is used. This affects the data rate, the on-board antenna properties, and also the choice in ground station. An overview of the frequencies commonly used in CubeSats is given below:

- **VHF & UHF:** The frequencies often used within VHF and UHF bands are around the ranges of 145-150 MHz and 400-440 MHz respectively. They are typically used with monopole or dipole antennae on the spacecraft, and Yagi antennae on the ground. As mentioned before, the ground stations can be built to be more powerful to compensate for the limited capabilities of the space segment. Typically, the VHF/UHF ground antennae are not too large as compared to dish antennae used for higher frequencies. They

are able to provide enough gain to signals that do not experience high losses. Therefore, VHF/UHF is often used in CubeSats orbiting in LEO, which are relatively close to Earth. However, the data rate in the VHF/UHF systems is often low, usually around 9.6 kbps. This can be sufficient for uplinking commands, though for downlinking large data this rate can be limiting.

- **S-band:** Frequencies of around 2025-2110 MHz for uplink and 2200-2290 MHz for downlink are also commonly found solutions for CubeSats, which are in the S-band. The on-board antennae that are available for this are patch antennae. On the ground, dish antennae are commonly used, ranging from diameters of 3 to 70 meters. The actual diameter needed from the antenna can be found from the link budget. The data rate in the S-band varies quite a bit among available COTS options. Values start at 128 kpbs and can reach up to 20 Mbps in some options.
- **X-band:** Lastly, even the X-band can be used in CubeSats, with frequencies of around 8025-8400 MHz. Similar to the S-band, patch antennae are used on board the satellites and dish antennae are used on the ground as well. Due to the higher frequencies, the data rate can reach up to 50 Mbps in some COTS options.

7.3.2. Link budget

The link budget is a key part of the TT&C subsystem. It allows to see how and at which rate the data from the satellites can be transmitted to the ground and vice versa. There is a very wide variety of options for the components of the spacecraft communication subsystem. For high-budget space missions, those components can even be designed individually. However, LICCA satellites will mostly rely on COTS components, as these are cheaper and often already tested for space missions. Thus, the LICCA's link budget is constrained by the properties offered by COTS components.

This section explains in detail the process of the link budget calculation. Overall, this process can be split in three iterations, representing the improvements made subsequently in order to reach the desired links. A preliminary version of the link budget was calculated in the Midterm Report [5, p. 44], and is referred to as the 'zeroth' iteration. This was used to give the design team an initial idea of the order of magnitude of the numbers to be considered for the links.

First iteration

In the first iteration, the general equations for the link budget calculation were identified [14]. Values for variables in those equations were estimated using either literature [32, 42, 72] or statistical data. The first equation starting the link budget is equation (7.1) with which the power flux density W_f can be calculated:

$$W_f = \frac{P \cdot L_l \cdot G_t}{4\pi S^2} = \frac{EIRP}{4\pi S^2} \tag{7.1}$$

where P is the power of the signal generated by transmitter, L_l is the loss factor from transmitter to antenna, G_t is the transmitting antenna gain, S is the distance between the transmitting and receiving antennae, and $EIRP$ is the effective isotropic radiated power.

This signal is then received by an antenna and receiver. The received power C can be calculated using equation (7.2) and equals to the product of power flux density W_f that reaches the antenna and the effective receiver aperture area A_r:

$$C = W_f \cdot A_r = \left(\frac{P \cdot L_l \cdot G_t \cdot L_a}{4\pi S^2}\right) \cdot \left(\frac{\pi \cdot D_r^2}{4} \eta\right) \tag{7.2}$$

In equation (7.2), the left hand side parentheses is the equation for W_f with additional atmosphere loss factor L_a that includes tropospheric and ionospheric attenuations. The right hand side parentheses describe area A_r, where D_r is the receiving antenna diameter and η is the receiving antenna efficiency.

The receiving antenna also has gain G_r which is defined as ratio of its effective aperture are A_r to the effective area of an isotropic antenna A_{is}. Area A_{is} is equal, by definition, to $(\lambda^2/4\pi)$ where λ is the wavelength of the transmitted signal and can be found by the simple relation $\lambda = c/f$ between the speed of light c and the signal frequency f. The antenna gain G_r therefore is calculated by equation (7.3):

$$G_r = \frac{A_r}{\lambda^2/4\pi} = \frac{(\pi \cdot D_r^2/4) \cdot \eta}{\lambda^2/4\pi} = \frac{\pi^2 \cdot D_r^2}{\lambda^2} \eta \tag{7.3}$$

The received power C is shown in equation (7.4), where space loss L_s is introduced and is equal to $(\lambda/4\pi S)^2$. The space loss is caused by the signal power dispersion during transmission.

$$C = \frac{P \cdot L_l \cdot G_t \cdot L_a \cdot D_r^2 \cdot \eta}{16S^2} = \frac{P \cdot L_l \cdot G_t \cdot L_a \cdot G_r}{16S^2} \cdot \frac{\lambda^2}{\pi^2} = P \cdot L_l \cdot G_t \cdot L_a \cdot G_r \cdot L_s \tag{7.4}$$

There are also reception losses, namely the antenna pointing loss L_{pr} and the reception feeder loss L_r. The antenna pointing loss can be calculated in decibels for each antenna with equation (7.5):

$$L_{pr} \text{ [dB]} = -12 \cdot \left(\frac{e_t}{\alpha_{1/2}} \right)^2 \tag{7.5}$$

Where e_t is the pointing offset angle and $\alpha_{1/2}$ is the antenna half power beamwidth. Note that this loss is given in decibels and must be converted to linear units when calculation is done in SI units. Reception feeder loss L_r is similar to the transmitting feed line loss L_l but on the receiving side and accounts for other losses occurring in the reception chain. Once these losses are included, the updated equation of the received power C is given by equation (7.6):

$$C = P \cdot L_l \cdot G_t \cdot L_a \cdot G_r \cdot L_s \cdot L_{pr} \cdot L_r \tag{7.6}$$

Once C is known, the received energy per bit E_b can be obtained with equation (7.7):

$$E_b = C \cdot \frac{1}{R} = \frac{P \cdot L_l \cdot G_t \cdot L_a \cdot G_r \cdot L_s \cdot L_{pr} \cdot L_r}{R} \tag{7.7}$$

where relation $1/R$ is the inverse of data rate R (expressed in bits/s) and denotes the duration of a single bit.

Besides the signal, the noise caused by random thermal motions of atoms and electrons in each component of the system has and impact on the link budget. The total received noise power over a given bandwidth is given by equation (7.8):

$$N = N_0 \cdot B \tag{7.8}$$

where N_0 is the white noise spectral density and B is the channel bandwidth. As mentioned above, the noise is caused by thermal motions, hence, it is convenient to express it with system noise temperature T_s:

$$N_0 = k \cdot T_s \tag{7.9} \qquad\qquad N = N_0 \cdot B = k \cdot T_s \cdot B \tag{7.10}$$

k Is the Boltzmann's constant. It also should be noted that noise temperature is not the actual physical temperature of a system or component and the two may differ.

Finally, E_b can be divided by N_0 to obtain the signal-to-noise ratio (SNR) for the link between ground and satellite:

$$SNR = \frac{E_b}{N_0} = \frac{E_b}{k \cdot T_s} = \frac{P \cdot L_l \cdot G_t \cdot L_a \cdot G_r \cdot L_s \cdot L_{pr} \cdot L_r}{R \cdot k \cdot T_s} \tag{7.11}$$

Equation (7.11) is called a *link equation*. This equation is fundamental for the link budget and it will be used in each iteration when updating the link budget. An overview of the gains and losses experienced by the transmission throughout the link budget is shown in figure 7.2. The example link shown in this figure is a downlink from the spacecraft to the ground station on Earth, and would have similar parameters if an uplink was considered.
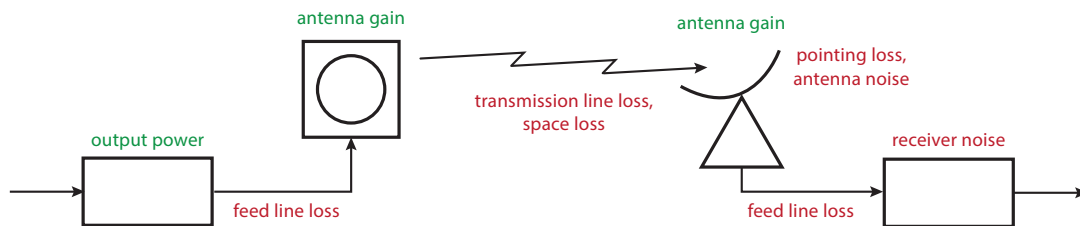
Figure 7.2: Overview of gains and losses experienced during transmission of a downlink.

Lastly, in the link budget the quantity differences are often too large, spanning from orders of magnitude of 10^{-23} to 10^4, or even higher. This makes the link equation more complex and less readable when such quantities are multiplied or divided. Thus, it is more convenient to express these terms in decibels. The use of decibels allows to add and subtract values instead of multiplying and dividing them, as well making the range of values not as large as in linear scale. Equation (7.12) demonstrates SNR expressed in decibels. It can be seen that denominator parameters from equation (7.11) are subtracted while numerator parameters are added which corresponds to logarithmic properties:

$$\frac{E_b}{N_0}[\text{dB}] = P + L_l + G_t + L_a + G_r + L_s + L_{pr} - 10 \log_{10} k - 10 \log_{10} R - 10 \log_{10} T_s \tag{7.12}$$

While a similar procedure was performed for the zeroth iteration in the Midterm Report [5], some parameters were missing and values, estimated for parameters present there, were not tailored to this specific mission. During the first iteration, however, more reasonable and realistic values for a space mission were identified. These values were found from other space missions [69] or in literature [32, 42, 72]. Nonetheless, the range of the final results was still too broad. Thus, a second iteration was indeed required to narrow down the link budget range.

Second iteration

In the second iteration, several options for COTS components were identified, which allowed to determine more realistic values for each parameter used in the link budget equations. Namely, the components for the "satellite side" were transmitters, receivers, transceivers, and antennae for VHF/UHF, S-band and X-band frequencies. The bands of frequencies taken under consideration are the most common ones for the CubeSats. These options can be seen in table 7.4. From that, realistic values for almost each parameter were obtained, with exception of individual parameters for some of the components, as those simply were not given. When it was the case, the average value of the other components was used.

The IG Spacecom transceiver operating in X-band was discarded at once as its power consumption is too high, given a 40 W constraint for the entire satellite. This left COTS components options for VHF, UHF and S-band only.

An initial selection of the ground stations was carried out in the Midterm report [5, p. 45], but a more detailed analysis was required for a more accurate selection. Concerning the ground segment, there were options of portable ground stations and those were also included in the list of possible options. Of course, a list of "fixed" ground stations was made as well because it was not clear if the portable ground stations, that have relatively small antennae, would be sufficient. This list is shown in table 7.5. Operating band, antenna dish diameter, and location are shown as well to give a general overview of these stations. All "fixed" ground station either belong to ESA/ESTRACK (European Space Tracking) or used by ESA as a part of their cooperative network.

Table 7.4: List of COTS components for the telemetry subsystem of a LICCA satellite

Manufacturer	Frequency band	Manufacturer	Frequency band
Transmitters		Receivers	
Endurosat[1]	S	Endurosat[1]	S
ISIS[2]	S	Nanoavionics (with Satlab)[3]	VHF
Nanoavionics[3]	S	Satlab[4]	VHF
IQ Spacecom[5]	S	Transceivers	
AAC Clyde Space[6]	S	Nanoavionics	S
Antennae		ISIS	S
Endurosat	S	GOMspace	S
GOMspace	S	Satlab	S
ISIS	S	IG Spacecom	S
Nanoavionics	S	Endurosat	UHF
IQ Spacecom	S	ISIS	UHF
Endurosat	UHF	Nanoavionics	UHF
ISIS	VHF/UHF	GOMspace	VHF/UHF
Nanoavionics	UHF	ISIS	VHF uplink, UHF downlink
		IG Spacecom	X

Table 7.5: List of options for ground stations

Ground station	Location	Band	Antenna diameter
Cebreros	Madrid	X, K_a	35 m
New Norcia	Perth	S, X	35 m
Malargüe	Buenos Aires	X, K, K_a	35 m
Kourou	French Guiana	S, X	15 m
Kiruna	Sweden	S, X	15 m, 13 m
Redu	Belgium	S , K_a	15 m, 13 m, 2.4 m
Santa Maria	Azores	S	5.5 m
South Point	Hawaii	S, X, K_u	13 m
Santiago	Chile	S, C, K_a	9 m, 12 m, 13 m
Troll	Antarctica	S, C, X	7.3 m
Svalbard	Norway	L, S, C, X, K	11.3 m, 13 m
Dongara	Close to Perth	S, X, K_a, K_u	13 m
TU Delft	Portable	VHF, UHF S (Rx only)	3m
ISIS	Portable	VHF, UHF S (Rx only)	3m
GOMspace	Portable	UHF, S	1.3 m
GAUSS Srl	Portable	VHF, UHF, S	1.5 m

Once ground stations and components were identified, the selection process began in order to find the most advantageous combination. First of all, the ground stations located too far in the North or South were discarded. Since the satellites will be in GEO above equator, having ground stations closer to the equator is more beneficial. This resulted in discarding Kiruna, Troll and Svalbard ground stations. Secondly, it was calculated that using deep space ground stations with very big antennae is also not necessary as a 12-15 m diameter antenna is sufficient. Furthermore, these big antennae operate in X band or higher frequencies, for which COTS components were not identified. Thus, Cebreros, New Norcia, and Malargüe ground stations were discarded. Then, it was calculated that the Santa Maria antenna of 5.5 m diameter was too small for a CubeSat in GEO operating in S-band, and was discarded as well. Finally, due to the European nature of this project, ground stations belonging to ESA are of a higher priority when selecting, thus, Santiago and South Point ground stations were discarded as these belong to Swedish Space Corporation.

After identifying the most suitable ground stations, the ground coverage of the satellites was analysed. By definition, the satellites will be above the equator as they are in geostationary orbit. The ground coverage of GEO satellites suitable enough for communications is approximately 70 degrees from the subsatellite point [42, p. 48]. Furthermore, the satellites of one constellation will be positioned with a longitudinal separation of 120 degrees with respect to each other. It should be noted that the satellites will be positioned in pairs consisting of one satellite for each of the two constellations, such that they can be injected into orbit at the same time. Along with this, one ground station can be used for each pair. That means that three ground stations will be used. The approximate positions across the world can be described as The Americas, Europe, and Australia.

In figure 7.3 the proposed distribution of the satellites is shown, only one constellation is included for simplicity. For each satellite, the ground coverage is approximated as 70×70 degrees. In reality, the coverage area is rounded when projected onto the earth, meaning that positioning the satellites in the corners should be avoided. Furthermore, the borders of the coverage area of each satellite are indicated by the dashed lines in the corresponding colors, and it can be seen that there is a slight overlap in the areas of each satellite. The positions can be summarised as follows. Satellite A is positioned at 110° West, satellite B at 10° East, and satellite C at 130° East. It can be seen that for satellite A only Kourou ground station is within its reach. For

---

[1] https://endurosat.com/, accessed 15/06/2020
[2] https://www.isispace.nl/, accessed 15/06/2020
[3] https://nanoavionics.com/, accessed 16/06/2020
[4] https://www.iq-spacecom.com/, accessed 15/06/2020
[5] https://www.aac-clyde.space/, accessed 16/06/2020
[6] https://www.satlab.com/, accessed 16/06/2020

satellite B, Kourou, Villafranca and Redu are within of a satellite reach. Villafranca will be used as the main ground station of satellite B, and Redu can be used as a backup station. For communication with satellite C, that will be on the opposite side of the Earth, the Dongara ground station will be used.
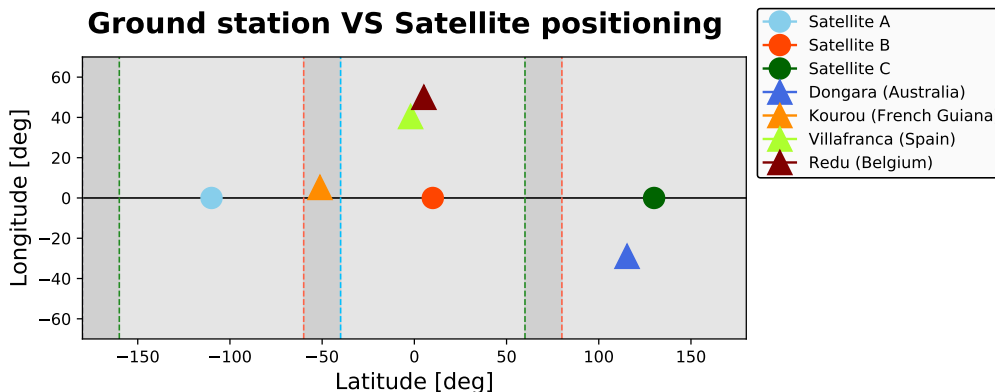
Figure 7.3: Longitudinal positioning of satellites with respect to chosen ground stations.

Finally, losses at each step of the signal flow were calculated or estimated more accurately with help of Stefano Speretta. For the transmitting feed line loss L_l and reception feeder loss L_r the value of -0.5 dB was used, which is a typical value for CubeSats. For transmission path losses, the detrimental effect of the atmosphere on the signal was divided into two: ionospheric losses and atmospheric losses, depending on where in the atmosphere the loss occurs. Atmospheric losses are then further divided in losses due to refraction, attenuation, scintillation and polarization. Refraction has a marginal effect due to the high elevation angle of the satellites from the ground station, and was hence neglected [32, 69]. Scintillation was also ignored, as for high elevation angles this loss is negligible [32, p. 416]. Polarization losses can also be ignored as not significant in the final link budget [69]. Finally, attenuation is further divided into losses due to molecular absorption and due to rain. An overview of the different components of the transmission path losses can be seen in.

Table 7.6: Transmission Path Losses Breakdown

Loss	Type	Type	Band	Value [dB]	Source
Ionospheric			UHF	0.4	[69]
			S	0.1	[69]
Atmospheric	Refraction		Both	Negligible	[32, p. 414]
	Attenuation	Molecular Absorption	UHF	0.2	[32, p. 415]
			S	0.38	[32, p. 415]
		Rain	UHF	0.1	[69]
			S	0.1	[69]
	Scintillation		Both	Negligigle	[32, p. 416]
	Polarisation		Both	Negligigle	[32, p. 416]

After taking into considerations all the different components, the transmission path losses for the UHF band are 0.7 dB and for S-band 0.58 dB.

When all parameters are known, link budgets for all possible equipment combinations can be calculated. The calculations showed that for payload and housekeeping data downlink only S-band can be used. This is due to the fact that there are no sufficiently big VHF and UHF antennae which makes SNR too high for CubeSats in GEO. The only exception when UHF can be used is the case of emergency. In this case, the bitrate cannot exceed 1000 bits/s. For uplink, however, both S-band and UHF can be used as uplink signals do not require high bitrates.

The possibility to use UHF is quite beneficial as it allows to use a portable ground station. This means that location of the ground station can be chosen more freely as it is up to engineers to decide where it should be positioned. Also, UHF ground stations can be used 24/7 whereas ESA ground stations will be only used once per day. It was found that the ISIS ground station is the only suitable option as the other two (GOMspace and GAUSS Srl) have too small antennae. Also, it was found that the signal from the satellite will have too high SNR when transmitting signal in S-band, thus, the portable ground station will only be used in UHF.

Lastly, it was decided to use transceivers for both S-band and UHF because if transmitters and receivers are

used separately, they take more space. Also, mostly transceivers are manufactured for CubeSats as it is a more popular solution. However, there are several options for transceivers that do not give a straightforward final solution. Thus, a proper trade-off is required in order to find the best solution. This trade-off is shown in table 7.7. Red colour indicates that this value is unacceptable and the corresponding component must be discarded. The green colour indicates the best option among the four components. It also can be seen that GOMspace transceiver is left out of the trade-off despite its outstanding characteristics. The reason for such a decision is that some values for GOMspace transceiver parameters raised questions that were not answered even after contacting the company.

Table 7.7: S-band transceiver trade-off

Company	Maximum transmit bit rate [Mbps]	Power consumption (Rx + Tx) [W]	Receive bit rate [Mbps]	Power consumption (Rx) [W]	Volume [U]
Nanoavion-ics	0.500	6.50	0.100	0.65	0.138
ISIS	4.300	13.00	0.0096	1.20	0.140
Satlab	0.512	5.00	0.128	0.55	0.138
IG Spacecom	4.000	13.00	0.064	4.50	0.259
GOMspace	7.000	8.25	3.000	0.08	0.038

Third iteration

In the third iteration the modulation type was along with bit error rate (BER) were chosen. The BER for the LICCA mission was chosen to be 10^{-6} at highest. This value was chosen following the LISA example [22, p. 174] where they used BER of 10^{-6} for their link budget. For the modulation type, the GMSK modulation type was chosen as that is now used in all ESTRACK ground stations as well as in the COTS components that will be used in the LICCA mission. This resulted in required SNR of 11.3 dB [8].

Furthermore, the distances from satellites to the ground stations were calculated more precisely to obtain more precise results in the link budget. Initially, it was assumed that a ground station is located precisely on the equator, and the satellite is right above the ground station. Now, the coordinates of the ground stations plotted in figure 7.3 can be used to calculate the distance between the satellites and the ground stations. This is done with the following calculation [56].

$$\gamma = \arccos\left(\sin LAT_{SAT} \sin LAT_{GS} + \cos LAT_{SAT} \cos LAT_{GS} \cos \Delta\right) \tag{7.13}$$

$$R_s = \sqrt{R_e^2 + r^2 - 2rR_e \cos \gamma} \tag{7.14}$$

In which LAT_{SAT} and LAT_{GS} are the latitudinal coordinates of the satellite and ground station respectively. Δ indicates the difference between the longitudinal coordinates of the satellite and ground station in question. Furthermore, R_e is the Earth radius, taken as 6378 km, and $r = R_e + h$ in which h is the orbital altitude, taken as 35 786 km for GEO. With these equations, the central angle γ is calculated, and finally the distance between the satellite and ground station R_s. Table 7.8 and table 7.9 show the link budgets for downlink and uplink, respectively, in both UHF and S-band.

Table 7.8: Link budget for downlink in both UHF and S-band.

Parameter	UHF	S-band	Source
General			
Signal frequency, f [MHz]	435	2245	Manufacturer data
Satellite to GS distance, S [km]	39260	39260	Calculated
Data rate, R [bits/s]	$1.2 \cdot 10^3$	$0.5 \cdot 10^{-6}$	Manufacturer data
Modulation type	GMSK	GMSK	Choice
Bit error rate, BER [-]	10^{-6}	10^{-6}	Choice
Transmitter			
Tx power, P [dBW]	3.01	0	Manufacturer data
Transmitting antenna gain, G_t [dB]	1.37	8.00	Manufacturer data
Feed line loss, L_l [dB]	-0.50	-0.50	Conservative assumption

EIRP [dBW]	3.88	7.50	Calculated (equation (7.1))
Channel losses			
Attenuation loss, L_a [dB]	-0.70	-0.58	Table 7.6
Space loss, L_s [dB]	-177.10	-191.35	Calculated (equation (7.4))
Antenna pointing loss, L_{pr} [dB]	0.00	0.00	Calculated (equation (7.5))
Total channel loss	-177.80	-191.93	Calculated
Receiver			
Receiving antenna gain, G_r [dB]	15.5	49.40	GS data
Reception feeder loss, L_r [dB]	-0.50	-0.50	Conservative assumption
Received power, C [dBW]	-158.92	-135.53	Calculated (equation (7.6))
Final values			
Received energy per bit, E_b [dB]	-189.71	-192.52	Calculated (equation (7.7))
System noise temperature, T_s [K]	264	85	GS data
Noise spectral density, N_0 [dB]	-204.38	-209.30	Calculated (equation (7.9))
Signal-to-noise ratio, SNR [dB]	14.68	16.78	Calculated (equation (7.12))
Required SNR [dB]	11.3	11.3	[8]
Link margin [dB]	3.00	3.00	Typical value
Remainder [dB]	0.38	2.48	Calculated

Table 7.9: Link budget for uplink in both UHF and S-band.

Parameter	*UHF*	*S-band*	*Source*
General			
Signal frequency, f [MHz]	436.5	2067.5	Manufacturer data
Satellite to GS distance, S [km]	40580	40580	Calculated
Data rate, R [bits/s]	$9.6 \cdot 10^3$	$128 \cdot 10^3$	Manufacturer data
Modulation type	GMSK	GMSK	Choice
Bit error rate, BER [-]	10^{-6}	10^{-6}	Choice
Transmitter			
Tx power, P [dBW]	20.00	26.02	Manufacturer data
Transmitting antenna gain, G_t [dB]	15.50	47.4	GS data
Feed line loss, L_l [dB]	-0.50	-0.50	Conservative assumption
EIRP [dBW]	35.00	72.92	Calculated (equation (7.1))
Channel losses			
Attenuation loss, L_a [dB]	-0.70	-0.58	Table 7.6
Space loss, L_s [dB]	-177.41	-190.92	Calculated (equation (7.4))
Antenna pointing loss, L_{pr} [dB]	0.00	-0.98	Calculated (equation (7.5))
Total channel loss	-178.11	-192.48	Calculated
Receiver			
Receiving antenna gain, G_r [dB]	1.37	8	Manufacturer data
Reception feeder loss, L_r [dB]	-0.50	-0.50	Conservative assumption
Received power, C [dBW]	-142.24	-112.06	Calculated (equation (7.6))
Final values			
Received energy per bit, E_b [dB]	-182.06	-163.13	Calculated (equation (7.7))
System noise temperature, T_s [K]	1000	1000	GS data
Noise spectral density, N_0 [dB]	-198.60	-198.60	Calculated (equation (7.9))
Signal-to-noise ratio, SNR [dB]	16.54	35.47	Calculated (equation (7.12))
Required SNR [dB]	11.3	11.3	[8]
Link margin [dB]	3.00	3.00	Typical value
Remainder [dB]	2.24	21.17	Calculated

7.4. Design methodology: tracking

This section will describe the methodology used in the design of the navigation part of the subsystem. Navigation, or orbit determination, is necessary for the spacecraft in order to know its position and to estimate its travel time. These two functions allow the spacecraft to determine when it should start communications or perform certain operations [74, p. 209]. Orbit determination can be performed in several ways. The ones considered for this mission are the following:

- DORIS receivers
- Laser tracking
- Radio communication
- GNSS receivers

Before being able to make a selection on what type of navigation to use, it is necessary to identify the required position accuracy, as this affects drastically the navigation subsystem. Requirement LICCA-SYS-Sub-Nav-2 specifies this, and sets the required accuracy to 1000m. This means that the position determination needed for the satellites is of medium to low precision, instead of requiring high-precision orbit determination. This consideration allows for the elimination of some methods to perform navigation, as they would provide unnecessary accuracy in tracking. The different options are now going to be considered, in order to choose the most optimal one for the application needed.

DORIS System

A DORIS system is a one-way Doppler tracking system, in which the frequency shift of a radio signal transmitted from a ground station is measured by a satellite. The ground segment of this network consists of 50 ground stations. This method would provide a higher position accuracy than required [56, p. 202]. Furthermore, the DORIS receivers available on the market are expensive, heavy and voluminous, all characteristics which make them not suitable for CubeSats. Considering the above considerations, this option is discarded.

Laser Tracking

Laser tracking relies on the use of lasers to measure the range between a laser station and a satellite, equipped with retroflectors. This method allows for high-precision tracking, with an accuracy of ± 1 cm [56, p. 203]. The on-board equipment required for this option consists solely of a corner cube retroflector, which is small, down to few mm in size[7], and does not require any power. Despite this, when looking at the ground segment required for this method, three laser tracking station would be necessary per satellite. Even if the two constellations would be positioned such that two adjacent satellites could use the same three stations, a total of nine stations would be needed, which is considered excessive. For this reason, together with the excessive accuracy reached, this option is discarded.

Radio Communication System

This method consists in using the communication system on-board the spacecraft to perform orbit determination. A signal is sent to the spacecraft from a ground station. This signal is then sent back by the spacecraft at the same frequency. In this way, the two way travel time is obtained, which can be calculated to a range. By looking at the frequency shift in the signal due to Doppler effect, the relative velocity of the spacecraft with respect to the ground station can be obtained. By combining this with the ranging measurements, the satellite orbital position and velocity can be determined [56, p. 195-197]. By comparing this measurement with a model of the theoretical orbit of the spacecraft, the remainder can be used to determine whether the satellite is in the correct orbit or needs to perform orbit maintenance. The on-board equipment needed for this option consists in an accurate clock to increase the precision of the measurement, and a transponder to send back the signal received in phase-lock. The former is already included in the payload, while the transponder used for telemetry could be made into a transponder by performing software implementation. Hence, this option would not require any additional equipment on board. On the downside, as the relative position of the satellite with respect to the ground station does not change in GEO, the relative velocity can be be measured less precisely than a satellite in LEO. Yet, thanks to software implementations, this method reaches an accuracy in the order of cm in ranging and in relative velocity (Stefano Speretta), without adding any extra component on-board, nor requiring different ground stations than the ones used for telemetry. For these reasons, this option is further considered.

GNSS Receiver

A GNSS receiver collects signals sent by satellites of Global Navigation Satellite System's constellations, and uses them to calculate the spacecraft's position and velocity states [56, p. 203]. The problem about using this method in GEO is that, as the GNSS satellites are in Medium Earth Orbit (MEO), 20 000 km, the spacecraft can only receive signals from the GNSS satellites in MEO on the opposite side of the Earth, as shown in figure 7.4.

---

[7]https://www.zygo.com/?/opt/components/cornercuberetroreflectors/, accessed 18/06/2020
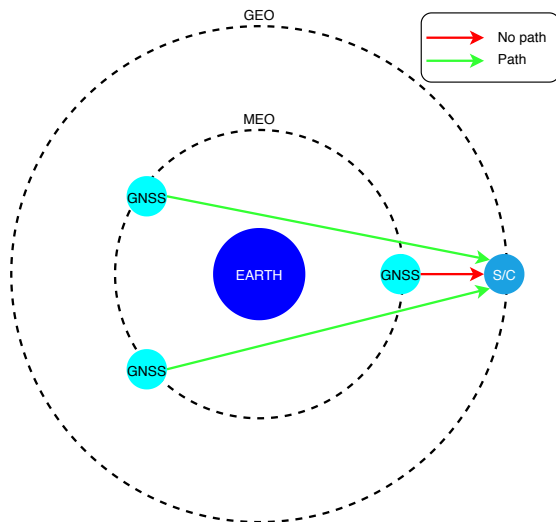
Figure 7.4: GNSS visibility from GEO
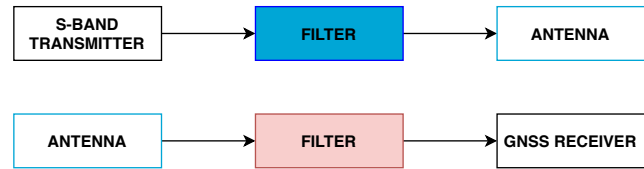
Figure 7.5: Extra filters required in case of GNSS tracking

Normally, the signals from four different satellites is needed to perform the triangulation necessary in order to track the spacecraft. This would not be possible for a spacecraft in GEO, as not at all times at least four of these satellites would be visible. Despite this, implementations on the software of the GNSS receiver allow for post-processing which makes it possible to determine the spacecraft's orbital position by processing the signal sent by only one GNSS satellite. With this method, the spacecraft would know its position and velocity at all times, without having to pass via a ground station. For this option, additional on-board equipment would be needed, namely a GNSS antenna and receiver, and filters. COTS components for GNSS antennae and receivers are compatible with CubeSats dimensions, 70x70x15 mm[8] and 100x100x15 mm[9] respectively, and do not consume excessive amounts of power. The filters are necessary in order to limit the effect of interference between the incoming GNSS signal, and both the uplink and downlink S-band signals.

The positioning of the filters in the T&T architecture is shown in figure 7.5. The blue filter would be needed to kill the noise due to the incoming GNSS signal, in order to let the S-band downlink signal be transmitted. The red filter would be needed to kill the high power signal incoming from the S-band uplink signal, in order to the weaker GNSS signal to be received.

Taking into account these considerations, and considering the tracking accuracy obtained being sufficient, this method is considered further.

In the next subsection, now that all the methods identified have been analysed, the remaining ones will be traded-off, in order to determine which one is optimal for the mission.

7.4.1. Trade-off

The remaining methods considered for tracking the spacecraft are using the radio communication system on-board the spacecraft, and using a GNSS system. The criteria identified for the trade-off are listed below. Note that the acronym of each criterion is used in table 7.11, for clarity of the layout.

Table 7.10: Criteria for tracking method trade-off

Criteria	ID	Explanation
Hardware complexity	HC	the number of extra hardware components required by the method
Software complexity	SC	the amount of extra software implementations required by the method
Reliability	R	how reliable each method is. This criteria takes into account the number of components that need to fail before tracking the spacecraft becomes impossible
Accuracy	AC	the accuracy obtained by the method
Autonomy	AU	the independence of the spacecraft from a ground segment to know its location and velocity
Mass	M	the extra mass due to the extra components
Volume	V	the extra volume due to the extra components
Power	P	the extra power due to the extra components

[8] https://www.isispace.nl/product/gps-patch-antenna/, accessed 18/06/2020
[9] https://www.cubesatshop.com/product/nss-gps-receiver/, accessed 18/06/2020

The method employed for this trade-off is an ordinal method, as these methods are to be preferred when knowing only qualitative information on the properties of the alternatives [35, p. 186]. More specifically, the majority rule was followed, in which of two alternatives, the alternative which is the most effective for the highest number of criteria wins the trade-off.

Table 7.11: Tracking method trade-off

	HC	SC	AC	AU	R	M	P	V	# of wins
GNSS	1	1	2	2	1	1	1	1	2
Radio communication	2	2	1	1	2	2	2	2	6

As it can be seen from the trade-off table above, the radio communication is chosen as the method to provide tracking for the spacecraft. Now that a method has been chosen, a more in depth functional breakdown of the navigation can be made. This is shown in figure 7.6, below.
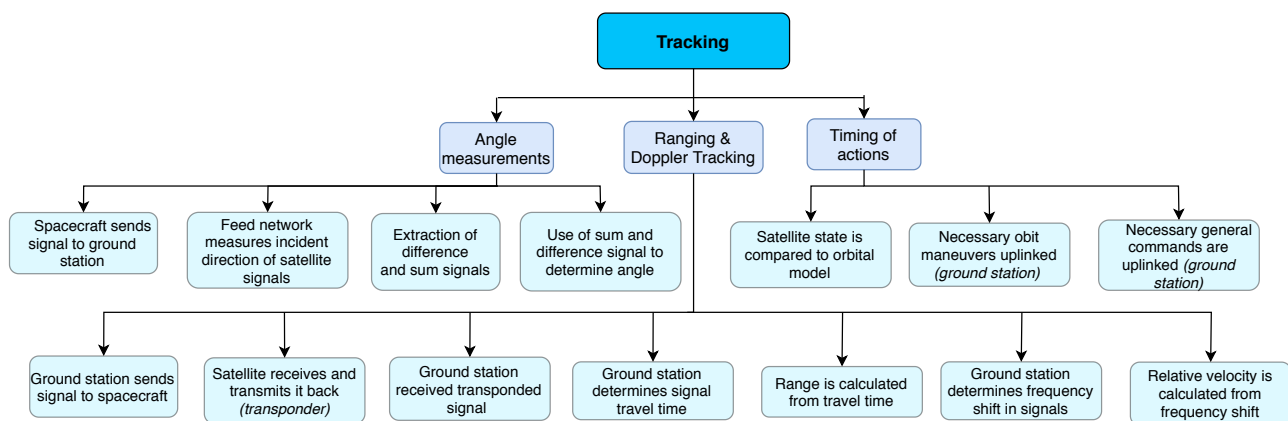
Figure 7.6: Functional breakdown structure of navigation subsystem

7.5. Risk

In this section, the risks associated with the TT&C subsystem are identified.

- **Incompatibility of frequencies between the antennae and the transceivers:** This applies for both downlink and uplink, and for both UHF and S-band. If the transceiver and the antenna work on two different frequency bandwidths, the spacecraft will not be able to communicate with the ground segment, making the mission purposeless. Also, a change in ground station will not mitigate this risk, as the problem would still be within the spacecraft itself.
- **Incompatibility of frequencies between the spacecraft and the ground station:** This applies for both downlink and uplink, and for both UHF and S-band.
- **Misaligned antenna:** If the spacecraft is not able to point the antenna towards the ground station, and the ground station becomes outside the beamwidth of the spacecraft antenna, communication will not be possible.
- **Different modulation types:** If the modulation type is different between the transmitter and the ground station, communication will not be possible.
- **Failure of component:** If one of the components were to fail, and no back-up is present, communication with the ground at the bandwidth of that components would not be possible anymore.
- **Wrong commands uplinked:** If the ground station sends the wrong commands to the spacecraft, the latter would perform non required maneuvers, risking to deorbit to undesired orbital planes.
- **Corrupted signal downlinked:** If the spacecraft sends a corrupted signal to the ground station, a possible gravitational wave detection might be missed, or the corrupted signal might be interpreted as a gravitational wave.

7.6. Sustainability

The components of the TT&C subsystem are mainly made of electrical components. When looking at the different COTS options, it was possible to see that the components offered by the various companies did not differ much in terms of dimensions and weight. Also, when looking at the elements that make up the COTS options, it was possible to see that these are almost identical for the different companies. Considering this, the materials and manufacturing processes used in the COTS options give little insight on their sustainability

impact, and hence no distinction can be made in the use of resources from each of the COTS components. The use of commercially available components, on the other hand, eliminates the need for a R&D phase, and also reduces the amount of component testing required. Both of these have a positive influence on the sustainability of the subsystem, as the overall use of resources is reduced. Furthermore, the usage of the ground stations can be employed as an indicator of the sustainability aspect of the subsystem [28]. Regarding this topics, in order to improve the sustainability of the mission, the team made the choice of not choosing ground station tracking. This modality of tracking would have required nine laser ground stations in order to track the six satellites which make up the two constellations. This was avoided by choosing to use the radio communication to perform tracking. In this way, the same ground station used for communication can be used for tracking, and the number of these can be kept at three.

7.7. RAMS

In this section, the reliability, maintainability, availability and safety of the telemetry, tracking and command subsystem.

7.7.1. Reliability

The elements composing the TT&C subsystem are all COTS components, most of which have flight heritage. For this reason, the reliability of each components is high, leading to a high reliability when considering the subsystem as a whole. Furthermore, in order to increase the reliability of the subsystem, in the subsystem architecture, two S-band antennae are included, for redundancy. This is also because the S-band antenna is used for telemetry and telecommand, as well as tracking, and is hence a critical component of the subsystem. The philosophy applied for this subsystem is thus fail safe.

7.7.2. Availability

The TT&C subsystem allows for communication with the ground once per day. Within the contact window, three different actions are performed:

- the scientific payload data is downlinked via the S-band channel from the spacecraft to the ground station
- tracking is performed by sending a two-way S-band signal between the ground station and the spacecraft.
- command signal is uplinked from the ground station to the spacecraft. The command signal can be transmitted in both S-band and UHF.

Since the spacecrafts are in GEO, the contact window is not determined by the amount of time the satellite is visible by the ground station, as this would be for the whole duration of the orbit. Instead, the contact window is determined by the amount of time the ground station can dedicate to the spacecraft, since the considered ground stations are important ESA ground station, used for many other space mission. Regarding the uplink of command using UHF, since for this an amateur antenna can be used, the availability is higher than for the S-band uplink, but on the other side the bit rate achievable is lower, hence increasing the required contact time to uplink the same amount of commands.

7.7.3. Maintainability

The TT&C subsystem is comprised of a space segment and a ground segment. Concerning the space segment, once positioned on the launcher the various components on-board the spacecraft cannot be inspected, nor replaced, nor fixed. Hence, maintainability on the space segment of the subsystem is not possible. On the other hand, the ground segment is easily accessible from Earth, and can be fixed whether something requires maintenance. Furthermore, in the eventuality that the spacecraft's TT&C subsystem is damaged and only able to transmit weaker signals, the link can be adjusted on the ground station side, thus maintaining active communication between ground and space segment. An additional consideration that can be made, is the possibility to uplink coding commands, allowing to fix software related problems on-board the spacecraft.

7.7.4. Safety

Three elements can be identified concerning critical safety functions of the subsystem under analysis. First, the command uplinked to the satellites will be encrypted. This is done in order to always have full control over the actions of the satellite, avoiding the possibility of an external party taking control over the satellites. Second, the tracking data will be used to make sure that the satellites are not going to collide with other satellites, in this way avoiding the creation of new space debris, as well as causing a premature end to two space missions. Third, the command uplinked to tell the satellite to initiate the end-of-life manoeuvre is necessary in order to ensure that the satellite will not deorbit into GEO, hitting other satellites and increasing space debris.

7.8. Final design

The final design of the telemetry and tracking system consists of the following elements. There will be two types of systems present in the satellites, namely a UHF system and an S-band system. For each system, the ground segment will be present in three locations on Earth, designated as The Americas, Europe, and Australia. Each segment will serve two satellites, one for each constellation.

The UHF communication link will primarily be used for uplinking commands to the satellites. Downlinking large amounts of data will not be possible with the UHF, though it would be possible to send small messages if needed in the event of an emergency. Furthermore, some small downlink messages can also be made available to amateur radio enthusiasts in return for using UHF frequencies. The on-board components consist of a COTS monopole antennae system and UHF transceiver, both manufactured by Nanoavionics. The UHF ground segment will use Yagi antennae, such as the ones available from ISIS. This is the antenna that is available at the EEMCS faculty of TU Delft. It is assumed that this antenna can be used to cover the Europe section. It is also assumed that similar antennae can be purchased from ISIS and placed at designated locations in The Americas and Australia.

The S-band communication is primarly for downlinking the scientific payload data, along with the housekeeping data. The tracking will also be done with this system. The on-board system will consist of an S-band patch antenna, produced by GOMSpace, along with the S-band transceiver made by Satlab. Two transceivers will be implemented on board for redundancy. The following ground stations have been identified as the primary stations to be in contact with out satellites: Kourou in French Guiana, Villafranca in Spain, and Dongara in Australia. They are part of the ESA ESTRACK network. A summary of all the on-board components and the used ground stations are given in table 7.12 and table 7.13 respectively, and an overall architecture of the TT&C subsystem can be seen in figure 7.7

Table 7.12: On-board components for telemetry and tracking.

Component	Quantity [-]	Mass [g]	Volume [U]	Power Rx+Tx [W]	Power Rx [W]
Nanoavionics UHF antenna	1	30	0.08	0	0
Nanoavionics UHF transceiver	1	8	0.01	0.5	0.5
GOMSpace S-Band patch antenna	1	110	0.19	0	0
Satlab S-Band transceiver	2	190	0.14	5	0.55
Total	**6**	**528**	**0.56**	**5.5**	**1.05**

Table 7.13: Selected S-band ESA ESTRACK ground stations.

S-Band ground stations	Country	Location	Dish size [m]
Kourou	French Guiana	+5° 15' 05.18", -52° 48' 16.79"	15
Villafranca	Spain	+40° 26' 33.23", -03° 57' 05.70"	15
Dongara	Australia	-29° 03', +115° 21'	13
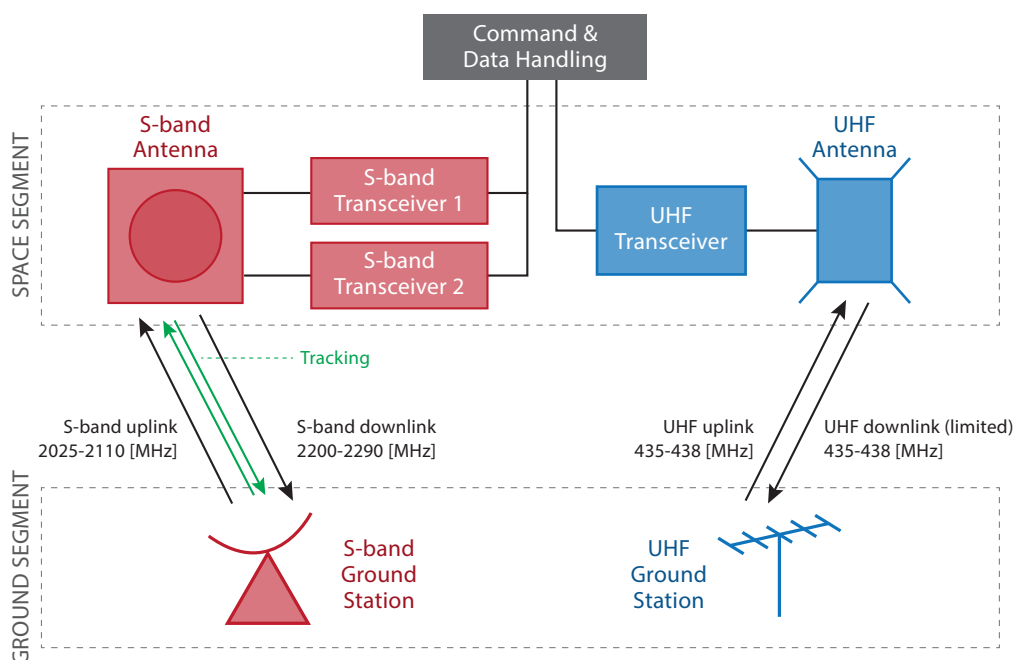
Figure 7.7: Architecture of TT&C subsystem.

8

Command & Data Handling

The Command & Data Handling (CDH) subsystem concerns all collection, computation and internal communication of data throughout the satellite. Furthermore, it must receive and interpret commands, and be capable of determining when it should perform manoeuvres.

8.1. Functional analysis

To start with the design of the CDH subsystem, the required functionality of the CDH subsystem needs to be analysed. For this, a Functional Breakdown Structure (FBS) was generated for the CDH subsystem. This FBS is given Figure 8.1. For the purposes of this diagram, it should be noted that the payload is considered a subsystem of the satellite.
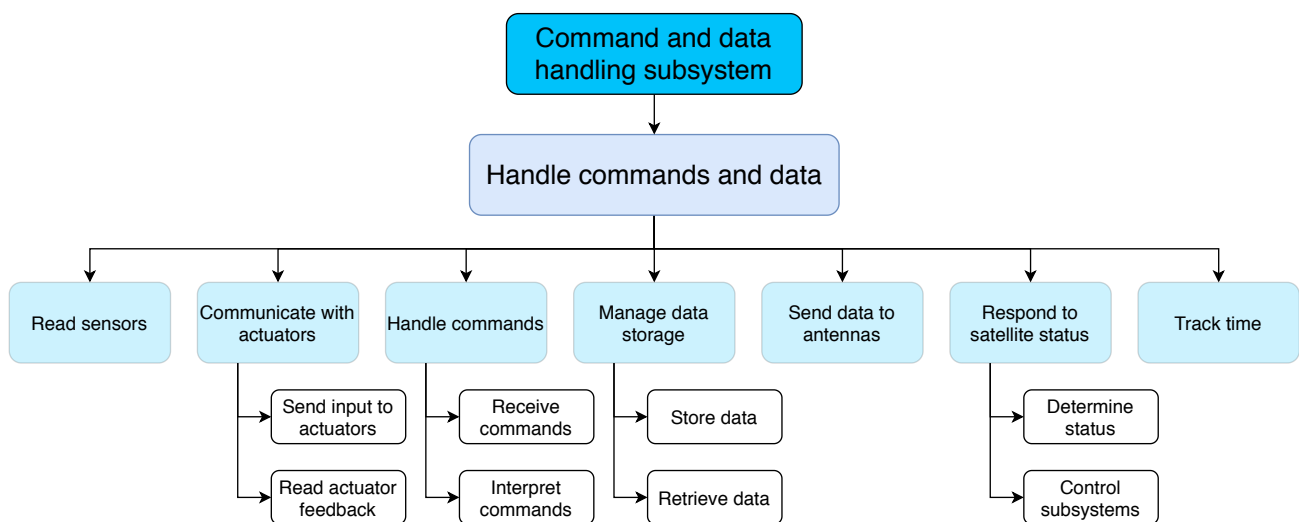
Figure 8.1: The functional breakdown structure of the CDH subsystem

It should be noted that the functionalities are mostly controlled by the *'Respond to satellite status'* functionality. That is to say, the CDH needs to be able to read sensors, but *when* the sensors are read is determined by the CDH's ability to respond to the satellite status. Furthermore, *'Control subsystems'* means the CDH should function as a control system for each subsystem, but the CDH may also determine a subsystems functionality is currently not required, and should be able to turn each subsystem on/off. These functionalities were used to identify the requirements that should be set on the CDH subsystem. The identified requirements can be found in the next section.

8.2. Requirements

The requirements for the CDH subsystem, as identified during the mission definition and exploration phase, can be found in the baseline report [3]. The updated requirements are shown in table 8.1. The changes made to the requirements can be found in table 8.2.

Table 8.1: CDH requirements

CDH	
LICCA-SYS-Sub-CDH-1	DELETED
LICCA-SYS-Sub-CDH-2	The CDH system shall handle at least 11300 bit/s.
LICCA-SYS-Sub-CDH-3	DELETED
LICCA-SYS-Sub-CDH-4	The CDH system shall be able to store 1.22 GB.
LICCA-SYS-Sub-CDH-5	The CDH system shall be able to activate the payload.
LICCA-SYS-Sub-CDH-6	The CDH system shall be able to deactivate the payload.
LICCA-SYS-Sub-CDH-7	DELETED
LICCA-SYS-Sub-CDH-8	DELETED
LICCA-SYS-Sub-CDH-9	The CDH system shall track the time of the mission.
LICCA-SYS-Sub-CDH-10	The CDH system shall be able to verify the functionality of the subsystems.
LICCA-SYS-Sub-CDH-11	The components of the CDH subsystem shall have a current TRL level of 7 or higher.

Table 8.2: The changelog of the CDH requirements

Requirement ID	*Changes*	*Rationale*
LICCA-SYS-Sub-CDH-11	Changed the TRL range to at least 7	A current TRL of 8 or 9 is also acceptable for this mission

8.2.1. Performance estimations

To generate the performance requirements for the CDH, a preliminary estimation had to be done regarding all sensors on the satellite. This list of sensors was generated using the design choices that are already made for the spacecraft at the time the CDH subsystem design was started, for example, the payload and ADCS sensors were already determined. For the other subsystems, preliminary estimations were made. The full list of sensors is shown in table 8.3.

Table 8.3: All sensors connected to the CDH subsystem in the satellite.

Subsystem/sensor	*Quantity* [-]	*Word size* [bit]	*Frequency* [Hz]	*Bit rate* [bit/s]
EPS				
Power source voltage (in)	1	8	1	8
Power source voltage (out)	1	8	1	8
Power storage	1	8	1	8
Power management	2	1	1	2
Thermal				
Power source thermocouple	2	16	0.1	3.2
Internal NTCs	4	8	0.1	3.2
Communication				
Antenna temperature	1	16	1	16
Transmit power	2	8	1	16
Tracking power level	1	8	1	8
Tracking temperature	1	8	1	8
Tracking time	1	32	1	32
CDH				
CPU power level	1	8	1	8
CPU temperature	1	8	1	8
EDAC (on/off)	1	1	5	5
Fault status	1	1	5	5
TM out (towards comm)	1	8	100	800

TC in (towards comm)	1	8	100	800
Propulsion				
Tank Gauge sensor	2	8	10	160
Propellant Flow sensor	8	8	2	128
Thruster Valve status	8	1	5	40
Thruster Control	8	8	1	64
ADCS				
Star sensors	2	8	10	160
Sun sensors	6	8	10	480
Earth sensors	1	8	10	80
IMU sensors	1	8	10	80
Actuators	8	8	10	640
Payload				
Payload Data	3	64	40	7680
Payload housekeeping	6	8	1	48
Payload ON/OFF	4	1	0.1	0.4
Total	**80**			**11300**

From the complete list of sensors, along with their word size and sampling frequency, the total bitrate can be estimated. It is assumed for now all sampled data is stored; although some readings may be processed to get more efficient parameters, and some readings may not be stored at all, assuming all read data is stored gives an upper limit to the required memory size. It is assumed that the data is downlinked every day; for redundancy, it is assumed the memory must be at least ten times larger, to take into account received commands, computed values, delayed downlinks and memory degradation due to radiation effects. The minimum storage memory size is then 9.76 Gbit, or 1.22 GB.

Table 8.4: The lines of code required per application/subsystem

Application/subsystem	#Lines of code
Executive	1000
Communication	4500
Attitude processing	7900
ADCS	33800
Attitude processing	4500
Fault detection	11500
Utilities	8800
Momentum management	3000
Power management	1200
Thermal control	800
Total	**77000**

The CDH subsystem must also have programmable memory. To get an estimate for the programmable memory size, the number of lines of code per subsystem was estimated [72]. This estimation can be seen in table 8.4. Once the total number of lines of code is estimated, this can be used to calculate both the programmable storage memory size, as well as the minimum processing speed.

With the total number of lines of code estimated, the required programmable memory size can be estimated. The required number of bytes per line of code is estimated at 10 bytes, once the code is compressed. The total required programmable memory size is then 0.518 MB.

Furthermore, the number of lines of code can be used to calculate the required processing speed. The processing speed is expressed in terms of instructions per second, or Hertz. For this estimation, is was assumed all lines of code per subsystem were ran at the average reading frequency of the sensors in that subsystem. Furthermore, it was assumed each line of code has, on average, five processor instructions. This would result

in a required processing speed of 0.442 million instructions per second, or Mips. Then, it is assumed each processor instruction requires 2 clock cycles. This would mean the minimum clock speed is 0.884 Mhz. This results in the following three performance requirements for the CDH subsystem:

- **Storage memory size:** 1.22 GB
- **Programmable memory size:** 0.518 MB
- **Clock speed:** 0.884 MHz

These requirements all used assumptions that can not be verified at this time, as these assumptions can only be verified when the software is developed and the sensors are selected. When the required software is either selected as a COTS package or developed, the required throughput can be calculated using the tools developed for this mission. These requirements all assume the upper limits on data processing and storage. The effects of radiation for the data processing is not taken into account here, and the risk that the performance of the CDH will be affected by radiation effects is mitigated in chapter 13. Still, the requirements are all very feasible with current CDH technology. Hence, these values will be used the design the CDH subsystem.

8.2.2. Connections
All connections of the sensors have to be compatible with the CDH. For now, it will be assumed all sensors and actuators are connected to the On-Board Computers (OBC) via an Input/Output (I/O) board. It is assumed the OBC and I/O board will communicate via an I^2C connection.

8.3. Design methodology
Developing a CDH subsystem that is capable of performing the required functions from scratch is considered non-feasible. Development costs would be very high, while the reliability and performance cannot be guaranteed. Hence, the design procedure will only consider COTS components. First, COTS OBC options are traded off. This trade-off is described in more detail in subsection 8.3.1. Then, I/O boards are discussed in subsection 8.3.2. Finally, the sensors are described in subsection 8.3.3.

8.3.1. OBC Trade-off
First, a large list of all available COTS OBC options was generated. Every option where not enough data was available was removed. Then, every option where the specifications did not meet the performance requirements was removed. All feasible COTS OBC opions are given in Table 8.5.

Table 8.5: All COTS OBC options that are feasible for the LICCA mission

Option	Name	Manufacturer	Mass [g]	Volume [U]	Power [W]
1	ISIS OBC	ISISpace	100	0.104	0.6
2	CP400-85	Hyperion Technologies	7	0.01	1
3	ATI OBC	ATI	24	0.03	1
4	DB-OBC-0402	Data Patterns	90	0.131	3
5	DSW OBC	Dream Space world	178	0.159	3
6	BAE RAD750 3U	BAE systems	549	0.16	10.8
7	OBC-P3	Space Inventor	150	0.15	3

All the options listed above are feasible in terms of the performance requirements, hence the trade-off selection procedure is not based off of these characteristics. However, the mass, volume and power consumption of each options also does not tell the whole story; each option has different characteristics in terms of possible connections, included Error Detection And Correction (EDAC) software, testing and qualification, radiation resistance, attachment options and redundancy. Hence, each option will be described in more detail, along with its pros and cons.

1. The ISIS OBC comes with different OS options, I^2C connections, integrated watchdog and fail-safe filesystem. However, it is not qualified for high radiation environments, and has little redundancy.
2. The CP400-85 has incredible physical characteristics, and a radiation tolerant storage. However, its other components are not radiation qualified, and it has no redundant components.
3. The ATI OBC has great physical characteristics, integrated EDAC and triple mode redundancy, and is radiation qualified up to 25krad. However, it has no I^2C connectivity, and uses 6 volts, which makes it more vulnerable to radiation than the other options, which all use 3.3 volts. Furthermore, ATI is located in Japan, decreasing the availability of this OBC.
4. The DB-OBC-0402 has built-in ADC for temperature monitoring and sensor interfaces, a fully redundant bus configuration and three I^2C connections, but lacks radiation qualification. Data Patterns is located in India, reducing its availability.

5. The DSW OBC has a 3-axis digital compass and 6-axis motion tracking, is qualified for up to 15krad of radiation, and has a high maximum clock rate of 866 Mhz, but lacks redundancy, vibration testing, and Dream Space World is located in South-Korea, reducing the availability.

6. The BAE RAD750 3U has high redundancy, and is incredibly radiation tolerant, but it is too heavy and power-consuming for this mission.

7. The OBC-P3 has two independently running OBCs resulting in very high redundancy. It has 1.5mm aluminium shielding, and it is vibration and radiation resistant. Furthermore, it has watchdogs and EDAC software. However, it would need to be customized to increase the storage memory size, as it can only store 2x32MB. Fortunately, the manufacturer indicates that it is customisable.

A formal trade-off cannot be done because the pros and cons of each option are fundamentally different. However, because the OBC-P3 fits most requirements and is customisable, the OBC-P3 is considered the best option. This option may be customised to fulfill the radiation hardness requirement, as described in more detail in subsection 8.4.2. Furthermore, it will be connected to an I/O board using its I^2C connectivity. The I/O board selection is described in more detail in subsection 8.3.2.

8.3.2. I/O board

The OBC needs to be connected to 80 different sensors. However, none of the OBC options can be directly connected to 80 different sensors. Hence, an I/O board is required for this mission. The selection of the I/O board is not done in this report, as it can be any lightweight I/O board that supports General Purpose Input/Output (GPIO) and I^2C connections. However, the selected I/O board should be included in the radiation hardness testing procedure as described in subsection 8.4.2.

8.3.3. Sensors and actuators

The selection of the sensors is done per subsystem. However, the CDH subsystem design requires that all sensors should be compatible with selected OBC and I/O board. All sensors and actuators should support either an I^2C or a GPIO connection. Furthermore, all actuators should function within a voltage range that can be achieved by the selected OBC and I/O board.

8.4. Risk

In this section, all risks which could cause the CDH to fail are described. The most important risks come from the radiation effects, which are described first, followed by radiation risk mitigation. Then, the description and mitigation of other risks is given.

8.4.1. Radiation effects

The risks coming from radiation effects can be split into two sections: the Total Ionising Dose (TID) and Single Event Effects (SEE). TID effects are long-term, gradual effects, whereas SEEs are instantaneous effects. The risks of both are described in more detail in this section.

Total ionising dose

The Total Ionising Dose (TID) is a measure for the total dose received by an object subjected to a low dose rate for an extended period of time. It mostly concerns space missions, but may also affect missions near nuclear reactors, or other radiation sources. While certain radiation sources may have instant effects on the OBC, the TID concerns the gradual degradation of the performance of the components.

Most of the effects the TID has on the OBC come from the changes in the Field-Effect Transistors (FETs). Both beta and gamma radiation can affect FETs. For beta radiation, the high energy of the electrons may knock the electrons inside FET gates out of the valence band. For gamma radiation, the energy of the photon may raise an electron into the conduction band, and the electric field may then remove the electron. In both cases, valence electrons are removed from the gate oxide, which changes the Threshold Voltage (V_{TH}) of the FET. For n-channel FETs, the V_{TH} decreases, whereas for p-channel FETs the V_{TH} will increase instead over time [63]. These changes to the properties of FETs over time may strongly influence the performance of the different components present in the OBC. The effects of the TID on the different components are listed below [63].

- **Processors:** the speed of the processors will decrease over time, as well as the throughput.
- **Memories:** The access time will increase.
- **Logic gates:** The delay will increase.
- **Oscillators:** The frequency of crystal oscillators can change, either increasing or decreasing.

As can be seen above, nearly all components will be affected negatively by the TID. However, the TID is quite easy to calculate, and the effects it has mostly affect the performance of the OBC, making the TID effects easier to take into account when designing an OBC for this mission.

The TID is typically expressed in rad. One rad is equivalent to 0.01 J/kg of absorbed radiation energy. Typically for space missions, the TID is in the order of several kilorads per year. To calculate the TID over the mission

lifetime, SPENVIS[1] will be used. From section 4.2, it was determined that the TID is around 50 000 to 5 000 rad (Si) per year, the OBC-P3 has an skin of 1.5 mm of aluminum, so it would need at least an additional 3 mm of equivalent aluminium shielding to stay under 20 000 rad (Si) for the whole mission. The 20 krad (Si), is based on what normal radiation hardened OBC can handle.

Single Event Effects

A charged high energy particles can go through the radiation shielding and create an ionising track, when passing through the depletion region of a piece of electronics. This ionization track can create holes and electrons which can change the state of that electronic component [55]. There are multiple effects these ionization track can have on semiconductor technologies in spacecraft [65].

- **Single Event Upset:** A high energy particle can cause an upset in semiconductors in spacecraft components [55]. This upset can cause a bit to flip, therefore corrupting the information stored. During the SEU the sensitive area of the storage device is hit and transfers enough energy to flip a bit [55]. The memory of the spacecraft is particularly at risk, therefore adequate protection is needed. Logic devices which include latches can also suffer from Single Event Upsets (SEU). These errors are called soft errors as they can be easily corrected [55].
- **Multiple Bit Upset:** During a Multiple Bit Upset (MBU) multiple bits of either memory or logic devices can be flipped at once. This event is more critical than the SEU as it is harder to detect and repair
- **Single Event Transient:** A Single Event Transient (SET) is a certain voltage spike in a node of an integrated circuit in a semiconductor [55]. This voltage spike might be converted to a transient voltage error and propagated to a storage element and be latched there, causing a soft error. It affects Analog and Mixed Signal circuits, and Photonics like fiber optics.
- **Single Event Functional Interrupt:** During a Single Event Functional Interrupt (SEFI) a semiconductor exhibits an unexpected change in its output [51]. During a SEFI event in a microprocessor a lockup can occur, the processor can go into standby, or the processor can get into an unknown state. A SEFI event in the memory is an event which results in an higher than expected error rate. These events occur in a cross-section of the device where minimal information is known about the device architecture. Therefore the error can only be detected by the malfunctioning of the device.
- **Single Event Latch-up:** During a Single Event Latch-up (SEL) a high energy particle makes an ionization track throughout the semiconductor [51]. This track can create a low-impedance path between the power rails of transistors. When the transistor is operating and a current flows a parasitic PNPn stucture can be triggered creating a hot spot and burning out the device. All CMOS or BiCMOS devices, e.g. microprocessors or batteries, are susceptible to SEL.
- **Single Event Burnout:** A Single Event Burnout (SEB) is an SEL in which due to the over-current the transistors can burnout making the device inoperable [51]. Devices which include a MOSFET or BJT structure are susceptible to SEB.
- **Single Event Gate Rupture:** During a Single Event Gate Rupture (SEGR) a high-energy can strike the gate electrode of an MOS-type semiconductor [51]. Power MOSFETs, Non-volatile NMOS structures, VLSIs, and linear devices, can suffer from SEGR. The particle can cause a conduction path in the oxide under the gate, the gate can then rupture or get damaged. The conductive path can create an electric field which temporarily exceeds the dielectric breakdown field strength of the gate oxide. This can result in permanent damage or loss of the device.
- **Neutron Induced Upset:** A Neutron Induced Upset (NIU) can be the same as a SIU but is caused by an neutron hitting an silicon atom, which then produces charged particles. These charged particles in turn can cause an single event effect.

8.4.2. Radiation tolerant architectures

The TID and SEE risks come with different architectures to minimize the risk. In this section, different design strategies for both effects are given.

Total Ionization Dose

The main risk caused by the TID is the deterioration of the OBC components. As the performance of the components cannot drop below acceptable levels, *space-grade* components can be selected. For the TID risk, the main parameter relevant while selecting/designing space-grade components is their rated radiation dose. The minimum TID the OBC should withstand in GEO can be calculated using SPENVIS. Most space-grade COTS components have rated radiation doses between 100 krad and 1M rad. However, these radiation hardened options can be very expensive, with long lead times and no supplier stock [65].

Instead, to significantly reduce cost, a design sequence is introduced in which non-space-grade COTS options are selected, tested, modified and analysed to fulfill the requirements. First, a COTS OBC which fulfills all other, non-radiation requirements (clock rate, storage etc.) is selected. At the start, the OBC-P3 will be selected for this procedure. Then, the required radiation hardness is determined by calculating the TID: this is done by determining the radiation dose rate and defining the total shielding of the OBC, and the TID is then determined

---

[1]https://www.spenvis.oma.be/, accessed 18/06/2020

using SPENVIS. Then, the OBC is tested by subjecting it to low doses of radiation. A radioactive source will be used for this. While the OBC is subjected to this radiation, its performance is tested. The radiation hardness of the COTS component is attained at the moment the OBC can no longer fulfill the performance requirements. At this point, the OBC can be analysed to see if the performance is bottle-necked. If only a few sub-components are bottle-necking the performance, they may be replaced with more radiation-hardened variants. These modified OBCs can then be tested again. If many sub-components are deteriorated, and the radiation hardness requirement is not fulfilled, a different COTS OBC should be tested and optimised instead. If the modified OBC or perhaps the original COTS OBC passes the required hardness tests, the design is qualified for use, and six of these units should be manufactured. This design sequence is shown in Figure 8.2
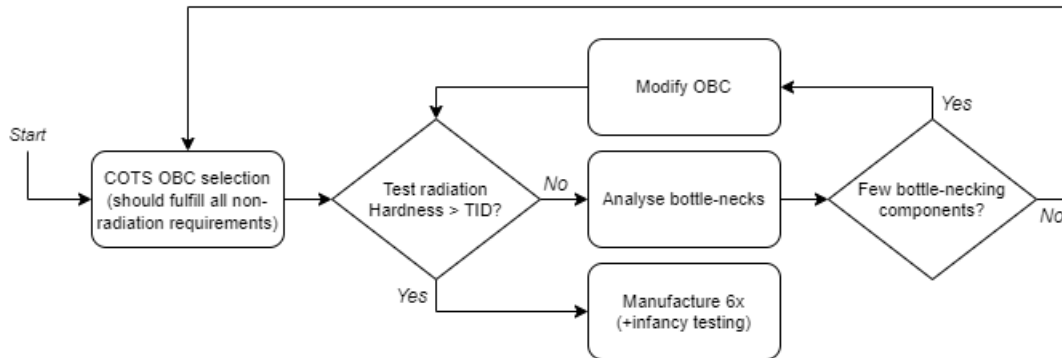

Figure 8.2: The design sequence for designing a radiation-hardened COTS OBC

Single Event Effects

Proper radiation shielding can decrease the chance of a SEE, but they will always be present and thus they have to be dealt with properly. There are different ways to design SEE tolerant systems, it can be done with installing extra pieces of hardware or using software to detect and correct the SEE [55]. All the different SEE have different ways to be dealt with, as there isn't one cures all. It is hard to determine the already in place SEE architecture of the OBC-P3. Therefore, the latter strategies are to be implemented or already implemented in the OBC. An always good working strategy to ground all electrical components to minimize the risk of SEL and SEGR.

Material choice of the components can have a big effect on the susceptibility of devices to SEE [65]. The use of Silicon on insulator which insulate the neighboring structure, such as two transistors, by lowering the parasitic capacitance, can decrease the effects of SEE. The Silicon on insulator and silicon on sapphire are both good ways to protect against the possibility of a SEL, but it does come at a price as it increases the size of the processor, and makes the processor much more expensive. Aluminum oxide can be used as a gate insulator and helps protects against SEB. Also the process of making the device, such as the temperature and the inert gas used, can increase the protection against SEE. This is only not verifiable as it is not know how the OBC components were made.

To counter the effect of SEE, fault tolerant systems can be use to prevent a fault turning into an error. A good way of making any space grade system fault tolerant is the use of redundancy in hardware or in software. Information and time redundancy are also good tools, these can be used such that fault detection and often fault tolerance can be achieved. There are a couple of techniques to achieve hardware redundancy [61]. Static techniques are designed to achieve fault tolerance trough the use of a voting mechanism. A voting mechanism is redundant hardware where multiple copies of the same tasks are made and then compared to each other [61]. An issue that arises with a voting system is that the voting system itself can be a single point of failure making it susceptible to faults or errors.

Dynamic techniques detect the existence of faults and perform a removal action of the hardware on the system. Examples are duplication with comparison, standby sparring, pair-and-a-spare, or a watchdog timer. In a pair-and-a-spare technique two modules operating at the same time, doing the same tasks and their results are compared against each other to provide error detection, this is a form of a voting system. A watchdog timer, assigns a certain time to a task, when no action is detected, it indicates a possible fault. The timer has to be reset after each task, the watchdog timer can be used for hardware or software fault detection. A hybrid technique combines the static and dynamic techniques. There are also software methods which can be implemented to achieve a more fault tolerant system. Such as consistency checks performed by the processor. Consistency checks consist of range checks, overflow, and underflow checks.

Capability checks such as memory tests or ALU tests, are done to verify the system on performing according to the expected capabilities. Code can also be used to detect and correct errors, to detect an error in a given structure Hamming Code can be used for single bit corrections and Reed-Salomon Code for multiple bit corrections.

To get an idea of the amount of SEEs that occur during two years GEO operation, a SPENVIS analysis was done. First the most critical components of the OBC had to be determined. Which are the flash, and memory of an OBC. The OBC-P3 uses Ferroelectric Random Acces Memory (FRAM) and NOR FLASH, both these are non-volatile meaning when there is a power cut information isnt lost. FRAM or FeRAM is immune to radiation and therefore very suitable for application in space [10]. However the CMOS structure for reading and writing the memory isnt radiation immune [10]. Therefore an analysis on the SEE occurrence for FRAM is very hard to do. A general value for FRAM LET threshold was taken, as it could not be determined what the manufacturer of the FRAM for the OBC-P3 was. Typical values for the LET for FRAM is between 20 and 40 MeV cm^2/mg, a bit crossection is in the order of 10^{-9} cm^2/bit [33]. Therefore a LET of 22 MeV cm^2/mg, a bit crossection of 1.5E-09 cm^2/bit was chosen. Giving a value from SPENVIS of 4.4E-02 bit^{-1} for 2 year GEO.

8.4.3. Other risks

The CDH subsystem has a vital function for the proper functioning of the spacecraft. Not only radiation poses a risk to the correct fulfilment of its task, there are many others which can cause the CDH and subsequently the spacecraft to fail. The most common ones are introduced by humans. Coding faults in the software can introduce an error in the spacecraft. Coding faults can even prevent the spacecraft from functioning, these coding faults should be found with proper verification and validation of the operating software of the spacecraft. Some of these coding faults can be solved after the spacecraft is in orbit, but if the operating software has a major fault then it might not be reparable. Electrical faults can also cause major problem to the CDH. Bad wiring or faulty connections, introduced by humans during assembly, can have disastrous consequences to the operation of the CDH.

Component corrosion, due to improperly stored components before launch, can create defects in the CDH. Mechanical damage due to vibrations and forces of the launch vehicle can introduces cracks or damage on the CDH components, a proper vibrational test has to be done to make sure the CDH can survive the launch stage of the mission. Due to the harsh space environment the thermal subsystem of the spacecraft needs to properly perform, when this is not the case thermal electric or mechanical stresses can be introduced into the CDH subsystem. These stresses can cause short or open circuits in the electrical components of the CDH. Soldering mistakes are often the cause of this, therefore the soldering joints should not be stress carrying.

When the CDH experiences a complete failure the mission can come to a premature end, when the satellite is not able to function anymore. Of all CubeSat failures 16-21%, 16% from begin of mission to 21% after 90 days, are due to failure of the CDH subsystem. It therefore is a critical subsystem and should be designed carefully. The OBC-P3 was chosen because of its excellent redundancy and pre-tested components.

8.5. Sustainability

The CDH is made in Denmark, therefore the CDH would need to be transported to the Netherlands for integration into the satellite. As it is a COTS option no R&D and little testing resources would have to be spend on the CDH, increasing its sustainability. The CDH consists of multiple cores made from silicon, it also has multiple Ferroelectric Random Access Memories (FRAM) made from iron. These are made by ARM which is a company situated in the UK, so the cores and memories would have to be shipped first to Denmark, this decreases the sustainability. The aluminium used for the casing can come from Denmark itself therefore decreasing the amount of resources spent on transport. The CDH does not have any explosive materials, therefore there is no risk for space debris due to explosion, or explosion during assembly. This increases the sustainability, by having a safe product. As Denmark has a lot of worker welfare laws, and environmental laws products made here hold a high sustainability standard.

8.6. RAMS

In this section, the reliability, availability, maintainability and safety characteristics of the CDH subsystem will be described.

8.6.1. Reliability

The OBC-P3 is highly reliable, as its two cores provide high redundancy. The OBC-P3 consists only of radiation total dose tested Electrical, Electronic and Electro-mechanical (EEE) components. Furthermore, it is vibration rated for all launch vehicles[2].

8.6.2. Availability

The OBC must always be available, as the rest of the subsystems are unable to function without it. The OBC is available even if one of the cores is reset by a watchdog or via command, since the OBC-P3 has two cores.

---

[2]http://space-inventor.com/wordpress/wp-content/uploads/2018/05/..., accessed 22/06/2020

8.6.3. Maintainability

Once the satellite is launched there will not be any possibility to do maintenance mechanical. It would be possible to do software updates during the mission, but this would only be done when a fault is detected. When the satellite is running smoothly then no scheduled software maintenance will be done. In case any issues do arise a time slot can be allocated to do the software update.

8.6.4. Safety

To identify safety risks a list of safety critical functions is made. The CDH forms the 'brain' of the satellite, hence it must always function to control the other subsystems. This is the first safety critical function: it must control the other subsystems. Secondly, the CDH must always be able to handle commands, otherwise it will never downlink the measurements, preventing the system from functioning. This is the second safety critical function: it must be able to receive commands. Lastly, it should always be able to send the measurements, giving the third safety critical function: It must be able to send stored data. As the assembly of the CDH may require soldering, which requires high temperatures, safety guidelines should be followed carefully. Furthermore, electricity should be handled carefully. Otherwise, the CDH is made out of non-explosive, non-toxic materials and is generally safe to handle.

8.7. Final design

The final CDH design will consist of one OBC-P3 unit, which consists of two cores, each with their own Central Processing Unit (CPU), Random Access Memory (RAM), programmable memory and storage memory. The first core will be dedicated to the ADCS control system, and the second core to all other command and data handling. The two cores will be connected, such that ADCS commands and data can be handled between the two cores. An I/O board will be selected and connected to the second core. The sensors will be selected such that they are compatible with the I/O board and OBC. In total, it is estimated that 80 sensors will be connected to the I/O board. The OBC and I/O board will be tested and qualified for their radiation resistance, as explained in section 8.4.2. Furthermore, proper validation and verification will be done for the code written, to prevent coding faults. Proper testing will be done to mitigate the risk of electrical faults, thermal stresses or mechanical stresses causing the CDH subsystem to fail. Storage, transport and soldering will be done carefully by professionals.

The mass, volume and power required for the CDH subsystem are given in table 8.6. The sensors are left out, as they are considered part of the relevant subsystem design. The I/O board does not consume power, as it is powered by the OBC. The characteristics of the OBC are given in table 8.7. The storage memory is not large enough, and should be customised. Customising the OBC is supported by the manufacturer, hence the storage memory may be increased by demand. If the required size (1.22 GB) cannot be provided by the manufacturer, the storage memory should be increased either by adding a separate storage memory module, or customising the storage memory manually. The customised storage memory should be included in all tests done.

Table 8.6: The mass, volume and power consumption of the CDH subsystem

Component	Mass [kg]	Volume [U]	Power [W]
OBC	0.15	0.15	3
I/O board	0.1	0.1	0
Margin	*10%*	*10%*	*10%*
Total	**0.285**	**0.285**	**3.3**

Table 8.7: The characteristics of the selected OBC.

Characteristic	Value	Unit
Clock rate	300	MHz
Programmable memory	1	MB
Storage memory	64	MB
Supply voltage	3.3	V
Aluminium shielding	1.5	mm

9

Electrical Power System

The EPS concerns all power generation, conditioning, and distribution systems to provide power to other subsystems. This system makes use of an external primary power source, namely solar panels, and an internal secondary power source, namely a battery.

9.1. Functional analysis

The EPS should provide enough power to all subsystems to operate. This power should be regulated to avoid the occurrence of one subsystem consuming the power of others. The EPS should also generate the right amount of power and this can be done via several options, such as a battery and a solar panel. An overview of the functions provided by the EPS were already identified in the baseline report [3] and are shown in figure 9.1.
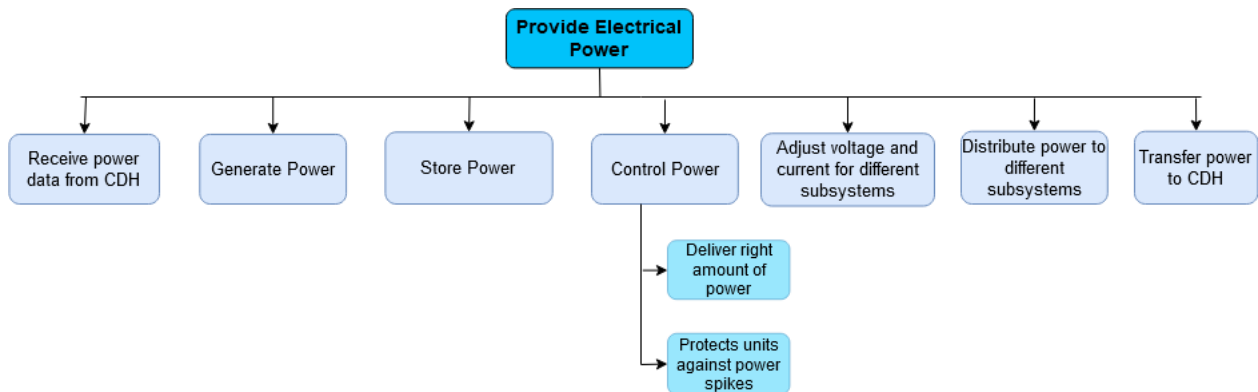
Figure 9.1: Functional breakdown structure of the EPS subsystem

9.2. Requirements

The requirements for the EPS can be found in the baseline report [3] and are shown below.

Table 9.1: EPS requirements

ID	EPS
LICCA-SYS-Sub-EPS-1	The total required electrical power shall not exceed 40W.
LICCA-SYS-Sub-EPS-2	The EPS shall be able to receive data from the CDH.
LICCA-SYS-Sub-EPS-3	The EPS shall deliver 30.60 W during daytime.
LICCA-SYS-Sub-EPS-4	The EPS shall deliver 31.0 W during eclipse.
LICCA-SYS-Sub-EPS-5	The EPS shall be able to store 90 Wh of energy.
LICCA-SYS-Sub-EPS-6	The EPS shall provide the right amount of power to each subsystem.
LICCA-SYS-Sub-EPS-7	The EPS shall adjust the voltage for each subsystem.
LICCA-SYS-Sub-EPS-8	The EPS shall provide the correct current type to each subsystem
LICCA-SYS-Sub-EPS-9	The EPS shall protect the system from power spikes.
LICCA-SYS-Sub-EPS-10	The EPS shall provide data about power regulation to the CDH subsystem.
LICCA-SYS-Sub-EPS-11	The power source of the EPS should have an efficiency of at least 31.8%.
LICCA-SYS-Sub-EPS-12	The components of the EPS subsystem shall have a current TRL of 7 or higher
LICCA-SYS-Sus-Sd-3.2	Batteries shall be discharged completely after the end of mission [36].
LICCA-SYS-Sus-Sd-3.3	Batteries shall incorporate safety mechanisms against break-up [36].

9.3. Design methodology

For the design of the EPS a solar cell for power generation and a battery for power storage are considered. These two were the valid options left from the design option tree as described in the baseline report [3]. On top of that a Power Conditioning Unit and a Power Distribution Unit were considered (PCU and PDU) to regulate power.

9.3.1. Basic set-up

First, the required power must be calculated in order to get an estimate of how much solar panel area is needed. For the first iteration it is assumed that the total power needed is 40 W, as this is a critical requirement and the design is made for the worst case scenario. The required power can be calculated with the equation (9.1):

$$P_{req} \cdot t_d = \frac{P_d \cdot t_d}{\eta_d} + \frac{P_e \cdot t_e}{\eta_e} \tag{9.1}$$

Where η_d and η_e are day and eclipse efficiencies, assumed to be 0.8 and 0.6 for the first iteration, respectively [74]. P_d and P_e are the power required during the day and eclipse, discussed more in detail in section 9.3.4. t_d and t_e are day and eclipse time, already determined in section 4.4.2.

9.3.2. Solar panel trade-off

Now that the required power is known, it is time to select a solar panel that can deliver this power. A couple of solar cells were considered for the trade-off, from Spectrolab[1], Azurspace[2], and CESI [3].

A trade-off was made between 11 different solar cells, taking into account the degradation (λ), efficiency (η) and mass density (M_d). Efficiency and degradation were considered to be the most critical parameters, as these influence the total area, which influences directly the volume and the configuration of the EPS system. The weight of the degradation was therefore estimated to be four, the weight of the efficiency to be three and the mass density was assigned a weight of one. These weights were then normalised for each parameter. The efficiency should be as high as possible and the degradation and mass density as low as possible to obtain an optimal design. The degradation and mass density were therefore inversed. The score is calculated with the following equation (9.2):

$$Score = p_\eta \cdot w_\eta + p_\lambda \cdot w_\lambda + p_{M_d} \cdot w_{M_d} \tag{9.2}$$

Here w is the weight of each parameter and p the score per parameter. The overview of each solar panel en their scores is presented in table 9.2.

Table 9.2: Solar Panels

Solar Panel	η (%)	λ (% per year)	M_d (mg/m^2)	Score	Norm
Weight	4	3	1		
XTE-SF	32.2	0.93	84	4.85	0.76
XTJ Prime	30.7	0.93	84	4.71	0.70
XTJ	29.5	0.93	84	4.59	0.64
UTJ	27.9	1.005	84	4.34	0.52
Silicon S32	16.9	1.99	32	3.26	0.00
TJ Solar Cell 3G28C	28.3	0.903	86	4.52	0.61
TJ Solar Cell 3G30C	29.8	0.705	86	5.08	0.88
QJ Solar Cell 4G32C	31.8	0.6815	86.15	5.33	1.00
CTJ-30 thin	29	1.16	50	4.52	0.61
CTJ-30	29.5	1.16	89	4.28	0.49
CTJ-LC	28	1.08	89	4.23	0.47

From the table it can be seen that the QJ Solar Cell 4G32C solar panel is the clear winner. A sensitivity analysis can be considered. However, from the table it can be seen that this solar cell has almost the highest efficiency and the lowest degradation. Therefore it was determined a sensitivity analysis was not needed.

---

[1] https://www.spectrolab.com/photovoltaics.html, accessed 11/06/2020

[2] http://www.azurspace.com/index.php/en/products/products-space/space-solar-cells, accessed 11/06/2020

[3] https://www.cesi.it/space-solar-cells/, accessed 11/06/2020

The area is then calculated with the following equation (9.3):

$$A = \frac{P_{req}}{\Phi \cdot \eta_{sp} \cdot cos(\theta) \cdot (1 - \frac{\lambda}{100})^t} \tag{9.3}$$

where ϕ is the solar flux, which is on average 1310 W/m^2 and t the lifetime of the satellite, estimated to be 2 years (see section 4.1).

The next step is to determine the configuration of the solar panels. It is determined that only three sides of the satellites will be used for solar panels, because the other sides are occupied by the thermal control subsystem (louvers) and the TT&C. A script is used to determine how much area of these three sides are in sunlight and for how long. It is combined with an eclipse tool that determines for every orbit whether the satellite is in eclipse or not (see section 4.4). An average orbit is taken to determine how much area is needed per side (A_{side}). In order to account for worst case scenarios the maximum incidence angle is taken (23.44 degrees) [15]. This determines the required area and the number of cells can be calculated. Finally, the total area of solar cells (A_{tot}) can be calculated. The final configuration is shown in section 9.7.

Now the total area is known, the total mass and volume of the solar panels can be calculated with equation (9.4) and equation (9.5).

$$m_{sp} = A_{solar-cell} \cdot M_d \cdot \#_{cells} \tag{9.4}$$

$$V_{solar-panels} = t_{solar-cell} \cdot A_{solar-cell} \cdot \#_{cells} \tag{9.5}$$

9.3.3. Battery trade-off
Now that the solar cell is chosen, an appropriate battery can be selected for this mission. The batteries considered for the trade-off and their specifications can be found in table 9.3.

Table 9.3: Batteries, taken from Clydespace [4], Eagle Picher, [5] SatSearch [6] and ISISpace [7]

Battery	Mass [g]	Voltage [V]	Volume [mm^3]	Specific) Energy
OPTIMUS-30	268	8.26	186330	30 Wh
OPTIMUS-40	335	8.26	236479	40 Wh
OPTIMUS-80	670	8.26	492326	80 Wh
CubeSat Battery Pack	240	6 - 8.4	216000	42 Wh
Li-Ion ICP-20	640	3 - 4.1	356384	150 Wh/kg
CubeSat Kit™ Battery Module 1	310	7.4	203040	40 Wh
6 Ah Space Cell	222	3 - 4.1	101296	105 Wh/kg
12 Ah Space Cell	465	3.6	175858	114 Wh/kg
Eagle Picher Space Cell	2020	4.1	802262	121.3 Wh/kg
43 Ah Space Cell	1270	3.6	496922	153 Wh/kg
ISISpace Battery Pack	252	3.6	210000	45 Wh

The total energy needed in eclipse needs to be calculated first. This determines how much batteries must be used in order to store enough energy. The energy is calculated using equation (9.6). Note that the total eclipse efficiency consists of the battery efficiency, the charge efficiency, the discharge efficiency and the efficiency of the Power Conditioning and Distribution Unit (PCDU).

$$E_{bat} = \frac{P_e \cdot t_e}{\eta_e \cdot \eta_{bat} \cdot \eta_{discharge-bat} \cdot DOD} \tag{9.6}$$

Now the required energy storage is known the batteries can be compared. The specifications of the batteries with an energy storage of 80 Wh can be found in table 9.4. The score is calculated in the same way as for the solar panel trade-off. Mass and volume are the only critical properties of the battery, the lifetime or cycles were considered before the selected battery could enter the trade-off. The weights for mass and volume are one and two, respectively. Volume is considered more critical, because the volume requirement of 12U should be taken into account. For mass there is no strict requirement.

---

[4]https://www.aac-clyde.space/assets/000/000/079/OPTIMUS_original.pdf?1564954960, accessed 11/06/2020
[5]https://www.eaglepicher.com/products/secondary-batteries-rechargeable/, accessed 11/06/2020
[6]https://satsearch.co/products/categories/power/battery, accessed 11/06/2020
[7]https://www.isispace.nl/product/ieps-electrical-power-system/, accessed 11/06/2020

Table 9.4: Battery trade-off

Battery	# batteries	Total Mass [g]	Total Volume [mm^3]	Score	Norm
Weight		1	2		
OPTIMUS-30	3	804	558990	1.85	0.47
OPTIMUS-40	2	670	472958	2.20	0.68
OPTIMUS-80	1	670	492326	2.15	0.64
CubeSat Battery Pack	2	480	432000	2.63	0.94
Li-Ion ICP-20	1	640	356384	2.72	1.00
CubeSat Kit™ Battery Module 1	3	930	609120	1.67	0.35
6 Ah Space Cell	4	888	405184	2.28	0.72
12 Ah Space Cell	2	930	351716	2.52	0.87
Eagle Picher Space Cell	1	2020	802262	1.11	0.00
43 Ah Space Cell	1	3.6	496922	1.79	0.43
ISISpace Battery Pack	2	504	420000	2.63	0.94

As can be seen from the table the scores are quite similar and thus a sensitivity analysis is needed. For this sensitivity analysis, three options will be considered, namely the CubeSat battery pack, the Li-Ion ICP-20 and the battery from the EPS system of ISISpace.

Sensitivity analysis

Since the normalised final scores of the battery trade-off lie close to each other, it is important to do a sensitivity analysis to see if the rightful winner is chosen. The first option to perform the sensitivity analysis is to change the weights. This is done in the graphs of figure 9.2.
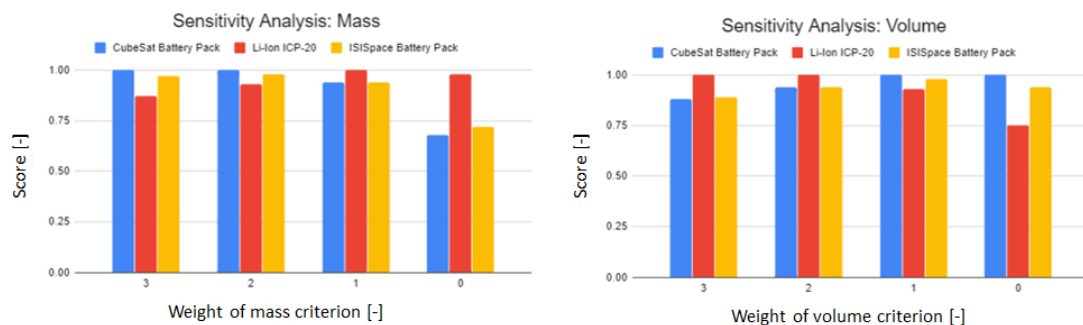
Figure 9.2: Battery trade-off sensitivity analysis

When looking at the figure, it can be seen that there is not one battery that always wins the trade-off. However, the three batteries chosen for the analysis have the highest score most of the times. Only if the mass is set to a weight of zero, the Cubesat battery pack and the ISISpace battery pack have a low score. This makes sense, since batteries with a low volume will now win the trade-off. However, for this trade-off it would not make much sense to remove mass as a criterion. When the volume weight is set to three, the '12 Ah Space Cell' will enter the top three. This battery has a relatively higher mass which will be less significant when the volume weight is increased. However, due to this higher mass and no better performance than the others, this will not be considered any further.

To conclude, for most criteria the same three batteries are in the top three of the trade-off. This means that the difference between these batteries is small so a decision has to be made based on small details. It can be seen in figure 9.2 that the Li-Ion ICP-20 wins the trade-off in most cases. Furthermore, this battery has a lifetime of 18 years in GEO which is beneficial for the mission[8]. Since the lifetime for the other batteries is not specified in GEO, it was decided that the Li-Ion ICP-20 battery will be used for the EPS subsystem in the LICCA mission. The DOD of the chosen battery is 0.8 and the efficiencies will be discussed in section 9.3.4. The battery is a COTS option and therefore it is assumed it complies to all safety regulations. The PCDU considered in section 9.3.4 also provides some safety regulations such that the battery will not be short circuited and is grounded.

---

[8] https://satsearch.co/products/oce-technology-lithium-ion-battery, accessed 11/06/2020

9.3.4. PCDU considerations and mass calculations

The last step in designing the EPS subsystem is to select a proper PCU and PDU, or a combined PCDU. The number of outputs that the PCDU system should provide is first estimated around 20. Outputs of this system are regulated buses of 3.3 V, 5 V, and 12 V and also unregulated buses such as the battery. Two options are considered, as can be seen in table 9.5. All the values have been multiplied by two, because two PCDU's will provide enough number of outputs. These PCDU's also include Battery Charge Regulators (BCR) and Maximum Power Point Trackers (MPPT) such that two complete systems can be compared.

Table 9.5: PCDU selection [9] [10]

PCDU	Total Mass [g]	Total Volume [U]	Power Consumption [W]	# of outputs
ISISpace PCDU	221.5	0.45	0.526	24
Starbuck NANO Plus	296	0.36	0.8	28

From the table it can be seen that it is not quite clear which option is the best. However, a lot more information is known about the Starbuck NANO Plus PCDU. This contains efficiencies and safety regulations. Furthermore, it provides more outputs, which results in more design freedom. Therefore the Starbuck NANO Plus PCDU is chosen for the LICCA mission.

The effective day and eclipse efficiencies can now be determined more precisely because the PCDU and the battery are known. Equation (9.7) and equation (9.8) are used to calculate these efficiencies. The values for the efficiencies are taken from the chosen PCDU [73] and the battery efficiency is assumed to be 95% [74].

$$\eta_d = \eta_{cond} \cdot \eta_{dist} \tag{9.7}$$

$$\eta_e = \eta_{cond} \cdot \eta_{dist} \cdot \eta_{bat} \cdot \eta_{charge-bat} \cdot \eta_{discharge-bat} \tag{9.8}$$

During the selection of the different components of the EPS, the required power changed. This was caused by a new iteration that determined different power consumptions for the subsystems. The power consumption per subsystem is given in table 9.6.

Table 9.6: Power per subsystem

Subsystem	Day	Eclipse
Payload	5.114	5.114
ADCS	9.9	9.9
Propulsion	1.89 or 9.6	1.89
Communication	5.5	0
CDH	3.3	3.3
Thermal	0	10
Structure	0	0
EPS	0.8	0.8
Total	**30.60**	**31.00**

During day and eclipse almost all subsystems consume the same amount of power, except for communication, thermal, and propulsion. It is determined communication is only used during the day (see chapter 7) and thermal only during eclipse to make sure every component stays within the specified temperature range (see chapter 10). For nominal operations, the propulsion system consumes 1.89 W. For preheat however, 9.6 W is needed. It is determined that the preheat is performed at other times than the telemetry, and the propulsion system can use the communication's 5.5 W. The remaining 4.1 W are added to the total power to be able to perform all necessary functions in different scenarios. The last step for the EPS is to estimate the total mass and volume which can be done by summing up the masses and volumes of the individual components.

9.4. Risk

The EPS consists of components which all can have a risk such that the mission fails. These risks should be identified in order to get an overview of what could happen and after that a mitigation strategy is performed to reduce the probability and/or the impact of these risks.

---

[9] https://www.isispace.nl/product/ieps-electrical-power-system/, accessed 11/06/2020
[10] https://www.aac-clyde.space/satellite-bits/eps, accessed 11/06/2020

The first component considered is the battery. Degradation of the battery is taken into account, but it can also happen that it degrades more than accounted for. This will influence the energy the battery can store and thus means that the satellite might not be able to activate all the systems every day. However the lifetime is estimated to be 18 years in GEO, which implies the chances this will happen are really small. The leakage of the battery should also be considered. Batteries tend to leak a lot, however this is tested thoroughly for the considered battery, thus the probability of occurrence is again small [25]. The chosen battery is a flight-proven COTS battery, so the leakage and degradation of the battery are not considered critical for the risk analysis.

The PCDU [73] also provides some safety mechanisms. The battery should be placed in the correct position, otherwise it can cause a short circuit. The battery should also be compatible with the PCDU, otherwise the PCDU can cause damage to the battery. Unrelated to batteries, the PCDU also has some risks. A few risks are stated in the user manual [73]. If the switch configuration is incorrect while a power is applied, the output of the BCR can be blown, which result in a failure of the EPS. Furthermore, exceeding maximum ratings (such as exceeding temperature ranges, vibration, and radiation levels) should be avoided.

Lastly the solar panels should be considered. They also have a degradation factor and a certain estimated efficiency. If these values are worse than stated, it could be the case that there is not enough power to supply all the subsystems. However this not considered as a critical risk and therefore it is not taken into account in the risk analysis. On top of that, the compatibility of the solar panels with the PCDU system should be considered and the creation of heat of the solar panels too, this could cause temperature problems. This will be analysed further in chapter 10. The last thing to consider is the failure of a couple of solar cells. These cells are quite small and fragile and therefore the chances are significant that at least one of them fails. This will lead to not enough power generation and thus should be avoided.

9.5. Sustainability

The EPS consists of multiple components, which should all be considered regarding sustainability. However the main element is the battery and discussed here. In the Baseline Report [3] some measures for a sustainable battery are identified. Here it is stated that safety mechanisms should be built in in order for the battery to not explode. The PCDU module incorporates a battery charge and discharge regulator systems, which accounts for this safety and includes these mechanisms [73]. The battery is discharged completely after EoL of the spacecraft.

9.6. RAMS

This section describes the reliability, availability, maintainability and safety characteristics of the EPS.

9.6.1. Reliability

As for all other subsystems, a fairly high reliability is required since there is no opportunity for maintenance. The EPS causes a large amount of CubeSat failures, approximately one third of all failures [46]. The design includes two PCDU's and thus also twice the safety mechanisms, which increases reliability. However, due to volume constraints no redundant solar cells nor battery are included, as explained in section 9.4. This means the EPS can not be considered as a reliable subsystem.

9.6.2. Availability

The solar panels first need to be deployed before the EPS can be activated. This is planned at the beginning of the operations and not adjusted afterwards. The solar arrays are sized to provide sufficient power to the spacecraft at every point in sunlit orbit. The battery can store power needed to survive eclipses and contains a margin. The EPS is therefore always available, assuming it to function correctly, to provide power.

9.6.3. Maintainability

During operations, it will not be possible to perform maintenance on the satellite. The functioning of the subsystem can thus not be corrected. Therefore the system is designed to have a high reliability and safety.

9.6.4. Safety

As mentioned in section 9.4, the PCDU contains safety mechanisms for the entire system. It protects the connections between the different components, for example it protects the PCU from overcurrent from the solar panels. It also protect overcharging and under-voltage of the batteries. Since all these safety mechanisms are present, the system can be considered safe. The solar panels can form a hazard due to degradation, but the solar cells used are tested and verified for longer missions, so the degradation will be limited. The functioning of the battery as well as the solar cells are safety critical functions. This means that if one of them fails, it is catastrophic for the mission.

The components of the EPS are designed to be safe, and thus not damage any equipment or other components. However, during manufacturing of the batteries safety precautions need to be made. Lithium is flammable and the ions can cause explosions. Once manufactured, this risk is no longer existent.

9.7. Final design

The final design of the EPS subsystem is determined using the design methodology described in section 9.3. The system consists of 6 solar panels, 2 on each side, covering 3 sides of the satellite. The solar cell used is the QJ Solar Cell 4G32C from Azurspace. It also contains a battery and a PCDU, which includes BCRs and a MPPT. The battery used is the Li-Ion ICP-20, the PCDU used is the Starbuck Nano Plus. A schematic overview is given in figure 9.3. Where the configuration of the solar panels is shown in more detail in figure 9.4.
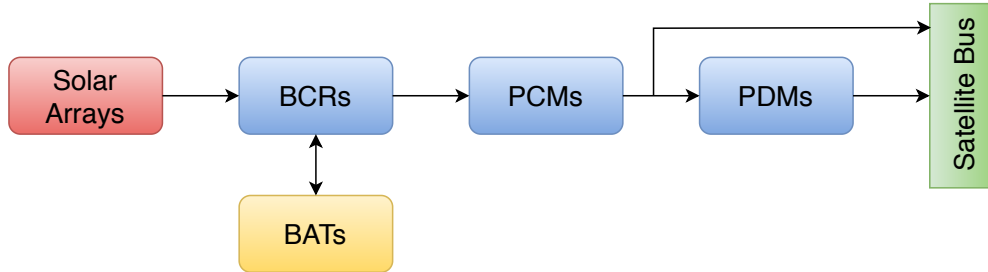
Figure 9.3: EPS configuration [73]
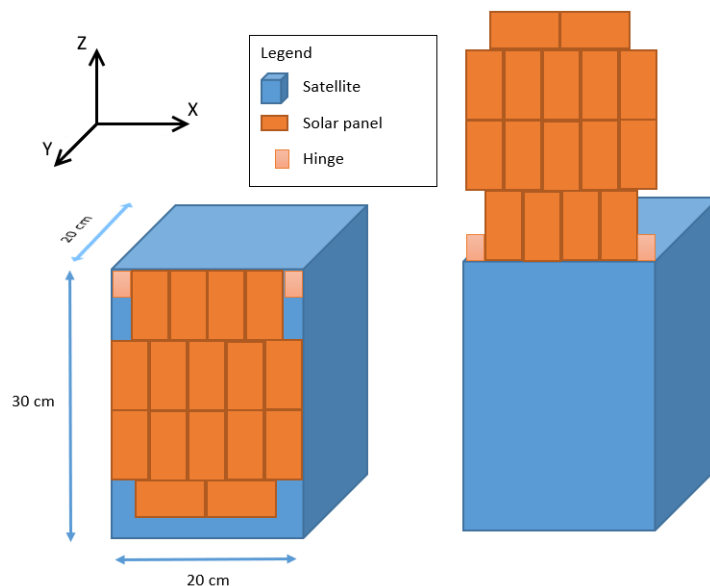
Figure 9.4: Solar panel configuration

As can be seen from the figure, one side of the satellite is shown where on the left figure the solar panel is shown in undeployed state and on the right figure it is shown in deployed state. This is then also done for two other sides of the satellite in order to provide enough power. The structure and deployment mechanisms of the solar panels will be described in more detail in chapter 11.

The general properties of the EPS subsystem can be found in table 9.8. More information about each property can be found in section 9.3. The mass and volume budgets can be determined using the masses and volumes of all different components. This result and the total mass and volume is shown in table 9.7.

Table 9.7: Mass and volume budget

Component	Mass [kg]	Volume [U]
Solar panels	0.2646	0.0338
Battery	0.640	0.356
PCDU	0.296	0.36
Total	**1.200**	**0.750**

Table 9.8: General properties of the EPS subsystem

Property	Value	Unit	Property	Value	Unit
Power consumption			Battery		
t_e	4320	s	DOD	0.8	-
t_d	82080	s	E_{bat}	90.2	Wh
P_d	30.60	W	Solar cell		
P_e	31.0	W	$\eta_{solar-cell}$	0.318	-
Efficiencies			θ	23.5	deg
η_{cond}	0.90	-	λ	0.6815	%
η_{dist}	0.90	-	M_d	68.15	mg/cm^2
η_{bat}	0.95	-	t	0.11	mm
$\eta_{charge-bat}$	0.89	-	A	0.0032	m^2
$\eta_{discharge-bat}$	0.89	-	Total area		
η_d	0.81	-	A_{req}	0.1063	m^2
η_e	0.61	-	A_{side}	0.09974	m^2
Required power			$\#_{cells}$	96	-
P_{req}	40.06	W	A_{tot}	**0.3072**	m^2

10

Thermal

The thermal control subsystem concerns the thermal regulation of the spacecraft. Its purpose is to keep all the different components of the spacecraft in their allowable temperature ranges.

10.1. Functional analysis

To come up with a proper design of the thermal subsystem, a functional analysis had to be done. In the FBS, five functions of the thermal subsystem are identified. These are in shown in Figure 10.1.
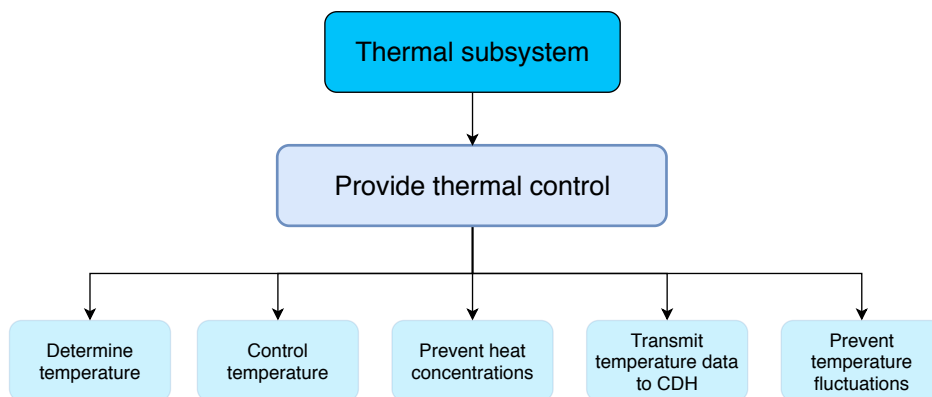
Figure 10.1: The functional breakdown structure of the thermal subsystem

10.2. Requirements

The requirements for the thermal control subsystem, as identified during the mission definition and exploration phase, can be found in the baseline report [3]. The updated requirements can be found in table 10.1. The changes made to these requirements with respect to the midterm report [5] are shown in table 10.2.

Table 10.1: The list of thermal control subsystem requirements.

ID	Thermal
LICCA-SYS-Sub-Thr-1	The thermal system shall measure temperature in Kelvin
LICCA-SYS-Sub-Thr-2	The thermal system shall maintain total temperature of the satellite in the range of 10-30 °C.
LICCA-SYS-Sub-Thr-3	DELETED
LICCA-SYS-Sub-Thr-4	The thermal system shall prevent a temperature difference within the spacecraft of over 20 °C.
LICCA-SYS-Sub-Thr-5	DELETED
LICCA-SYS-Sub-Thr-6	The thermal system shall be able to transfer the thermal data to the CDH system.
LICCA-SYS-Sub-Thr-7	The components of the thermal subsystem shall have a current TRL level of at least 7.

Table 10.2: The changelog of the thermal requirements

ID	Changes	Rationale
LICCA-SYS-Sub-Thr-2	Changed the temperature range	After iteration 1, the temperature range of all COTS components was found. These ranges overlapped between 283.15 K and 303.15 K
LICCA-SYS-Sub-Thr-5	Removed	This requirement now overlaps with requirement LICCA-SYS-Sub-Thr-2

10.3. Design methodology

The thermal control subsystem has to keep all the different subsystems in their ideal temperature range, as this ensures proper functioning of the subsystems. It requires inputs from other subsystems and the space environment has to be taken into account. The temperature of components in space fluctuates a lot. This temperature fluctuation is caused by the solar irradiance, and the infrared radiation from Earth.

A temperature range was identified for all the subsystems. This temperature range was based on the highest minimum temperature and the lowest maximum temperature of all the components. Therefore, this could be taken as the maximum temperature range possible for that subsystem without failure or proper functioning of the subsystem itself. The ranges can be found in table 10.3.

Table 10.3: Temperature ranges subsystems

Subsystem	Minimum temperature [°C]	Maximum temperature [°C]
Payload	10	60
ADCS	-20	40
Propulsion	-	-
Communication	-40	85
CDH	-40	55
EPS	10	30

From table 10.3, it was deduced that the temperature range is between 10 °C and 30 °C. This means that the temperature could not be below 283.15 K and not exceed 303.15 K. Therefore, the thermal control subsystem needs to keep the temperature of the spacecraft in between this temperature range. The thermal control system tries to keep the entire spacecraft in this range to minimise temperature differences which could influence the payload measurements. It should be noted that for the selected thruster, no certified temperature range was available. For now, it is assumed this temperature range does not further limit the design space.

As temperature sensors, Resistance Temperature Detectors (RTD) may be used. These are very small, require very little power, and their selection is thus not driving for the design of the thermal subsystem. For example, the 6 W 161 from Innovative Sensor Technology is 1.6 x 1.2 mm^2, can measure temperatures between -200 C

and 600 C, and consumes 0.1 mW of power[1]. First, the principle of establishing a heat balance is explained in section 10.3.1, followed by the design methodology for the thermal subsystem, in section 10.3.2. Afterwards, in section 10.3.3, a separate heat balance is made for the solar panels, which is then evaluated.

10.3.1. Heat balance

Heat is transferred from a medium with a high temperature to a medium with a low temperature, according to the second law of thermodynamics. The Sun has a major influence on the amount of heat generated on the spacecraft. Therefore it has to be determined what area is exposed to the Sun. First, the solar irradiance was calculated for variable distances to Earth. This is done by assuming the Sun to have an effective radiating temperature of 5 870 K [74]. This is calculated by making use of equation (10.1), and assuming that the Sun is a black body emitter, meaning that its emissivity is one, $\epsilon = 1$ [74].

Knowing the radius of the sun to be 696 340 km, it is calculated that the total power emitted is $3.856 \cdot 10^{26}$ W. Based on conservation of energy, and assuming the energy is emitted in all directions equally, the inverse square law was used, $q \propto 1/r^2$ [74]. Knowing the distance to Earth, the solar flux varies between 1328 W/m^2 in aphelion and 1440 W/m^2 in perihelion.

To determine the amount of solar irradiance reflected by Earth, the albedo has to be determined. The albedo of Earth can vary dependably on the position of the spacecraft. Since the satellites orbit in GEO, this position is constant. The albedo factor can vary from 0.05, open ocean, to 0.6, high clouds or icecap. As the satellites will be in orbit around the equator, where warm weather, rain clouds, and oceans exist, a range of 0.1-0.5 was chosen for the albedo factor. To calculate the albedo flux, equation (10.2) [74], has been used.

$$T_e = \sqrt[4]{\frac{q_{emitted}}{k}} \qquad (10.1)$$

$$F = \left(\frac{R_{planet}}{R_{orbit}}\right)^2 \qquad (10.3)$$

$$J_a = a \cdot J_s \cdot F \qquad (10.2)$$

$$J_{IR} = k \cdot T_{IR}^4 \qquad (10.4)$$

Where a is the albedo factor, and F the visibility factor. The visibility factor depends on where the spacecraft is, during eclipse the F is zero, but when the spacecraft is on the Sun lit side of the Earth, equation (10.3) [74] can be used. The Earth, as any other planet, radiates infrared energy. This value depends on the effective radiating temperature of the planet, which can be calculated with equation (10.4) [74]. For Earth, the effective temperature is taken to be 255 K, with an equivalent planet flux of 240 W/m^2 [74].

Knowing all external heat sources, a balance could be made to get an estimate of heat absorbed by the spacecraft. Equation (10.5) was used to find the received heat from the external sources [74]. In this equation, ϵ is the emissivity, α the absorptivity and J the intensity. Subscripts s, a and IR refer to solar radiation, albedo, and IR radiation respectively. The A_i refers to the projected area, where i stands for the incoming radiation. $A_{surface}$ is the total surface area. ϵ is used for the infrared spectrum, as this is a different frequency than the solar irradiance. The emissivity is used according to Kirchhoff's law, and the absorptivity and emissivity of a material at identical temperature are essentially equal [74].

$$\dot{Q}_{absorbed} = \alpha_s \cdot J_s \cdot A_i + \alpha_s \cdot J_a \cdot A_i + \epsilon_{IR} \cdot J_{IR} \cdot A_{surface} \qquad (10.5)$$

Another source of heat that has to be taken into account is the heat produced by the other subsystems. To get an estimate for this, it needs to be known how much power is consumed, on what efficiency the system operates, and over what period of time the system is active. An estimate of the power dissipated by the different subsystems can be found in table 10.4.

Table 10.4: Power dissipated by subsystems

Subsystem	Minimum [W]	Maximum [W]
Payload	0	1.68
ADCS	0	1.118
Propulsion	0	0.1
Communication	0	1.2
CDH	0.55	1
EPS	0	6.04

To make the heat balance of the spacecraft, the emissivity factor has to be determined. This property varies per material or paint layer. The same goes for the absorptivity factor, which can be freely chosen according to

material choice. The emissivity of the spacecraft was calculated using the equation (10.6) [74].

$$\dot{Q}_{emitted} = \sqrt[4]{\frac{J}{\epsilon \cdot k \cdot A}}$$

(10.6)

Where J is the total heat the spacecraft experiences, ϵ the emissivity factor and k the Stefan Boltzmann constant. Having the internal heat generated and external heat received, and knowing the amount of heat dissipated, the heat balance can be made. To find the areas exposed to the sun, a program was made to find the maximum and minimum surface exposed to the Sun during the lifetime of the spacecraft. Then, to balance the heat, a study was done into different materials and heat dissipation techniques, such as louvers. Table 10.5 was constructed to get an estimate of the absorptivity and emissivity of different materials.

Table 10.5: Absorptivity and emissivity of different materials

Material	Solar absorptance	Hemispherical emissivity
Black paint	0.96	0.75
Aluminized teflon 5 mil	0.14	0.78
Silvered teflon 5 mil	0.09	0.8
Aluminized kapton foil 2 mil	0.42	0.72
Aluminized kapton foil metal side	0.12	0.05
White paint	0.17	0.82
OSR without glue gaps	0.09	0.76
Solar cell Si	0.75	0.82
Solar cell GaAs	0.91	0.81
CFRP	0.92	0.82

Having identified the heat flow coming from the external and internal sources, and the calculated emissivity, the heat balance was set up, from which an equilibrium temperature was calculated. This was done by taking the background temperature of space and adding the difference from $\dot{Q}_{in}$ and $\dot{Q}_{out}$ to get the equilibrium temperature of the spacecraft.

10.3.2. Thermal subsystem

The thermal subsystem of the spacecraft is designed using a heat balance. For many of the variables in the heat balance, the value depends on the status of the satellites. For example, the area irradiated by the Sun depends on the orientation of the spacecraft. To calculate the total temperature range to which the spacecraft can be subjected, minimum and maximum values are used for all heat balance calculations. The albedo radiation, the albedo factor and visibility factor can also vary greatly. Furthermore, the heat generation from the different subsystems can also vary, as shown in table 10.4. A special case that has to be accounted for is when the spacecraft does not receive solar irradiation due to an eclipse. The temperature range is calculated separately for eclipses, to determine whether a heat source is required. The total temperature range, both for eclipsed and nominal scenarios, is given in table 10.6. As can be observed, the temperature can vary greatly. During eclipses the temperature drops far below the accepted temperature range.

Table 10.6: Temperature range for the spacecraft, during nominal situation and eclipsed

	Nominal temperature [°C]	Eclipsed temperature [°C]
Minimum incoming heat	-66.81	-164.50
Maximum incoming heat	137.30	68.60

The main problem comes from the eclipsed situation. The lack of solar irradiance during an eclipse significantly decreases the heat flowing into the system. To compensate for this, heat sources can be added. However, a heat source alone would need to generate about 12W of power to compensate for the solar irradiance. This is far over the budget allocated to the thermal subsystem, and is thus considered an unacceptable design choice.

Instead, thermal louvers were considered. Thermal louvers can be either opened or closed, but do not require power to be controlled. In the opened state, the louvers expose the underlying material to the environment. In the closed case, the underlying material is isolated; only the louver material is exposed. The emissivity of louvers can be very low, down to 0.03 using louvers with a TRL of 7 [30]. The underlying material will

be aluminised kapton foil, which has an emissivity of 0.72. By opening or closing the louvers, the effective emissivity of the spacecraft can be altered. Two 20x20cm² sheets of louvers will be installed, on both 20x20cm² surfaces on the spacecraft. By controlling the louvers, the effective emissivity of the spacecraft can be varied in the range of 0.045-0.2175.

Using the louvers, the temperature can thus be controlled. To establish the controllable temperature range, the emissivity of the spacecraft is varied. The controllable ranges are given in table 10.7. The temperature range that be can controlled using the louvers is given for minimum and maximum heat income conditions.

Table 10.7: Controllable temperature range using louvers for all conditions

Minimum incoming heat	Nominal temperature [°C]	Eclipsed temperature [°C]
Maximum emissivity	-66.8	-164.5
Minimum emissivity	32.8	-112.0
Maximum incoming heat	Nominal temperature [°C]	Eclipsed temperature [°C]
Maximum emissivity	3.7	-42.7
Minimum emissivity	137.3	68.6

The controllable temperature range depends on the spacecraft conditions. For example, in the minimum incoming heat situation while not eclipsed, the temperature can be controlled in the range from -66.8 °C up to 32.8 °C using only the louvers. The overlap between all temperature ranges, for all different conditions, is the total controllable temperature range. However, the temperature range while eclipsed in minimum incoming heat conditions is very low, with the maximum temperature being -112.0 °C. Hence, the temperature for minimum incoming heat conditions while eclipsed cannot be controlled using only louvers. To resolve this issue, a 6.6 W heat source will be added to the spacecraft. While not eclipsed, the controllable temperature range is 3.7-32.8 °C, hence the heat source does not need to be active in nominal conditions. As can be seen in table 10.8, the heat source resolves the temperature range issue.

Table 10.8: Controllable temperature range using louvers and a 6.6 W heat source active while eclipsed

Minimum incoming heat	Nominal temperature [°C]	Eclipsed temperature [°C]
Maximum emissivity	-66.8	-66.8
Minimum emissivity	32.8	32.8
Maximum incoming heat	Nominal temperature [°C]	Eclipsed temperature [°C]
Maximum emissivity	3.7	-42.7
Minimum emissivity	137.3	68.6

Now, for all different conditions, the temperature can be controlled using the louvers and active heat source in the range of 3.7-32.8 °C. This means that, through all conditions, the temperature can be kept constant within this range by designing a proper control system for the spacecraft temperature. The heat sources will consist of multiple resistances spread throughout the satellite, to allow the heat to spread more quickly. Although 6.6 W is still above the budget dedicated to the thermal subsystem, this can be accounted for by assuming that the satellite will never downlink data to earth during an eclipse. This is a fair assumption, as downlink happens only once per day, and the maximum eclipse time is of 72 minutes, as calculated in section 4.4.2. This means the power budget dedicated to the downlinking components of the communication subsystem can be used for the thermal subsystem during eclipses.

10.3.3. Solar panels

The heat generation and radiation of the solar panels was not considered during the design of thermal subsystem. This was done because all solar panels are deployable, hence if it is assumed no heat can flow through the connecting hinges, the solar panels can be considered thermal systems. For this reason, the solar panels can be analysed as isolated thermal systems, using the same heat balance methods. The temperature ranges were calculated for the solar panels, and are given in table 10.9.

Table 10.9: Temperature range for the spacecraft, during nominal situation and eclipsed

	Nominal temperature [°C]	Eclipsed temperature [°C]
Minimum incoming heat	-138.4	-237.14
Maximum incoming heat	83.167	-273.12

The maximum temperature range that solar panels can typically handle is -110 to 110 °C. While the maximum temperature will never exceed 110 °C, the minimum temperature is far too low. This is due to the fact that while eclipsed, the only source of heat is the black body radiation from earth, which generates very little heat. However, it is unlikely that the temperature of a solar panel would actually approach -273.14 °C, as the eclipse periods are not long enough for the temperature to stabilise. Hence, for the solar panels, simulations were done to estimate the minimum temperature reached during eclipses. It was assumed the starting temperature for this simulation was the minimum nominal temperature, -138.4 °C. The results of this simulation can be seen in figure 10.2.
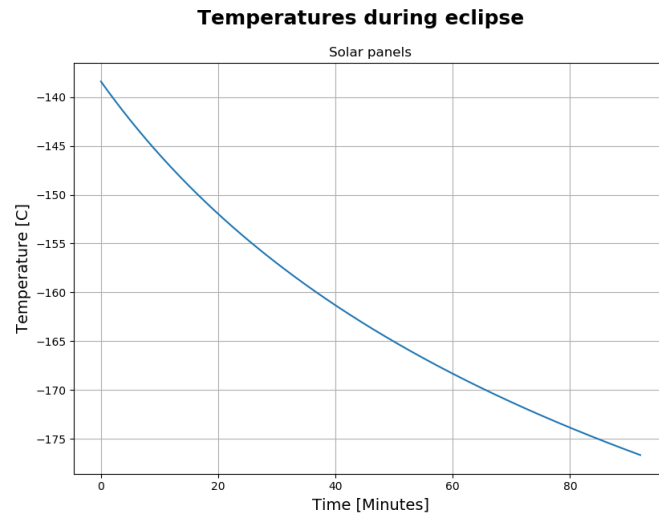

Figure 10.2: The temperature of a solar panel over the maximum eclipse period

For the simulation, it was assumed the solar panels are made of AlBeMet, a beryllium and aluminium metal matrix composite material, with a thickness of 2 mm. The width is 200 mm, and the height is 280 mm, as is required for the EPS subsystem. From this simulation, it can be determined that the minimum temperature the solar panels will be subjected to is -176 °C. Both the initial and the final temperature of this simulation are too low for a solar panel. To resolve this, heaters can be activated if the temperature is getting too low. However, this would require more cables to run through the hinges, while the assumption that the hinges can completely prevent heat transfer would still need to be verified.

Instead, the hinges connecting the solar panels to the spacecraft can be designed to allow for the transfer of heat between the solar panels and the rest of the spacecraft. This would mean the solar panel temperature can effectively be controlled by the louvers and heat sources of the spacecraft body itself. To model this, the heat flow through the hinges is estimated using equation (10.7). It should be noted that the constant k depends on the selected material and the geometry of the hinge, and the selected value for k should be taken into account whilst designing the hinge.

$$\dot{Q}_{sc,sp} = k \cdot (T_{sc} - T_{sp}) \tag{10.7}$$

The temperature of the solar panels and spacecraft body during an eclipse has been simulated over the maximum eclipse period. It is assumed the initial temperature is 20 °C for the spacecraft body and all solar panels. The results are plotted for different values of k, and can be seen in figure 10.3.

To save power, the thermal control system should not heat up the spacecraft body beyond 20 °C. It can be observed that, for values of k above 0.2 W/°C, too much heat starts flowing away from the spacecraft body, reducing its temperature below 20 °C. This should be prevented, as the temperature may never reach below 10 °C, to comply with the temperature range of the batteries. However, the temperature of the solar panels may not drop below -110 °C. If k has a value of 0.016 W/°C, the spacecraft body temperature remains constant, and the solar panel temperature does not drop below 110 °C in minimum incoming conditions. This would thus fulfill all thermal subsystem requirements for the solar panels and spacecraft body. Hence, the hinge should be designed for this value of k.

Since the hinges allow for heat transfer between the spacecraft body and the solar panels, the controllable temperature range needs to be recalculated. While exposed to sunlight, the controllable temperature range is not altered. Due to the orientation of the solar panels, only four can be exposed to sunlight simultaneously, all at an angle of 45 °. The other two solar panels will cool down, reducing the heat of the spacecraft body. However, during an eclipse, the heat transfer would further reduce the temperature of the spacecraft body. To compensate for this, the maximum power of the heat sources needs to be increased to 10.0 W. With the increased heat source power, the controllable temperature range remains 3.7-32.8 °C.

Temperatures during eclipse
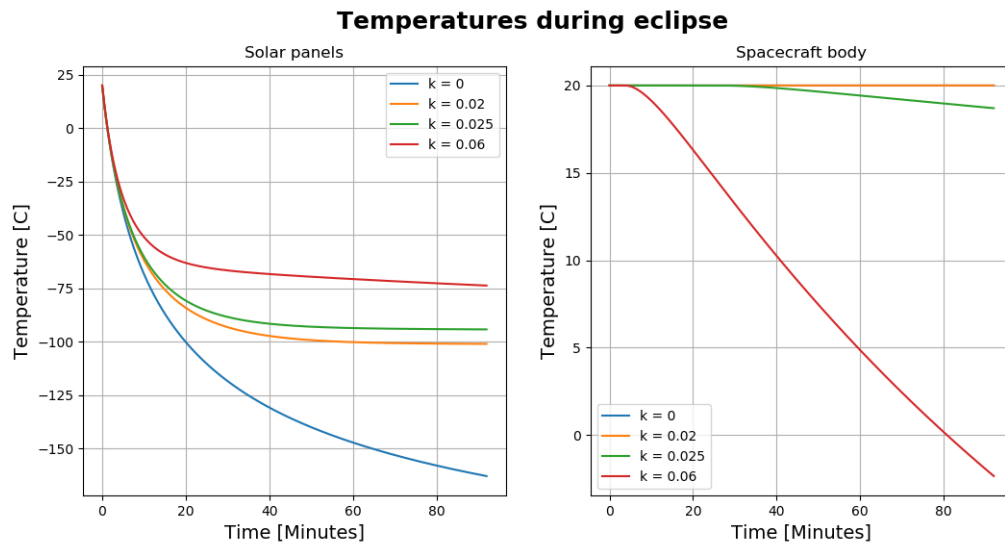
Figure 10.3: A simulation of the temperatures over the maximum eclipse period, solar panels on the left, and spacecraft body on the right

10.4. Risk

The thermal control system faces many risks over its lifetime, some of these risks can end the mission prematurely and thus have to be mitigated. Many of the risks a thermal control subsystem faces come from the environment the satellite operates in. Due to the high doses of radiation and charges particles, many of the different components of the subsystem can fail or degrade over time.

Due to the high doses of radiation, components in space have the tendency to degrade over time. This is especially the case for electronic components. The thermal control system operates many different sensors and a heater, it also has a control software which is run by the CDH. The heater can degrade over time and not provide enough heating anymore to the subsystems. This can cause systems to freeze or to lose efficiency. The loss of efficiency can cause the EPS not to deliver enough power to the satellite anymore and subsystem to go seize to operate properly.

The software of the thermal control system is susceptible to SEE. These effects can cause faults which can result in errors, stopping the software from running. If the software stops running or wrong data is calculated, then there might be too much or too little heating provided. The space environment can charge the outside of the spacecraft. This charging can speed up the degradation of the materials chosen for the thermal insulation, which can have a devastating effect on the thermal regulation of the spacecraft. The insulators and thermal blanket can loose partly their absorptivity and emissivity, therefore changing the thermal balance. The springs on the louvers can deteriorate and change their specific thermal expansion coefficient partly, but this effect will be minor.

The springs of the louvers can break during the launch or deployment of the satellite. Also, during manufacturing small defects can be introduced. This has a major effect on the thermal regulation of the spacecraft. If the louvers fail to open properly, the temperature in the spacecraft can climb which in turn creates thermal stresses. Thermal blankets and insulation have proven in the past to get caught in the deployer because of the snug fit. Lastly, heat concentrations may form if non-ductile materials used within the spacecraft.

10.5. Sustainability

The thermal control system louvers are made in the US, so they would need to be shipped to Europe, which decreases the sustainability of the thermal control system. The materials used in the thermal control subsystem are titanium, aluminised kapton foil, and copper. All these materials need to be shaped and processed, this costs large amount of resources, and is therefore not very sustainable. As the R&D and testing is already done on the louvers, many resources can be saved. The heater works on internal resistance, so primarily copper wires are used for this. This subsystem does need to be tested, which cost large amounts of resources, thus decreasing its sustainability.

10.6. RAMS

In this section, the RAMS characteristics of the thermal subsystem are described.

10.6.1. Reliability

The louvers are highly reliable, showing no signs of performance degradation after 12 900 cycles, vibrations, vacuum and radiation testing [30]. The heat sources should be tested. Due to their simple functionality principle, requiring a power circuit and a resistance, they are highly reliable. The coating, made of aluminised kapton foil, is a commonly employed heat-protection material. It has been utilised for over 50 years, for example during the Apollo Lunar Module[2]. The coatings are thus proven technology, and are highly reliably.

10.6.2. Availability

The louvers are always available during operations. Because they contain moving parts, payload measurements may become less accurate during active usage. However, the temperature should be regulated to prevent thermal failures. Hence, the louvers have priority over the measurements. The heat sources are only available during eclipses. The coatings are not actively controlled, but functionally, they are always available.

10.6.3. Maintainability

The thermal subsystem cannot be maintained physically once launched. However, the louvers and heat sources can be controlled directly by the OBC, hence the control system can be altered if the temperature regulation is not deemed optimal during the mission.

10.6.4. Safety

The main function of the thermal subsystem is to prevent overheating or undercooling of any of the components. This includes three safety critical functions: the functioning of the coatings, louvers and heat sources. The coatings and louvers are made of aluminised kapton foil and aluminium, respectively. These materials are non-flammable, easy to work with, and thus are deemed safe. The heat sources will be made out of circuits with high resistance. Testing of the heat sources must be done carefully, as they may overheat.

10.7. Final design

The thermal subsystem will consist of Resistance Temperature Detectors (RTD), a coating, two sheets of louvers, and internal resistances as a heat source. The coating will be made of aluminised kapton foil (2 mil), and will be applied to the outside of the satellite, as well as the backs of the solar panels. This material has an absorptivity of 0.12 and an emissivity of 0.05. Since it is applied to the outside of the spacecraft, its volume is neglected. The louvers will cover the two 20x20 cm surfaces of the spacecraft, with an absorptivity and emissivity of 0.03. If opened, they will expose the underlying coating of aluminised kapton foil (metal side), which has an absorptivity of 0.42 and an emissivity of 0.72. The louver thickness will be 6.5 mm, fitting within the 1 cm space around the CubeSat in the deployer. Since it is on the outside of the structure, its volume is not included in the volume budget.

The internal resistances will occupy little volume and mass, but the cables may add more to the volume and mass required. The total required power for the internal resistances is 10.0 W. Lastly, to account for the temperature range of the solar panels, the connecting hinges should be designed to allow heat to flow through it at a rate of 0.016 W/°C.

The thermal subsystem can freely control the temperature of the spacecraft body anywhere between 3.7 °C and 32.8 °C. Since the acceptable temperature range of the spacecraft body is is 10 °C to 30 °C, the thermal subsystem should keep the spacecraft body temperature constant at 20 °C.

The total mass, volume and power requirements can be found in table 10.10. As the thermal subsystem will only require power during eclipses, when the TT&C will be inactive, the power required is set at 4.5 W. This value is the difference between the maximum power of the thermal subsystem (10 W) and the maximum power of the TT&C subsystem (5.5 W).

Table 10.10: The characteristics of the thermal subsystem

	Mass [kg]	Volume [U]	Power [W]
Coating	0.023	0	0
Louvers	0.4	0	0
Heaters	0.01	0.01	4.5
Total	**0.433**	**0.01**	**4.5**

---

[2]https://pfinspace.com/lmdata/, accessed 16/06/2020

<div align="right">

11

Structure

</div>

The structures subsystem provides structural integrity to the spacecraft and protects all other subsystems for the harsh space environment. It also needs to be able to survive all the loads the spacecraft encounters during it lifetime.

11.1. Functional analysis

A functional analysis was done on the structure subsystem of the spacecraft. This functional analysis is used to come up with the requirements and produce a proper design. Six functions of the structures system were identified which have to be fulfilled for a proper functioning of the subsystem. These can be found in the FBS as shown in figure 11.1.
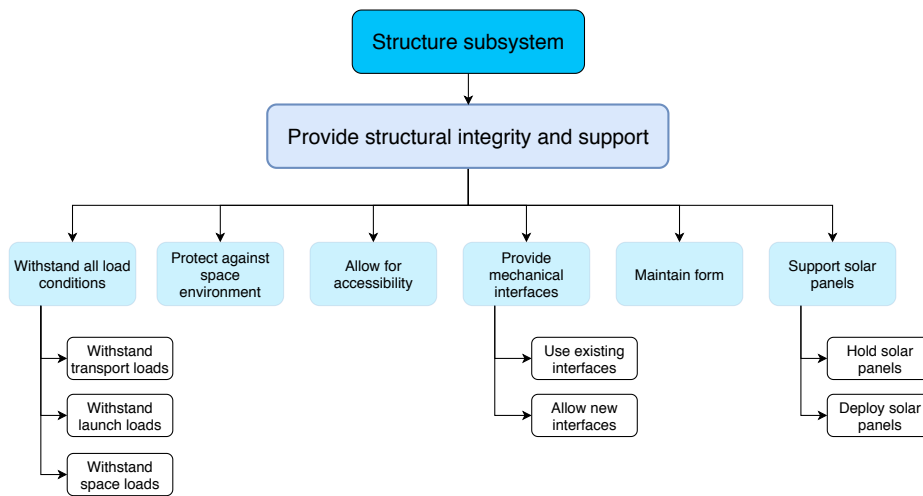
Figure 11.1: The functional breakdown structure of the structure subsystem

11.2. Requirements

The requirements for the structure of the spacecraft, as identified during the mission definition and exploration phase, can be found in the baseline report [3]. The updated requirements can be found in table 11.1.

Table 11.1: The list of structures subsystem requirements.

ID	Structures
LICCA-SYS-Sub-Str-1	DELETED
LICCA-SYS-Sub-Str-2	Structural system shall maintain elastic deformation of the spacecraft below <tbd>during all phases of the mission.
LICCA-SYS-Sub-Str-3	The total volume of the structures containing all spacecrafts shall not exceed 12U.
LICCA-SYS-Sub-Str-4	The structural system shall withhold quasi static load of at least 6 g's.
LICCA-SYS-Sub-Str-5	The structural system shall withhold vibrations due to launch of 100 Hz.
LICCA-SYS-Sub-Str-6	DELETED
LICCA-SYS-Sub-Str-7	The structural system shall be able to withstand a Total Ionising Dose of 20 000 Rad.
LICCA-SYS-Sub-Str-8	DELETED
LICCA-SYS-Sub-Str-9	The structural system shall provide attachment point for subsystems.
LICCA-SYS-Sub-Str-10	DELETED
LICCA-SYS-Sub-Str-11	The structural system shall provide interface with the deployers.
LICCA-SYS-Sub-Str-12	DELETED

| LICCA-SYS-Sub-Str-13 | DELETED |
| LICCA-SYS-Sub-Str-14 | The components of the structural subsystem shall have a current TRL level of at least 7. |

Table 11.2: ADCS Requirements changelog

ID	*Change*	*Rationale*
LICCA-SYS-Sub-Str-12	Deleted.	The torques experienced during launch are at most 30 Nm, this has a negligible effect on the stiffened structure. During operations the ADCS does introduce torques on the structure but these are also small, 1.5E-03 Nm.

11.3. Design methodology

The structure needs to be able to survive all the launch loads and protect the subsystems from the space environment. The structure also needs to provide mechanisms to hold and deploy the solar panels. All this has to be done with a minimized weight. First the main structure design is explained, where an analysis on the launches loads is done, and the radiation shielding is designed. After which the release and holding mechanism of the solar panels is designed in more detail and evaluated.

11.3.1. Main structure

The structure was designed working from the requirements and the functional analysis. The structure of a spacecraft consist of two different parts, a primary and a secondary structure. The primary structure is the load bearing structure which supports all other subsystem during launch and carries all the loads the satellite experiences. Therefore when the primary structure fails the whole satellite will collapse. To mitigate a catastrophic collapse of the primary structure a load and frequency analysis was done after a COTS option was chosen. The secondary structure of the spacecraft contains all structures which only need to support themselves. These include the thermal blankets and solar panels. When the secondary structure fails the structural integrity of the spacecraft does not change, therefore no structural analysis was done on the secondary structure.

To fulfil the requirements an analysis on COTS structures was done. The advantage of using a COTS structure is the mitigation of design, verification and validation costs. A small trade-off was done to come up with a suitable COTS option. Material choice and the weight of the primary and secondary structure were of high importance. The material choice directly influences the ability of the structure to provide adequate radiation protecting to the subsystems inside the spacecraft. The denser the material the better radiation protecting it provides. However denser materials also increase the weight, therefore these two have to be weighted off against each other. Material choice also influences the thermal expansion and contraction properties of the spacecraft. Isotropic materials have the same properties in all directions, this means that it will expand or contract evenly across the material. Carbon Fiber Reinforced Plastics (CFRP) do not have these isotropic properties. This means that one side may expand more than the other, increasing the stresses on the structure itself.

It is needed to know how much the structure will heat up and cool down to make a choice of material. Thermal expansion and contraction can create stresses in the structure or disrupt measurements due to the increase or decrease of the length of the spacecraft. Material choice is also influenced by outgassing regulations and the ability to survive the space environment, without any premature degradation. Most spacecraft structures are made from aluminium 6061-T6 or 7075, which both have isotropic material properties. The aluminium 7xxx series have a higher yield stress than the 6xxx series aluminium, but it has a worse thermal conductivity and a lower specific heat capacity, the electrical conductivity is also lower. The 6xxx series of aluminium is less dense than the 7xxx series. Both series of alloys have around the same modulus of elasticity, and are therefore both very stiff.

CFRP components are very strong, but anisotropic. This means that the material does not have the same properties in all directions. CFRP can also degrade rapidly due to the outgassing of certain polymers used. This means more molecules are outgassed, and due to the regulations on outgassing set by different space agencies and governments, a lot of testing would be required to insure the compliance to these laws. The TRL of structures with CFRP is generally lower than from aluminium ones. The following options were analysed more closely, table 11.3.

Table 11.3: Different cubesat structures data

Company	Primary structure weight [kg]	Secondary structure weight [kg]
ISISpace	1.5	0.5
SPACEMIND	1.43	0.32

More COTS option were investigated, primarily from NANOAVIONICS and Hyperion. These provide integrated busses and not separate structures, therefore these were not taken into account. The choice of structure is based on the following factors: sustainability, cost, material choice, and TRL. The sustainability of the structures is determined by distance from supplier to integration site, and environmental standards at place of manufacturing. Cost is based on the listed price on the websites[1][2]. Material choice is based on the material used in the primary and secondary structure. TRL is based on documents from ESA and NASA. A decision was made to use the structure of ISIS, as it has a proven TRL of 7 [23], and a manufacturing facility close to the integration site. The price difference between the ISIS and SPACEMIND structure is very small. Even thought the SPACE-MIND structure has a lower listed price, it needs more options to make it suitable for the LICCA mission„ these include shear panels, and a secondary structure, and make the price difference with ISIS very small. The ISIS structure provides 1.5 mm thick shear panels.

The ISIS structure is made in the Netherands, from aluminum 6082-T6, and has a TRL of 7. The CubeSat structure is listed for 11 950 EUR. The SPACEMIND structure is made in Italy, from aluminum with CFRP options and stainless steel threads, the TRL is not known. The structure is listed for 9 980 EUR, but this does not include all different options and is excluding shear panels.

After the COTS option from ISIS was chosen an analysis on the structure was done. A CAD model was made in CATIA, with the same materials and dimensions as the 12 U ISIS structure. Due to the thrusters of the ADCS, a hole in the structure had to be made to be able to account for deployment. It was determined that the maximum launch loads experienced by the structure would be 6 g of lateral acceleration and 2 g longitudinal. The model was simplified by making the following assumptions.

- All subsystems are rigidly connected to the primary structure.
- All subsystems are not load carrying.
- All subsystems are rigid, so they do not deform during launch.

An analysis on the vibrations and the accelerations on the structure was done. From the CATIA analysis it was determined that the structure would be able to survive the 6 g loads with a maximum deformation of 0.001 mm. No stresses were found higher than the yield stress, 220 MPa for 6082-T6 aluminium. Therefore it was concluded that the spacecraft structure can survive the launch loads. After this analysis, a simplified analysis was done on one of the columns of the structure. The columns are the vertical corners of the structure, made from Al6082-T6. The thickness was taken to be 1.5 mm, the width and length were taken as 10 mm and the height to be 340.5 mm[3]. An Euler buckling analysis was done with the following assumptions.

- The bottom of the column is rigidly connected to the deployer, the top is free.
- All loads are acting from the top of the column.
- The maximum load a single column can experience is 3/8 of the total load all four columns have to withstand.

To calculate the buckling load of the column equation (11.1) was used.

$$P_{cr} = \frac{\pi^2 EI}{l_e^2} \tag{11.1}$$

Where EI is the flexural stiffness, and l_e is the effective length of the column, which for this case is two times the length. As the column is symmetric, the moment of inertia around the x- and y-axis are the same, both are 0.63E06 mm^4. The modulus of elasticity is 69 GPa, and the effective length is two times 340.5 mm. This results in 9 300 kN of force to buckle one of the columns. To determine the most plausible failure mode, the stress calculated from this force is 182 GPa, which is almost a thousand times higher than the yield stress of 220 MPa, so the material will yield before buckling. Equation (11.2) was used to calculate the stress in the material when a force of 9 300 kN is applied on an area of 51 mm^2.

$$\sigma = \frac{P}{A} \tag{11.2}$$

The maximum load was determined by using the weight of the subsystems, and knowing their placement it was

---

[1] https://www.isispace.nl/product/12-unit-cubesat-structure/, accessed 16/06/2020
[2] https://www.npcspacemind.com/store/#!/SM12/p/172169670/category=44131123, accessed 16/06/2020
[3] https://www.isispace.nl/product/12-unit-cubesat-structure/, accessed 22/06/2020

determined that only the propellant tank could be neglected in the analysis because it is situated at the bottom of the spacecraft. The mass used was 19 kg. This is based on the weight of the payload, ADCS, TT&C, CDH, EPS, Thermal, and the structure itself, including a safety margin of 10 %. Using again equation (11.2), and a force equivalent of 6 g's, due to the launch loads experienced by the structure, the weight times the gravitational acceleration of 9.81 m/s^2, results in a stress of 22 MPa in one column. This is well below the yield stress of Al6082-T6, therefore the structure will survive the launch loads. However because of the adjustments made to facilitate the ADCS thrusters, a full analysis still needs to be done in compliance with ISIS. Therefore, a lot of proper testing is needed to be able to comply with laws, and launcher specifications, which cost a lot of extra time and money.

After analysis of the structure, a decision on the skin thickness had to be taken to provide adequate radiation shielding to the components inside the structure. Using the estimations made in chapter 8 and section 4.2, a skin thickness estimation could be made. The ISIS structure includes shear panels with a thickness of 1.5 mm made from Al6082-T6. These panels occupy all surfaces. This is however not needed as the skeleton of the structure can on its own withstand the launch loads. The radiation shielding also does not have to be evenly spread as some subsystems can withstand more radiation than others. The most critical subsystems were determined to be CDH, Payload, and ADCS.

These subsystems are all situated in the top of the satellite, therefore local skin thickness increase would only be needed for the top of the spacecraft. From section 4.2 it was determined that around 3 mm of skin thickness would be enough to stop a substantial amount of radiation. Therefore, at the location of critical subsystems a skin thickness of 3 mm is needed. A larger thickness would only increase the weight and not drastically reduce the radiation, as Bremsstrahlung cannot be neglected. The propellant tank is made from titanium and therefore provides, from the bottom up, a good amount of radiation shielding. Therefore, the local skin thickness is decreased to 0.5 mm on the bottom. The most critical parts of the payload will be situated near the top of the spacecraft and therefore the skin will have a thickness of 3 mm. The louvres on the top and the bottom of the spacecraft provide and equivalent thickness of around 2 mm of aluminium, this was based on the thickness and material the louvres are made of. Therefore only 1 mm of skin thickness will be added at the top of the satellite. This will create a radiation protection bubble of 3 mm to all subsystems in the top half of the spacecraft. Local increases of thickness can be added when the components need extra shielding.

11.3.2. Solar panel structure

Another part of the structural design is the solar panels. For the solar panels, the width and height come forth from the EPS power requirements. 16 solar cells must be on each solar panel, facing outwards. The solar panels must be deployable, and the deployment system must bring the panels from the folded position to their deployed position, a full 180°rotation. First, the design methodology of the solar panels will be given, followed by the hinge design and the deployment mechanism.

Solar panels
First, the structure on which the solar cells can be installed must be designed. The layout of the solar cells has been already determined. For this analysis, the solar panel orientation and coordinate system is defined as shown in figure 9.4.

Each of the solar cells is 4x8cm. The total height of the panel must thus be 28cm, and the width will be 20cm. The total area will be at least 512cm², to support the solar cells. For the initial analysis, it is assumed the solar panel is rectangular, with dimensions of 28x20cm, for a total area of 560cm².

For the solar panels, the thickness and a material must be selected. The main drivers of these design parameters come from the loads and vibrations experienced while inside the launcher, and during deployment. Three materials were considered; aluminium alloys Al2024T6[4], Al6061T6[5], and aluminium beryllium matrix composite AM162-AlBeMet[6].

The properties of these materials can be found in table 11.4. Once one of these three materials is selected, it can be compared to different versions of that alloy, to select the optimal one for this mission.

Table 11.4: Properties of some aluminium alloys/composites

Property	Al2024T6	Al6061T6	AM162-AlBeMet	Unit
Density	2.77	2.70	2.10	g/cm³
Modulus	72	70	193	GPa
Poisson's ratio	0.33	0.33	0.17	-
Yield strength	345	276	386	MPa

[4]http://asm.matweb.com/search/SpecificMaterial.asp?..., accessed 15/06/2020
[5]http://asm.matweb.com/search/SpecificMaterial.asp?..., accessed 15/06/2020
[6]https://materion.com/-/media/files/beryllium/albemet..., accessed 15/06/2020

To select the material and thickness, the failure modes have to be identified. The following failure modes were identified for the solar panels:

1. Failure due to longitudinal loads experienced during launch.
2. Failure due to lateral loads experienced during launch.
3. Failure due to vibrational resonance experienced during launch.
4. Failure due to forces experienced during deployment.

The fourth item is a major driver during the deployment mechanism design, hence it is not considered for the design of the solar panel structure The structure will be designed such that its mass is minimal, but none of failure modes 1-3 will occur.

The longitundal loads experienced during launch introduce normal stresses on the solar panels. The maximum normal force the solar panel will experience can be estimated using equation (11.4). Here, $F_{n,max}$ is the maximum force experienced, m_{sp} is the mass of the solar panel, $a_{l,ax}$ is the maximum acceleration of the launcher and g is the gravitational acceleration on earth. This maximum force occurs near the hinge. The maximum experienced stress during launch can then be calculated using equation (11.3).

$$\sigma_{max} = \frac{F_{n,max}}{w \cdot t} \qquad (11.3) \qquad\qquad F_{n,max} = m_{sp} \cdot (a_{l,max} + g) \qquad (11.4)$$

Here, σ_{max} is the maximum stress, w is the width of the solar panel, and t is the thickness of the solar panel. The solar cells and cables will also add weight. The selected solar cells have a weight per area of 50mg/cm²[7]. Hence, the total weight of the solar cells will be about 25g. This is increased to 40g to include cables.

The lateral accelerations may introduce a shear force on the solar panels. The maximum shear stress occurs near the hinges, as this is where the structure must carry the mass of the entire solar panel. The maximum shear stress can be calculated using equation (11.4) and equation (11.3). If the launcher points towards zenith, gravity will not affect the lateral accelerations. However, as the launcher will not necessarily point exactly towards zenith at the point of maximum lateral acceleration, gravity is taken into account.

The last failure mode is due to vibrational resonance. If the lowest eigenfrequency of the solar panel is lower than the highest frequency occurring in the launcher, resonance may cause the solar cells to get loose, and potentially cause the solar panels to fail. To account for this, the lowest eigenfrequency of the solar panel is calculated. The lowest eigenfrequency of the solar panel corresponds to the vibrational mode where the solar panel is modelled as a bending cantilever beam. In this case, the spring constant k can be calculated using equation (11.5). Here, E is the E-modulus of the material, I_{xx} is the moment of inertia about the x-axis, and l is the length of the beam, in this case the length of the solar panel. The moment of inertia depends on the cross-section of the beam around which the bending occurs. For the solar panel, the moment of inertia I_{xx} can be calculated using equation (11.6). The spring constant can be used to determine the first natural frequency ω_n of the solar panel, using equation (11.7).

$$k = \frac{3EI_{xx}}{l^3} \qquad (11.5) \qquad\qquad I_{xx} = \frac{w \cdot t^3}{12} \qquad (11.6) \qquad\qquad \omega_n = \sqrt{\frac{k}{m_{sp}}} \qquad (11.7)$$

The material and stiffness should be selected to minimise the weight of the structure, while ω_n must be larger than 120 Hz. Although the highest occurring frequency in the launcher is 100 Hz, a 20% margin is added for safety.

Since two solar panels must be placed on top of each other, both with solar cells facing towards the structure, they must be held in place such that neither solar panel is damaged. Four supports will be added to the solar panels, as shown in orange in figure 11.2.
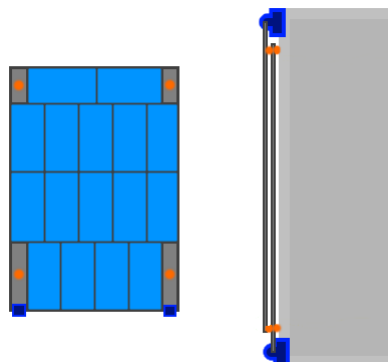

Figure 11.2: The solar panels configuration, supports are colored orange

[7]https://artes.esa.int/projects/next-generation-upright-metamorphic-4junction..., accessed 15/06/2020

As can be seen on the right, these supports will prevent the solar cells from being damaged. The supports must be designed to absorb impact, but durability and radiation resistance are not large issues, as they are not used after deployment. The minimum strength of the supports should be designed such that it can handle both direct impacts and continuous forces.

Hinge design

The hinge must be designed to withstand the forces applied to the solar panels during launch. Furthermore, the hinges must be designed such that the deployment of the solar panels does not destroy the solar panels. To analyse the maximum forces acting on the hinges, the maximum forces experienced during launch are calculated using equation (11.4), both for longitudinal and lateral forces. The forces are modelled as acting on the center of the solar panel, as shown in figure 11.3.

In figure 11.3, L_x and L_y are the maximum lateral and longitudinal forces during launch respectively, and $R_{a,x}$, $R_{a,y}$ and $R_{b,y}$ are the reaction forces of hinge a and b in the direction of the x-axis and y-axis. The reaction force in the x-direction of hinge b is left out of the analysis, as the problem would become statically indeterminate. Without the reaction force in the x-axis direction of hinge b, the maximum forces acting on each of the hinges can be determined using equilibrium of forces and moments. It should be noted that, for the equilibrium of moments, the moment is taken about the position of hinge b, with clockwise positive.
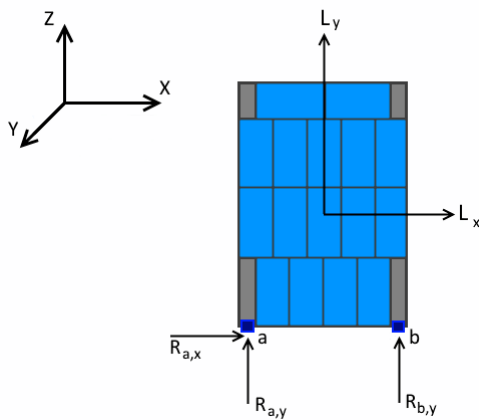
$$\Sigma F_x = L_x + R_{a,x} = 0 \qquad (11.8)$$

$$\Sigma F_y = L_y + R_{a,y} + R_{b,y} = 0 \qquad (11.9)$$

$$\Sigma M_b = L_y \frac{w}{2} + L_x \frac{h}{2} + R_{a,y} w = 0 \quad (11.10)$$

Figure 11.3: The forces acting on the solar panels

In equation (11.10), w and h are the width and height of the solar panel respectively. For L_x and L_x, both the minimum and maximum values are taken into account to calculate the maximum magnitude of the reaction forces on the hinges.

Furthermore, the hinges can be spring-loaded. If the hinges are spring-loaded, the solar panels are deployed and kept in place automatically. The deployment can be prevented using a HRM, as described in the next section. For reference, the deployment angle of the solar panels is considered 0°before deployment, and 180°after deployment. To fully deploy the solar panels, the spring must have a free spring angle θ_0 of at least 180°. However, to make sure the solar panels never deviate from their deployment angle of 180°, the springs must be pre-loaded, such that θ_0 is larger than 180°. The spring constant k must be selected such that the spring can overcome frictional forces, but that the solar panels will not be damaged during deployment. The moment the torsional spring will apply to the solar panel is given in equation (11.11).

$$M = 2k \cdot (\theta_0 - \theta) \qquad (11.11)$$

This moment should be able to overcome the frictional forces. It should be noted the moment is doubled, since two identical hinges will be used, and both will be spring-loaded. The maximum rotational energy of the solar panel can be calculated by calculating the maximum potential energy of the spring. It is assumed the hinge fully blocks rotations at 180°. The maximum rotational energy at 180°is then given in equation (11.12).

$$E = 2(\frac{1}{2}k\theta_0^2 - \frac{1}{2}k(\theta_0 - 180)^2) \qquad (11.12)$$

In simple terms, this equation states the maximum rotational energy is equal to the difference in potential spring energy between folded and deployed positions. The maximum deflection during deployment can be calculated using the spring constant of the solar panel as given in equation (11.5). For the maximum accelerations, both translational and angular, it should be verified that the solar panels always remain deployed at 180°.

Hold and Release Mechanism

A Hold and Release Mechanism (HRM) must be introduced that holds the solar panels in place, and can deploy the solar panels when desired. The simplest such mechanism uses a nylon wire to keep the solar panels in place, and a circuits with burn resistors. The wire is attached to the solar panel on one end, and to the burn

circuit on the other end. The circuits will be activated only once, to cut the nylon wire, thus allowing the solar panels to deploy. It has been proven experimentally that this concept can work on CubeSats for 20x30cm² solar panels [68]. However, after cutting the wire with the burn circuit, one end of the nylon wire can float freely in space. Assuming the six nylon wires, one for each solar panel, would be 20 mm long, 0.5 mm thick, with a density of 1150 kg/m³, the center of mass of the spacecraft can fluctuate around $2.71 \cdot 10^{-8}$ m. The ranging accuracy of the payload is 10^{-12} m. Hence, these fluctuations are too large. To prevent the nylon wires from floating freely, a small retractable reel with casing will be installed on each solar panel. This reel will continuously apply a tensile force on the wire. Once the wire is burned, the nylon wire will be fully reeled in, preventing fluctuations to the center of mass of the spacecraft. This reel has to be reliable, but does not need to have a high radiation resistance, since it will only be used once during deployment.

11.3.3. ADCS thruster deployment

The space available on the outside of the structure, between the spacecraft and the deployer, is 10 mm [8]. The skin thickness is 3 mm, and the solar panels are 3 mm thick each, which means the total required space is about 9 mm. However, it was determined that the ADCS subsystem requires thrusters that protrude of the structure at least 4 mm. Two of these thrusters are required, on two sides where solar panels are located as well. This would mean the ADCS thrusters cannot fit. To resolve this issue, a deployment mechanism is introduced for the ADCS thrusters. This deployment mechanism will be similar to the solar panel deployment mechanism, with nylon wires, a burn circuit and springs. A nylon wire and burn circuit will be attached to the structure. A cylindrical hole will be created for the ADCS thruster to fit. On the inside edge of this hole, damping elements will be attached, to prevent damage. A retractable reel with casing will be attached to the ADCS thruster, to reel in the nylon wire after deployment. It should be noted that this retractable reel must consistently exert a tensile force on the nylon wire. This tensile force must be significantly larger than the force exerted by the springs, to prevent the ADCS thruster from deploying prematurely and damaging the solar panels. Springs will be placed between the structure and thrusters to deploy the thrusters after the nylon wire is cut. Using this HRM and deployment mechanism, the solar panel design does not have to be altered.

11.4. Risk

Failure of any component of the structure can have serious consequences for the continuation of the mission. The risks therefore need to be identified and mitigated.

11.4.1. Main structure

The main structure of the spacecraft does not face many risks, but some can have a catastrophic effect on the mission. There is always a possibly that the main structure is not able to withstand the launch loads, this can be caused by defects in the material or improper manufacturing and assembly. If the main structure would not be able to survive the launch loads, the mission would end before the deployment. Another risk is the deformation of the structure during launch or during any other mission segment. The structure can become too cold or too hot and this can cause thermal stressed on the structure. A risk related to the ADCS in the structure is that the ADCS thrusters may fail to deploy, or fail to function properly after deployment.

11.4.2. Solar panels

The solar panel is a rectangular plate with solar cells attached. One risk is that the solar cells become loose as the solar panel vibrates. If the solar cells become loose, they may no longer function. Another risk is that the solar cells are damaged due to contacting the structure during launch.

The solar panel deployment mechanism has two risks. Firstly, the solar panel may either not deploy at all due to the hinges not generating a large enough moment to overcome frictional forces. Secondly, the solar panel may be damaged during deployment if the hinges generate a too large moment. The HRM may fail due to the burn circuits not being able to cut the nylon wire, thus tests should be performed. It should also be inspected that the burn circuit does not damage the satellite during operation. Another HRM risk is the failure of the retractable reel. The reel should be tested separately from the solar panel, to verify it will always store the remaining nylon wire in the casing. Lastly, the solar panel deployment and HRM are tested in a larger system test of the entire mechanism.

11.5. Sustainability

The structure of the satellite comes from the ISIS space in the Netherlands. The structure is made from aluminium 6082-T6 which is more easy to manufacture and from, therefore using less energy than higher strength aluminium such as 7075. Aluminium has less outgassing than other materials therefore decreasing the amount of space pollution and decreasing the amount of charged particles in the GEO, compared to the use of CFRP. Using COTS option decreases the amount of resources spend on R&D and testing, this has an positive influence on the sustainability. The structure of the structure is not made of any hazardous or explosive materials, therefore having a positive impact on the sustainability and decreasing the risk of explosion in space.

---

[8] https://www.isispace.nl/wp-content/uploads/2015/12...., datasheet 12U CubeSat deployer, accessed 22/06/2020

11.6. RAMS

In this section, the RAMS characteristics of the structure subsystem will be described.

11.6.1. Reliability

The main structure is quality tested for functionality, vibrations, mechanical shocks and thermal cycling[9]. The solar panel structure is made from AlBeMet, which is radiation resistant[10], and functions well in a space environment[11].

The hinges, springs, nylon wire and burn circuit need to be selected/designed, hence their reliability can not be estimated. However, they utilise relatively simple technology, hence selecting/designing highly reliable components should be a relatively simple process.

11.6.2. Availability

The main structure is always available. The solar panels are permanently available after deployment, as they should never retract. The burn circuits are available after the deployment of the solar panels, but since they serve no purpose, they should not be used.

11.6.3. Maintainability

No physical maintenance can be performed on the structure during operation.

11.6.4. Safety

One safety critical function of the main structure are to hold the subsystems in position. If components move, cables may disconnect, potentially causing the system to become inoperable. Another safety critical function is to protect the internal components from the space environment. Many components, including the OBC and sun sensors, are vulnerable to radiation, and this may cause the system to fail. Furthermore, the successful deployment of the solar panels and ADCS thrusters form two safety critical functions.

The main structure and solar panel structure have no hazardous properties. The spring-loaded hinges are designed for the solar panels, which weigh less than 250 g each. Hence, they also form no danger. The burn circuits should be treated very carefully. Nylon has a melting point of up to 272 °C[12], which can cause skin burns within an exposure time of a second[13].

11.7. Final design

The characteristics of the structure can be found in table 11.5. The structure itself takes no volume of the spacecraft, as it allows for a inside volume of 12 U. Note that the solar panels occupy no volume, since the solar panels are on the outside of the structure. Only the burn circuits must be inside the structure.

The structures will have a width and length of 226.3 mm, and a height of 340.5 mm, excluding the the skin thickness. Measured from the bottom of the satellite the first 170.25 mm of height, for all four the side panels, will have a skin thickness of 0.5 millimetres, for the second 170.25 mm the skin thickness increases to three millimetres. The top of the structure has a panel of 1 mm thick. The bottom does not have an extra panel due to the presence of the louvers and the effective shielding it provides. The skeleton weight is very low because the skeleton consist of thin walled beams, therefore having a low weight and high stiffness. The main structure has a hole cut out to provide place for the ADCS thrusters.

The six solar panels will each be rectangular and effectively 3 mm thick. The base structure is made from AlBeMet, and will be 2.0615 mm thick. The solar panels will be deployed using two hinges. The two hinges of the solar panels in the top position will be positioned 3 mm away from the structure. For the thermal subsystem, the hinges should also have a heat conductivity of 0.016 W/°C. All hinges are spring-loaded, and allow rotation up to 179°(±1°). For the HRM, 1 nylon wire will be attached to a retractable reel with casing. 1 reel will be used per solar panel. Structural supports are added to the solar panels, to prevent the solar cells from touching the structure. The final design of the solar panels can be seen in figure 11.5.

---

[9] https://www.isispace.nl/product/12-unit-cubesat-structure/, accessed 18/06/2020

[10] https://materion.com/-/media/files/beryllium/albemet-materials/..., accessed 18/06/2020

[11] https://materion.com/-/media/files/beryllium/..., accessed 18/06/2020

[12] http://polymerdatabase.com/polymer%20physics/Polymer%20Tm%20C2.html, accessed 17/06/2020

[13] http://burncentrecare.co.uk/about_burned_skin.html, accessed 17/06/2020

Table 11.5: The characteristics of the structure

	Mass [kg]	Volume [U]	Power [W]
Structure			
Skeleton	0.422	0	0
Total structure	0.422	0	0
Radiation shielding			
Side panels top half	1.2	0	0
Side panels bottom half	0.2	0	0
Top panel	0.14	0	0
Total radiation shielding	1.54	0	0
Solar panels			
Structure	1.5	0	0
Hinges (with springs)	0.1	0	0
HRM	0.1	0.01	0
Total solar panels	1.62	0.01	0
ADCS thrusters			
Total ADCS thrusters	0.12	0.05	0
Total	**3.7**	**0.06**	**0**
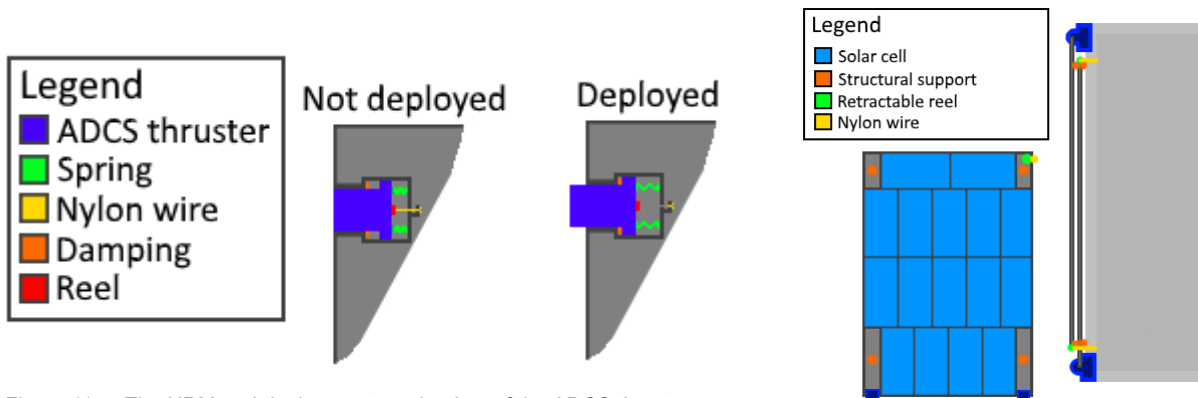
Figure 11.4: The HRM and deployment mechanism of the ADCS thrusters

Figure 11.5: The final design of the solar panels

The ADCS thrusters are kept in place using a nylon wire and a cylindrical hole, which are attached to the main structure. This hole is 26.4 mm long, have an internal diameter of 64 mm, and is 3 mm thick. The damping element is 3.2 mm thick, and is shaped to fit the ADCS thruster nicely. This way, the ADCS thruster protrude 4 mm relative to the skin once deployed. Beyond the damping elements, the structure expands as a square hole with internal dimensions of 89x89 mm to fit the ADCS thruster, and prevent free rotation of the thruster, and a back plate. Two springs and a retractable reel with casing will be attached to the ADCS thruster, to hold, release and deploy the ADCS thruster. The springs will be attached to the back plate. A nylon wire will be attached to the reel and an attachment to the back plate, to make room for the burn circuit. The nylon wire must be attached such that the thruster is retracted 5 mm from its deployed position. The full design is shown in figure 11.4. The ADCS thrusters can not be deployed until after the solar panels are deployed. The cables attached to each ADCS thruster must be slightly longer, to allow for the movement of 5 mm.

System characteristics

This chapter will show the system characteristics. First of all, the configuration of the satellite is presented in section 12.1. Then the cabling is discussed in section 12.2. Next, the external systems are discussed in section 12.3 and the operations in section 12.4. Then the budgets are presented and discussed in section 12.5. The system characteristic diagrams are shown in section 12.6 and finally the cost of the mission is estimated in section 12.7.

12.1. Configuration

The configuration of the LICCA satellite is presented in figure 12.1. The components of different subsystems can be seen inside the structure. The radiation shielding panels of the satellite are not shown in this figure (only a small bit can be seen on the left) as the components inside the satellite would be not visible then.

In figure 12.1, the satellite is shown from the side facing nadir. On this side, four antennas are visible, which form the UHF connection. Right above the UHF antenna, the S-band antenna can be seen (squared patch) The dual telescope can be seen in the middle. The six solar panels are shown in orange, facing east, west and zenith. The green cylinder on the right side is the ADCS thruster. The propellant tank is shown in blue. The main thruster is connected to this tank facing zenith. The thruster is hence is not visible here. On the top and bottom, the thermal louvers are visible.

The configuration of the LICCA satellite might be prone to changes during next design phases, if components have different sizes than expected or will be needed to be placed in a different place withing the satellite.
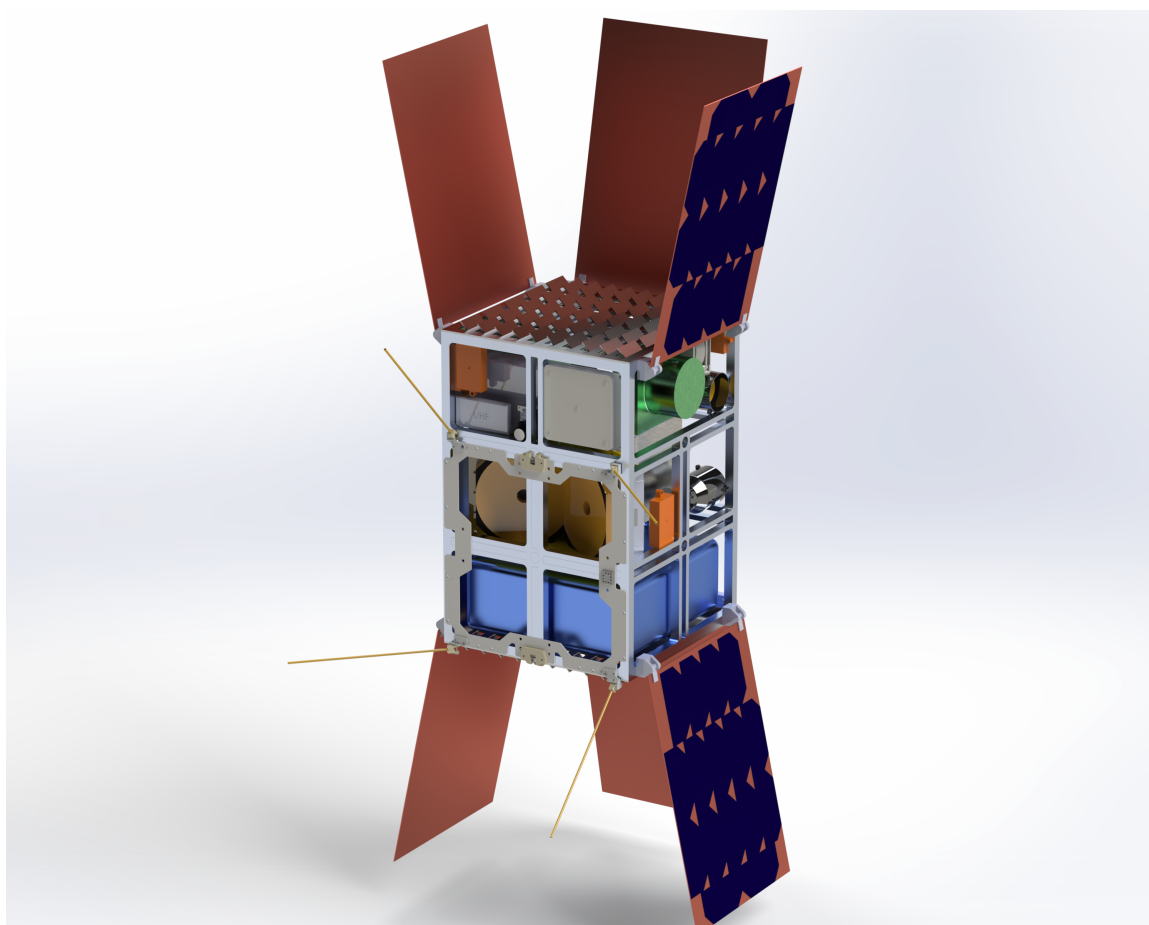
Figure 12.1: The configuration of the spacecraft

12.2. Cabling

Cables are used throughout the spacecraft to deliver power or transfer data. A general estimate on the weight of the cables of a spacecraft is around 10-20% of the spacecraft dry mass. Cable management in spacecraft is very important as it can lead to failure or to incorrect measurements. A common failure is the failing of the I^2C connectors due to improper shielding or due to the lack of overcurrent protection. These I^2C connectors caused some catastrophic satellite failures and a great amount of bus lockups [38]. Alternatives to the I^2C connectors are SPI and RS-232 connections [38]. The SPI and RS-232 have different issues as they cannot be implemented with all COTS options. Therefore, satellites normally have different data buses for different tasks [38]. The OBC-P3 however does not have SPI or RS-232 connection and therefore they cannot be implemented in combination with this OBC[1]. Possible explanations for the high failure rate of I^2C connectors can be the lack of separate handshaking lines, the high amount of nodes connected to the bus, not having differential signalling, not having enough radiation shielding, or the state-machine of the I^2C hardware and firmware have errors [38].

Proper testing on the data bus of the spacecraft will thus be important, and the sensitivity of these connections cannot be overlooked during further design. Other wiring in the spacecraft consist of electrical connections to supply power to the subsystems. Proper design and analysis of the wiring will have to be done, as there are some risks to be taken into account. The electrical wiring of the spacecraft needs to have sufficient room to radiate the heat it generates. Packing too many wires closely together can cause the temperature of the wires to rise and even to burn the protective layer around the copper. The loosing of the protective layer can cause short circuit, which can cause failure of the satellite. The resistivity of copper also increases with increasing temperature this causes the EPS to lose efficiency.

Another risk with improper placement of wires is the electromagnetic field which can be created when current runs through a wire. This electromagnetic field can interfere with the payload measurements, and thus will need to be modelled to counter the disturbances caused by it [71]. The Lorentz force acting on the wire can also cause minor changes in the centre of mass of the spacecraft [71].

12.3. External Systems

This section describes all the external systems that the CubeSats will employ to ultimately reach GEO, namely the launcher and the transfer vehicle.

12.3.1. Launcher

To reach orbit, the satellites need to be launched. In the Midterm Report [5] all launchers that would be able to bring the spacecraft to GEO in 2030 are identified. However, there are some aspects that need to be taken into account when selecting one. The project is connected with European institutions, therefore a European launcher is chosen. The mission is designed to be compatible with European launch regulations. It supports the European economy and is thus beneficial for sustainability from a social-economic perspective.

In this scenario, three launchers remain: Soyuz, Ariane 5 and Ariane 6. The satellites are designed to be compatible with any of these launchers (e.g. the highest launch loads are designed for). The vehicles launch form Kourou in French Guyana into a GTO with equal characteristics: 250 km perigee altitude, 6 ° inclination and 80 km apogee altitude accuracy.

The selection of a launcher also depends on the development of Ariane 6 and accompanying retirement of Ariane 5. The situation in 2030 is not fully known yet, so both options are taken into account.

The Ariane 5 provides spaces for auxiliary payloads to be carried along with the main payload. These are the spots that will be taken by the mission. The Ariane 5 Structure for Auxiliary Payload (ASAP5) provides different kind of configurations, namely four mini satellites (120 to 300 kg), eight mirco satellites (less that 120 kg) or two mini satellites and six micro satellites[2]. The Ariane 6 will have a similar configuration for auxiliary payloads with the capability of transferring more mass more efficiently [3]. Soyuz has a slightly different configuration, according to the Arianespace Structure for Auxiliary Payloads for Soyuz (ASAP-S). It allows to embark up to four micro satellites (up to 200 kg) or one mini satellite (up to 400 kg) [4]. However, this mission occupies two mini satellites, as will be explained in section 12.3.2. This should preferably be launched at once. Therefore one auxiliary payload structure in the Soyuz is not sufficient and this option is discarded. The CubeSats will therefore be launched with either Ariane 5 or Ariane 6, depending on availability.

12.3.2. Transfer Vehicle

Reaching GEO turns out to be a major challenge for this mission due to the volume and power constrains. In chapter 6, it was concluded that the CubeSats would have to be brought to this orbit. Fortunately, the space industry is getting more efficient year by year. This leads to the establishment of new companies with the

---

[1]http://space-inventor.com/wordpress/wp-content/uploads/2018/05/..., accessed 18/06/2020
[2]https://www.brown.edu/Departments/Engineering/Courses/, accessed on 29/06/2020
[3]https://www.arianespace.com/wp-content/uploads/2018/04/, accessed on 29/06/2020
[4]https://www.arianespace.com/wp-content/uploads/2015/09/, accessed on 30/06/2020

purpose of bringing satellites to a desired orbit. One of these companies is Momentus Space. Their objective is to bring satellites to their orbits, using the expendable transfer vehicle Vigoride, of which the most important parameters are presented in table 12.1. Unfortunately, not all six CubeSats fit in one vehicle due to the mass limitation. Therefore, one Vigoride will be used for each constellation of three CubeSats.[5]

Three CubeSats will be mounted on the Vigoride inside their deployers. This assembly will then be placed in the ASAP5 as a mini satellite, implying that the total mass of the satellite should be under 300kg. The total estimated mass of the assembly, with the mass of the CubeSats estimated in section 12.5 and the mass of the deployers with the necessary shielding, breakdown in section 12.3.3, is around 299.6 kg.

Table 12.1: VIGORIDE datasheet [6]

Parameter	Value
Wet Mass (98.5% of propellant) [kg]	212.15
Max Payload (GTO to GEO)[kg]	120
LICCA mission payload [kg]	87.45
LICCA mission transfer time [months]	1.2

Note that for sustainability and mass considerations, only the necessary propellant is taken on board (including 10% margin). Now the plan is to use the Vigoride in this mission. However, this selection may be influenced by future developments in this space taxi market, more sustainable or cheaper.

12.3.3. Deployer
To survive the transfer from GTO to GEO, adequate radiation shielding is required. To determine the required aluminium shielding, an analysis in SPENVIS was done, making use of the MULASSIS model. From this analysis was determined that an equivalent aluminium shielding of 4 mm would be required to minimize the TID on the CubeSats. After the transfer of two months from GTO to GEO the TID of the CubeSats would be around 100 rad. Which means the CubeSats can start their mission without a significant experienced TID. As the deployer has an equivalent aluminium shielding of 1.5 mm [7], this was deduced from the materials used and the CAD models. Therefore, an additional shielding of 2.5 mm would need to be added. This gives a total mass for the deployer (5.65kg) and for the aluminium shielding, making use of aluminium 6081-T6, of 1.2 kg.

12.4. Mission operations planning
This section gives an overview of the mission operations. Three main phases were identified and need deepening, these phases are also depicted in the Functional Flow Diagram(FFD) and mentioned in the Functional Breakdown Structure(FBS). The diagrams can be found in appendix A. The focus in this chapter lies on the insertion into orbit, operations and EoL phases.

12.4.1. Injection into orbit
Injection into orbit includes reaching GEO, initialising the satellite and reaching the correct formation.

Reaching GEO
The arrival to GEO is planned as follows. First of all, Ariane 5 or 6 takes two VIGORIDE satellites with a total of six CubeSats of the LICCA mission, in their deployers, to GTO as secondary payload. Once in GTO, VIGORIDE brings the CubeSats to GEO, in 1.7 months, where they are deployed.

Initialisation
Once in GEO, the spacecraft subsystems are activated. The solar panels are deployed, such that sensors become visible and the thruster is liberated. Contact is made with the ground and the spacecraft's orbit and attitude are determined.

---

[5]https://momentus.space/rides/, accessed 26/06/2020
[6]https://momentus.space/rides/, accessed 26/06/2020
[7]https://www.planetarysystemscorp.com/wp-content/uploads/, datasheet CubeSat Deployer, accessed on 29/06/2020
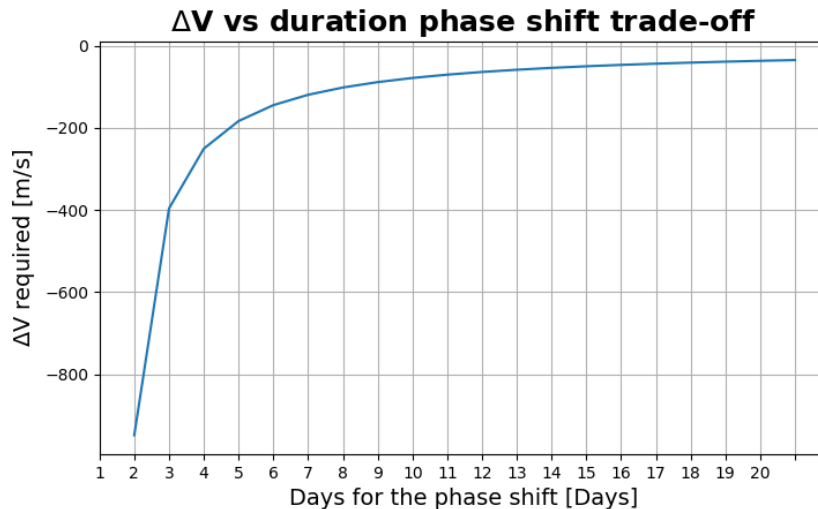
Figure 12.2: Relationship between ΔV and phase shift maneuver duration

Formation

To get the constellation into an equilateral triangle, a phase shift of 120°between each satellite has to be performed. The satellites of each constellation will be deployed at around the same place in GEO. Therefore, to get a phase shift of 120°between each satellite in the constellation, a couple of manoeuvres have to be planned. The satellites will be called one, two, and three, where satellite one is the reference satellite. To get a phase shift of 120°between satellites one and two, the latter needs to slow down. This can be done by increasing the apogee of the orbit of satellite two. This means satellite two will slow down relative to satellite one, and a phase shift of 120°can be achieved. To get satellite three in a phase shift of 120°with satellite one and two, either a phase shift of -120°or 240°with satellite one is needed. It was chosen to do a phase shift of -120°, as this would mean both the phase shifts of satellite two and three can be done simultaneously. Therefore, the perigee of satellite three is lowered, and the satellite speeds up relative to satellite one. A trade-off was made between the duration of the manoeuvre and the ΔV required as shown in figure 12.2, equation (4.1), equation (4.4) from section 4.3 were used. From which a manoeuvre duration of 7 days was deduced. When the constellation is formed, the payload's laser should be pointed towards the receiving satellite. First, the spacecraft attitude is determined and controlled accurately. The laser is now pointed towards the computed location of the receiving satellite and can be moved by the Piezo stage. If the other satellite does not receive any signal, the laser will spiral out until the satellites find each other. This locating should be repeated after every manoeuvre during which the spacecraft is rotated. When the signal is in view, the measurements can be started.

12.4.2. Operations

The subsystems work simultaneously during operations, as represented in function four of the FFD and FBS. The functional analysis per subsystem can be found in the designated chapters. Nominally, all subsystems are continuously active. However, there are some exceptions to this which will be described next.

Housekeeping and scientific data are gathered in orbit. They are stored in the memory of the CDH. Once per revolution the data is sent to the ground station via downlink. Details can be found in chapter 7. Due to power regulations for heating, this downlink is planned during daytime.

After 15 days, the satellites might have drifted from their original position. Therefore a realignment manoeuvre is required. This manoeuvre is described in section 4.3. The sequence is as follows: deactivate payload, rotate, burn, rotate back, find other satellites, measure again.

12.4.3. End-of-Life

After an operational lifetime of two years, the EoL manoeuvre shall be performed. The procedure can be seen in function 5 of the FFD and FBS. The satellites are brought to a graveyard orbit, located 300 km above GEO. At this point in the mission, the spacecraft subsystems might still be able to function properly. If this is the case, the measurements can continue in the graveyard orbit. An important factor in the continuation of the measurements is the amount of propellant left in the tank. Since no extra propellant is taken on board of the spacecraft (because there was no volume for this), the tank could be empty. However, when calculating the propellant needed for the realignment manoeuvre, the propellant needed for a maximum drift was calculated. This means that there might be propellant left after two years of operational lifetime, if the satellites do not drift in the worst possible direction every time.

To summarise, the mission might continue in the graveyard orbit if there is enough propellant left to do the realignment manoeuvre. Furthermore, the subsystems are prone to failure at this point of the mission, due to radiation for example. Therefore the EoL manoeuvre is performed after two years of operational lifetime, independent of the functioning of the spacecraft at that time. To not let a possible extension of lifetime go to waste, the measurements can be picked up in the graveyard orbit.

The measurements are proceeded until the subsystems are no longer able to function properly. At that point the left propellant is burned and the batteries are discharged completely. The remaining systems are shut down and the mission ends.

12.5. Budgets

This section summarises all subsystems into final budgets. The subsystem designs were based on the budgets presented in the Midterm Report [5]. The values are no longer based on estimates and statistics, but determined by the design. Further development of the mission may imply slight changes to the budgets, therefore still some margins are included. The margins follow the ECSS regulations [67]. The section presents the power, mass and volume budgets. In addition, the ΔV budget can be found under Astrodynamics (see section 4.3).

12.5.1. Power budget

The power budget is presented in table 12.2. The budget is split up in power needed during daytime and eclipse, since this can differ per subsystem. More information on when which subsystem is active and how the power is distributed can be found in section 9.3. The total power needed during daytime is 30.60 W. Note that this is not simply the summation of the power of each subsystem, but the maximum that is reached by active subsystems during daytime. The total power during eclipse equals 31.00 W.

These powers can be compared to the estimated values from the previous phase of the project, including margins [5]. The power was estimated to be within the range of 27.88 to 58.25. The final values are at the lower limit of this range, and thus well under the requirement of 40 W.

The margins applied are the following [67]:

  • 5% for subsystems that consist of merely COTS components
  • 10% for subsystems that use COTS components with minor modifications
  • 20% for subsystems with components under development

Most subsystems use COTS components. The propellant tank of the propulsion subsystem would be enlarged, thus this is seen as a modification. This however would not influence the power budget, since only the thruster consumes power for propulsion and this is a COTS component. The payload and structure contain components that need to be fully developed: the transponder and the solar panel structure respectively.

Table 12.2: Power budget

Subsystem	Margin	Daytime [W]	Eclipse [W]
Payload	20%	5.114 ±1.02	5.114 ±1.02
ADCS	5%	9.9 ±0.495	9.9 ±0.495
Propulsion	5%	1.89 ±0.0945 or 9.6 ±0.48	1.89 ±0.0945
Communication	5%	5.5 ±0.275	0
CDH	5%	3.3 ±0.15	3.3 ±0.15
Thermal	5%	0	10 ±0.5
Structure	20%	0	0
EPS	5%	0.8 ±0.04	0.8 ±0.04
Total		**30.60 ±2.28**	**31.00 ±2.30**

12.5.2. Mass budget

The mass budget can be found in table 12.3. After several iterations, the mass converged to a value of 22.3 kg. The value estimated in the midterm was 18.36 kg with a margin of 16% [5]. The final mass is higher, even above the upper limit. This is however not considered a problem since mass has no hard constraints.

On top of the mass estimated for the subsystems, 15% of the total mass is added for cabling. This includes cabling of the power system and the command and data handling. More information about this estimate can be found in section 12.2. The margins used for the mass budget are the same as for the power budget, with the difference that in the mass budget the modification to the propellant is accounted for.

Table 12.3: Mass budget

Subsystem	Margin	Mass [kg]
Payload	20%	5.75 ±1.15
ADCS	5%	2.77 ±0.139
Propulsion	10%	4.50 ±0.450
Communication	5%	0.528 ±0.0264
CDH	5%	0.285 ±0.0143
EPS	5%	1.20 ±0.060
Thermal	5%	0.433 ±0.0217
Structure	20%	3.81 ±0.636
Total		**22.3 ±2.50**

12.5.3. Volume budget

The last budget presented is the volume budget in table 12.4. The volume should not exceed 12 U. This constraint was an important driver for the design. The value estimated in the midterm was 9.6 U, in a range of 5.68 U to 13.53 U [5]. The final volume occupies 10.9 U. This is close to but slightly higher than the estimated value. This table regards the inside volume of the spacecraft, and thus not includes for example louvers and solar panels mounted on the sides. The outer volume is determined by the CubeSat deployer in the launcher and provides an extra 10 mm on every side. The budget does also not account for cabling, since the volume of cabling is considered negligible in the architecture of the spacecraft. Since mostly COTS components are used, it is difficult to place all components to use the CubeSat volume efficiently. However a configuration was worked out to fit the components in the structure, as is shown in section 12.1. Here it can be seen that the constraint of 12 U is met.

For the volume budget, no margins are included [67]. The volume growth should however be monitored constantly, based on the available volume of 12U. The architecture should be adaptable to this. Components subject to potential volume growth are identified in the sensitivity analysis in chapter 14. Other margins that cause potential volume growth have already been incorporated in the mass and power budgets, therefore it is deemed not necessary to include them in the volume budget.

Table 12.4: Volume budget

Subsystem	Volume [U]
Payload	4
ADCS	0.971
Propulsion	4.1
Communication	0.559
CDH	0.285
EPS	0.75
Thermal	0.1
Structure	0
Total	**10.9**

12.6. System characteristic diagrams

Diagrams which characterise the systems were created during the preliminary design phase as described in the midterm report [5]. In the detailed design phase, these diagrams were utilised and maintained. The updated diagrams are presented here.

12.6.1. Software Block Diagram

The software block diagram gives an overview of the utilised software, along with how the software communicates internally and externally. Since the CDH subsystem utilises two cores, functionally there will be two different OBCs. OBC 1 will function as the main OBC, whereas OBC 2 will function mainly as the ADCS control system. The software block diagram is given in figure 12.3.
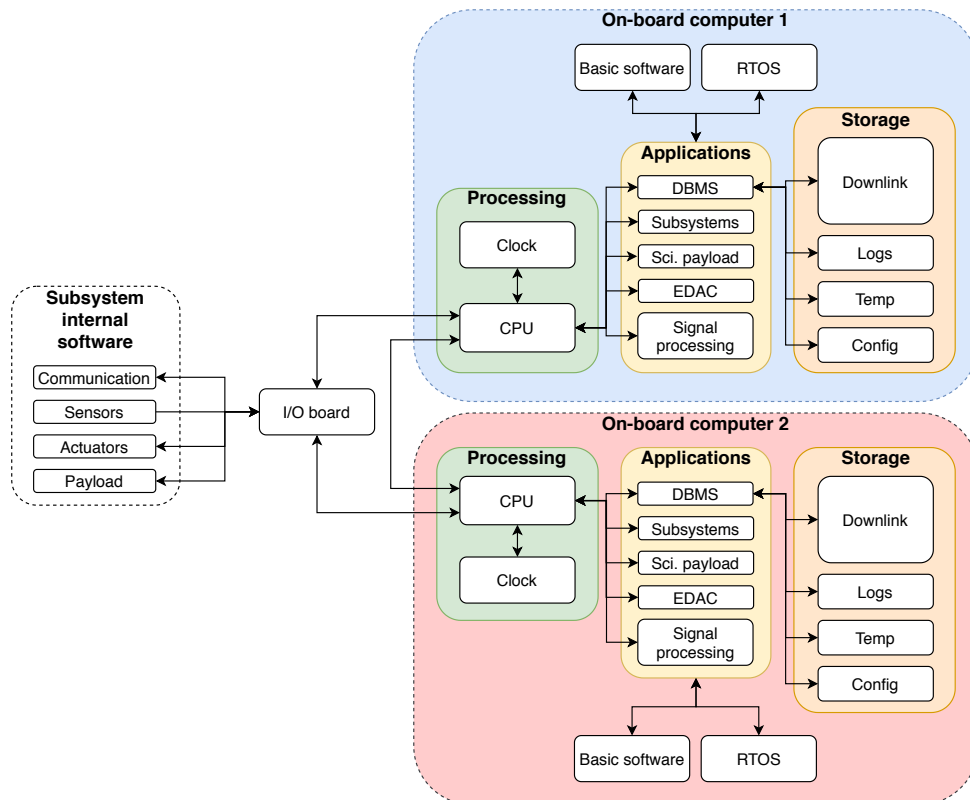
Figure 12.3: The software block diagram

The subsystem internal software for the communication, sensors, actuators and payload are all connected to the OBCs via one I/O board. Since either OBC must be capable of overtaking the other OBC's functionality if the other must be reset due to faults, both OBCs can communicate with the subsystem internal software via the I/O board. Furthermore, the OBCs can communicate directly with each other, such that the OBCs are aware of the status of the other OBC is case either needs to be reset. Since both OBCs must be able to fulfill the tasks of the other OBC, they contain identical software.Both OBCs run on Real-Time Operating Software (RTOS), and contain applications for DataBase Management Software (DBMS), subsystems, the payload, EDAC software and signal processing software. The DBMS controls the storage, including the mass storage for downlink, as well as storage for logs, temporary data (temp) and configuration (config). Although both OBCs have an internal clock, it should be noted that the payload contains an atomic clock. This clock will also be connected via the I/O board, as it may be useful for more accurate timestamps of the payload data.

12.6.2. Hardware Block Diagram
The hardware block diagram in figure 12.4 visualises the hardware and electronics used in the satellite. Per subsystem all components that provide readings or react to commands are presented. As previously mentioned, there are two CDH cores, the main core OBC 1 and a core used for ADCS, OBC 2. Generally commands are received via the uplink and distributed by OBC 1. This can be seen in the diagram as an arrow accompanied by 'CMD' for command. The commands for the ADCS are passed through via OBC 2. Within for example the EPS, the commands are distributed further by the PCDU electronics. The sensors of the subsystems provide readings, which are processed by the OBCs. Arrows with 'RDG' represent these readings. The readings are sent towards the ground station via downlink. In this diagram the UHF system is used for uplink and the S-band for downlink, which are the main purposes of these systems. Both systems could potentially be used for both uplink ad downlink, but this is left out for simplicity.
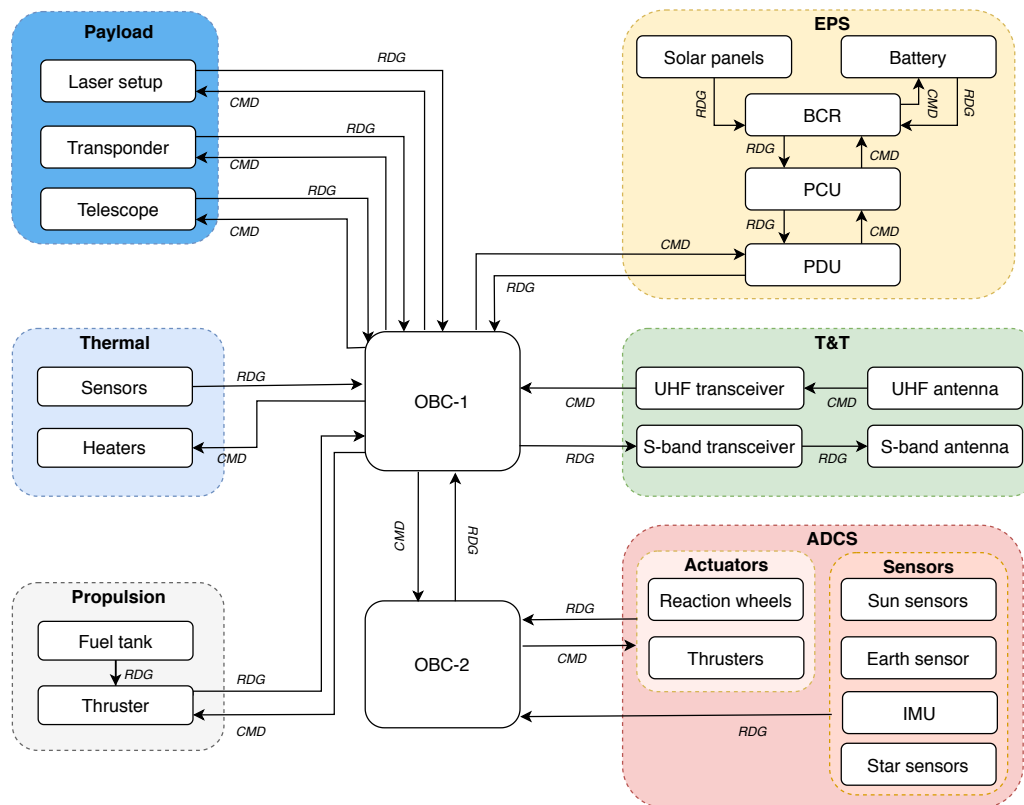
Figure 12.4: Hardware Block Diagram

12.6.3. Electrical Block Diagram

The electrical block diagram shows the electrical connections between the EPS and all other subsystems and their components figure 12.5. The EPS consists of 6 solar panels, a battery and an EPS dock, which includes two PCUs and PDUs. The solar panels are connected by the BCRs, which includes multiple MPPTs to allow for the connection with two opposing solar panels [73]. This dual connection with two solar panels is only possible when the solar panels are facing opposite to each other, where one panel is in the sun and the other only receives light from the Earth albedo effect. Therefore four BCRs are needed, as there are six solar panels of which four are facing opposite from each other. The EPS from Clyde Space consist of two EPS boards and one EPS dock. The Motherboard has three BCRs and the daughterboard has six. These motherboards are connected to the EPS dock which in turn is connected to the undervoltage protectors. The undervoltage protector protect the PCU from damage due to voltages below the design criteria [73]. The PCU has four different voltage suppliers, 3.3V, 5V, 12V, and an unregulated BATV. The PCU in turn is connected to the PDU, which has 3x3.3, 3x5,2x12, and 2xBATV buses [73]. All the sensors and actuators of the satellite are then connected to the different buses. The sun sensors are divided into two different parallel circuits, both running on five volts. The reaction wheels are also connected in parallel with each other. All the different circuits amperages are below the maximum allowable ones. The antennas are connected in parallel, containing a switch box, this is done to decrease the need for a third PCU and PDU pair. This does mean however that they cannot be operated all at the same time otherwise the current through the wire will be too high, but this would not pose a problem to the functioning of the spacecraft. The OBC has only one connection to the EPS as it is build as a single module with its own PDU to distribute the power between the two cores.
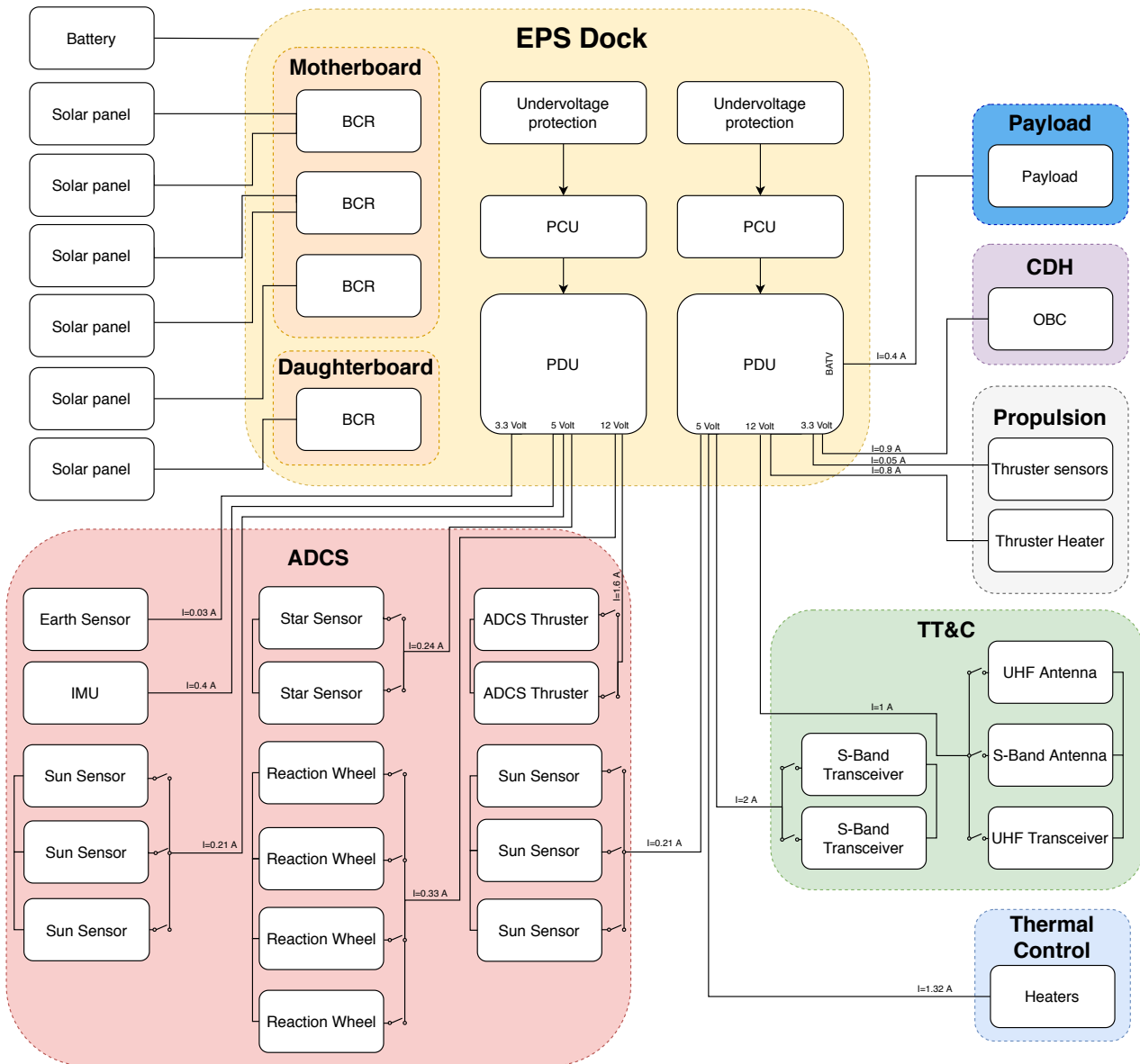
Figure 12.5: The electrical block diagram

12.6.4. Data Handling Block Diagram

The data handling block diagram gives an overview of how the spacecraft handles data internally. Since the CDH subsystem contains a OBC-P3 component, which contains two independent OBCs, the two OBCs are distinguished in the data handling block diagram. The diagram is given in figure 12.6.
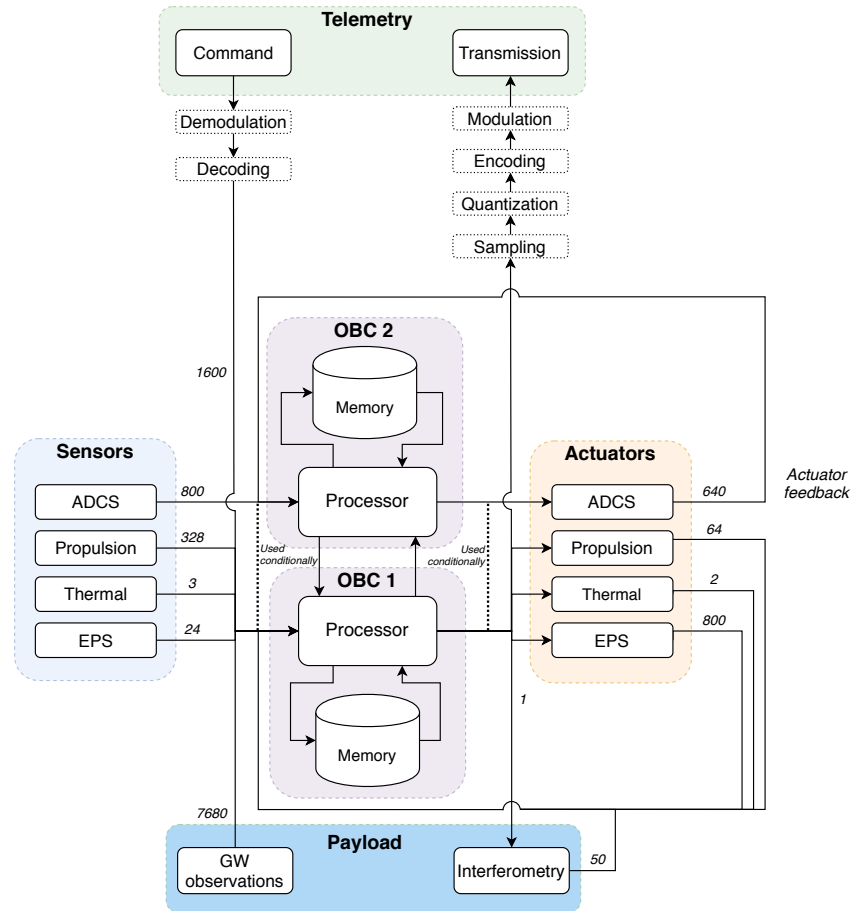
Figure 12.6: The data handling block diagram

In the data handling block diagram all subsystems occupying sensors are listed. The ADCS sensor data enters the processor of OBC 2, and the other sensor data enters the processor of OBC 1. Similarly, OBC 2 controls the ADCS actuators, and OBC 1 controls all other actuators. The processors of OBC 1 and OBC 2 are connected, since housekeeping data from and commands for the ADCS must be transferred from OBC 2 to OBC 1. Furthermore, in case one of the OBCs fails or is being reset, the other OBC will detect this via the processor of the non-functional OBC. The other OBC will take over its functions. In this condition, the dotted lines are used, which marked with *"Used conditionally"*. On the top of the diagram, the telemetry is shown. For transmission, the data will be sampled, quantized, encoded and modulated first, such that it can be transmitted. Received commands must be demodulated and decoded. Lastly, the payload will nominally be operated by OBC 1. The numbers indicate the datarate of the different data flows. These values are given in bits per second (bits/s). The complete list of sensors and actuators is omitted for a better overview. The complete list of sensors and actuators, along with their functionality, can be found per subsystem in the relevant chapters.

12.6.5. Communication Flow Diagram

Data will flow within the system between the various subsystem in the satellites, between the different space and ground segments of the mission, and between the segments and their environment. An illustration of this communication flow is given in figure 12.7. The arrows in the diagram are accompanied by small texts that specify the sent signal.

The scientific payload that is on board measures fluctuations in distance cause by gravitational waves. Several other subsystems receive inputs from the environment as well, such as the ADCS and the EPS. The scientific data gathered by the payload and the housekeeping data of the subsystems is fed to the CDH. The CDH then routes this data to the TT&C subsystem to be downlinked. The TT&C consists of an S-band link and a UHF link, which can be seen in the diagram. The S-band will be capable of higher data rates, and is used to downlink both scientific and housekeeping data. The UHF data rate is very limited, and should only be used for downlinking housekeeping data in the event of an emergency. Furthermore, as a courtesy to the amateur radio enthusiasts for using the UHF frequency band, messages of a limited size can be downlinked to them. The rest of the data from the downlink is gathered at the command centre. Tracking data is included in this, as it is performed by the S-band ground station. The scientific data is then sent to the data processing facilities, along with further distribution and storage as necessary.

At the command centre, commands are issued and sent out to the ground stations to be uplinked. The uplink of commands will primarily occur with the UHF system, as it is assumed that these will be owned by the LICCA mission, or in any case less frequently used than the ESTRACK ground stations, and thus largely available. Nevertheless, the capability for uplinking from the S-band ground stations is also present and can be used if necessary and possible. Once again, the TT&C receives the commands and passes these on to the CDH. From there, the CDH processes and executes the commands for the relevant subsystems.
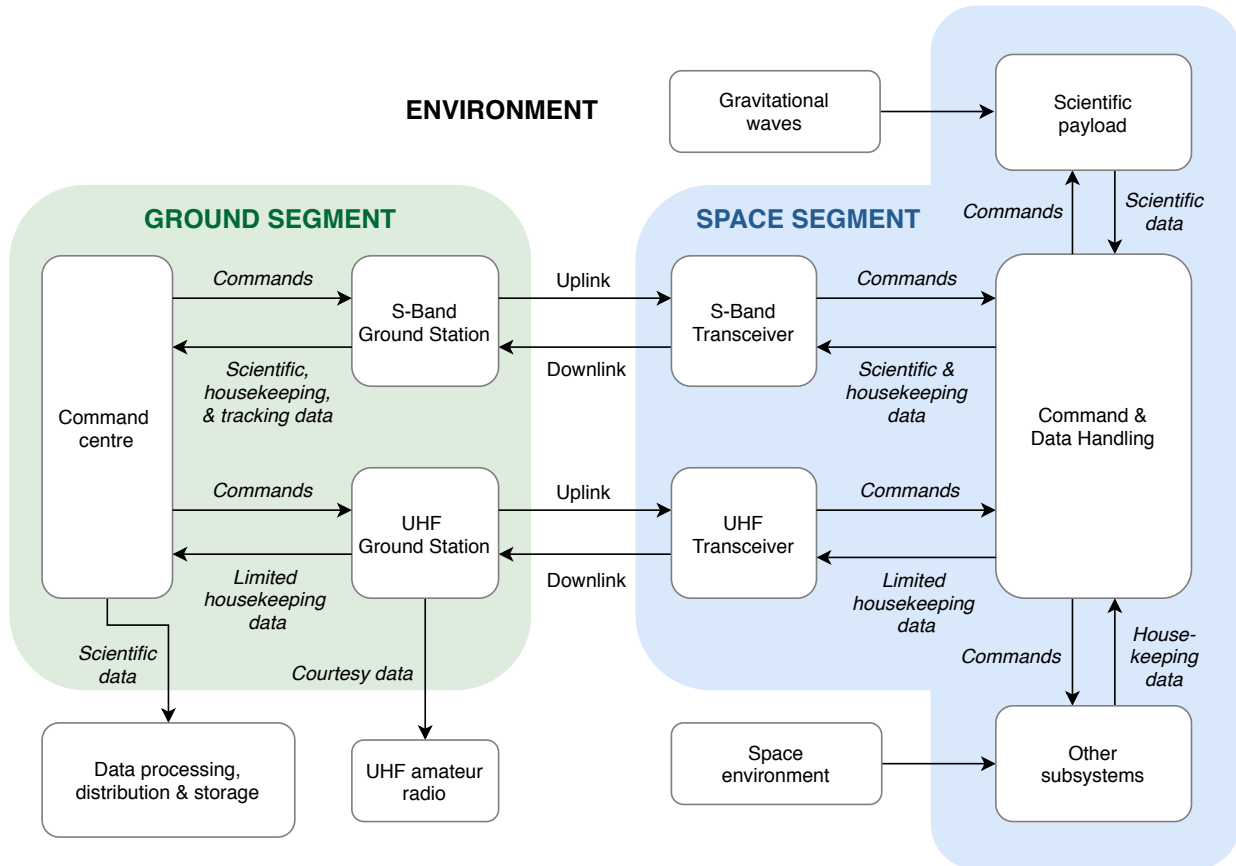
Figure 12.7: The Communication Flow Diagram.

12.7. Mission cost

This section describes the cost of the mission and the division of the 20 million EUR budget. It should be noted that the budget will cover all aspects of the mission except for the launch and operational costs. In order to analyse how much money is needed for the different stages of the design, a Cost Breakdown Structure (CBS) is made. As can be seen in figure 12.8, the mission is split into five phases: design, research & development, verification & validation, production and operations. For all these phases, an estimation of the cost was made. The diagram is an AND tree, meaning that the cost of the five phases is the sum of the blocks under that phase. Note that the operations branch is indicated with a dotted line, since, as aforementioned, it is not part of the mission budget, but was presented in the diagram for completeness.

For the design phase, the cost are estimated as follows. The design phase consists of the DSE, detailed design and documentation. The costs for these three phases are taken from the project Gantt chart, shown in figure A.6 and figure A.7, in which the total amount of hours spent in each phase and the corresponding wage were identified. The results can be seen in figure 12.8.

For research and development, the cost was estimated by taking 10% of the design and testing phase [72]. The major components that have to be developed are the transponder system, and a propulsion system capable to perform the transfer from GTO to GEO.

For verification and validation, the cost is dependent on the lines of code. As explained in section 8.2, approximately 77 000 lines of code are needed in designing this mission. For the cost a price of €10 per line of code was taken [54], resulting in €770 000 for verification and validation.

Next, an estimation is made for the production phase, which consists of transport, testing, manufacturing and the price of the COTS components. For transport of the components, it is assumed that a component travels for 3 000 km on average, due to the country of origin being in Europe for most components but from the USA for

ADCS components, and a price of €3 per kilometre is assumed [28]. For the transport of the satellites, a similar estimations was done. However, since the testing facilities are close to the Delft, a lower distance of 300 km was taken for the average travel distance. Another difference is that these travel distances have to be doubled, as the satellites have to go to the testing facility and come back to be assembled. The estimation for the cost of testing and manufacturing was taken from the project Gantt chart. The price of the COTS components was simply looked up. If the price of the used component was not found, the price of a similar component was used as an estimation. When this was not possible, such as for the ADCS subsystem, an estimation was made based on the cost of an ADCS unit for a 12 U Cubesat with a similar pointing accuracy from Blue Canyon Technologies[8]. Regarding the battery, since no similar components were found, an estimation based on its size was made [74]. In order to make a conservative estimate, and due to the uncertainties for certain components, a margin of 10% was taken [67].

The final phase is the operational phase. Although it is required to make an estimation of the cost of this phase, it will not be taken into account in the 20 million EUR budget. The cost of the operational phase comprises launch and operational cost. For the launch, a cost of €21 600 per kg is assumed [32, p. 248]. For the ground station, an estimation was made about the duration of uplink, downlink and tracking time. This was multiplied by an estimated cost per minute[9], which was then multiplied by the expected mission duration, resulting in the number shown in figure 12.8. For the transfer from GTO to GEO, the price was found to be €3 554 880 [10]. Note that the total price of the LICCA mission is the sum of all the phases, multiplied by an average inflation of 2% per year[11]. Since the launch is in 2030, ten years will be taken into account for inflation.
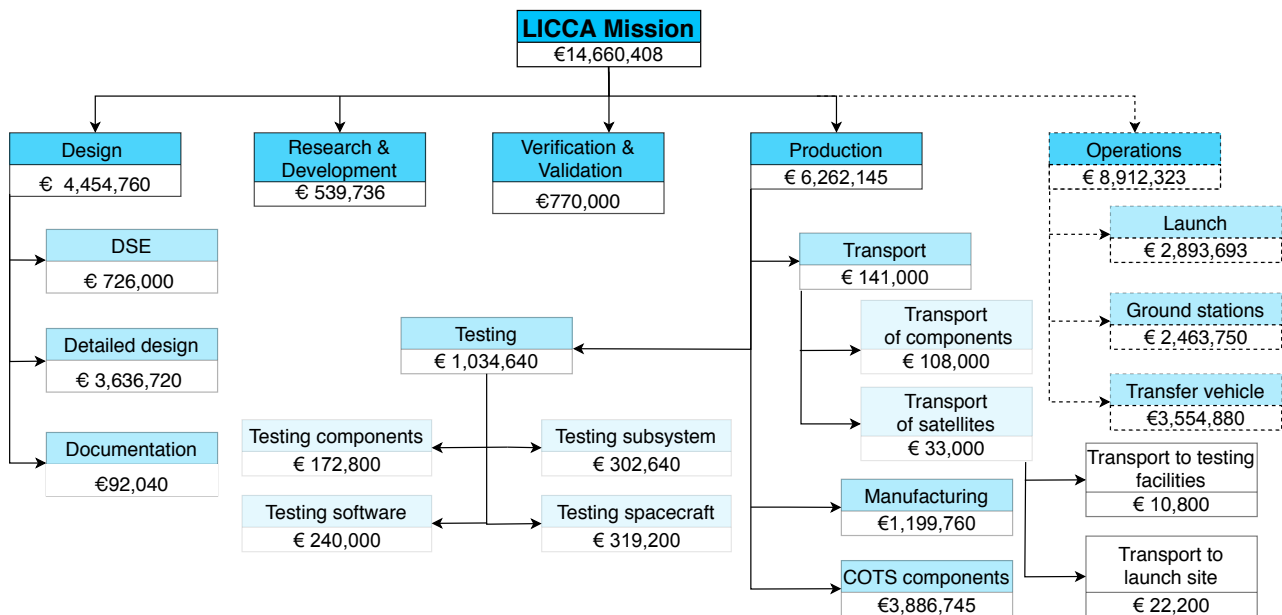
Figure 12.8: The Cost Breakdown Structure of the LICCA mission

13

Technical Risk Management and RAMS

This chapter describes the risk management of the technical aspects of the mission, including manufacturing and design. Furthermore, the RAMS characteristics are assessed regarding the entire system. The risks and RAMS characteristics are discussed per subsystem in the previous chapters. In this chapter they are summarised and investigated generally. Section 13.1 describes the identification of general risks as well as gathering all risks already identified for each subsystem. After that, a risk mitigation is presented in section 13.2. Section 13.3 discusses reliability, in section 13.4 the availability is looked at, maintainability can be found in section 13.5 and section 13.6 addresses the safety of the system.

---

[8] https://www.bluecanyontech.com/, accessed 18/06/2020
[9] https://aws.amazon.com/ground-station/pricing/, accessed 18/06/2020
[10] https://momentus.space/, accessed on 29/06/2020
[11] https://tradingeconomics.com/netherlands/inflation-cpi, annual inflation rate, accessed 18/06/2020

13.1. Identification of risks

In the subsystem chapters, a risk identification was performed. In table 13.1, the risks stemmed from that process are listed. In the table, two numbers are stated next to each risk: the first one indicates the likelihood of the risk, whereas the second indicates the impact of the risk. Throughout the risk analysis, some general risks were identified, and are now analysed below. First, the risks already identified in previous design stages are listed below [5]:

- **G1:** An assembly error occurs
- **G2:** The design fails to meet the requirements when testing
- **G3:** There is an error in the data interpretation
- **G4:** A subsystem fails
- **G5:** Schedule delays
- **G6:** Integration delays
- **G7:** Surpass budget
- **G8:** DELETED
- **G9:** There are no existing similar missions yet
- **G10:** A satellite is hit by space debris
- **G11:** Data loss during downlink
- **G12:** Launch failure
- **G13:** Damage during storage and transportation of components

Table 13.1: Risks identified in subsystem design

ID	Risk	(L,I)	ID	Risk	(L, I)
	Payload			*ADCS*	
PL1	Many components that can fail	(2,3)	A1	Radiation	(4,3)
PL2	Inaccurate pointing of lasers	(2,3)	A2	Temperature	(3,3)
PL3	Failure transponder system	(3,3)	A3	Sensor failure	(2,4)
PL4	Mirrors not oriented in the correct way	(1,4)	A4	Centre of mass variation	(1,3)
	Propulsion			*Thermal*	
Pr1	Stress concentrations in propellant tank	(4,3)	T1	Thermal balance is changed due to loss of absorptivity and emissivity	(2,2)
Pr2	Propellant tank leakage	(1,4)	T2	Springs of the louvres can break during launch	(1,4)
Pr3	Failing EoL manoeuvre due to lack of propellant	(1,3)	T3	Heat concentrations form due to non ductile materials	(2,2)
	TT&C			*CDH*	
TT1	Incompatibility of frequencies between antennas and receivers	(1,4)	C1	Total ionising dose	(4,3)
TT2	Incompatibility of frequencies between satellite and ground station	(1,3)	C2	Critical SEE	(1,5)
TT3	Misaligned antenna	(1,3)	C3	Non critical SEE	(4,2)
TT4	Different modulation types	(1,3)	C4	Coding faults	(3,2)
TT5	Component failure	(2,4)	C5	Electrical faults	(2,2)
TT6	Wrong commands uplinked	(1,3)	C6	Component corrosion	(1,3)
TT7	Corrupted signal downlinked	(2,4)	C7	Soldering mistakes	(2,3)
	EPS			*Structure*	
E1	Battery causing a short circuit	(3,3)	S1	Main structure can not withstand loads	(1,4)
E2	Incorrect switch configuration	(2,2)	S2	Deformation of the structure	(1,4)
E3	Exceeding maximum ratings	(2,4)	S3	Structure becomes too hot or too cold	(2,4)
E4	Failure of solar panels	(1,4)	S4	Damage of solar cells due to vibration during launch	(1,4)
	Cabling		S5	Solar panels damaged during deployment or do not deploy at all	(2,4)
Ca1	Failure of I^2C connectors	(3,4)	S6	Failing of the HRM	(2,4)
Ca2	Heat generation in wires	(2,2)	S7	Failure of the retractable reel	(1,3)
			S8	ADCS thruster deployment failure	(3,4)

On top of these, new generic risks are added in the current design phase. Below, their identification and analysis is described.

- **G14:** *Failure of the EoL manoeuvre. (1,3)* When the mission is at its end, an EoL manoeuvre is performed. If this manoeuvre fails, the satellites might end up in the wrong orbit. In this eventuality, the mission, comprising of six satellites, would contribute extensively to the creation of space debris.
- **G15:** *Misfit of the satellite in the deployer. (1,4)* The satellites will be in a deployer during launch. This deployer has a predetermined size and if the satellites do not fit, the launch will become impossible.
- **G16:** *The GTO to GEO transfer fails. (2,5)* Since the transfer from GTO to GEO can not be done by the CubeSat itself, it was chosen to let a transfer vehicle produce the required ΔV. However, if this transfer vehicle fails or Momentus is not able to deliver their vehicle in time, the LICCA satellites do not end up in GEO.

13.2. Risk maps

The identified risks can now be presented in risk maps. The risk maps are split into the subsystem risks and the general risks, presented in figure 13.1a and figure 13.1b, respectively. Critical risks are risks in the yellow, orange and red zones. Note that in figure 13.1b, risk G16 is shown after mitigation since it is the only risk in this map that needs mitigation.

(a) Original risk map subsystems   (b) Mitigated risk map general system
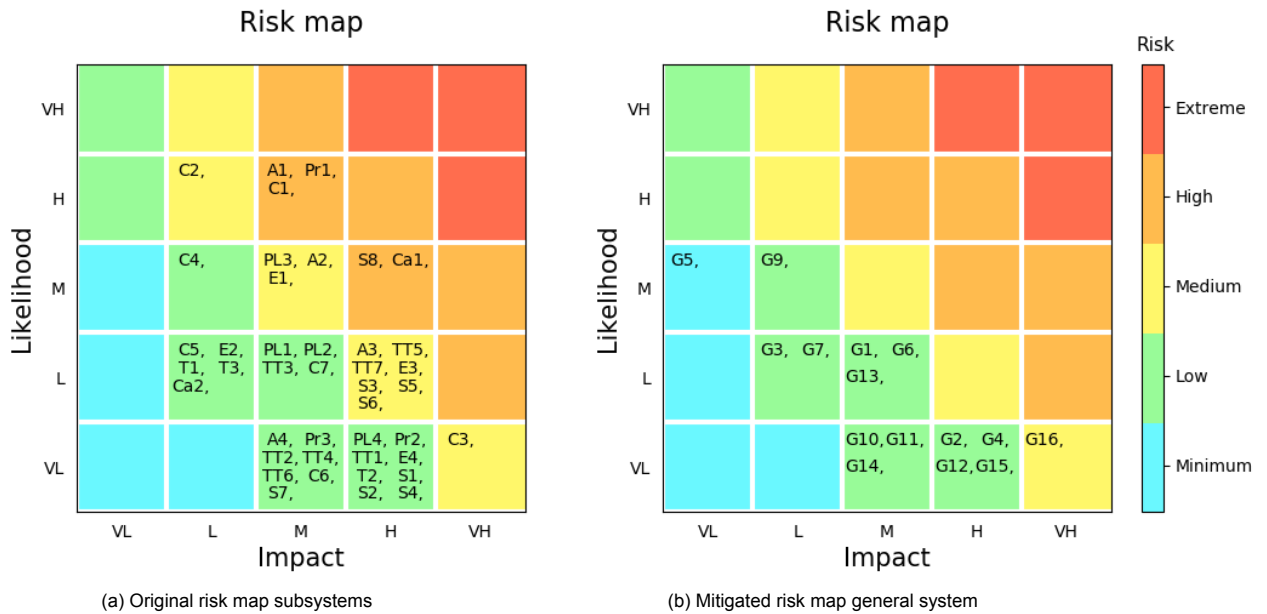
Figure 13.1: Original risk maps including mitigation for the general system

It can be seen that some risks are in the critical zone, and must therefore be mitigated. A mitigation strategy for each of these critical risks is given below:

- **PL3:** Since the transponder system requires development, the chances of failure are higher than for components that were already part of previous space missions. However, once the design of the transponder system is completed, thorough research will be done into the feasibility of the system. Furthermore, the system will undergo many tests, simulating the space environment and its mission conditions, thus lowering the likelihood of failure during the mission.
- **A1:** The amount of radiation the ADCS components are certified to withstand ranges from 9 krad to 30 krad. Therefore, additional protection has to be included in order to mitigate this risk. These includes adding a layer of protective material, protective lenses for sensors requiring a field of view, and filtering the signal obtained by these to account for possible deviations. These measures will decrease impact and likelihood of the risk.
- **A2:** Whenever large temperature fluctuations occur, either active thermal control or placement of a component compensating the temperature gradient has to be performed, which decreases the probability.
- **A3:** To mitigate this risk, multiple sensors are installed in the satellite. These are: two star sensor, one Earth sensor and one Sun sensor. Adding redundancy to the system decreases the impact.
- **Pr1:** Since the propellant tanks of the LICCA satellites have an unusual shape, stress concentrations occur. However, extensive testing will reduce the likelihood of failure of the tank. Since a broken tank can not be repaired in space, the tank will be tested and redesigned if necessary, until the tank is a reliable component of the satellite.

- **TT5:** All components run the risk of failure. In the case of the TT&C, failure in the components would mean the inability to communicate with the satellite. This would make the satellite useless and the mission fail. Two separate communication channels have thus been included,one for UHF and one for S-band. Also, two S-band transceivers have been included in the design, making the TT&C more resilient to component failure.
- **TT7:** Errors in the downlink can occur due to noise. For this, a significant BER has been employed in the SNR calculations in the link budget. Furthermore, an encoding method can be used to add redundant bits that can allow for error-correcting of the signal.
- **C1:** Since non-space-grade COTS OBC options are typically not qualified for the TID experienced in GEO, a procedure is suggested where a COTS OBC is tested for performance after being exposed to a radioactive source. It is exposed to this source until the TID equals the expected TID in GEO over the lifetime of the mission. If the performance has degraded too much, it is either modified if the performance is bottle-necked, or a different COTS OBC is selected. This procedure is described in more detail in section 8.4.2.
- **C2:** Critical SEE can be mitigated by the use of redundant hardware or software architectures. SEL can be mitigated by making sure all semiconductor elements are grounded, to prevent sudden voltage spikes. Increasing the thickness around the components can also help, decreasing the chance of a SEE.
- **C3:** Non-critical SEE can be mitigated by the use of redundant hardware and software or by the use of specialised hardware which can detect SEU and correct them. Extra shielding can decrease the chance of a SEE.
- **E1:** A short circuit should always be avoided. This can be mitigated by extra protection of surrounding materials, which will decrease the impact. Furthermore, checks can be made to see whether the battery is correctly aligned [73], which decreases the likelihood.
- **E3:** Exceeding maximum ratings can be avoided by proper testing of all components used to ensure compatibility. On top of that, protection of the components is added to make sure the EPS system stays within their radiation and temperature margins. This will decrease the probability.
- **S3:** A too large temperature difference can be mitigated by use of an active thermal control system, which is described in chapter 10 in more detail. This decreases the likelihood of this event.
- **S5:** Solar panels have a high probability of taking damage during deployment or even fail to deploy correctly, because their deploying mechanism is complex. Proper testing ensures safety and therefore decreases the likelihood of failure.
- **S8:** The failure of the deployment of the ADCS thrusters must be avoided. Thorough testing will be done on the deployment mechanism, especially since new components are used for it. This will decrease the probability. By considering redundant components in this new system, the impact could also be decreased.
- **Ca1:** The risk of failure of I^2C connectors can be mitigated by adding wires and a bus for redundancy. Besides that, a watchdog circuitry can be added. A watchdog timer times how long it takes for signal to go from one point to another, if this takes too long, the system will reset, and the signal is send again. Bus lockup protection may also be added [38]. This will all decrease the probability of this risk.
- **G7:** This risk was already mitigated, but a new mitigation strategy is added. When the budget is surpassed, the concept can always be adjusted from six to three satellites.
- **G16:** The risk of the transfer not occurring can be mitigated by testing. Furthermore, if other missions in the coming years successfully use this transfer vehicle, it is a more confident solution for the LICCA mission. Since the launch is only in 2030, maybe new companies will enter the space taxi market, meaning that the LICCA mission can choose the best option. This way the likelihood of the transfer failing or not occurring will decrease.

After the mitigation, new risk maps were made in order to visualise the main differences, which is shown for general risks in figure 13.1b and for subsystem risks in figure 13.2. It can be seen that there is only one risk left in the critical zone, which is G16. Since this is something that is designed in the next stages of the mission, it is important to take this risk into account and update the risk map when necessary.
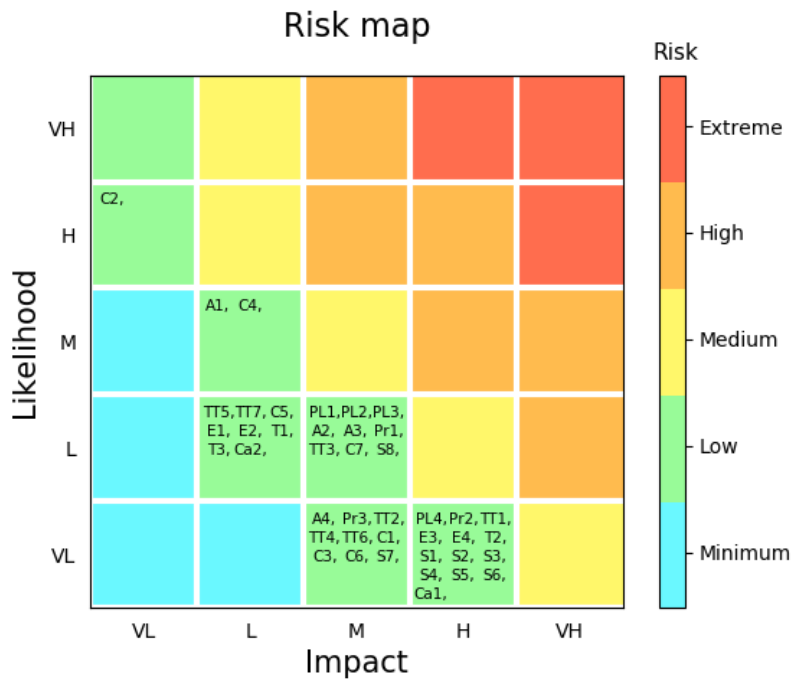
Figure 13.2: Mitigated risk map general system

13.3. Reliability

Reliability is defined as the probability of the system functioning, and thus one minus the probability of failure. The probability of failure can be estimated based on the probability of a risk occurring and its impact on the functioning of the system. As is evaluated in chapter 13, the risks are fairly low. After mitigation all risks receive a score of 0.24 or lower. Nevertheless there are many risks identified, which increases the general probability of failure. Taking everything into account, risk originating from the subsystems and general risks, the reliability is estimate at 0.58. Note that this is simply an order of magnitude estimate and the reliability of this mission will be investigated more closely. A reliability of 90% is considered high, and a probability of 50% is considered the lower limit [74]. A high reliability is desired, but CubeSats are known for not achieving this.

Reliability estimates are often based on comparable missions, thus for this project the statistical reliability of CubeSats is investigated. Due to infant mortality in CubeSats the reliability degrades rapidly, but it stagnates over time. At the moment of launch the reliability of CubeSats is over 80%. After two years the reliability is approximately 0.56 [47]. This is taken as a baseline and in the following it is discussed what variables in the design could influence this number.

During the design, extensive use was made of COTS components. These components are verified and flight-proven, which results in high reliability. Some components are not developed for this missions orbit, and may degrade due to radiation. A few components need to be developed entirely, which imposes uncertainties. These effects are likely to cancel each other out and this will does not affect reliability greatly. During next phases of the mission, numerous tests are planned for further development of the design. Testing improves reliability significantly.

Due to volume constraints, not many redundant components for the subsystems can be taken on board. However during the design margins are taken into account. This approach has some influence on reliability. Contingencies during operations can be handled by these margins, but when a component fails no redundant component can take over. Overall this philosophy diminishes reliability. The failure of one component would be catastrophic and would mean failure of the system.

A measurement system consists of a triangle of three active satellites. This means that three interferometers are taken on board. The reliability of one interferometer is fairly low, since the technology is not fully developed yet. However three interferometers contains a form of redundancy, meaning that certain components can fail without affecting others. More information about this can be found in section 3.6, where the reliability of the payload is discussed.

The general focus of this chapter lies on the characteristics of the spacecraft, but emphasis can be laid on the constellation. The constellation consists of two independent trios of spacecraft and provides two independent datasets. This means that if something happens to one constellation, the other can still provide measurements. This increases reliability.

13.4. Availability

The main focus of availability for this mission lies on the availability of data. The availability of measurements was discussed in section 3.6. Measurements can continue for 15 days, after which a realignment manoeuvre is needed. During the burns of this realignment, measurements are interrupted. However due to the presence of two constellations, continuously one dataset can be available. Housekeeping data is constantly monitored by the CDH and internally commands can be given at any time.

The data is sent to the ground system once per day via downlink, but the spacecraft are available for receiving commands via uplink at every moment during orbit. The availability is thus twofold. The satellites can always be reached, but it can take up to an entire revolution before response to the ground is given.

13.5. Maintainability

Once in orbit, the spacecraft can no longer be reached physically and no mechanical maintenance is possible. This means that no reparation is possible when component fails. To account for this the system needs to be highly reliable and contingency margins need to be accounted. Nevertheless software updates can be performed, sent via uplink and processed by the CDH.

13.6. Safety

Safety critical functions are identified per subsystem. There are many, since LICCA is a pioneer mission and tight constraints needed to be handled, resulting in for example no redundant components. However safety features and mechanisms are incorporated in the entire system to mitigate these safety critical functions. The spacecraft parameters are monitored and reacted to constantly by the CDH. The spacecraft is prevented from becoming space debris by making sure the propellant tank and battery can not explode. Safety for the spacecraft components is disregarded for this mission, since every component failure would be catastrophic. In the perspective of the influence of a malfunction, the spacecraft can be considered safe. The environment and people involved would not suffer from a failure of a component, as is guaranteed by sustainability measures.

14
Sensitivity Analysis of Final Design

To investigate how strong the final design is, a sensitivity analysis is performed. The sensitivity analysis investigates what the influence of uncertainties is on the design. In section 14.1 the uncertainties in the design are identified per subsystem. Their margins are put to a maximum and a minimum, to obtain a best and a worst case scenario. The power, mass and volume budgets for both these scenarios are listed in section 14.2. Section 14.3 discusses what the influences of these adaptations have on the design.

14.1. Uncertainties in the design

In this section, the uncertainties per subsystems are identified. Since mostly COTS components are used for the design, not much uncertainty is involved. However some margins were kept during the design phase, which are set to their highest and lowest value to obtain the best and worst case scenarios.

Payload: The payload is still under development, and therefore prone to uncertainties. The payload consists of three parts: the laser setup, the transponder and the telescope. The laser setup includes margins for electronics: 20% for mass and 10% for power. Since the values for the components are actually known, for the best case scenario, the margins can be set to zero. However, if the final laser setup is more complicated, the electronics could add mass and power. Therefore, upper limit margins are chosen to be 30% for the mass and 20% of the volume. The telescope needs to be designed partly, but the technology is already developed, as described in chapter 3. Therefore a good estimate can be made, for the mass of the body this is 40% and for the pupil 5%. During design, the body can become heavier or lighter, thus a range of 30% to 50% is chosen. The pupil is fairly small and will thus not change much further. However, to investigate the best case and worst case scenarios, the margin was adapted to 2% and 10% respectively. The transponder is a different story. This component needs to be fully designed and not much is known yet. This implies large uncertainties. The margin for electronics is in this case taken very wide, ranging from 10% to 100%. How these adjustments change the budgets can be found in table 14.2.

ADCS: ADCS comprises sensors and actuators which are all COTS components, and therefore not changes much. However, a misalignment of the pointing of the used thrusters should be considered. This will be at maximum 2 degrees, which means more thrust is needed for realigning. This results in more propellant mass, which is calculated, and equal to 4 g. This change is neglected as it is very small. The same holds for the change in volume.

Propulsion: Propulsion includes propellant mass, which is determined by the total ΔV needed for all the manoeuvres. Originally a margin of 10% was added here for uncertainties. Since now the worst and best case conditions are considered, this margin is changed to 0% for best-case condition and 20% for the worst case condition. The result of this is a change in propellant mass, which directly increases or decreases the total mass of the propulsion subsystem. This also implies a change in volume, as mass and volume are directly related. Another uncertainty considered is the margin of the rounded corners in the propellant tank calculation. This margin was originally taken as 10%, but now two extreme cases are considered, namely a margin of 5% and 25%. This again increases or decreases the mass and also the volume. The results of the changes can be found in table 14.2. Considering the power, the worst case scenario occurs when the preheat of the thruster is necessary at the moment the downlink is active, especially if this happens during eclipse, when also the thermal system requires power.

Telemetry, Tracking & Command: For power considerations during the design of the satellite, it is assumed that the daily downlink occurs during daylight and the TT&C system does not require power during eclipse. This is however not guaranteed. It depends on the regulations of the ground system and is considered an uncertainty. Downlink during eclipse has major consequences for the design, as can be found in table 14.2. Other uncertainties regarding the TT&C system are also considered. The exact position of the satellites may already be occupied in GEO. However it is secured that the used ground stations will be in view. Another uncertainty is the noise, but this can be remedied by lowering the bit rate. As mentioned above regarding propulsion, the TT&C system being active during preheat and eclipse largely influences the required power.

CDH: Uncertainties for CDH lie in failure of connections and radiation protection for the I/O board. A connection that fails frequently is I^2C, but this can be avoided by means of testing. The amount of radiation protection needed is more difficult to estimate. Hyperion, the company which produces the I/O board, states that the protection should be enough, implying a best case condition of a mass of 7 g, a power of 0.55 W and a volume of 0.01 U. In the worst case condition, radiation protection is added and another board is used for redundancy. This is explained more in detail in chapter 8. The result can be found in table 14.2.

EPS: The uncertainty for the EPS lies in the efficiencies. What if an efficiency turns out to be higher or lower than expected? In the best case scenario, daylight as well as eclipse efficiencies are both 100%, and no energy is lost. This leads to a total amount of 78 solar cells, as compared to 96 in the nominal case. Reducing the efficiencies to 60% during daytime and 45% during eclipse, which is considered the worst case scenario, implies the need of 129 solar cells. For power storage, extra batteries are needed, and another battery type was deemed more suitable in this case. The chosen battery is the battery pack included in the Modular EPS from ISISpace [1]. Three batteries of this type are needed. This worst case scenario has large consequences on the design, especially for the structure subsystem.

Thermal: Uncertainties in the thermal subsystem come from temperature fluctuations and concentrations, as well as degradation of materials. Therefore, a margin of 10% was assumed for both the upper and the lower limit of the estimated mass and volume, as this means, for example, more or less louvers are needed.

Structure: For the structure subsystem, uncertainties lie in the shielding material, in the material of the hinges, and in the deploy mechanisms for the ADCS thrusters and solar panels. For shielding, a worst case condition implies more shielding is needed, meaning that 1.5 kg of mass must be added. For the deploy mechanisms, a margin of 10% was assumed for both the upper and the lower limit. This only holds for this part of the structure, thus 10% of 1.68 kg. The explanation where this mass come from can be found in chapter 11.

Cabling: Added mass for cabling was found to vary between 10% and 20% of the final mass for comparable CubeSat missions (see section 12.2). Therefore these values were taken as best and worst case scenario. The volume of the cables is negligible compared to the total volume of the spacecraft.

---

[1]https://www.isispace.nl/wp-content/uploads/2019/12/..., accessed on 18/06/2020

14.2. Renewed budget range

All the important parameters that have changed due to the uncertainties are given in table 14.1. More detailed information about each subsystem can be found in table 14.2. Table 14.2 visualises the new adapted budgets for power, mass and volume. They contain both the best and worst case scenario.

Table 14.1: Most important differences between worst and best case conditions

Parameter	Best Case	Worst Case
Power [W]	27.37	46.60
Mass [kg]	19.63	26.84
Volume [U]	10.51	11.63
Battery	Li-Ion ICP-20	ISIS battery pack
# batteries	1	3
# solar cells	78	129
CDH component	Hyperion CP400-85	Space Inventor OBC-P3

Table 14.2: Renewed budgets: minimum and maximum

Subsystem	Minimum Power [W]	Maximum Power [W]	Minimum Mass [kg]	Maximum Mass [kg]	Minimum Volume [U]	Maximum Volume [U]
Payload	4.63	5.61	4.93	6.38	4	4
ADCS	9.9	9.9	2.84	2.84	1.13	1.13
Propulsion	5.99	11.5	4.35	4.97	3.97	4.50
Communication	5.5	5.5	0.528	0.528	0.559	0.559
CDH	0.55	3.3	0.007	0.285	0.01	0.285
EPS	0.8	0.8	1.15	1.41	0.75	1.04
Thermal	0	10	0.390	0.476	0.09	0.11
Structure	0	0	3.65	5.48	0	0
Total	**27.4**	**46.6**	**19.6**	**26.8**	**10.5**	**11.6**

14.3. Influences on subsystems

After the identification of uncertainties for each subsystem, the influence of the renewed budgets on the system should be discussed. The first part describes the worst case conditions, and the second part the best case conditions. In these parts, all the parameters are considered separately from each other, which means, for example, a worst case scenario for mass does not necessarily imply the power is in worst case conditions too. The considered parameters can be found in table 14.1, except for volume, since it is directly related to mass.

14.3.1. Worst case scenario

In the worst case scenario, the influence of maximum power, mass and volume on the design is assessed.

ADCS

If the mass and/or the solar panel size increases, the moment of inertia also increase. This influences the time to perform the slewing manoeuvre. With the maximum mass, this gives a slewing time of 150 s. Due to an increase in mass, also the propellant mass slightly goes up. The momentum also increases, but remaining within its margins. If the solar panels become very large, jitter would come into play. This will increase the noise during measurements and decreases the pointing stability.

Propulsion

The mass is the only important parameter for the propulsion subsystem. An increase in mass results in more propellant mass needed for all manoeuvres. The new propellant mass becomes 4.82 kg, which results in an increase in propellant tank mass as well. The total mass becomes 5.78 kg, which is around 1.3 kg higher than the official propulsion mass budget. The volume increases to 5.22 U, which is an increase of around 1.1 U. This is undesired, as this would increase the total volume above 12 U.

EPS

Power is the main driver for the EPS. If this is increased, the system enlarges. The main influences on the power are what subsystems are active simultaneously. For the worst case scenario this means all subsystems require power at the same time. The maximum power value was found to be 46.6 W. This is a theoretical analysis, since the required power is constrained to 40 W. For completeness, however, the influence on the design of a power of 46.6 W is investigated. For this amount of power, up to 102 solar cells are needed. All subsystems being active during eclipse implies complications for the battery. More energy needs to be stored, and again another battery type should be chosen. The Li-ion CubeSat Battery Pack [2] is the best option for this scenario, and four of these batteries are needed.

Thermal

The most important design parameters concerning the design of the thermal subsystem come from the heat balance. If the power consumption increases, and the subsystems uses power less efficiently, the minimum temperature of the spacecraft reaches 39.4 °C in maximum conditions, which is above the allowed limit. Placement of materials with higher emissivity underneath the louvers decreases this temperature to 31.0 °C. Experimental coatings can be used instead of aluminized kapton foil. A material with an absorptivity of 0.03 would reduce the minimum temperature to 10.9 °C, which is acceptable.

If the size of the solar panels changes, the hinges may need to be redesigned to prevent overheating or undercooling of the solar panels. In the case of an eclipse, larger solar panels emit more heat, thus more powerful heat sources are required. When not eclipsed, the solar panels may generate more heat, which may mean better heat sinks are required.

Structure

In the maximum mass case, the structure is not certified to be able to withstand the loads and vibrations. Simulations and tests would be needed to verify the structural integrity of the design. If the structure is deemed too weak to handle 26.8 kg, a redesign may be required. If the wall thickness is increased, the structure may withstand higher loads without requiring a redesign of the configuration.

If the EPS requires larger solar panels, which must support a total of 129 cells, the solar panels need to be redesigned. The dimensions of the solar panels must be increased, which cannot be done without a fundamentally different solar panel design. Options to consider are folding solar panels; only one of the two solar panels per side would need to be able to fold, and the new design could support up to 144 solar cells.

14.3.2. Best case scenario

In the best case scenario the budgets are set to their minimum. This has a positive influence on the design, which is identified per subsystem below.

ADCS

In the best case scenario for the ADCS, the opposite happens than in the worst case scenario. A mass decrease causes a moment of inertia decrease and a propellant decrease. The slewing time then equals 115 s.

Propulsion

Again the mass is the only important parameter for propulsion looking at the best case. Using this mass, it was calculated that the propellant mass becomes 2.98 kg. This decreases the propellant tank as well. The total mass then becomes 3.95 kg, which is 0.55 kg less than the official budget. The volume decreases as well, the new volume becomes 3.62 U, which is about 0.5 U smaller than the budget.

EPS

Reduced power leads to smaller EPS components. Given a power of 27.4 W, only 87 solar cells are needed. The power to store during eclipse also decreases, this means the battery gains more contingency margin.

Thermal

If the EPS has an efficiency of 1, the controllable temperature range increases. Any temperature between -16.5 °C and 60.0 °C can be maintained. The reduced solar panel size reduces the power required to heat the spacecraft during eclipses to 7.8 W.

Structure

The structure could be lighter, as the mass reduction implies it has to withstand less loads. However, this requires re-certification of the COTS structure option, and may thus not be considered worth the effort.

The solar panels could reduce in size, as only 78 solar cells need to be deployed. Without a fundamental redesign of the solar panels, this means three of the six solar panels may be reduced in size, to 16x20 cm². The smaller size means they are less susceptible to vibrations, thus their thickness may also be reduced, to reduce mass. This means the HRM and deployment mechanisms need to withstand lower loads, thus their mass may decrease.

---

[2] https://satsearch.co/products/imt-srl-cubesat-battery-pack, accessed on 18/06/2020

14.3.3. Concluding remarks

As a consequence of adaptions needed to cope with the worst case scenario, which are described in section 14.3, the volume of the satellite would become more than 12 U. This is undesired and should therefore be avoided. Another consequence is that even more solar cells and batteries are needed, which results in too fragile solar panels, which is undesired as well. The ADCS gets more problems with manoeuvring of the satellite. The thermal subsystem requires more power to heat during eclipses, and may require heat sinks.

The functioning of the worst case scenario is highly unlikely, and therefore in a later design stage the uncertainties should be decreased in order to see whether the design is feasible or not. It should be noted however that this worst case scenario is also not likely to happen, which implies the design is assumed to be feasible for now until the contrary is proven.

As a consequence of the best case scenario, the volume, mass and power decrease, which results in more design freedom. Furthermore, the solar cells and number of batteries decrease, which is an advantage for the structure and thermal subsystem. Solar panels can be made smaller, which results in a more rigid design and the deployment mechanism carries less loads. Less solar panels and batteries also means less heat generation and therefore less louvers and thermal control is needed. In this scenario more components can be added for redundancy, or even more precise and/or reliable components can be considered.

As can be seen from the final design, the original budgets are on the lower side of the new budget range, which implies the design is fairly strong. The probability of the design to tend towards the worst case scenario during further development is small.

15

Verification & Validation Procedures

In this chapter the verification and validation procedures are presented. The procedures are divided into software testing, presented in section 15.1, where all the design tools used in the process are verified and validated, and product testing, presented in section 15.2, where a plan on the verification and validation of the satellites is laid out.

15.1. Software testing

Software testing is an extremely important process for design. Its purpose is to determine if a tool is suitable to be employed in the design process. Software testing comprises verification and validation. Software verification is the process where it is determined whether the software performs as intended [57]. It is carried out on every software used in the design and the standard approach is to divide the code in units. The inputs and outputs of these units are then tested. The next step is to test the complete systems, here all inputs are taken into account and the collaboration between units is checked. In certain occasions where a code is composed by one unit, a system test is not required as it would just be a redundant unit test.

Software validation is the process where the accuracy of a predictive model is assessed based on the comparison of a prediction to experimental results [57]. This process can be realised in three different methods according to the availability of the experimental data. The first and most optimal method is using physical inputs in the model and comparing the output of the model to an actual physical output. This is, however, limited by the availability of these inputs and output. The second method is to compare the output of the model with experimental data with conditions that are as similar as possible to the model. For example, comparing the modelled disturbances for a 12U CubeSat to a 6U CubeSat in the same orbit. This method has plenty of limitations as the objective and requirements of the missions can differ. The third method is comparing the model to a more detailed model. For example, comparing an analytical model of the stress distribution in a structure to a finite element analysis of the same structure. This method in some cases is not considered validation as the comparison is not with experimental data. For the scope of this project this is considered a valid method, as the design is still in the research and development stage. Although, the limitations of the validation model must be stated.

15.1.1. Solar Illumination Model

This code computes the position of the Sun relative to Earth and relative to a satellite in GEO. From this is was calculated when the satellite was in eclipse and which sides were illuminated and at which angle of incidence. This tool was used in order to ultimately compute the torque disturbances due to the Sun's radiation and size the solar arrays.

Verification

Unit 1 - Calculate orbital parameters: The orbital period formula is verified by checking the outcome of the code. When using the Sun's gravitational parameter and the distance to Earth, the period is 365 days. In addition, the formula for the periapsis is verified using again the same values of Earth's orbit the outcome should be $1.47 \cdot 10^8$ km.

Unit 2 - Position of Earth relative to the Sun: To verify that the outcome of the Sun's relative position to the one of Earth is correct, nine points were obtained for an interval of four years. This way each point represents the Sun's position every half period. The outcome is shown in figure 15.1, which gives a predictable result: the position of the Sun oscillates between the perihelion and aphelion every half period. Furthermore, the reason why after one orbital period the point "Year 1" differs from "Year 0" in the x-y plane by about $\frac{\pi}{2}$ has to do with the fact that leap-years exist. As the division between the total orbital period of the Earth around the Sun is 365.265 days, there will be an offset of the Earth position of about $\frac{\pi}{2}$ $[rad]$ in the x-y plane with respect to its initial place, because this period is 0.265 days longer than 365 days year. Therefore, in order to have a better estimation of the Earth position with respect to the Sun, there is a leap-year every four years in the calendar that accounts for this offset.
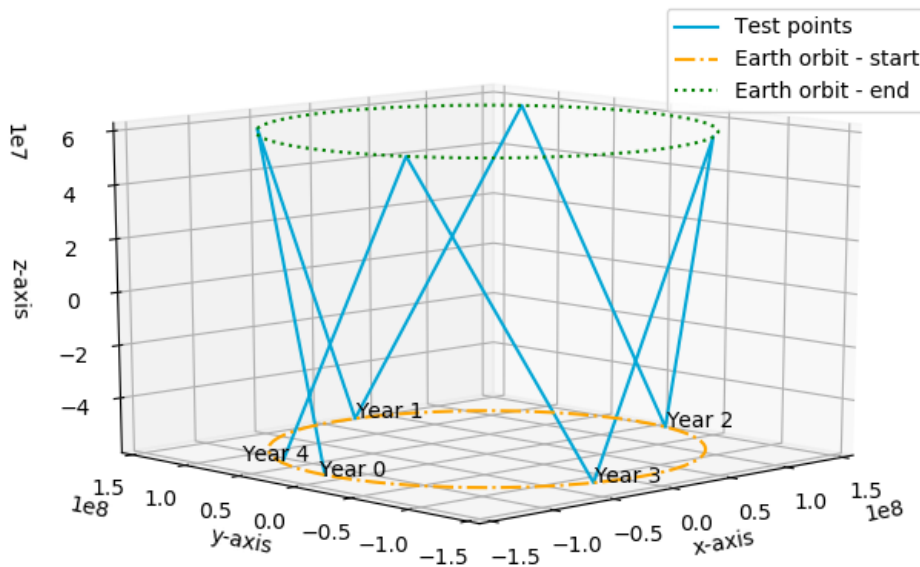
Figure 15.1: Verification of Sun position relative to Earth every half year

Unit 3 - Illuminated area: To test if this unit works, an extreme case is checked. If the satellite faces the Sun directly without inclination, only one face should be illuminated and the total illuminated area should be equal to that face. This is done by setting the incidence angles between the Sun and the satellite to 0 °. The results in fact matched to 0.06 m^2, not including solar panels.

System: To test the system works together without any major issue the inputs are varied to test nominal and edge cases and see if the outcome is as predicted. These tests are shown in table 15.1 and the output is the torque.

Table 15.1: Testing different cases in the solar illumination model

Test	Expected Maximum Torque [Nm]	Actual Maximum Torque [Nm]
J = 0	0	0
c = 0	Inf	Inf
d = 0 (Sun Earth Distance)	Inf	Inf

Validation

To validate this model the satellite illumination simulation of SPENVIS was used. SPENVIS can model the variation in solar radiation for one face of a satellite in GEO orbit, shown in figure 15.2. The periods of the two models are compared and they result to be exactly the same, proving that the correct modeling was done for the faces of the satellites. Moreover, the maximum of this graph is 1290 W/m^2 only 5% off the value used in the developed model, as shown in table 15.2. Therefore, the results can be expected to be accurate if the

system and units work. It is important to note that this validation method can only be use during this stage of the design to check if the output values are in the right order of magnitude. The satellite illumination model on SPENVIS has been validated by the Royal Belgian Institute for Space Aeronomy and this is the most accurate model available for the DSE. However, SPENVIS still has limitations. For example, the solar flux can not be varied and the moon is not taken into account. For further design stages the solar illumination model will need to be validated against some experimental data for small or nano- satellites in GEO.

Table 15.2: Comparing SPENVIS to the Solar illumination model

Parameter	*SPENVIS*	*Solar irradiation model*	*Deviation*
Period [hr]	12	12	0%
Maximum Power [W/m^2]	1290	1367	5.6%
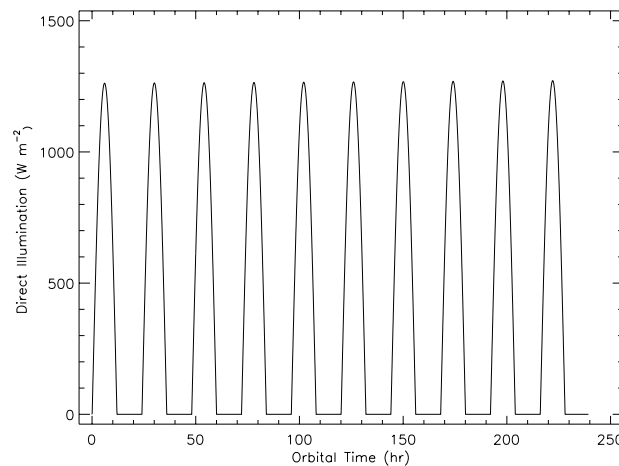
Figure 15.2: SPENVIS Simulation of Solar illumination [1]

15.1.2. Manoeuvres model

This script calculates the required ΔV needed for every manoeuvre that is considered. First of all the orbital parameters are determined, after which the ΔV for every manoeuvre is calculated using only two different functions.

Verification

Unit 1 - Calculate ΔV for a Hohmann transfer: The required ΔV for a Hohmann transfer is calculated using orbital parameters, a departure altitude and a target altitude. Two edge cases are considered, one is what happens when these altitudes are equal and what happens when there is a major difference between these altitudes. Equal altitudes implies zero ΔV. A major difference in altitude implies a lot of ΔV, however it should be noted that this does not always hold. The ΔV gradually increases with altitude to a certain peak point, after which it decreases again and it converges to the escape velocity. This means with a lot of difference in altitude, the ΔV becomes more or less equal to the ΔV required for an escape, which is 3.27 km/s, assuming an initial altitude of 0 (Earth's surface) [70].

Unit 2 - Calculate ΔV for a phase shift: The required ΔV for a phase shift is calculated using orbit parameters, the amount of shift you would like to end up with and the number of orbits taken for the transfer. Again two edge cases are considered. One taking zero shift, the other one taking 1000 days for transfer. Zero shift implies zero ΔV and 1000 days for transfer would mean that per transfer not much ΔV is needed and thus is expected to be close to zero.

Regarding the trustworthiness of the values, the outputs are compared with the AE1222-II course reader [74] and this way the numbers are verified. Orbit maintenance was already taken from this reader and therefore already verified. The tests are summarised in table 15.3.

---

[1]https://www.spenvis.oma.be/, accessed 17/06/2020

Table 15.3: Manoeuvres model tests

Test	Output[km/s]	Expected Output[km/s]
Hohmann		
$r_{dep} = r_{tar}$	0	0
$r_{tar} \gg r_{dep}, r_{dep} = 0$	3.27	3.27
Phase shift		
phase = 0	0	0
1000 transfer days	$6.83 \cdot 10^{-4}$	Close to 0

System test: This script comprises of two main units thus to fully verify the systems a manoeuvre which does both a Hoffman transfer and a phase shift is selected to be tested: the circulation manoeuvre. To test this manoeuvre an inversely proportional relationship between the two units was found, as the maximum drift is a constant value. Working on the assumption that the spacecraft will have maximum drift, the higher the loss in altitude, the lower is the phase shift. This relationship can be seen in figure 15.3, and proves the correct integration of the units.
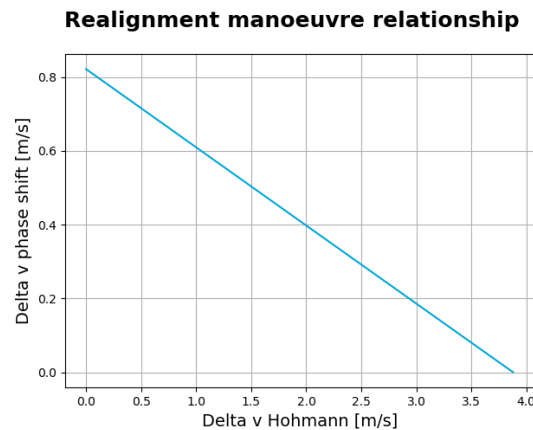
Figure 15.3: Relationship between the Hoffman transfer and the phase shift

Validation
The ΔV for every function needs to be validated. For Hohmann, the formula is validated with the AE1222-II course reader [74] using an initial orbit of 200 km (LEO) and a final orbit of 35786.136 km (GEO). The result of the model is 3.93 km/s, compared with 3.95 km/s from the reader and as this lies within the 5% margin, this is accepted.

For the phase shift, a more precise way of calculation (the validated model) is used and compared to the output from the made model. The inputs used are a phase shift of $-\frac{2}{3}\pi$, a transfer time of seven orbits (seven days) and some orbital parameters. The 'validation model' outputs a ΔV of 102.47 m/s [19]. The model for calculation outputs 101.6 m/s, which lies within the 5% margin and thus is accepted to be correct.

15.1.3. Propulsion model
This script calculates the propellant mass and volume needed when considering chemical propulsion. Besides that, it calculates the time it would take when using electric propulsion to proof that that is not an option.

Verification
Unit 1 - Transfer time: This unit determines the time it takes for several electric propulsion options going from a circular orbit to another circular orbit. Inputs are mass, thrust, specific impulse, initial and final altitude. The considered cases are: equal initial and final altitude, zero specific impulse and a super high thrust ($10^{90}N$) which should all result in a transfer time of 0. The last check is a huge difference between initial and final altitude, which results in a fixed number ($m \cdot g_0 \cdot \frac{I_{sp}}{T}$).

Unit 2 - Rocket equation: This unit calculates the propellant mass knowing the required ΔV, the initial mass and the specific impulse. The following test cases are considered: zero initial mass and zero ΔV, which should both result in a propellant mass of 0. The last test case is a high ΔV. A high ΔV (30000 m/s or higher) should result in a propellant mass close to the initial mass.

Unit 3 - Calculate propellant tank dimensions: This unit calculates the dimensions of the propellant tank using a certain thruster (EPSS 1C). Input is propellant volume, which basically determines the structure. Two test cases are considered, when the propellant volume is zero and when propellant volume is large. Propellant volume of zero means a tank mass of zero, and a really large propellant volume means a large mass for the propellant tank is needed.

Trustworthiness of numbers here is verified with literature [74]. This also immediately tests 'normal cases', therefore as can be seen before only edge cases are considered as test cases. The tests are summarized in table 15.4.

Table 15.4: Propulsion model tests

Test	Output	Expected Output
Transfer time [s]		
$r_{dep} = r_{tar}$	0	0
$I_{sp} = 0$	0	0
$T = 10^{90} \ N$	0	0
$r_{tar} >> r_{dep}, m = 10 \ kg$		
$I_{sp} = 100 \ s, T = 0.981 \ N$	1.00	1.00
Rocket equation[kg]		
$m_i = 0$	0	0
$\Delta V = 0$	0	0
$\Delta V = 30000 \ m/s, m_i = 20 \ kg$	20	20
Propellant tank[m^3]		
$V_{prop} = 0$	0	0
$V_{prop} = 10^{99}$	inf	inf

System test: This script calculates impulsive, chemical propulsion, and non-impulsive manoeuvres, electrical propulsion. The non-impulsive manoeuvres only used the first unit, transfer time, while the impulsive part uses both rocket equation and propellant tank dimensions. Thus, only the second manoeuvre needs to be tested, as the time transfer has already been tested in the unit tests. To test this input value for the specific impulse will be change first to 3000s and then to 10. The calculation were then done by hand with these same inputs, always keeping 2 decimal place and the code was modified to keep 2 decimal places after every computation, the result was exactly the same as expected, presented in table 15.5.

Table 15.5: Testing the system by hand

Test	Output Code $[\mathbf{mm^2}]$	Output by hand $[\mathbf{mm^2}]$
$I_{sp} = 3000s$	166.89	166.89
$I_{sp} = 10s$	12771.42	12771.42

Validation

The transfer time formula is validated using an example [19]. Inputs are m = 1000 kg, I_{sp} = 10000 s,T = $2.5 \cdot 10^{-3}$ kN, r_{tar} = 42164 km, r_{dep} = 6671 km. Result is 21.03 days, which is exactly the same result as the model explained in chapter 6 and therefore validated.

The rocket equation is validated using the ADSEE 1 reader [74]. Using an initial mass of 1000 kg, a ΔV of 2000 m/s and a specific impulse of 305.81 s result in a propellant mass of 487 kg. The code, using the same inputs, produces a mass of 487 kg, which is exactly the same and thus validated.

Propellant tank calculations have been validated by a different way of calculation of the tank volume. The volume of the thin-walled cuboid is calculated with the following formula:

$$V_{tank} = V_{outer} - V_{inner} = (l + t) \cdot (b + t) \cdot (h + t) - (l - t) \cdot (b - t) \cdot (h - t) \tag{15.1}$$

where l, b and h are dimensions of the cuboid and t the thickness. It is just the volume of a cuboid subtracted from another volume. Inputs used are l = 1 m, b = 2 m, h = 3 m and t = 0.001 m. The result is $0.0220m^3$, compared with $0.0227m^3$ found by the model described in chapter 6. This lies within the margin of 5% and is therefore validated to be correct.

15.1.4. EPS model

This model calculates all the required power, the total solar panel area needed, the mass and volume of the solar panels and the energy needed for eclipse.

Verification

Unit 1 - Power required and energy needed for eclipse: This function calculates the total power required by the EPS system based on the power consumption of other subsystems, efficiencies and some orbital parameters. 2 test cases are defined, one is a day efficiency of 0%, which should result in infinite power. The other one is a required power in eclipse and day of 0 W, which should result in a required power of 0 W. Orbital parameters have already been verified before and are therefore not considered in these tests.

The energy needed for eclipse has the same input parameters, except for the DOD of the battery. This value is just taken from the chosen battery and other parameters have been verified before, therefore no tests are needed for this calculation.

Unit 2 - Solar panel dimension calculation: This function calculates solar panel dimensions based on the total required power and the parameters of the chosen solar cell. Other input parameters are solar flux, incidence angle and lifetime. Considered test cases are:

- Baseline test case with an incidence angle of 23.5 degrees, the input parameters of the chosen solar cell, a solar flux of $1310 \ w/m^2$ and a lifetime of 2 years.
- Change incidence angle to 0 degrees, result should be that less solar cells are needed and thus less volume and mass.
- Change incidence angle to 90 degrees, the result should be an infinite number of solar cells.
- Change in lifetime to infinite years. The output should be an infinite number of solar cells.
- Change in solar flux to 0. The output should be an infinite number of solar cells.
- Change in required power to 0. The output should be 0 solar cells.

Table 15.6: EPS model tests

Test	Output	Expected Output
Power required and eclipse energy[W]		
$\eta_d = 0$	inf	inf
$P_d = 0 \ and \ P_e = 0$	0	0
Solar panels[# of panels]		
$Baseline$	31	31
$\theta = 0$	29	27-31
$\theta = 90$	inf	inf
$\phi = 0$	inf	inf
$P_{req} = 0$	0	0

The model has been verified using literature [74] to see if the right inputs result in the right outputs. The above described unit tests are made to see how it acts when edge cases occur.

System test: For this model the only input that is passed on from unit 1 to unit 2 is the required power(P_{req}) which already has been tested in the unit test. Thus the relationship between the unit has already been proven and a system test is not required.

Validation

Validation of required power energy needed for eclipse is done using the ADSEE 1 reader [74]. An example is used with the following inputs: p_d = 450 W, p_e = 450 W, η_d = 0.8, η_e = 0.6, T = 6.7 h and T_e = 1.25 h. From this follows a required power of 734.5 W, which is exactly the same for the model used in chapter 9 and therefore validated to be correct. The found efficiencies for day and eclipse in the model used in chapter 9 were 0.81 and 0.61, respectively. The reader assumes these values as 0.8 and 0.6. The difference is really small and in this way the values taken by the model are validated.

The solar panel dimension calculation method is validated using a tool [2] which states an area of $0.09m^2$ should deliver 15 W. For a power of 15 W in the used model with an efficiency of 15.8% and a lifetime of 10 years, the required area becomes 0.0846 m^2. It could be that some area is added to connect the solar cells in the validated model, which is not included in the used model. Since the outputs lie relatively close to each other it is validated to be correct.

---

[2]https://www.solar-estimate.org/solar-panels-101/how-many-square-feet-of..., accessed 22/06/2020

15.1.5. ADCS model

This model is a spreadsheet that computes all the torque required by different maneuvers and creates a momentum budget to be are to choose the reaction wheels.

Verification

Unit 1 - Torques by thrusters: The verification procedure starts by setting the two thrusters along the x-axis in the two opposite walls of the CubeSat facing the exterior. Then, if each thruster applies a thrust of 1 N on each nozzle, the outcome can be calculated by hand. First, there will not be a torque in the x-axis, which is the case in the spreadsheet too. Then, the values of the torques around the y and z axis in absolute value can be calculated by using $T_{y,z} = \sin{(45°)} \cdot d_x$, where $T_{y,z}$ is the torque around y and z axes and d_x is the distance to the origin in the x-axis. This formula gives indeed the same result as the spreadsheet. In order to verify that the signs are correctly applied, it is recommended to evaluate the values using the right-hand rule. For this case this was the procedure done and it gave correct results.

Unit 2 - Momentum Budget: To verify this unit the time and moment of inertia where set to zero and, as can be seen the results matched what was expected. This is shown in table 15.7.

Table 15.7: Testing the system by hand

Test	Output Code [Nms]	Output Expected [Nms]
$t = 0$	Inf	Inf
$I = 0$	Inf	Inf

System test: In this model units are developed independently from each other and then they all come together in the momentum budget. Testing the inputs of this part can therefore be considered system testing.

Validation

Validating this model proved to be of extreme difficulty due to the lack of information available. This means that the ADCS will need to be thoroughly tested throughout the design process. Table 15.8 presents the maximum torque and angular storage of the Delfi-n3Xt mission, a 3U CubeSat orbiting in LEO. The comparison between this satellite and the LICCA mission can be regarded as useful to check the order of magnitude of the parameters, but this cannot be considered a full validation of the design tool and in further advancements of this project more accurate validation and testing is required. The LICCA project values for torque and angular storage momentum are as expected much higher than the Delfi-n3Xt, and the order of magnitude is similar, but this comparison has too many limitations to be considered valid enough, the difference in size, the difference in the mission objective, the orbit, and the stability requirements.[26]

Table 15.8: Comparing ADCS parameters

Mission	Maximum Torque [mNm]	Angular storage momentum [Nms]
Delfi-n3Xt	0.09	1.5E-3
LICCA	7	0.1

15.1.6. Thermal model

The thermal model calculates the heat generated by every subsystems, as well as the flux due to the Earth and the Sun and computes a heat balance for the satellite

Verification

Unit 1 - Heat Balance: To test this unit and effective way is to change the impact of different components of the heat balance and check the responses of the temperature. The test goes as follows: firstly, the impact of the Sun is taken out, this should results the heat balance to be comprise only of Earth flux and Heat generated, dropping drastically the temperature, then the heat generation of the subsystems, this should also drop drastically the temperature, and finally the Earth flux, which should have a negligible effect, results are shown in 15.9. This kind of sensitivity analysis shows that the unit works and responds as predicted to different inputs.

System test: This script only comprises of one single unit, thus, by testing that unit the system is tested.

Table 15.9: Testing the sensitivity of the systems

Test	Average Value[T]	Deviation from original value[%]
No Sun	2.08	-96
No Earth Flux	54.29	0
No Heat Generation	-6.53	-112

Validation

The thermal component is an extremely important part of the LICCA mission as this is one of the first times that a CubeSat orbits in GEO. This means that the literature for heat balance is very limited, for this reason only the heat generation is used to validate this model, but thorough thermal test will be carried out on the satellites as mentioned in section 15.2. The internal heat generation is compared with the MinXSS-1, a 3U CubeSat orbiting in LEO.[52] The heat load for this CubeSat is lower than the LICCA project as this satellite is much smaller and requires much less power, 19 W maximum power. This values leads to a ratio of 47.5% between the maximum powers. As noticeable in table 15.10 , the ratio between the heat generation is higher that 47.5%, this was expected as the MinXSS-1 is an older and less efficient satellite.

Table 15.10: Heat generation variation between CubeSats

Parameter	LICCA	MinXSS-1	Ratio
Min Heat Generation[W]	3.45	1.67	48.4%
Max Heat Generation[W]	5.10	3.31	64.9%

15.1.7. Solar array temperature simulation

This model predicts the temperature drop of the solar array during eclipse.

Verification

Unit 1 - High heat flow: If the hinges of the solar panels allow a lot of heat to flow, the temperature of the solar panels and spacecraft body should remain equal. The heat flow contant was set to $k = 10$, and indeed the temperatures remained equal ($\epsilon_{\Delta T}$ < 1-E5).

System test: To test this system a comparison with an example is done. A two-body isolated system with heat flow example has been found from the University of British Columbia[3]. As this example does not account for heat emission, the emissivity in the simulation has been reduced to 0. The results were compared, and found to be equal (ϵ_T < 1E-3).

Validation

To validate this simulation the rate at which the temperature of the solar array drops in eclipse is compared with the Nimbus 2 mission of NASA. This mission orbits in LEO causing limitations to this comparison, but, the Sun is still has the mayor influence on the temperature. The results, presented in table 15.11 show a deviation of 8.2% an acceptable number comparing the possible uncertainties and difference between the mission, like the the flux of Earth, the heat cause by atmospheric drag in LEO. To calculate the rate it was assumed that the solar arrays started at maximum temperature in both cases[9].

Table 15.11: Temperature dropping rates in eclipse

	LICCA	Nimbus 2	Deviation
Temperature drop [°C/min]	-2.43	-2.63	8.2%

15.1.8. CDH model

This model computes the clock speed, together with the storage of the satellite.

Verification

Unit 1 - Clock Speed Calculations: To verify the CDH model, similar calculations were found in Space Mission Analysis and Design[72]. The inputs were entered into the CDH model, and it was verified that the outputs are identical.

System test: This model comprises of one unit therefore a system test is not required.

---

[3]https://www.phas.ubc.ca/~kiefl/ch15_part2.pdf

Validation

Validation of the CDH model is carried out by using the Space Mission Engineering Development resource.[72] The authors provide the lines of code needed for to operate the FireSat II and the clock speed needed for there lines of code. If the CDH model is applied with the FireSat II inputs, it can be noticed that the clock speed is faster than the minimum clock speed calculated, the large discrepancies is due to the implementation of safety margins, which are not implemented in this calculation of the CDH model. According to the ESA for data rate should be at least 50%, so the real deviation is 2% [67]. The results are shown in table 15.12.

Table 15.12: Clock Speed of FireSat II

	CDH Model	FireSat II	Deviation
Clock Speed[Hz]	7.70E+06	1.170E+07	52%

15.1.9. Radiation model

The SPENVIS tool was used to model the radiation at GEO, this is an engineering tool developed by ESA. [4]

Verification

This tool, begin developed by the ESA, has already been verified at both a unit and system level, therefore it is safe to say that the model work correctly and no verification is required. Although, it is important to verify the way it has been used by the team, for example If the inputs are correct and if the correct model has been used. To verify the data retrieved from SPENVIS a literature study was done into normal values for TID in GEO orbit. Missions in GEO to measure the total radiation dose experienced were done by a couple of satellites, named CRES, METEOSAT-3, GSAT-2, and KITSAT-1 [60]. GSAT-2 used five dosimeters, all protected by varying level of thicknesses of aluminum. One dosimeter was placed at the center of the satellite to measure the radiation at the core of the spacecraft. It was found that the dosimeters experienced from 42 130 rads/year to 376 rads/year [60]. Taking a normal skin thickness into account set on around 2-3 millimeters for CubeSats would yield around a dose of 5 000 rads/years for the inside of the CubeSat during solar maximum. This is very compliant with the data retrieved from SPENVIS running a similar simulation. Therefore, the data retrieved from SPENVIS was assumed to be verified as it has been proven that the team uses the model correctly.

Validation

The validation process for a tool like SPENVIS is a challenge. This tool uses IRENE radiation environment model that specifies the natural trapped radiation environment, the fluctuations of radiations around Earth cannot be modelled analytically, but using stochastic modelling. This implies that there is no way of getting an exact answer from a input but rather a probabilistic answer. Thus, to the only methods to validate this model are by actually flying the modelled orbit and detecting the naturally trapped radiation or performing very precise experiments in a particle collider. As this tool is employed by ESA and other European national space Agencies it is safe to assume that the results will be accurate enough for this phase of the project.

15.1.10. Communication model

This model calculates the link between the ground stations and the spacecrafts, in order to check whether the signals sent are powerful enough to be detected and received.

Verification

Unit 1 - Conversion from linear SI units to dB: In order to check whether the conversion from Si unit to decibels was performed correctly, a unit test was performed. The equations below show how to calculate the signal to noise ratio both in SI units and in dB.

$$SNR = \frac{E_b}{k \cdot T_s} = \frac{P \cdot L_l \cdot G_t \cdot L_a \cdot G_r \cdot L_s \cdot L_{pr} \cdot L_r}{R \cdot k \cdot T_s} \tag{15.2}$$

$$SNR[\text{dB}] = P + L_l + G_t + L_a + G_r + L_s + L_{pr} - 10\log_{10}k - 10\log_{10}R - 10\log_{10}T_s \tag{15.3}$$

To be able to perform the latter, all the variables have to be converted to dB. To check whether this was made correctly, the signal to noise ratio value in dB calculated with equation (15.3) was converted to linear SI units by using the relation $[SI] = 10^{\frac{[dB]}{10}}$. An example of the difference between the two results obtained can be seen in table 15.13. As the SNR calculated in this way and the one obtained from equation (15.2) are the same, the conversion can be considered correct and verified.

---

[4]https://www.spenvis.oma.be/, accessed 17/06/2020

Table 15.13: SI to dB conversion verification

Value obtained with equation	Value obtained with conversion	Difference
3524.644872	3524.644872	3.354E-13 %

Unit 2 - Correct implementation of equation: As the link budget relies on only one equation, verifying this last one is sufficient to verify the model. In order to do that, '0's have been plugged in for each variable. When plugging in '0's on the nominator of the equation, the SNR became 0, while when plugging in '0's in the denominator, Excel gave the #DIV/0! error.

Validation
In order to validate the result obtained by the communication model, two checks were performed.

EIRP: The first one consisted in comparing the EIRP value for the uplink obtained from the model with the ones found in the CCSDS document on ground station, [18]. This was done fore each of the ESA ground stations selected. As the two values coincide, the EIRP calculation of the model has been validated.

Link: In order to validate the whole model, the values of the variables taken from the Delfi-n3xt mission, [69], were plugged in. The final result of signal-to-noise ratio coincided, and hence the model can be considered validated.

15.1.11. Coverage area model
This model is used to plot the positions of the ground stations as well as the satellites. The coverage area of the satellite that is suitable for radio communication is approximated to span 70 degrees in each direction from the subsatellite point, which is taken at the equator since the satellites are in GEO. In the plot produced by this model, the coverage area is approximated as 70×70 degrees. It should be noted that one should be cautious of ground stations in the corners of these approximated coverage areas. With this plot, a visual check can be done to see if the ground stations will be within the coverage area of the satellites.

Verification
Unit 1 - Conversion of geographic coordinates to decimal degrees: This function takes the elements of a geographic coordinate as input, namely the degrees, minutes, and seconds. A value in decimal degrees is given as the output. The following tests have been performed to test this function. The edge case of filling in zeros was tested to see if it would indeed produce zero as an output. Furthermore, 60 arcmin is equal to one degree, and the same counts for 3600 arcsec. Both of these were tested as inputs to check if one would be the output. The results are summarised in table 15.14.

Unit 2 - Calculation of distance from satellite to ground station: This function calculates the distance from the satellites to the ground station. Since the coordinates of the ground stations have already been converted in this model, it was chosen to use these values to calculate the distance. The inputs for this calculation are thus the longitudinal and latitudinal coordinates both the satellite and ground station, along with the Earth radius R_e and the orbital height h. The output is the distance between satellite and ground station. The following tests have been performed. First, the longitudinal and latitudinal coordinates of both the satellite and the ground station have been filled in to be equal at zero for both, and the orbital height is set to zero. This would indicate that the satellite is at the exact same position as the ground station, and therefore the calculated distance should be zero. Second, the coordinates for the ground station are both set to zero, and the same goes for the coordinates of the satellite. The orbital height is set to that of GEO, namely 35 786 km. This should also the result of the distance calculation, since in this scenario the satellite is exactly over the ground station. The results of the tests are shown in table 15.14.

Table 15.14: Coverage area model tests

Test	Output	Expected Output
Geographic coordinate conversion[°]		
$D = 0, \ M = 0, \ \ S = 0$	0	0
$D = 0, \ M = 60, \ S = 0$	1	1
$D = 0, \ M = 0, \ \ S = 3600$	1	1
Distance between satellite & ground station[km]		
$LONG_{SAT} = 0, \ LAT_{SAT} = 0, \ LONG_{GS} = 0, \ LAT_{GS} = 0, \ h = 0$	0	0
$LONG_{SAT} = 0, \ LAT_{SAT} = 0, \ LONG_{GS} = 0, \ LAT_{GS} = 0, \ h = 35786$	35786	35786

System test: This model comprises of two units, but the first is a simple conversions, therefore performing a system test would consist in checking again the second unit, which would be redundant. For this reason a system test is not considered necessary.

In order to validate this model the satbeams database was employed. This website states the location of most of the commercial satellites along with the correspondent coverage. For the coverage area model the position of the satellites as well as the position of the ground stations. Figure 15.4 show that the Echostar 10 at 110°West can see the Kourou groud station, the E Echostar 21 at 10°East can see the Villafranca station and the Chinasat 6C at 130°East can see the Dongara ground station. All the mentioned satellites are in GEO.
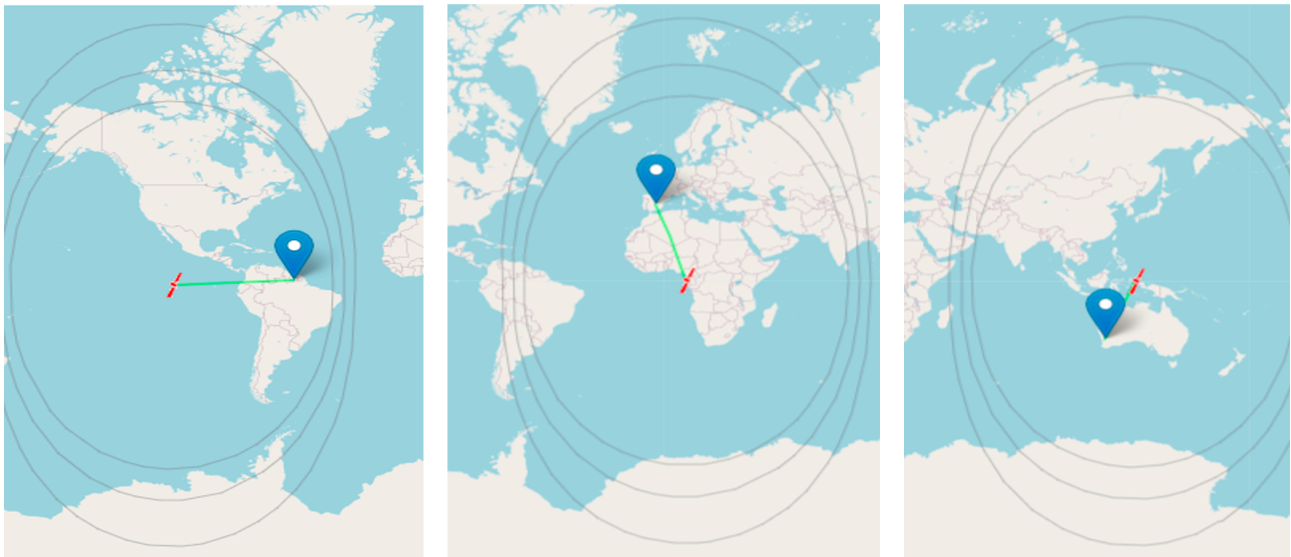
Figure 15.4: Coverage area of varius satellites. On the left the Echostar 10, in the center the E Echostar 21 and on the right the Chinasat 6C

15.2. Product testing
This section presents the testing of the LICCA satellites divided into product verification and product validation.

15.2.1. Product verification
Product Verification is defined as the proof of compliance with design solution specifications and descriptive documents. In order to achieve this objective, a methodical approach is crucial. The following steps will ensure a successful product verification: start with a validated set of requirements, models, personnel and other resources [48]. Then develop a project philosophy, which will be used to list the verification requirements. The former list will be used to define more detailed test plans, including the facilities and models that will be used. For the purpose of this report only the driving requirements will be analysed and tested, in later stages of project development this approach will need to be applied to all the requirements.

The choice of a test philosophy plays an important role in CubeSat projects as it significantly affects the cost, risk and scheduling of the mission. The LICCA mission satellites are primarily assembled with COTS components, many of them with flight heritage. This may lead to the choice of using a protoflight philosophy, cheap and risky. On the other hand, it is very important to keep in mind that this mission will orbit in GEO, making the flight heritage of the components almost obsolete, as most CubeSats orbit in LEO[16]. For this reason, a traditional prototype philosophy will be used for the purpose of verification. This choice implies the development, and validation, of a qualification model, a dedicated model which shall be flight representative in terms of design, materials and tooling. This model will be subjected to all the qualification tests, at levels which are beyond what is expected. In addition, the flight model itself, model to be launched, will be used for all the acceptance tests.

The next stage of product verification is creating a verification requirement matrix, shown in table 15.15. This table describes, for every driving requirement, a method of checking whether the system meets that requirement and on which unit the requirement will be tested, namely parts, Qualification Model (QM) or Flight Model (FM). There are four verification methods: inspection, inspecting the product itself to check if the requirement is met, analysis, using a mathematical model, demonstration, carrying out the actual operation, or test, test the product under operational conditions [48].

Table 15.15: Verification Matrix

ID	Source Requirement	Verification Rationale	Units
LICCA-SYS-Perf-01	The system shall be able to detect gravitational waves in the 1-10 Hz band.	Analysis, it can be checked with an analysis if the gravitational waves detected by LICCA are in the 1-10 Hz frequency band. Models can be made to analyse the events that correspond to the wave and if these events produce a gravitational wave in the specified frequency band.	FM
LICCA-SYS-Perf-09	The constellation of satellites shall be flying with a distance of 72 000 km from each other.	Analysis, for the satellites to be 72 000 km apart from each other, an analysis can be made to predict the launch and the injection in the target orbit. This way the necessary manoeuvres can be determined and the final distance between the satellites as well.	FM
LICCA-ST-Perf-01	The spacecraft shall carry a low power laser payload for interferometry.	Inspection and test, the fact whether the spacecraft carries a low power laser can be checked by inspection. However, it can also be tested by turning on the payload and check the amount of Watts that the laser delivers is lower than 0.1 W.	Parts, FM
LICCA-SYS-Bud-01	The spacecraft shall be compliant with the CubeSat form factor i.e. it should be made up of multiple cubic units each of 10 cm x 10 cm x 10 cm.	Inspection, to see if the spacecraft is compliant with the CubeSat form factor can easily be verified by inspection.	QM,FM
LICCA-SYS-Bud-02	The spacecraft shall have a size of≤12U.	Inspection, similar to the previous requirement, the size of the satellite can be verified easily by inspection.	QM, FM
LICCA-SYS-Bud-06	A Commercial Off-The-Shelf (COTS) option shall be identified during the design of each subsystem, and included in the trade-off.	Analysis, by reading the reports and analysing the components used in the final design it can be seen whether COTS components are applied to the spacecraft.	Parts
LICCA-ST-Bud-01	The launch date shall be 2030.	Analysis, the launch date can be verified by analysis. The launch date is scheduled in advance and will be determined prior to the launch.	N.A.
LICCA-ST-Cost-01	The cost of the mission shall not exceed 20 million euro, excluding the launch cost and operation.	Analysis, an analysis can be made of all the components and their corresponding cost. This way it can be checked if the design stays within the allocated budget.	FM
LICCA-ST-21	The mission shall comply with space laws set by the United Nations.	Analysis, it will be analysed if all relevant aspects of the mission comply with the space laws set be the United Nations. The relevant aspects will need to be analysed (by a professional) and compared to the set laws to determine if they are compliant.	FM
LICCA-ST-26	The system shall comply with the space laws of The Netherlands.	Analysis, it will be analysed if all relevant aspects of the mission comply with the space laws of The Netherlands. The relevant aspects will need to be analysed (by a professional) and compared to the set laws to determine if they are compliant.	FM
LICCA-SYS-Sub-01	The use of COTS components for the system shall be maximised.	Analysis, for every component of the satellite, during (conceptual) design, it will be checked if there is a COTS component available to maximise the use of COTS component and to minimise the need for development of new components.	FM

LICCA-SYS-Sub-Ad-04	The ADCS shall provide a pointing accuracy of 0.0023 rad.	Analysis, the pointing accuracy of the ADCS shall be analysed via calculations and a model, concerning orbital parameters, as the accuracy can only be determined in space and not directly on Earth.	QM, FM
LICCA-SYS-Sub-EPS-01	The total required electrical power shall not exceed 40W.	Analysis, an analysis can be made to check the power consumption of all the subsystems. Combining this can be done to check if the power of 40 W is not exceeded.	FM
LICCA-SYS-Sub-PI-01	The interferometers shall operate with a maximum angle deviation of 5 arcmin.	Test, the maximum deviation angle of the laser can be tested by pointing the laser and measure the accuracy to see it the devialtion is lees that 5 arcmin	Parts
LICCA-SYS-Sub-PI-02	The variation in power of the lasers that compose the interferometers shall not exceed 150 mW.	Test, the actual lasers that will be used as payload can be tested in laboratory and the power they use can be measured to see if it exceeds 150mW.	Parts
LICCA-SYS-Sub-PI-03	The variation in frequency of the lasers that are part of the interferometers shall not exceed 167 THz.	Test, the actual lasers that will be used as payload can be tested in laboratory and the frequency of the signal they send can be measured and compared.	Parts
LICCA-SYS-Sub-PI-04	The distance from the interferometers to the centre of mass of the spacecraft shall not exceed 4 cm.	Inspection, after the entire satellite is manufactured, the actual distance from the interferometer components to the centre of mass of the spacecraft can be inspected.	QM, FM
LICCA-SYS-Sub-PI-05	The payload shall have a TRL of 3 or higher.	Inspection, the development of the technology of the scientific payload can be evaluated to inspect if the TRL is 3 or higher.	Parts
LICCA-SYS-Lt-01	The spacecraft lifetime shall be at least two year.	Analysis, the spacecraft will be functional for its entire lifetime if all subsystems are functional for this lifetime. The degradation (for example due to radiation, loading or working cycles) of each subsystem can be analysed in order to determine this.	FM
LICCA-SYS-Cost-04	The spacecraft shall be launched along with other missions.	Inspection, it can simply be checked if the spacecraft is launched along with other missions.	FM
LICCA-SYS-S&R-02	The system reliability shall be at least at End-of-Life conditions.	Analysis, the reliability of the system can be approximated accurately by mathematical models.	QM, FM
LICCA-SYS-Sub-Str-4	The structural system shall withhold vibrations due to launch of 100 Hz.	Test, the test shall conduct a modal survey using vibration table. The test can be considered successful when 100 Hz are withhold	QM, FM
LICCA-SYS-Sub-Str-5	The structural system shall withhold quasi static load of at least 6 g's.	Test, The test shall apply a static load of the satellite. It will be considered passed if after 1 000 N the performance is unaffected	QM, FM
LICCA-SYS-Sub-Str-7	The structural subsystem shall provide radiation shielding for all subsystems to a subcritical level.	Test, the ionising dose shall be tested in a facility with Heavy ions. The test shall be considered successful if the performance of the satellite is unaffected.	Parts, QM, FM
LICCA-SYS-Sub-5	The spacecraft shall be able to withstand a shock of <tbd>N.	Test, the test shall apply a shock to the satellite and it will be considered a pass if after <tbd>N the performance is unaffected	QM, FM

LICCA-SYS-Sub-6	The spacecraft's performance shall be unaffected by the electromagnetic environment.	Test. The test will consist in applying radio waves to the object and the performance should be unaffected	QM, FM
LICCA-SYS-Sub-Thr-2	The thermal system shall maintain total temperature of the satellite in the range of 10 - 30 °C.	Test, the test shall apply cyclical heat simulating real-life conditions and if the performance is unaffected then the test will be consider passed.	QM, FM

The verification requirement matrix represents a strategy to verify the product. The next step is to develop a technical plan on how to gather the evidence that a requirement has been verified, Test and Verification Requirements (TVR). Verifying requirements by analysis and inspection is straightforward: once the correct method is carried out, as described in the verification rationale, the outcome will be either a pass or a fail. The focus of the technical plan is on the requirements which need to be tested. The tests which concern the verification of the product are environmental tests and functional tests [48]. Table 15.16 presents the environmental tests that need to be carried out on the models with the requirements that need to be complied.

Table 15.16: Environmental tests to be carried out with testing facility

TVR ID	Source Requirements	Unit	TVR Operator	TVR Type
1	LICCA-SYS-Sub-Str-4, LICCA-SYS-Sub-Str-5 LICCA-SYS-Sub-5	QM, FM	CubeSat Support Facility (ESA)	Electrodynamic Shaker test
2	LICCA-SYS-Sub-Thr-2	QM, FM	CubeSat Support Facility (ESA)	Thermal Vacuum test
3	LICCA-SYS-Sub-Str-7	Parts	Cyclotron Resource Centre (UCL)	Heavy Ion Radiation test
4	LICCA-SYS-Sub-6	QM, FM	Maxwell Test Chamber(ESA)	Electromagnetic Compatibility test
5	LICCA-SYS-Sub-Thr-2	QM, FM	Environmental Test Facilities(ISIS)	Thermal cycling

A major source of issues in space comes from the launch and the natural space environments. This is why the thorough testing of the product in simulated environments is crucial. As already previously mentioned two models will be developed for verification: the QM and the FM. Both these models will undergo almost the testing campaign at different loads, the only exception is the shock test which will only be carried out on the qualification model to not damage the hardware of the flight mode and risk jeopardising the lifetime. During this campaign functional tests will be paired with environmental tests to check the performance of the product in space conditions, shown in figure 15.5. Functional tests will comprise in a set of tests which will verify that the requirements, to be tested, are met at all levels. These tests need to be further developed in later stages of the design process, once all the functions of the satellite are better defined. Some examples are: testing the capability of the payload, checking the solar array deployment mechanism, testing if the propulsion can still be receive data from the CDH, etc. It is important to note the absence of the radiation testing in this diagram, this is due to the fact that the diagram only portrays the testing sequence of the QM and FM. Radiation testing will be carried out on the singular components.
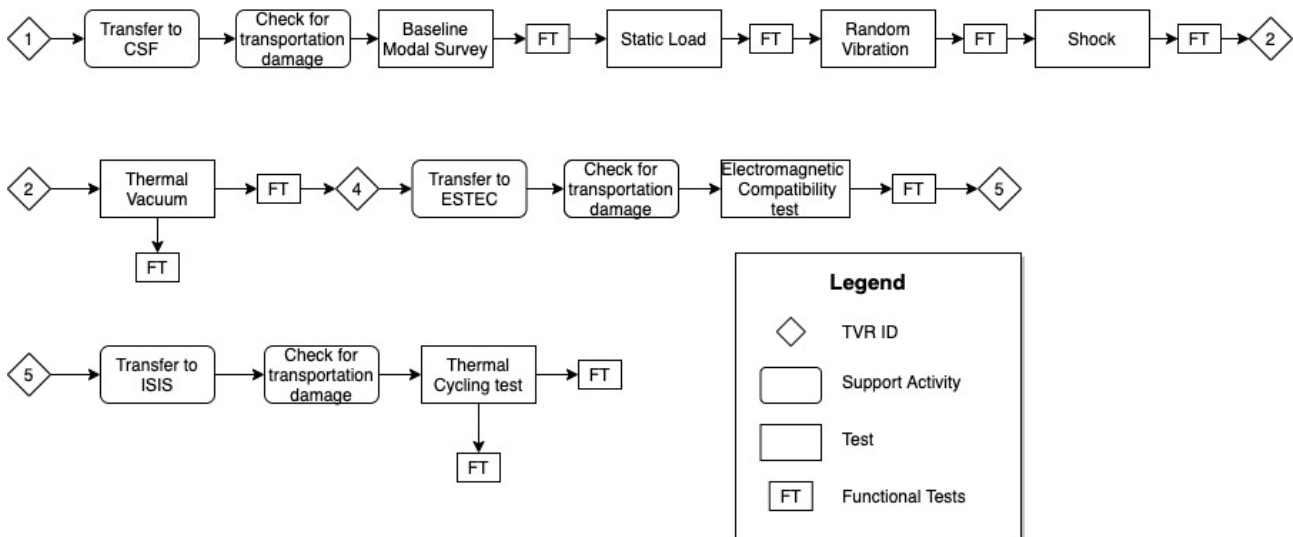
Figure 15.5: LICCA mission test campaign sequence

Finally, the requirements that pass the tests should be ticked off in a compliance matrix. Appendix A presents this kind of matrix for the initial stage of the project, where requirements are considered complied simply if the system is designed to meet that requirement, without being inspected, demonstrated, analyzed or tested. This matrix will very probably be subjected to change once the product verification starts and the method just presented is applied to all the requirements.

15.2.2. Product validation

Product Validation begins once the product is completely, or close to, verified. It focuses on meeting the true expectation of the costumer. The validation of the systems may, at first glance, appear a duplicate of product verification but in reality it focuses on the overall system with the objective of predicting unexpected behaviour. For this reason the focus of validation is on what happens in practice and not on the requirements.[48] The following techniques are the most commonly used for this validation:

- **End-to-End Information System Testing:** Show compatibility of project information systems.
- **Mission Scenario Tests:** Demonstrate that flight hardware and software can execute the mission under flight-like conditions (nominal & contingency) without real timeline.
- **Operations Readiness Tests:** Demonstrate that all elements of the ground segment (e.g. software, hardware, people, facilities) accomplish the mission plan using real timeline.
- **Stress-Testing and Simulation:** Assess system robustness to variations in performance and fault conditions.

Similarly to the product verification, to effectively validate the product, a validation matrix is necessary to plan the validation methods against the costumer expectations and key operational behaviours. These two components are identified with the help of a fault tree, figure 15.6. This tree is crucial for planning different ways to stress the systems under realistic and extreme conditions.[48]
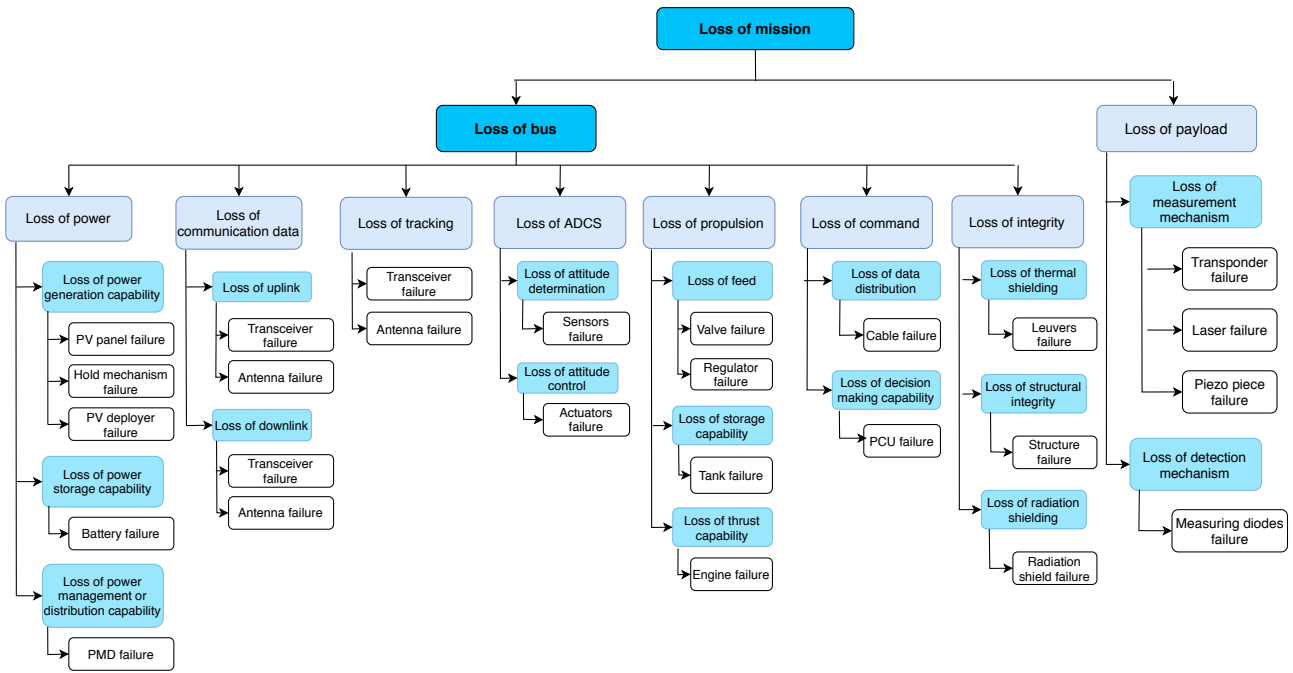
Figure 15.6: LICCA mission fault tree

The validation matrix presents capabilities of the mission that are to be validated along with the corresponding method. The tools and test facilities can be assumed to be the same ones used for the verification due to the closeness of these two activities. It is extremely important to note that not all capabilities can be tested during a ground-based validation event because not all flight elements work outside the space environment. The validation matrix presented in table 15.17, contains only the capabilities of the system identified at this stage of the design process, with further advancements in the design and more contact with the costumers this matrix should be extended.

Table 15.17: Validation Matrix

Validation Capabilities	End-to-End Information System Testing	Mission Scenario Tests	Operations Readiness Tests	Stress-Testing and Simulation
Detect Gravitational Waves in the frequency of 1-10Hz	x	x	x	
Optimize the intensity of the laser detected by the satellites	x	x	x	
Complete a realignment manouver without one reaction wheel				x
Communicate to ground station with a broken transponder				x
Determine the attitude in eclipse with a broken star sensors		x		x

16

Conclusion and Recommendations

In this chapter the conclusion, section 16.1, and the recommendations, section 16.2, are presented.

16.1. Conclusion

The need for the LICCA mission is as follows: *"To gain a more comprehensive view of the gravitational wave frequency spectrum, the mission will provide complementary measurements to the frequencies of current and planned gravitational wave measurements by detecting in the range of 1-10 Hz."* The objective of this project was to transform the idea of measuring gravitational waves with CubeSats to a conceptual design. To do so, the general characteristics of the mission have been determined, namely the astrodynamics, sustainability, risk characteristics, RAMS and financing, along with the design of each of the subsystems.

In the phases leading up to the detailed design, design concepts were generated and a winner was selected through a trade-off. The winning concept consists of six CubeSats in geostationary orbit, in which there are two independent constellations of three satellites. The payload of each satellite employs a Sagnec interferometer sending and reflecting lasers to the other CubeSats in the constellation. This interferometer was chosen as it best fit a CubeSats due to its low complexity. For the design of the rest of the subsystems, the use of Commercial Off-The-Shelf components has been implemented as much as possible. The main results of the subsystem designs are presented in table 16.1. Overall, the use of COTS components simplifies and accelerates the design process of the mission. The flight heritage of these greatly improves the reliability. The drawback is that the components will not be tailored for the mission resulting in unnecessary redundancies.

From the design of the subsystems design there are two major conclusions. The first one being, the transfer from GTO to GEO cannot be done with a 12U CubeSat for this mission with the technology available today. However, there are solutions to get to GEO, the best identified one was the use of a developing transfer vehicle. The second major conclusion is that the GEO radiation environment is very harsh for COTS components that are mainly designed for LEO. This implied, firstly, a large the use of radiation shielding and secondly, the fact that all the components will be thoroughly tested for radiation tolerance.

The reliability of the systems is estimated to be around 56%, this low number due to the low redundancy of the system caused by volume constrains. Moreover, from the verification and validation section it was concluded that a flight model and a qualification model will be developed to ensure appropriate testing. Testing facilities in Europe where also identified, like the CubeSat Support Facility and the Maxwell Test Chamber from ESA, the Cyclotron Resource Centre from UCL, and Environmental Test Facilities from ISIS.

The main system characteristics concluded that the launch will be made with either Ariane 5 or Ariane 6. Following this, the spacecrafts will arrive in GEO by piggybacking off Vigoride. Moreover, the constellation will need to realign every 15 days to correct for the drift. Then, the End-of-Life manoeuvre will consist of entering a graveyard orbit after the mission lifetime is exceeded. If enough functionality is remaining in the satellites, the measurements can continue from this graveyard orbit.

Finally, for the financing of the mission, the estimated cost of the mission is about 14.66 million EUR and the operation costs is around 8.91 million EUR. Finally, from the system analysis it is concluded that the mass range is between 19.6-26.8 kg and the power oscillates from 27.4-46.6 W.

Table 16.1: System Characteristics

Satellites		TT&C	
Mission Duration	>2 years	Uplink	S-band: 2025-2110 [MHz]
No. of spacecraft	6		UHF: 435-438 [MHz]
No. of constellations	2	Downlink	S-band: 2200-2290 [MHz]
Configuration	CubeSat (12 U)		UHF: 435-438 [MHz]
Mass (per satellite)	22.3 kg	Tracking type	Radio communication system
Size (per satellite)	30x20x20 cm	Ground segment	
Power (per satellite)	30.6 W	S-band: ESTRACK	Kourou, Villafranca, Dongara
Geometry		UHF: ISIS Amateur	Anywhere
Constellations	Equilateral	CDH	
Orbit	GEO	Cores	2
Arm Length	72 000 km	No. of sensors	80
GW frequency	1 - 10 Hz	EPS	
Payload		Solar Array Area	0.307 m^2
Measurement method	Sagnac, TDI	PCDU	includes BCRs and MPPT
Reflecting system	transponder	Thermal	
ADCS		Active	Heaters
Pointing accuracy	0.13 °	Passive	Louvers, Coating
Propulsion		T-range	288.15-293.15 K
Type	Chemical	Structure	
Tank shape	Cuboid with round corners	COTS skeleton	ADCS thruster deployer
		Hold and release mechanism for solar panel	

16.2. Recommendations

To end this report some recommendations are given for further research into the LICCA mission. The main steps that would follow beyond the DSE have been outlined in the project Gantt chart, as shown in figure A.6. Based on the final design that has resulted from this DSE, several recommendations can be given for these next steps.

Further research is required for the transfer from GTO to GEO, that is not feasible for the CubeSats within the constraints of the LICCA mission. However, multiple solutions can be considered in order to resolve this issue. First of all, research can be conducted into electrical propulsion. With this it can be considered to use more power such that higher thrust levels can be reached. Another option for further research is to investigate the feasibility of extending to a 16 U CubeSat. This allows for larger tanks, and consequently more propellant, which can be taken along and might be enough for the transfer. When this transfer is deemed feasible, it was already determined for the LICCA mission how the satellites should transfer into GEO. After three revolutions in GTO, the phase change between the satellite already orbiting GEO and the one that is about to do the transfer is 114°. This means that an additional manoeuvre is needed for only 6°. This way the least ΔV is needed to achieve the triangular constellation. Another benefit for extra propellant that can be taken on board would be to extend the lifetime of the mission.

If these measures are out of the possibilities for this mission, a transfer vehicle can still be used to reach GEO. At this point in the mission, Vigoride was considered the best option. By the time of launch, other opportunities might rise, which outperform Vigoride. Since the CubeSat deployer is compatible with a variety of external systems, the new developments should be considered and investigated.

For the telecommunications of the mission, the following aspects can be considered and further developed. A longitudinal position has been selected based on optimal positioning for the ESTRACK ground stations that have been selected. The GEO orbit is highly populated, and it would have to be investigated if these longitudinal positions would indeed be available for the LICCA CubeSats. Furthermore, it is recommended to investigate the use of commercial ground stations, such as KSAT, Amazon GS, Leaf Space, and Infostellar. Currently, they have ground stations that are capable of communicating with CubeSats in LEO, but their networks are expected to expand in the near future. Then these ground stations might be sufficient for the LICCA communications, which would provide more flexibility in their positioning and usage.

For the EPS a redundant battery can be considered in the future. This increases the reliability of the system, however it increases mass and volume. This could thus only be implemented when there is enough volume left. Besides, the two PCDU's now used could be split up in 1 PCU and 2 PDU's to decrease mass, volume and power of the EPS. Further research will determine how feasible this option is.

To decrease the weight of the structure more research has to be done in localised radiation shielding. This would decrease the mass of the structure and better protect the components of all subsystems against radiation effects. More radiation hardened components can also become available in the future helping decrease the mass and extent the lifetime of the CubeSat. A full analysis has to be done on the structure to make sure it complies with all laws and launcher specification.

The pointing stability for the ADCS is another factor that has to be looked in more detail. As the payload subsystem is designed to detect the phase shifts between the sent and received laser beams, any disturbance experienced by the CubeSat in the frequency range in which gravitational waves are expected to be detected have to be reduced so they will not interfere with the results obtained from the experiment. This was managed partially with the Piezo stage, but its performance should be looked into with more detail together with the frequencies of the disturbances that the satellite could experiment in such a environment. Furthermore, the option of integrating the main propulsion subsystem with the ADCS thrusters could be looked into with more detail because this could allow the mass and volume to be reduced if both subsystems either share the tank or the thrusters.

A last aspect that requires developing is the integration testing, a plan needs to be drafted to check the assembly of the different sensors, the functional integration of spacecraft subsystems and the integration between the CubeSats, deployers, transfer vehicle and launcher.

Bibliography

[1] F. Witte A. Chanoine, Y. Le Guern, T. Soares J. Huesing, and L. Innocenti. Integrating sustainability in the design of space activities: development of eco-design tools for space projects. In *Proceedings of 5th CEAS (Council of European Aerospace Societies) Air & Space Conference*, 2015.

[2] B.T. Melter A. Schmidt. A.A. Jensen, L. Hoffman. Life Cycle Assessment (LCA) - a guide to approaches, experiences and information sources. Technical report, European Environment Agency, 8 1997.

[3] J. Achterberg, F. Bagchus, I. Boshuizen, T. Eppenga, S. Falckenheiner, F. Magri, G. Mettepenningen, J. Oduber, P. Silvagni, V. Tunjov, and F. Weijand. *Baseline report, Small Satellites for Gravitational Waves Observation*. Delft: Delft University of Technology, 2020.

[4] J. Achterberg, F. Bagchus, I. Boshuizen, T. Eppenga, S. Falckenheiner, F. Magri, G. Mettepenningen, J. Oduber, P. Silvagni, V. Tunjov, and F. Weijand. *Project Plan, Small Satellites for Gravitational Waves Observation*. Delft: Delft University of Technology, 2020.

[5] J. Achterberg, F. Bagchus, I. Boshuizen, T. Eppenga, S. Falckenheiner, F. Magri, G. Mettepenningen, J. Oduber, P. Silvagni, V. Tunjov, and F. Weijand. *Midterm report, Small Satellites for Gravitational Waves Observation*. Delft: Delft University of Technology, 2020.

[6] Arianespace. *Ariane 6 user's manual*. ArianeGroup, 2018.

[7] T. Asai, K. Yamada, and I. Jikuya. Fuel-efficient low-thrust transfer in elliptic orbits. *Trans. JSASS Aerospace Tech. Japan*, 12(29):1–9, 2014.

[8] Hlwun Moe Aung, Win Zaw Hein, and Hla Myo Tun. Performance evaluation of gsm transmission over different modulation schemes (bpsk, qpsk, gmsk). *International Journal of Scientific and Research Publications (IJSRP)*, 4(4):1–5, 2014.

[9] M. J. Barrett and R. G. Lyle. Spacecraft solar cell array. *NASA*, December 1971.

[10] A. L. Bosser. Single-event effects of space and atmospheric radiation on memory components, 2017.

[11] G.H. Bruntland. World commission on environment and development. *Our common future*, 1987. Vol. 17, pp. 43–66.

[12] E. Canuto, C. Novara, L. Massotti, D. Carlucci, and C. Perez Montenegro. *Spacecraft Dynamics and Control - The Embedded Model Control Approach*. Elsevier, 2018. ISBN 978-0-08-100700-6.

[13] D. Castelvecchi. Hunt for cosmic waves to resume. *Nature*, 2015. Vol. 525, No. 7569, pp. 301–302.

[14] A. Cervone. Aerospace design and system engineering elements ii - spacecraft telecommunications, Sept 2019.

[15] H. Chen and J. Zheng. *Analyze on GEO Satellites Output Power Variation*. Atlantis Press, 2012.

[16] J. Chin, R. Coelho, J. Foley, A. Johnstone, R. Nugent, D. Pignatelli, S. Pignatelli, N. Powell, J. Puig-Suari, W. Atkinson, J. Dorsey, S. Higginbotham, M. Krienke, K. Nelson, B. Poffenberger, C. Raffington, G. Skrobot, J. Treptow, A. Sweet, J. Crusan, C. Galica, W. Horne, C. Norton, and A. Robinson. *CubeSat 101 - Basic Concepts and Processes for First-Time CubeSat Developers*. NASA CubeSat Launch Initiative, October 2017.

[17] LIGO Scientific Collaboration. Instrument science white paper, 2016.

[18] CCSDS committee. *CCSDS historical document - CCSDS radio frequency and modulation system - Earth Stations*. Consultative Committee for Space Data Systems, May 1997.

[19] H.D. Curtis. *Orbital Mechanics for Engineering Students*. Elsevier, 2014.

[20] S. Pautonnier R. Drai D. Desiderio, M. Lovera. Magnetic momentum management for a geostationary satellite platform. *Proceedings of the 47th IEEE Conference on Decision and Control*, December 2008.

[21] K. Danzmann. *Laser Interferometer Space Antenna: A proposal in response to the ESA call for L3 mission concepts*. Albert Einstein Institute Hannover, 2017.

[22] K. Danzmann and LISA Science team. Laser interferometer space antenna: A cornerstone mission for the observation of gravitational waves. *NASA*, September 2000.

[23] R. Carlino G. Defouw A.D. Perez A.G. Karacalıoğlu B. Klamm A. Rademacher J. Schalkwyck R. Shimmin J. Tilles S. Weston E. Agasid, R. Burton. *State of the Art Small Spacecraft Technology*. NASA Ames Research Center, Small Spacecraft Systems Virtual Institute, December 2018.

[24] B. Dobrotin J. Scull R. E. Fischell D. Fosth J. Kelly A. J. Fleig H. Perkel R. E. Roberson-J. Rodden B. Tinling S. O'Neil-F. J. Carroll R.F. Bohling E. P. Blackburn, D. DeBra. Nasa space vehicle design criteria - spacecraft magnetic torques, 1969.

[25] ECSS Secretariat. Li-ion battery testing handbook, 2015.

[26] J. Bouwmeester J.M. Kuiper E.H. Dekens, G.F. Brouwer. Development of a nano-satellite reaction wheel system with commercial off-the-shelf motors, 2010.

[27] B. Tabea C. Benoit A. Ciroth C. Cucuzzella C. Gensch J. Hébert P. Lesagne A. Manhart E.S. Andrews, L. Barthel and P. Mazeau. Guidelines for social life cycle assessment of products. Technical report, United Nations Environment Programme, 2009.

[28] ESA LCA Working Group. Space system Life Cycle Assessment (LCA) guidelines, 2016.

[29] P Escobal. Methods of orbit determination, RE Krieger Pub. *Co, Huntington, NY*, 1976.

[30] A. Evans. Design and testing of the cubesat form factor thermal control louvers, 2019.

[31] F Froes, M Qian, and N. Niinomi. Titanium for consumer applications, 2019.

[32] F. Chatel G.E. Dorrington J.B. Farrow N.P. Fillery C.R. Francis G. Hall J.M. Houghton J.B. Moss T. Ransom K.M. Redford-C.J. Savage R.E. Sheriff D. Stanton-M.N. Sweeting A.R.L. Tatnall C.I. Underwood G.S. Aglietti, M. Bandecchu. *Spacecraft System Engineering*. John Wiley & Sons, Ltd, 4th edition, 2011.

[33] V. Gupta. Analysis of single event radiation effects and fault mechanisms in sram, fram and nand flash : application to the mtcube nanosatellite project. *Electronics. Université Montpellier*, 52, 2017.

[34] D. Haeseler, V. Bombelli, P. Vuillermoz, R. Lo, T. Marée, and F. Caramelli. Green propellant propulsion concepts for space transportation and technology development needs. In *ESA Special Publication*, 2004. Vol. 557.

[35] Ir. R.J. Hamann and Prof. Dr. Ir. M.J.L. van Tooren. *Systems Engineering & Technical Management*. Delft University of Technology, 2006.

[36] Inter-Agency Space Debris Coordination Committee (IADC). IADC space debris mitigation guidelines. Technical report, 9 2007.

[37] ITR. *International Telecommunication Regulations - Melbourne - (WATTC-88)*, 1988.

[38] E. Gill J. Bouwmeester, M. Langer. Survey on the implementation and reliability of cubesat electrical bus interfaces. *CEAS Space Journal*, June 2017.

[39] C. Han J. Guo. Where is the limit: The analysis of cubesat ADCS performance. *The 4S Symposium*, May 2016.

[40] C. Jo D. Chang J. Lee, Y. Choi. Design of a prismatic pressure vessel: An engineering solution for nonstiffened-type vessels. *Ocean Engineering*, 142:639–649, 2017.

[41] Hui-Zong Duan Yun-Gui Gong Shoucun Hu Jianghui Ji Qi Liu Jianwei Mei Vadim Milyukov Mikhail Sazhin Cheng-Gang Shao Viktor T. Toth Hai-Bo Tu Yamin Wang Yan Wang Hsien-Chi Yeh Ming-Sheng Zhan Yonghe Zhang Vladimir Zharov Ze-Bing Zhou Jun Luo, Li-Sheng Chen. Tianqin: a space-borne gravitational wave detector, 2015.

[42] M.O. Kolawole. *Satellite Communication Engineering*. Marcel Dekker, Inc., 2002.

[43] I. Kök. Comparison and analysis of attitude control systems of a satellite using reaction wheel actuators. *Luleå University of Technology Department of Computer Science, Electrical and Space Engineering*, October 2012.

[44] S. Lacour, A. Kellerer, J. Woillez, M. Nowak, F. Vincent, L. David, V. Lapeyrère, A. Le Tiec, O. Straub, and P. Bourget. SAGE: using CubeSats for gravitational wave detection. *Space Telescopes and Instrumentation 2018: Ultraviolet to Gamma Ray*, July 2018. doi: 10.1117/12.2313639.

[45] S. Lacour, F.H. Vincent, M. Nowak, A. Le Tiec, V. Lapeyrere, L. David, P. Bourget, A. Kellerer, K. Jani, J. Martino, et al. SAGE: finding IMBH in the black hole desert. *Classical and Quantum Gravity*, 36(19), 2019.

[46] M. Langer and J. Bouwmeester. Reliability of cubesats – statistical data, developers' beliefs and the way forward. *In Proceedings of the 30th Annual AIAA/USU Conference on Small Satellites*, 2016.

[47] M. Langer, M. Weisgerber, J. Bouwmeester, and A. Hoehn. A reliability estimation tool for reducing infant mortality in cubesat missions. *IEEE Aerospace Conference*, 2017. 7943598.

[48] Larson, Kirkpatrick, Sellers, and Verma. *Applied Space Systems Engineering*. Mc Hill, Boston, MA, 2014. ISBN 978-0073408866.

[49] A. Kajo M. Mirghani, A. Tagelsir. Hardware selection for attitude determination and control subsystem of 1u cube satellite. *International Conference on Computing, Control, Networking, Electronics and Embedded Systems Engineering*, September 2015.

[50] V.K. Mani, A. Cervone, and F Topputo. Chemical propulsion system design for a 16u interplanetary cubesat, 2018.

[51] L. M. S. Martines. Analysis of LEO radiation environment and its effects on spacecraft's critical electronic devices. *Embry-Riddle Aeronautical University*, 2011.

[52] J.P. Masonaand, B. Lamprechtband, and T.N. Woods. Cubesat on-orbit temperature comparison tothermal-balance-tuned model predictions. *Chloe Downs*, 2014.

[53] D.R. Mattie and T.R. Sterner. Review of ammonium dinitramide toxicity studies. Technical report, Air Force Research Laboratory, 2011.

[54] J. Melkert. Dse weekly videos, 2020.

[55] G.C. Messenger and A.S. Milton. *Single Event Phenomena*. Springer US, Boston, MA, 1997. ISBN 978-1-4615-6043-2. doi: 10.1007/978-1-4615-6043-2_2. URL https://doi.org/10.1007/978-1-4615-6043-2_2.

[56] O. Montenbruck and E. Gill. *Satellite Orbits - Models, Methods, Applications*. Springer, 1st edition, 2000.

[57] E. Mooij, Z. Papp, and W. van der Wal. AE3212-II Lecture notes: Simulation, Verification and Validation. Delft University of Technology, February 2020.

[58] R. Noomen. AE2230-I, lecture 3: Eclipse, maneuvers, 2019. Flight and Orbital Mechanics, lecture slides.

[59] Atem de Carvalho R., Estela J., and Langer M. *Nanosatellites: Space and Ground Technologies, Operations and Economics*. John Wiley & sons Ltd, June 2020.

[60] B. Ravinarayana, N. Upadhyaya, and R. Kulkarni. Total radiation dose at geostationary orbit. *Nuclear Science, IEEE Transactions on*, 52:530 – 534, 05 2005. doi: 10.1109/TNS.2005.846881.

[61] V. Savani, M. Akash, and N. Gajjar. Single event upset mitigation techniques implementaion based on

tmr. 01 2010.

[62] R. Schneider, V. Ferrari, S. Matarrese, and S. F. Portegies Zwart. Low-frequency gravitational waves from cosmological compact binaries. *Monthly Notices of the Royal Astronomical Society*, 324:797–810, 2001.

[63] J. R. Schwank. Basic mechanisms of radiation effects in the natural space environment, 1994.

[64] D.M. Seymour, B.D. Mason, W.I. Hartkopf, and G.L. Wycoff. Binary star orbits. II. preliminary first orbits for 117 systems. *The Astronomical Journal*, 123:1023–1038, 2002.

[65] D. Sinclair and J. Dyer. Small satellites ssc 13-iv-3 radiation effects and cots parts in smallsats. 2013.

[66] R.A. Spores, R. Masse, S. Kimbrel, and C. McLean. *GPIM AF-M315E Propulsion System*. Aerojet Rocketdyne and Ball Aerospace and Technologies Corporation, 2013.

[67] SRE-PA & D-TEC staff. Margin philosophy for science assessment studies. Technical report, ESA, 06 2012.

[68] H. Oh T. Park, B. Chae. Development of 6u cubesat's deployable solar panel with burn wire triggering holding and release mechanism, 2019.

[69] A. Tindemans. Delfi-n3xt - End-to-end analysis an design of the satellite communication links. System design of the communication subsystem of the Delfi-n3xt nanosatellite. Master's thesis, Delft University of Technology, June 2010.

[70] D.A. Vallado. *Fundamentals of Astrodynamics and Applications*. Springer Science & Business Media, 2011.

[71] P. van Kampen. Lorentz contraction and current-carrying wires. *European Journal of Physics*, 29(5): 879–883, jun 2008. doi: 10.1088/0143-0807/29/5/002. URL https://doi.org/10.1088%2F0143-0807%2F29%2F5%2F002.

[72] J.R. Wertz, D.F. Everett, and J.J. Puschell. *Space Mission Engineering: The new SMAD*. Microsom Press, 2011.

[73] A. Wright. User manual: 3rd generation EPS range - no inhibits, 2017.

[74] B.T.C. Zandbergen. *Aerospace Design & Systems Engineering Elements I. Part: Spacecraft (bus) design and sizing*. Delft: Delft University of Technology, 2017.

[75] B.T.C. Zandbergen. *Aerospace Design & Systems Engineering Elements I. Part: Launch Vehicle design and sizing*. Delft: Delft University of Technology, 2017.

Appendix: Diagrams

Compliance matrix

The compliance matrix checks whether all requirements are met. The driving requirements are coloured green, and the killer requirements are coloured orange. The requirements that have been deleted in this report, as mentioned in their related subsystem sections, are omitted. The '-' sign indicates that a requirement was identified as out of the scope of the DSE and can only be checked in further phases of the mission. Following, an explanation of why requirements are not met is given:

- **LICCA-SYS-Sub-Prp-2:** As described in section 6.3, the propulsion system would become too large to be compliant with 12U if ΔV for the transfer manoeuvre needs to be accounted for. The volume constraint was considered more important to meet for this mission, since it is a user requirement.

- **LICCA-SYS-Sub-L&m-5:** As a consequence of not performing the transfer manoeuvre, the satellites will not be ejected from the deployer into a transfer orbit, but immediately into the target orbit.

Requirement	Compliance	Requirement	Compliance	Requirement	Compliance	Requirement	Compliance
User Requirements		LICCA-ST-20	-	***Hazardous materials***		LICCA-SYS-Sub-Str-4	-
Performance		LICCA-ST-21	✓	LICCA-SYS-Sus-Hm-1	✓	LICCA-SYS-Sub-Str-5	✓
LICCA-SYS-Perf-01	✓	LICCA-ST-22	✓	LICCA-SYS-Sus-Hm-1.2	✓	LICCA-SYS-Sub-Str-7	-
LICCA-SYS-Perf-03	-	***European Union***		LICCA-SYS-Sus-Hm-1.4	✓	LICCA-SYS-Sub-Str-9	✓
LICCA-SYS-Perf-05	✓	LICCA-ST-23	-	LICCA-SYS-Sus-Hm-2	✓	LICCA-SYS-Sub-Str-11	✓
LICCA-SYS-Perf-06	✓	LICCA-ST-24	-	LICCA-SYS-Sus-Hm-4	✓	LICCA-SYS-Sub-Str-12	-
LICCA-SYS-Perf-07	✓	***Government***		LICCA-SYS-Sus-Hm-5	✓	LICCA-SYS-Sub-Str-14	✓
LICCA-SYS-Perf-08	✓	LICCA-ST-26	✓	***Subsystems***		***CDH***	
LICCA-SYS-Perf-09	✓	LICCA-ST-27	✓	LICCA-SYS-Sub-1	✓	LICCA-SYS-Sub-CDH-2	✓
LICCA-ST-Perf-01	✓	***Space Agencies***		LICCA-SYS-Sub-2	✓	LICCA-SYS-Sub-CDH-4	✓
Safety & Reliability		LICCA-ST-28	-	LICCA-SYS-Sub-3	✓	LICCA-SYS-Sub-CDH-5	✓
LICCA-SYS-SR-01	✓	***Industry***		LICCA-SYS-Sub-4	✓	LICCA-SYS-Sub-CDH-6	✓
LICCA-ST-SR-02	✓	LICCA-ST-29	-	LICCA-SYS-Sub-5	✓	LICCA-SYS-Sub-CDH-9	✓
LICCA-ST-SR-03	✓	LICCA-ST-30	-	LICCA-SYS-Sub-6	✓	LICCA-SYS-Sub-CDH-10	✓
Sustainability		LICCA-ST-31	-	***ADCS***		LICCA-SYS-Sub-CDH-11	✓
LICCA-ST-Sus-01	✓	LICCA-ST-32	-	LICCA-SYS-Sub-Ad-1	✓	***TT&C***	
LICCA-ST-Sus-02	✓	***Launch Service provider***		LICCA-SYS-Sub-Ad-2	✓	LICCA-SYS-Sub-TTC-1	✓
LICCA-ST-Sus-03	✓	LICCA-ST-33	✓	LICCA-SYS-Sub-Ad-3	✓	LICCA-SYS-Sub-TTC-2	✓
LICCA-ST-Sus-04	✓	***Transportation and storage companies***		LICCA-SYS-Sub-Ad-6	✓	LICCA-SYS-Sub-TTC-3	✓
Engineering budgets		LICCA-ST-36	-	LICCA-SYS-Sub-Ad-7	✓	LICCA-SYS-Sub-TTC-4	✓
LICCA-SYS-Bud-01	✓	LICCA-ST-37	-	***Navigation***		LICCA-SYS-Sub-TTC-9	✓
LICCA-SYS-Bud-02	✓	***Assembler***		LICCA-SYS-Sub-Nav-1	✓	LICCA-SYS-Sub-TTC-11	✓
LICCA-SYS-Bud-03	✓	LICCA-ST-38	-	LICCA-SYS-Sub-Nav-2	✓	LICCA-SYS-Sub-TTC-12	✓
LICCA-SYS-Bud-04	-	LICCA-ST-39	-			LICCA-SYS-Sub-TTC-13	✓
LICCA-SYS-Bud-05	✓	LICCA-ST-40	-			LICCA-SYS-Sub-TTC-14	✓
LICCA-SYS-Bud-06	✓	LICCA-ST-41	-	LICCA-SYS-Sub-Nav-6	✓	LICCA-SYS-Sub-TTC-15	✓
LICCA-SYS-Bud-07	✓	LICCA-ST-42	-	LICCA-SYS-Sub-Nav-7	✓	***Thermal***	
LICCA-ST-Bud-01	✓	LICCA-ST-43	-	***EPS***		LICCA-SYS-Sub-Thr-1	✓
Cost		***Satellite operator***		LICCA-SYS-Sub-EPS-1	✓	LICCA-SYS-Sub-Thr-2	✓
LICCA-ST-Cost-01	✓	LICCA-ST-44	-	LICCA-SYS-Sub-EPS-2	✓	LICCA-SYS-Sub-Thr-4	✓
LICCA-ST-Cost-03	✓	LICCA-ST-45	-	LICCA-SYS-Sub-EPS-3	✓	LICCA-SYS-Sub-Thr-5	✓

LICCA-ST-Cost-04	✓	*Ground station operator*		LICCA-SYS-Sub-EPS-4	✓	LICCA-SYS-Sub-Thr-6	✓
Stakeholder Requirements		LICCA-ST-46	-	LICCA-SYS-Sub-EPS-5	✓	LICCA-SYS-Sub-Thr-7	✓
TU Delft		*External experts*		LICCA-SYS-Sub-EPS-6	✓	*Propulsion*	
LICCA-ST-01	✓	LICCA-ST-48	✓	LICCA-SYS-Sub-EPS-7	✓	LICCA-SYS-Sub-Prp-1	✓
Scientific Community and Universities		**System Requirements**		LICCA-SYS-Sub-EPS-8	✓	LICCA-SYS-Sub-Prp-2	x
LICCA-ST-02	-	*Mission*		LICCA-SYS-Sub-EPS-9	✓	LICCA-SYS-Sub-Prp-3	✓
LICCA-ST-03	-	LICCA-SYS-Perf-01	✓	LICCA-SYS-Sub-EPS-10	✓	LICCA-SYS-Sub-Prp-4	✓
LICCA-ST-04	-	LICCA-SYS-Perf-09	✓	LICCA-SYS-Sub-EPS-11	✓	LICCA-SYS-Sub-Prp-5	✓
LICCA-ST-05	-	LICCA-ST-Perf-01	✓	LICCA-SYS-Sub-EPS-12	✓	*Legal*	
LICCA-ST-06	-	*Sustainability*		*Payload*		LICCA-SYS-Leg-1	✓
LICCA-ST-07	-	*Space debris*		LICCA-SYS-Sub-Pl-1	✓	LICCA-SYS-Leg-2	-
Sponsors		LICCA-SYS-Sus-Sd-1	✓	LICCA-SYS-Sub-Pl-2	✓	LICCA-SYS-Leg-3	-
LICCA-ST-08	✓	LICCA-SYS-Sus-Sd-2	✓	LICCA-SYS-Sub-Pl-3	✓	*Lifetime*	
LICCA-ST-09	✓	LICCA-SYS-Sus-Sd-2.1	✓	LICCA-SYS-Sub-Pl-4	✓	LICCA-SYS-Lt-1	✓
LICCA-ST-10	✓	LICCA-SYS-Sus-Sd-2.2	✓	LICCA-SYS-Sub-Pl-5	✓	*Cost*	
LICCA-ST-11	✓	LICCA-SYS-Sus-Sd-2.3	✓	*Launch and mission planning*		LICCA-ST-Cost-01	✓
LICCA-ST-12	-	LICCA-SYS-Sus-Sd-3	✓	LICCA-SYS-Sub-L&m-1	-	LICCA-SYS-Cst-2	✓
Media		LICCA-SYS-Sus-Sd-3.1	✓	LICCA-SYS-Sub-L&m-3	✓	LICCA-SYS-Cst-3	✓
LICCA-ST-13	-	LICCA-SYS-Sus-Sd-3.2	✓	LICCA-SYS-Sub-L&m-4	✓	LICCA-SYS-Cst-4	✓
LICCA-ST-14	-	LICCA-SYS-Sus-Sd-3.3	✓	LICCA-SYS-Sub-L&m-5	x	LICCA-SYS-Cst-5	✓
Public		LICCA-SYS-Sus-Sd-3.4	✓	LICCA-SYS-Sub-L&m-6	✓	*Safety & Reliability*	
LICCA-ST-15	-	*End-of-Life*		LICCA-SYS-Sub-L&m-8	✓	LICCA-SYS-S&R-1	✓
LICCA-ST-16	-	LICCA-SYS-Sus-El-1	✓	LICCA-ST-Bud-01	✓	LICCA-SYS-S&R-2	✓
LICCA-ST-17	✓	LICCA-SYS-Sus-El-2	✓	LICCA-SYS-Sub-L&m-10	✓		
United Nations - Office for Outer Space Affairs		*Ground*		*Structures*			
LICCA-ST-18	✓	LICCA-SYS-Sus-G-1	✓	LICCA-SYS-Sub-Str-2	-		
LICCA-ST-19	-	LICCA-SYS-Sus-G-2	✓	LICCA-SYS-Sub-Str-3	✓		
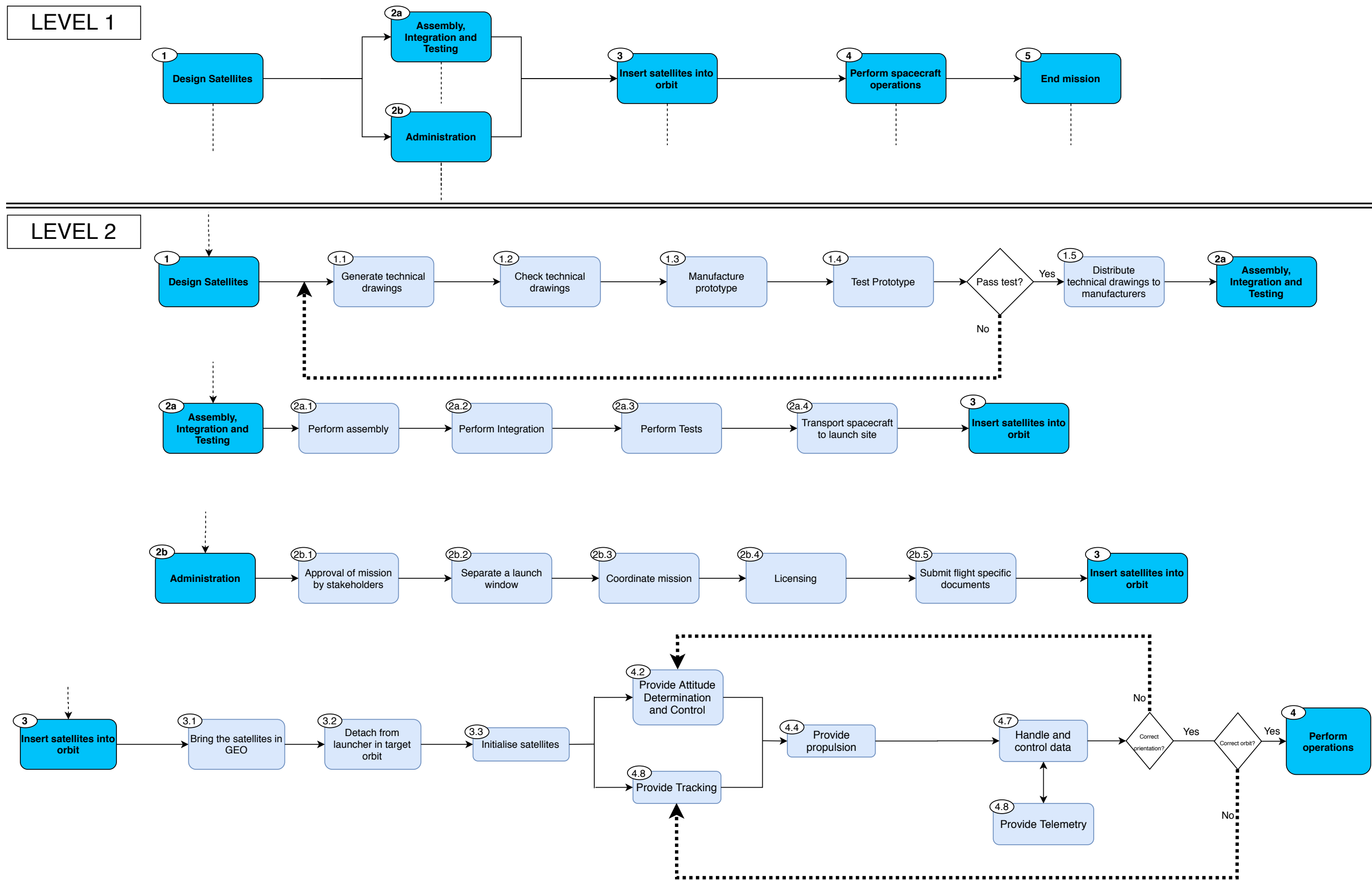
Figure A.1: Functional Flow Diagram - part 1

LEVEL 2
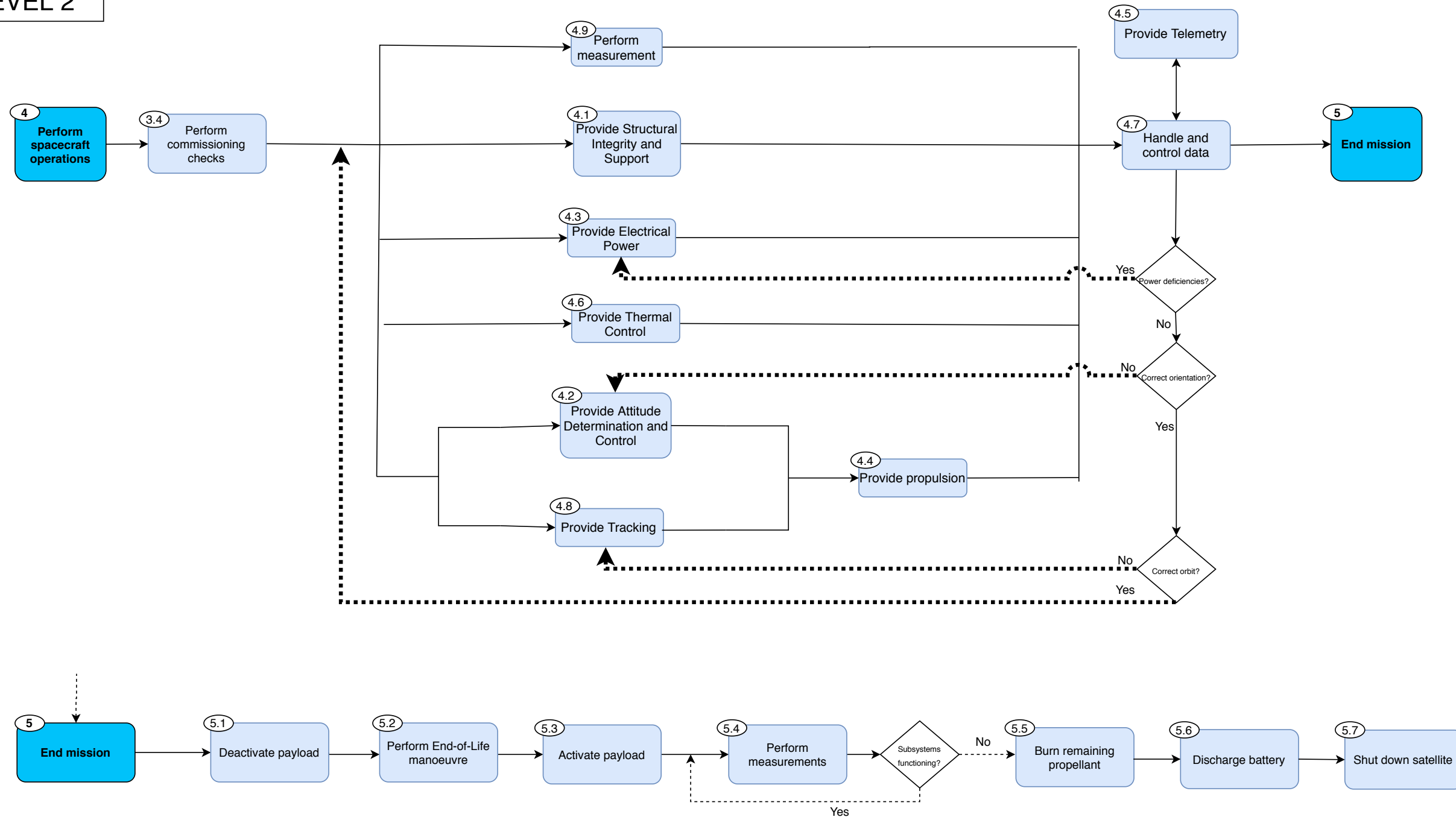
Figure A.2: Functional Flow Diagram - part 2

LEVEL 3
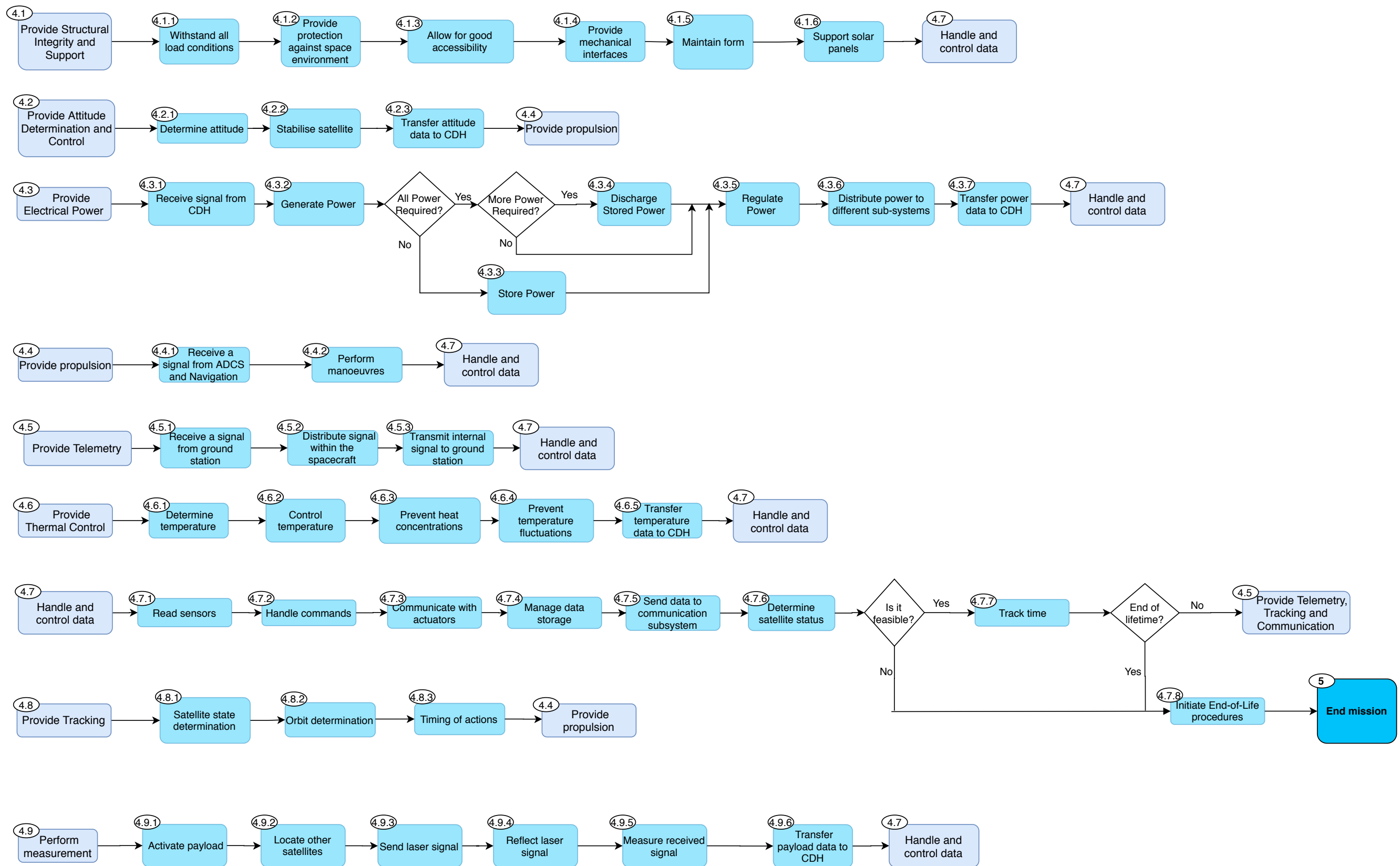
Figure A.3: Functional Flow Diagram - part 3
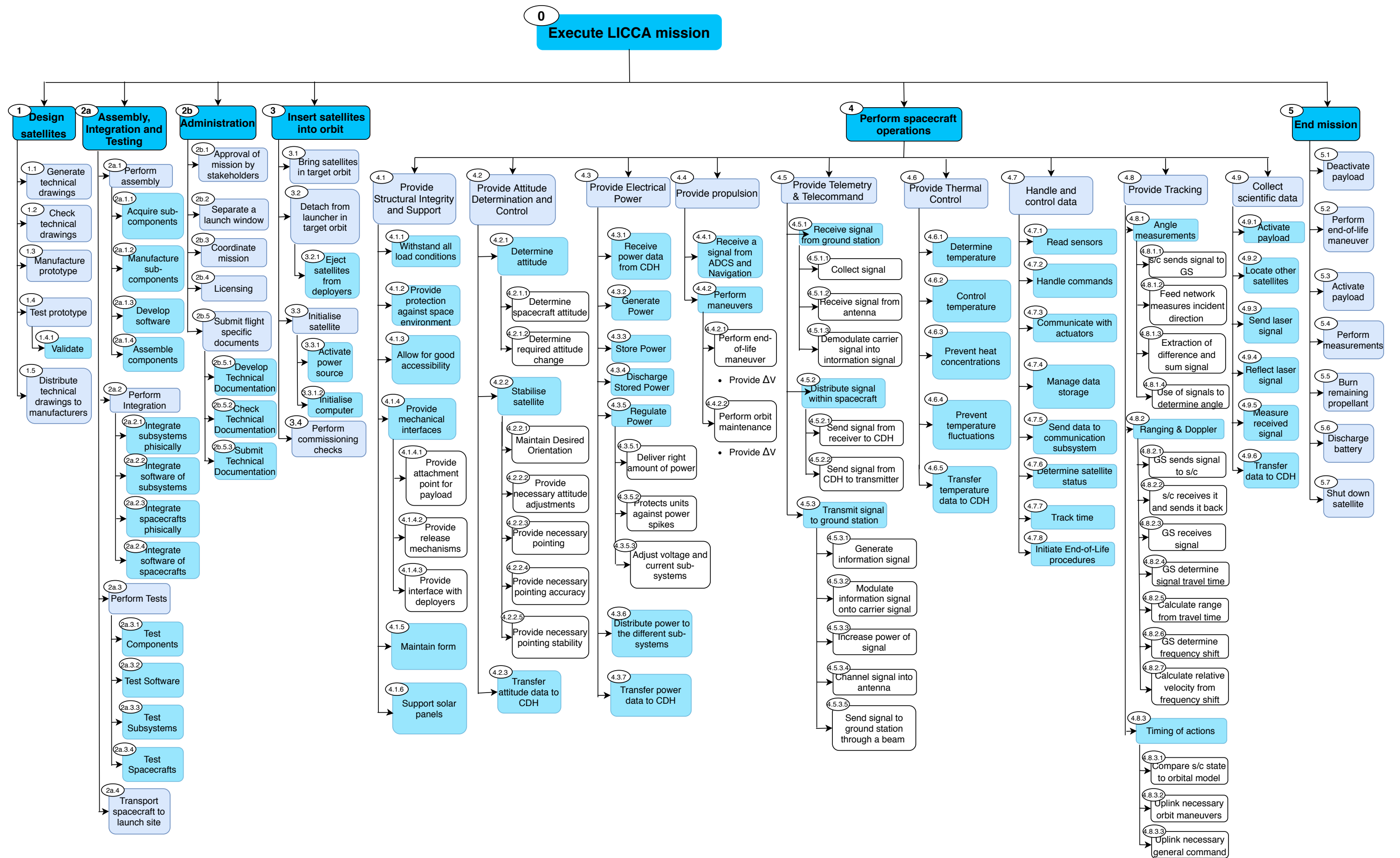
Figure A.4: Functional Breakdown Structure

Payload	Constellation Requirement (72 000km)	Pointing Accuracy		Pre-processing necessary Size/rate of data	Power requirement	Temperature Range	Mass and Volume			
	Astro-dynamics	Disturbance torque	DeltaV Required		Radiation levels	Eclipses	External Temperature Range	Radiation levels	Orbital characteristics	Coverage
		ADCS	Momentum (for dumping)			Power requirement	Temperature Range Heat Generation	Mass and Volume		
			Propulsion			Power requirement	Temperature Range Heat Generation	Mass and Volume thrust force		
		Antenna pointing accuracy		**Telemetry & Tracking**	Size/rate of data	Power requirement	Temperature Range Heat Generation	Mass and Volume		Size/rate of data
				Size/rate of data	**CDH**	Power requirement	Temperature Range Heat Generation	Mass and Volume		
		Array pointing accuracy and size				**EPS**	Temperature Range Heat Generation	Mass and Volume		
						Power requirement (if active)	**Thermal**	Mass and Volume		
		MMOI	Possibility of attachment Total mass	Possibility of attachment		Possibility of attachment	Temperature range Materials	**Structure**	Mass and Volume	
	Injection orbit						Loads during launch		**Launcher**	
	Desired coverage			EIRP Frequency band						**Ground system**

Figure A.5: Design N2 chart

ID	Task Mode	Task Name	Duration	Start	Finish	Predecessors
1		**DSE phase**	**55 days**	**Mon 20-4-20**	**Fri 3-7-20**	
2		Concept development, merit and feasibility review	23 days	Mon 20-4-20	Wed 20-5-20	
3		Conceptual design	32 days	Thu 21-5-20	Fri 3-7-20	2
4		Detailed design	**610 days**	**Mon 6-7-20**	**Fri 4-11-22**	
5		Design components and prototype	300 days	Mon 6-7-20	Fri 27-8-21	3
6		Generating technical drawings	20 days	Mon 30-8-21	Fri 24-9-21	5
7		Checking technical drawings	10 days	Mon 27-9-21	Fri 8-10-21	6
8		Manufacture prototype	100 days	Mon 11-10-21	Fri 25-2-22	7
9		Test and evaluate prototype	90 days	Mon 28-2-22	Fri 1-7-22	8
10		Execute readjustments	90 days	Mon 4-7-22	Fri 4-11-22	9
11		**Administration**	**783 days**	**Mon 30-8-21**	**Wed 28-8-24**	
12		Approval of mission by stakeholders	390 days	Mon 30-8-21	Fri 24-2-23	5
13		Separating a launch window	131 days	Mon 27-2-23	Mon 28-8-23	12
14		Mission coordination	262 days	Tue 29-8-23	Wed 28-8-24	13
15		Licensing	87 days	Mon 27-2-23	Tue 27-6-23	12
16		**Submit flight-specific documents**	**219 days**	**Tue 29-8-23**	**Fri 28-6-24**	
17		Develop technical documentation	153 days	Tue 29-8-23	Thu 28-3-24	13
18		Check technical documentation	22 days	Fri 29-3-24	Mon 29-4-24	17
19		Submit technical documentation	44 days	Tue 30-4-24	Fri 28-6-24	18
20		**Assembly, integration and testing**	**913 days**	**Mon 27-2-23**	**Wed 26-8-26**	
21		**Assembly**	**326 days**	**Mon 27-2-23**	**Mon 27-5-24**	

Engineering 1;Engineering 2;Engineering 3;Engineering 4;Engineering 5;Engineering 6;Engineering 7;Engineering 8;Engineering 9;Engi

Engineering 1;Engineering 2;Engineering 3;Engineering 4;Engineering 5;Engineering 6;Engineering 7;Engineering 8;Engineering 9;Eng

Engineering 1[50%];Engineering 2[50%];Engineering 3[50%];Engineering 4[50%];Engineering 5[50%];Engineering 6[50%

Engineering 1[50%]

Engineering 1

Manufacturing 1[80%];Manufacturing 2[80%];Engineering 1[80%];Engineering 2[80%]

Engineering 1[60%];Engineering 2[60%]

Engineering 5[50%];Engineering 6[50%]

Administrative 1[20%];Engineering 2[20%];Engineering 4

Administrative 1[20%];Engineering 1[20%]

Engineering 1[30%];Engineering 6[30%]

Administrative 2[50%];Administrative 3[50%]

Engineering 2[30%]

Administrative 1[50%];Engineering 4[50%]

Administrative 1[20%]

Project: Project Gantt chart - Co
Date: Tue 19-5-20

Task		Project Summary		Manual Task		Start-only		Deadline	
Split		Inactive Task		Duration-only		Finish-only		Progress	
Milestone		Inactive Milestone		Manual Summary Rollup		External Tasks		Manual Progress	
Summary		Inactive Summary		Manual Summary		External Milestone			

Page 1

Figure A.6: Project Gantt Chart - Part 1

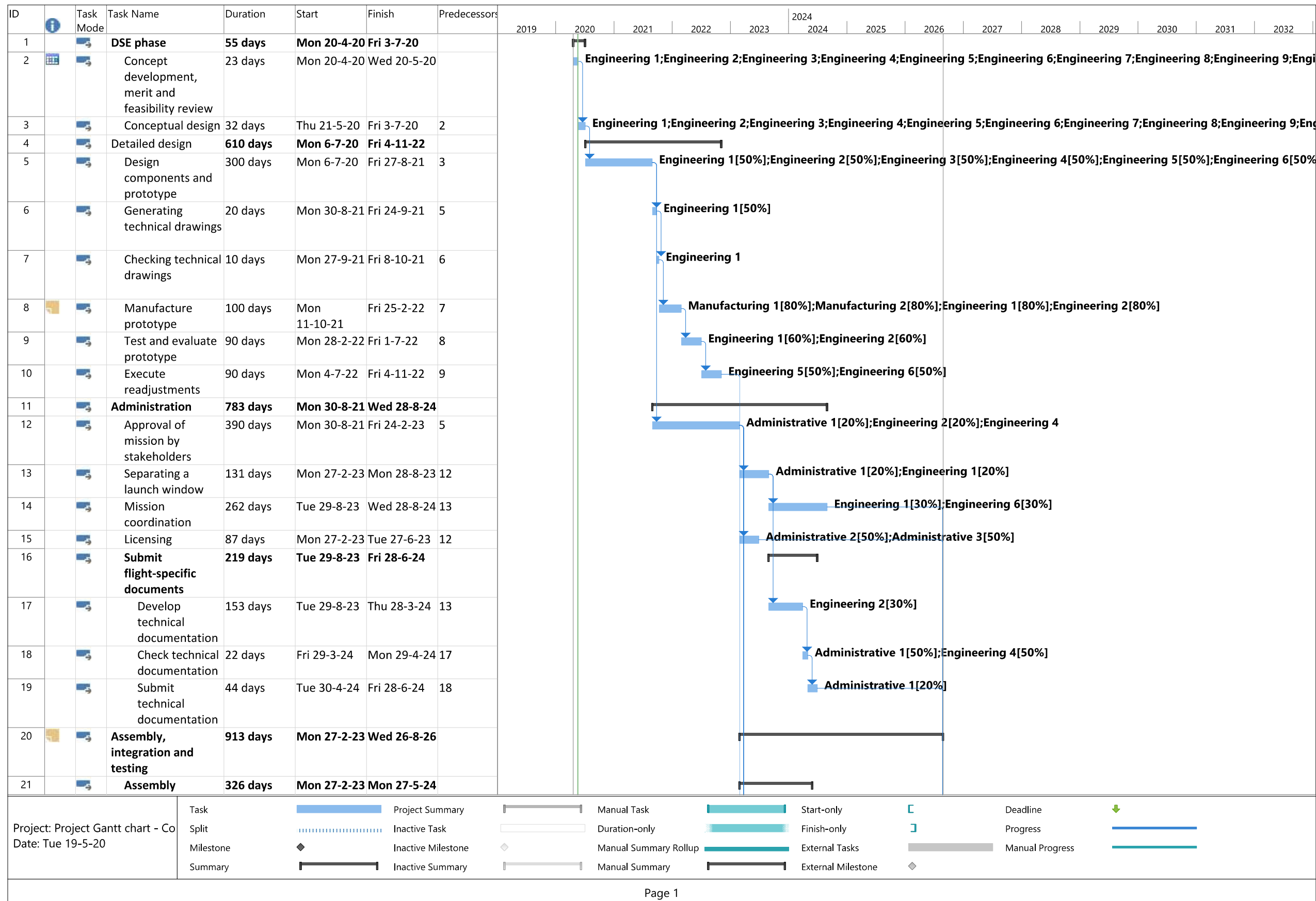| ID		Task Mode	Task Name	Duration	Start	Finish	Predecessors
22			Acquisition of sub-components	220 days	Mon 27-2-23	Fri 29-12-23	12;10
23			Manufacturing sub-components	260 days	Mon 27-2-23	Fri 23-2-24	12
24			Develop software	200 days	Mon 27-2-23	Fri 1-12-23	12
25			Assemble components	66 days	Mon 26-2-24	Mon 27-5-24	22;23;24
26			**Integration**	**420 days**	**Mon 22-4-24**	**Fri 28-11-25**	
27			Physical integration of subsystems	66 days	Tue 1-10-24	Tue 31-12-24	32;33
28			Software integration of subsystems	30 days	Mon 22-4-24	Fri 31-5-24	33
29			Physical integration of spacecraft	44 days	Tue 30-9-25	Fri 28-11-25	34
30			Software integration of spacecraft	22 days	Tue 30-9-25	Wed 29-10-25	34
31			**Test**	**710 days**	**Mon 4-12-23**	**Fri 21-8-26**	
32			Test components	90 days	Tue 28-5-24	Mon 30-9-24	25
33			Test software	100 days	Mon 4-12-23	Fri 19-4-24	24
34			Test subsystems	194 days	Wed 1-1-25	Mon 29-9-25	27;28
35			Test spacecrafts	190 days	Mon 1-12-25	Fri 21-8-26	29;30
36			Transport spacecraft to launch site	3 days	Mon 24-8-26	Wed 26-8-26	15;14;35;1!

Figure A.7: Project Gantt Chart - Part 2